U.S. Department of Energy
Office of Advanced Automotive Technologies
1000 Independence Avenue S.W.
Washington, DC 20585-0121

FY 2002

Progress Report for Automotive Lightweighting Materials

Energy Efficiency and Renewable Energy
Office of Transportation Technologies
Office of Advanced Automotive Technologies
Vehicle Systems Team

Robert Kost **Vehicle Systems Team Leader**

January 2003

This report was prepared as an account of work sponsored by an agency of the United States Government. Neither the United States Government nor any agency thereof, nor any of their employees, makes any warranty, express or implied, or assumes any legal liability or responsibility for the accuracy, completeness, or usefulness of any information, apparatus, product, or process disclosed, or represents that its use would not infringe privately owned rights. Reference herein to any specific commercial product, process, or service by trade name, trademark, manufacturer, or otherwise, does not necessarily constitute or imply its endorsement, recommendation, or favoring by the United States Government or any agency thereof. The views and opinions of authors expressed herein do not necessarily state or reflect those of the United States Government or any agency thereof.

CONTENTS

1. INTRODUCTION 1

2. AUTOMOTIVE ALUMINUM R&D 9

A. Active Flexible Binder Control System for Robust Stamping 9
B. Warm Forming of Aluminum—Phase 2 19
C. Hydroformed Aluminum Tubes 23
D. Electromagnetic Forming of Aluminum Sheet 27
E. Aluminum Automotive Closure Panel Corrosion Test Program 33

3. ADVANCED MATERIALS DEVELOPMENT 39

A. Low-Cost Powder Metallurgy for Particle-Reinforced Aluminum Composites 39
B. Low-Cost Cast Aluminum Metal Matrix Composites 43
C. Exploratory Study into Improved Formability and Strength of Automotive Aluminum Sheet Alloys with an Electric Field 49
D. Magnesium Powertrain Cast Components 53
E. Solid Oxygen-ion-conducting Membrane Technology for Direct Reduction of Magnesium from Its Oxide at High Temperatures 59
F. Understanding the Economics of Emerging Titanium Production Processes 67
G. Preparation of Closed Metal Cell Composites 71
H. Structural Reliability of Lightweight Glazing Alternatives 77
I. Structural Cast Magnesium Development 87

4. POLYMER COMPOSITES R&D 93

A. Development of Manufacturing Methods for Fiber Preforms 93
B. Composites-Intensive Body Structure Development for Focal Project 3 99
C. Thermoplastic Composite Sheet Manufacturing 103
D. High-Volume Processing of Composites 111

5. LOW-COST CARBON FIBER 115

A. Low-Cost Carbon Fibers from Renewable Resources 115
B. Low-Cost Carbon Fiber Development Program 121
C. Low-Cost Carbon Fiber for Automotive Composite Materials 133
D. Microwave-Assisted Manufacturing of Carbon Fibers 137

6. RECYCLING 143

A. Recycling of Polymer Matrix Composites 143
B. Recycling Assessments and Planning 149

7. ENABLING TECHNOLOGIES 153

A. Durability of Lightweight Composite Structures 153
B. Creep, Creep Rupture, and Environment-Induced Degradation of Carbon-Reinforced and Glass-Reinforced Automotive Composites 159

C. Modeling of Composite Materials for Energy Absorption 165
D. Intermediate-Rate Crush Response of Crash Energy Management Structures 177
E. Composite Crash Energy Management 181
F. Energy Absorption in Adhesively-Bonded Composites 189
G. Long-Life Electrodes for Resistance Spot Welding of Aluminum Sheet Alloys and Coated High-Strength Steel Sheet 193
H. Plasma Arc Welding of Lightweight Materials 199
I. Performance Evaluation and Durability Prediction of Dissimilar Material Hybrid Joints 203
J. Joining of Dissimilar Metals for Automotive Applications: From Process to Performance 211
K. Nondestructive Evaluation Tools for Evaluation of Laser-Welded Metals 217
L. Nondestructive Evaluation Techniques for On-Line Inspection of Automotive Structures 221
M. Technical Cost Modeling 227

8. HIGH-STRENGTH STEELS 231

A. Modeling of High-Strain-Rate Deformation of Steel Structures 231
B. Enhanced Forming Limit Diagrams 245
C. High-Strength Steel Stamping Project 249
D. Hydroforming Materials and Lubricants Project 253
E. High-Strength Steel Joining Technologies Project 255
F. Sheet Steel Fatigue Characterization 257
G. Strain Rate Characterization 261
H. High-Strength Steel Tailor-Welded Blanks 263
I. Tribology 267

Appendix A: ACRONYMS AND ABBREVIATIONS 271

1. INTRODUCTION

Automotive Lightweighting Materials R&D

Technology Development Manager
Joe Carpenter

Technology Development Manager
Rogelio Sullivan

As a major component of the U.S. Department of Energy's (DOE's) Office of FreedomCAR and Vehicle Technologies Program (FCVT), Automotive Lightweighting Materials (ALM) focuses on the development and validation of advanced lightweight materials technologies to significantly reduce automotive vehicle body and chassis weight without compromising other attributes such as safety, performance, recyclability, and cost. Through many of its technology research programs, DOE has supported the government/industry Partnership for a New Generation of Vehicles (PNGV) since inception in 1993. In 2002, PNGV was replaced by FreedomCAR, and new, longer-term goals were set. FCVT and ALM are refocusing their goals accordingly.

The specific goals of ALM are

1. By 2004, develop and validate advanced material technologies that will be needed to meet technical goals:
   - Enable reductions in the weight of body and chassis components by 50% and vehicle weight by 40% (relative to 1994 comparative vehicles)
   - Exhibit performance, reliability, and safety characteristics comparable to those of conventional vehicle materials
   - Be cost-competitive, on a life-cycle basis, with costs of current materials
2. By 2011, develop and validate advanced material technologies that will
   - Enable reductions in the weight of body and chassis components by at least 60% (relative to 1994 comparative vehicles)
   - Exhibit performance, reliability, and safety characteristics comparable to those of conventional vehicle materials
   - Be cost-competitive, on a life-cycle basis, with costs of current materials

ALM is pursuing five areas of research: cost reduction, manufacturability, design data and test methodologies, joining, and recycling and repair. The single greatest barrier to use of lightweight materials is their high cost; therefore, priority is given to activities aimed at reducing costs through development of new materials, forming technologies, and manufacturing processes. Priority lightweighting materials include advanced high strength steels, aluminum, magnesium, titanium, and composites such as metal-matrix materials and glass- and carbon-fiber-reinforced thermosets and thermoplastics.

Collaboration and Cooperation

ALM collaborates and cooperates extensively in order to identify and select its research and development (R&D) activities and to leverage those activities with others. The primary interfaces have been and still are with the Big Three domestic automotive manufacturers, namely the FreedomCAR Materials Technical Team, the Automotive Composites Consortium (ACC), and the United States Automotive Materials Partnership

(USAMP). This collaboration provides the means to determine critical needs, to identify technical barriers, and to select and prioritize projects. Other prominent partners include such organizations as the Aluminum Association, the American Iron and Steel Institute, the American Plastics Council, the Vehicle Recycling Partnership, the Society for the Advancement of Material and Process Engineering (SAMPE), the International Magnesium Association, the International Titanium Association, and the Auto Parts Rebuilders Association. ALM also coordinates its R&D activities with entities of other U.S. and Canadian federal agencies. Interactions with the DOE Office of Industrial Technologies (OIT) and High-Strength Weight Reduction Materials Program (HSWR) and with the Department of Natural Resources of Canada (NRCAN) are especially important by virtue of overlaps of interests in lightweight materials.

Once selected, R&D projects are pursued through a variety of mechanisms, including cooperative research and development agreements (CRADAs), cooperative agreements, university grants, R&D subcontracts, and directed research. This flexibility allows the program to select the most appropriate partners to perform critical tasks. The ALM efforts are conducted in partnership with automobile manufacturers, materials suppliers, national laboratories, universities, and other nonprofit technology organizations. These interactions provide a direct route for implementing newly developed materials and technologies. Laboratories include Argonne National Laboratory (ANL), Lawrence Berkeley National Laboratory (LBNL), Lawrence Livermore National Laboratory (LLNL), Los Alamos National Laboratory (LANL), Oak Ridge National Laboratory (ORNL), Pacific Northwest National Laboratory (PNNL), and Sandia National Laboratories (SNL). PNNL manages the Northwest Alliance for Transportation Technologies, drawing on expertise and developments in the Northwest. ANL oversees recycling efforts, and ORNL provides overall technical management, including management for the DOE cooperative agreement with USAMP.

Research areas and responsible organizations

Coordinated area	Organization
Production and fabrication of aluminum	The Aluminum Association, HSWR, OIT, Natural Resources of Canada (NRCAN)
Production and fabrication of magnesium	International Magnesium Association, NRCAN, HSWR
Recycling, reuse, repair of automotive parts and materials	Auto Parts Rebuilders Association, OIT, Vehicle Recycling Partnership, American Plastics Council
Fabrication of steel and cast iron	American Iron and Steel Institute, the Auto/Steel Partnership, HSWR
Fundamental materials research	DOE Office of Energy Research, National Science Foundation
High-volume composite processing	Department of Commerce—National Institute of Standards and Technology's Advanced Technology Program
Materials research for defense applications	Department of Defense
Materials research for space applications	National Aeronautics and Space Administration
Crashworthiness	Department of Transportation
International vehicle material R&D	International Energy Association
Production and fabrication of titanium	The International Titanium Association
Production and fabrication of composites	American Plastics Council

FY 2002 Accomplishments

To meet the goals set forth for the program, ALM is developing materials and material processing technologies; validating these technologies through fabrication and evaluation of representative, non-proprietary test components; and developing adequate design data to facilitate their beneficial application. The research is balanced between nearer-term objectives and longer-term, higher-risk research. As the techni-

cal barriers are removed, the technology is made available to industry. Because of the broad area of research and the limited resources, projects have been selected to overcome the most significant barriers within the technical areas that the materials community considers higher-risk but that, if successfully developed, would result in significant progress toward ALM's goals.

Metals and Alloys

Low-Cost Cast Metal Matrix Composites

Metal matrix composites (MMCs) exhibit a number of benefits for automotive applications. Unfortunately, several barriers, including cost, durability, and manufacturability, have limited their widespread application. This project seeks to make these materials more attractive by reducing the costs of the raw materials, the processing methods, and the downstream operations. The focus of the project is an innovative brake system. However, instead of using a common cast-iron brake rotor design and direct materials substitution with aluminum-MMC, an approach tried in the past with poor results, the goal is to design from scratch a geometry that can exploit the properties of an aluminum-MMC material with good performance. With this approach, Visteon Chassis Systems and the project team believe that a functional aluminum-MMC brake rotor can be produced and used on a typical mid-size passenger vehicle. Under a no-cost, non-disclosure agreement, Visteon has provided an appropriate and novel brake rotor design that will be used for prototyping and evaluation purposes. Based on the two casting methods selected for prototyping of aluminum-MMC brake rotors (squeeze and centrifugal casting), a cost-shared contract with THT Presses was established for the design and fabrication of the appropriate casting dies. Furthermore, THT Presses will cast the prototype rotors at the Casting and Composite Technology Center. In FY 2003, it is anticipated that approximately 80 prototype rotors will be produced for testing and evaluation.

Warm Forming of Aluminum

In a recently completed Phase I project, a team consisting of representatives from original equipment manufacturers (OEMs), universities, materials suppliers, and the National Center for Manufacturing Sciences (NCMS) successfully demonstrated the feasibility of warm forming technology and its potential to significantly improve the formability of aluminum. That work involved developing modified 5000-series aluminum alloys, producing blanks, and performing warm forming trials on a Dodge Neon door inner with deep drawn profiles. Trials were performed at an industrial stamping supplier, where the component was formed in a single die stage with one hit. The equivalent steel panel required two stages. The results of Phase I indicated that additional developments were required in the alloy chemistry, the lubrication system (washability and paintability), the temperature management of the forming dies, and blank preheating, if "production" feasibility were to be demonstrated. In Phase II, Pechiney Rolled Products provided five different alloys composed of varying formulations containing magnesium, manganese, chromium, zirconium, copper, or scandium. Laboratory tests at the University of Michigan identified grain size as critical to warm forming. Warm forming tests using rectangular cups on selected alloys demonstrate that the formability of these alloys should be greater than that of the materials studied in Phase I. Infrared Technologies will deliver an infrared heater to be used for continued evaluation of the production feasibility of this technology. Parallel activities are focusing on the lubrication system and thermal management.

Dodge Neon door inner panel.

Magnesium Powertrain Cast Components

Although magnesium has been demonstrated to significantly reduce weight at acceptable automotive costs in many areas of the vehicle, structural powertrain components have not benefited from the use of this material.

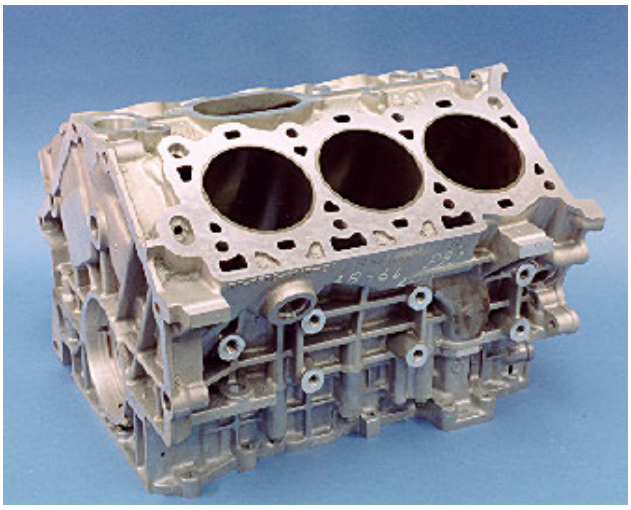

The Ford 2.5-L Duratec engine block.

A project led by USAMP is addressing this issue by focusing on overcoming the major barriers limiting the use of magnesium in these applications. The engine chosen for the project is the Ford Duratec. The components of this V-6 engine to be designed for magnesium are the block, the bedplate, the structural oil pan, and the front cover. The team—consisting of 44 companies and organizations that are key magnesium alloy producers and casters, the Big Three auto makers, and a number of universities and other R&D organizations—has made substantial progress on Phase I. In Phase I, the focus is on three areas: (1) evaluating and selecting alloys that can withstand the operating temperatures of the engine without deforming under load (creeping), (2) developing finite element analysis design and cost models of the engine and its magnesium components, and (3) identifying the fundamental scientific challenges of using magnesium alloys and casting processes for powertrain components. Seven high-pressure die casting alloys and three sand casting alloys were selected for inclusion in the alloy evaluation database. The castability trials for the die casting alloys have been completed, and properties of these alloys have been measured and compared. Final tests of the sand cast alloys are also nearing completion. A bedplate has been identified for use in assessing the potential of the most promising alloys. The team has also completed computer-assisted drawing files for the engine components and initiated finite element analyses. Computational fluid dynamics and heat transfer analyses were completed, and structural analysis and design are progressing rapidly. Casting and solidification modeling have also been initiated. Successful completion of these tasks will lead to a decision to proceed with Phase II in FY 2003. Phase II will comprise three tasks: (1) casting engine components, (2) developing a comprehensive magnesium database, and (3) conducting validation tests on assembled engines. This project is an aggressive attempt to address key concerns regarding the future prospects for a magnesium-intensive powertrain.

Modeling of High Strain Rate Deformation of Steel Structures

During the past decade, the finite element modeling (FEM) of vehicle crashworthiness has become fully integrated in vehicle design and analysis. The limiting technology has now become the accuracy of the FEM components, e.g., constitutive models, element technology, and contact algorithms. ALM is supporting a project aimed at developing numerical modeling guidelines for strain-rate-dependent materials in crashworthiness computations. The scope of the project is to study specific, experimentally well-defined structural problems in automotive impact using combinations of modeling approaches and to identify the trends, influences, and direct effects of the modeling techniques used. During FY 2002, research focused on developing experimental results based on crushing circular tubes and using these results to identify the modeling approaches and their relative importance to the accuracy of the predictions. The developed models have shown overall excellent agreement with crush tests and have provided an explanation of the test results and the relative effect of the test method

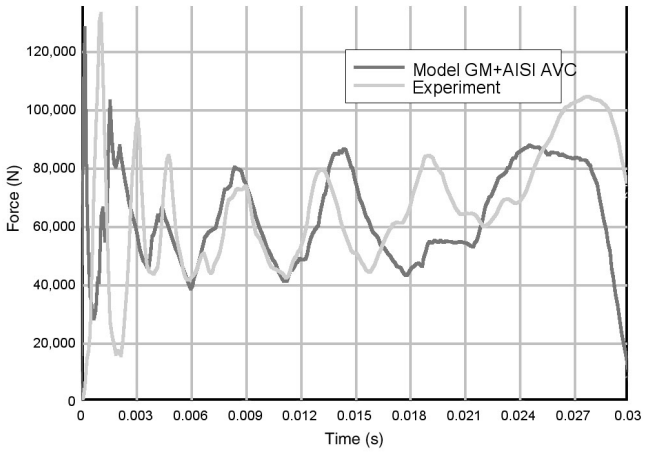

DP600 drop tower simulation.

and tube imperfections. A comparison of the force–time diagram from a drop tower test of circular tubes of DP600 steel and the results of the model can be seen in the accompanying figure. These encouraging results will be used in FY 2003 to model the crush of rectangular tubes, model the damage that the advanced high-strength steel experiences during the deformation, and incorporate the effect of processing into the models.

Composites

Low-Cost Carbon Fiber

One of the highest-priority technical needs is the development of low-cost carbon fibers. Carbon fiber composites are the lightest material available for making primary automotive structures. Their use in automotive structural composites could reduce the body and chassis weight of vehicle components by up to 67%. Currently, the use of these advanced lightweight composites in primary automotive structures is limited because carbon fibers are much more expensive than traditional automotive materials. To address this challenge, research is being conducted to reduce the cost of materials being converted into carbon fiber and the cost of production processes used for making carbon fiber.

Originally, the overall effort had four projects aimed at developing low-cost carbon fiber precursors. That field was reduced to two projects in a previous year. One nearer-term, medium-risk project focuses on using commodity-grade polyacrylonitrile (PAN) precursor, which could reduce finished fiber costs by up to $1.60 per pound. One longer-term, higher-risk project uses lignin-based precursors, which could reduce carbon fiber prices to near $3 per pound.

Textile-Grade PAN Precursors

During 2002, the technologies were developed to produce lower-cost carbon fiber precursor using commodity-grade PAN on a small-scale production line. Commodity textile-grade PAN is commercially available in large quantities at about half the cost of large-tow PAN precursors. Chemical pretreatment and thermal processing methods were developed using textile-grade PAN precursors. Appropriate mechanical and chemical properties were determined, and spools of fiber were produced on a small-scale production unit. Finished fiber spools were created using textile fiber produced by Sterling, Inc., in Pensacola, Florida. The next step will be to incorporate the chemical pretreatment into the fiber production facility and provide textile-grade fiber for use in all the other ALM technology development projects. The project should conclude in about 9 months and be ready for implementation into full-scale production facilities shortly afterward. It is critical that this fiber be used in the other processing and structural development projects so that industry will learn what differences there are between its behavior and that of conventional fibers. The resulting reduction in carbon fiber price is projected to be $1.51 per pound.

Textile PAN being processed into carbon fiber.

Lignin-Based Carbon Fiber Precursors

It is expected that commodity-grade textile precursor will allow penetration of carbon-fiber-based composites into the automotive market at significant levels by meeting the $5 per pound goal for carbon fiber. However, for carbon fiber composites to become more prevalent as structural materials, carbon fiber prices must approach $3 per pound. The second precursor project seeks to meet that goal by using lignin as a feedstock. Lignin is a by-product of paper making and is often burned in paper mills to recover its energy value. It can be purchased on the open market for $40 per ton. During this year, preliminary technical development was completed. Continuous strands of lignin-based precursor were made and processed into carbon fiber. These early tows contained only a few filaments each and had filament diameters larger than those of conventional

Multi-filament processing unit.

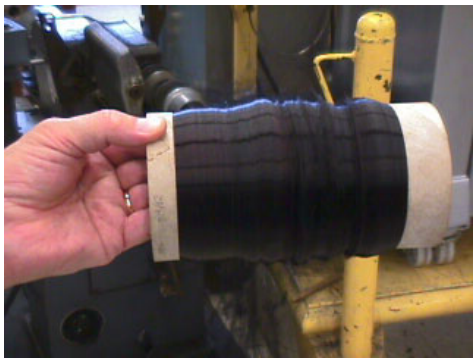

Carbonized lignin-blend fiber.

fibers. These materials allowed development of the technologies for handling the raw fiber during subsequent processing. Chemical and mechanical tests verified that this class of precursor can be successfully made into carbon fiber. The next step for this technology is to develop the capability to spin and subsequently process multi-filament tows.

Microwave-Assisted Plasma Processing of Carbon Fiber Precursors

In addition to developing lower-cost precursors, ALM has been working on developing lower-cost production methods for converting precursors into carbon fiber. In previous years, a process was demonstrated that used microwave energy to produce carbon fibers; it required processing times that were only a fraction of the time necessary using conventional methods. The tow size of carbon fibers was small; the process, after initial development, was small; and the output line speed was only starting to be scaled up. However, during the last year, a new microwave-assisted plasma (MAP) unit was designed and built to handle large-tow precursors at greatly enhanced speeds. The unit can process 48-K tows at line speeds of 120 inches per minute, which is faster than the speed of conventional carbon fiber lines. The mechanical properties of the fibers produced met and often exceeded the properties of fibers made from the same precursor on a conventional thermal line. The next obstacle to be addressed in this program is simultaneous production of multiple tows.

Newest MAP carbon fiber production unit.

Recycling of Polymer Matrix Composites

One major concern associated with using polymer-based composites in automotive structures is that, historically, it has not been economical to recycle these materials. This project is developing methods for recycling carbon-fiber–based polymer composites cost-effectively by recovering the high-value carbon fiber and reusing it in appropriate applications. In previous years, the project evaluated three processes to separate carbon fibers from polymer matrix composite (PMC) scrap. Those processes were thermal treatment, chemical treatment, and thermal shock. The thermal treatment method was chosen as the one showing the most promise. Economic analysis showed that this method will have a potential investment payback of less than two years.

During FY 2002, carbon fibers were recovered at ANL from PMC panels that were made with known fibers and substrates supplied by Hexcel Carbon Fibers. The recovered fibers were evaluated by Hexcel and ORNL for their potential for subsequent reuse. The fibers were shown to have a high shear strength and high oxygen concentration on the surfaces, which indicated that they have good potential to adhere to matrix resins

without the need for additional surface treatment. The physical and morphological characteristics of the recovered fibers were nearly identical to those of virgin fibers.

Hexcel used the recovered fibers to make new PMC panels that were physically identical to those from which the fibers had come. The data showed only a 10% reduction in stiffness and 12% reduction in the short beam shear strength. It did, however, show a significant reduction in tensile properties. It was shown that these fibers can be used to make carbon fiber composites and that the most likely application will be to make sheet molding compound composites that require chopped fibers.

Typical PMC panel before thermal treatment (left). Recovered carbon fibers after treatment (right).

Thermoplastic Composite Sheet Manufacturing

Polymer matrix composites have a combination of properties required to achieve significant reductions in vehicle mass compared with conventional materials. Although they are widely regarded as having the most potential for weight savings, their application is severely restricted by fundamental issues in achieving the required production volumes and in the cost of basic materials. This project has identified carbon fiber thermoplastic matrix composites as having significant potential to meet structural property requirements and to achieve rapid processing cycles similar to those for stamping metal components. Automotive applications will be more widespread if two other fundamental issues can be addressed: thin-walled structures (for optimum structural performance and minimum weight) and Class A surfaces in semi-structural components. Developing the thermoplastic composites to meet these requirements will require a combination of experimental approaches, materials and process modeling, and modification of materials forms and processing methods to achieve an optimum manufacturing process.

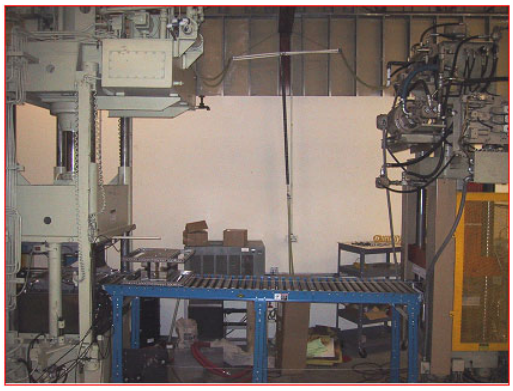

Two-press system with tool shuttle.

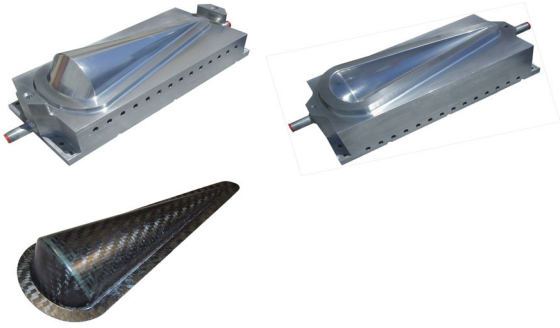

Generic cone-shaped heated and cooled mold for formability and process envelope studies.

During FY 2002, a two-press system was completed, installed, and demonstrated in operation using a single modified cone tool. Operation showed a need for emphasis on tool design, specifically optimizing tool mass and heating and cooling times. The results showed that current material forms cannot be processed within cycle times that are compatible with automotive production cycle goals. The project goal is materials that either require shorter consolidation times or are pre-consolidated. A new seven-sided forming tool was designed to allow structural testing and show the effects of slope angle on structural integrity. A numerical model was developed that predicts 2×2 foot twill unconsolidated fabric shear behavior to simulate properties useful for macro models of stamp forming. Critical process parameters were determined for the test material, and a process methodology was developed to determine the balance among pressure, time, and temperature for reinforced thermoplastic systems.

Intermediate Strain Rate Test Machine

The ACC's Energy Management Group and FreedomCAR Materials Technical Team, along with the national laboratories, is undertaking development of the knowledge base, both analytical and experimental, that will lead to a predictive capability for composites and metals subjected to crash events. Previous research has demonstrated a dramatic difference in the energy absorption of steels and composite tubes when they are tested quasi-statically and dynamically. The difference in the operating material responses between these two failure rates is not understood, but it is critical to designing automotive structures that provide occupant safety during both low- and high-speed crashes. It is known that the dynamic response is controlled largely by the material response as the failure mode transitions from one type to another at intermediate strain rates. Currently, there is no practical method to study the crush response of tubes or other material forms tested at intermediate strain rates.

MTS and ORNL, in conjunction with the ACC, have designed and built an intermediate strain rate tester that will allow the study of materials crushed at these in-between strain rates. The machine can operate at rates of up to 160 inches per second and at loads of as high as 60,000 pounds. The machine has been built and the verification testing completed at MTS. It will be installed at the National Transportation Research Center at ORNL in early FY 2003. It will be used to test aluminum, steel, and composite materials and components at a range of predetermined strain rates.

Future Direction

FY 2002 marked the middle of a second ALM phase to run between around FY 2000 and FY 2004. In the first phase, between about FY 1994 and FY 2000, ALM showed that glass-fiber–reinforced PMC automotive structures could be manufactured at about the same cost as structures made of the currently used steels but could not meet the PNGV goal of 40% overall vehicle weight reduction. It also showed that acceptable automotive structures made of aluminum could achieve the weight reduction goal, but at a slight cost premium. In its Ultralight Steel Autobody (ULSAB) program, which ran chronologically parallel to and independent of the ALM first phase, the steel industry showed that high-strength steels could be used to produce a body-in-white (BIW) that would be cost-neutral (or even lower in cost) compared with bodies made of current steels; however, the BIW could not meet the weight reduction goal. Some of the technologies developed by ALM and in the ULSAB are already on production vehicles; and it is now apparent that aluminum, PMCs, and advanced high-strength steels are serious technical and economic contenders for eventually replacing some or all current steels when market conditions are suitable.

In the current second phase, earlier efforts in aluminum research are being advanced while more attention is being focused on materials such as advanced high-strength steels, carbon-fiber–reinforced PMCs, and magnesium and on issues associated with manufacturing and recycling automotive components made of all those materials. The North American steel industry joined ALM in the effort to show that the advanced high-strength steels could meet PNGV goals. But in FY 2002, PNGV was replaced by FreedomCAR and new, longer-term goals were set, including a cost-neutral 60% weight reduction in the body and chassis by 2011. So the shift toward carbon-fiber–reinforced PMCs and magnesium that began before FreedomCAR formed was serendipitous in that it is apparent that these materials will play a significant role in achieving the 2011 weight reduction goals. Thus current ALM efforts are expected to continue as-is through FY 2003 and FY 2004.

Planning for what will replace the current efforts in FY 2005 and beyond is beginning and will continue in FY 2003 and 2004. It appears that the "low-hanging fruit" of aluminum, fiber-reinforced PMCs, and advanced high-strength steels that ripened over the past few decades may have been "picked" by the end of ALM's second phase in FY 2004, at least in the technical feasibility stage. Initial thoughts are that ALM's focus may bifurcate, with proportionately less work on technical feasibility and more on exploring the feasibility of several very novel concepts and on demonstrating a few technologies that have been proven technically but that industry cannot or will not pursue on its own in a timely manner.

2. AUTOMOTIVE ALUMINUM R&D

A. Active Flexible Binder Control System for Robust Stamping

Project Leader: Tom Balun
Ford Motor Company
Vehicle Operations General Office, C290, 17000 Oakwood Blvd.
Dearborn, MI 48121
(313) 322-4951; fax: (313) 337-2706; e-mail: tbalun@ford.com

Project Administrator: Mahmoud Y. Demeri
FormSys Inc.
40180 Woodside Drive South
Northville, MI 48167
Phone/fax: (734) 462-274; e-mail: mdemeri@peoplepc.com

Technology Development Manager: Joseph Carpenter
(202) 586-1022; fax: (202) 586-1600; e-mail: joseph.carpenter@ee.doe.gov
Field Technical Manager: Philip S. Sklad
(865) 574-5069; fax: (865) 576-4963; e-mail: skladps@ornl.gov

---

Contractor: U.S. Automotive Materials Partnership
Contract No.: DE-FC05-02OR22910

Objective

- Develop and demonstrate, on an industrial scale, an optimized closed-loop flexible binder control system that can be installed in presses to improve the quality, reduce the variability, and maintain the accuracy of stampings made from aluminum alloys and ultra-high-strength and stainless steels. The system will also reduce cost for developing and setting production tools.

Approach

- Conduct open-loop control demonstration of flexible binder technology.
- Develop methodology and guidelines for designing and building flexible binders.
- Develop computer simulation and process optimization capabilities for flexible binders.
- Develop a closed-loop flexible binder control system with appropriate sensors.
- Demonstrate closed-loop control of the flexible binder system on an industrial part.
- Evaluate the technical and economic feasibility of flexible binder technology.

Accomplishments

- Developed and experimentally verified a mathematical model that represents the press system dynamics, using a specially designed single-cylinder test rig. The model will be used to design appropriate feedback controllers to manipulate pressure levels in hydraulic cylinders and to simulate the binder control closed-loop system.

- Based on analytical modeling, validated a nonlinear control strategy for pressure control in a hydraulic cylinder representative of the binder force actuation system. The validation was conducted in a scaled experiment ramp-step pressure profile with good tracking performance.
- Completed an 18-step process for designing and building flexible binders and issued a technical report.
- Completed conical cup experiments simulating single-point binder force control to verify wrinkle and fracture criteria in sheet metal forming. The criteria will be used to define failure in sheet metal forming simulation and to develop optimized binder force trajectories for successful stampings.
- Used the gradient method to optimize blank holder force (BHF) trajectories in conical cup drawing.

Future Direction

- Transfer the old control unit (Erie's) to Magna for evaluation and repair.
- Arrange with the Institute for Metal Forming Technology in Germany (IFU) to modify the DOE-owned Yoshida/front fender die and control unit so that the hardware can be used in a mechanical press environment. The hardware is to be shipped to Troy Design and Manufacturing (USA) for set-up and testing.
- Extend non-linear control analysis to multi-cylinder systems.
- Evaluate the fatigue properties and determine stress concentrations and allowable stresses in flexible binders.
- Evaluate proposals and initiate work on developing a closed-loop control system for flexible binders.
- Initiate cost analysis and feasibility studies for the flexible binder control technology.

Introduction

Significant weight savings can be achieved by replacing parts made from mild steel with parts made from lightweight materials (aluminum and magnesium alloys) and high-specific-strength materials (ultra-high-strength and stainless steels). Such materials are less formable than mild steel, and parts made from them lack dimensional control because of the significant amount of springback that they produce after forming.

Traditional stamping leaves no flexibility in the stamping process for using difficult-to-form materials and for responding to process variations (e.g., lubrication, material, die wear, blank placement) that can lead to stamping inconsistencies or even failure. It has been found that failure caused by wrinkling or tearing is highly dependent on the magnitude and trajectory of the binder force. Recently, dynamic variation of the binder force during the forming stroke has been shown to affect formability, strain distribution, and springback. Optimal forming trajectories can be obtained under constant and variable binder force conditions, but there is no guarantee that process variables will remain constant during the stamping process. Specifying a binder force trajectory is not easy because the part shape changes during forming. Also, stresses in the part cannot be determined because the coefficient of friction is not a controllable quantity and it varies from location to location. Therefore, the forming process must be controlled, and a closed-loop system with an appropriate local control parameter (friction, draw-in) must be used to track a pre-determined optimum control parameter trajectory.

The scope of this project involves using flexible binder control technology in conjunction with innovative tool designs and closed-loop control to produce robust processes for stamping aluminum and high-strength steel automotive panels. The focus of this project is to implement binder and feedback process control in the stamping industry to increase the robustness of the forming process and to improve the quality and consistency of stampings. This technology will use computer simulation and process optimization to predict optimum binder force trajectories that can be entered into programmable hydraulic cushions to control binder actions in mechanical and hydraulic presses.

Task 1: Conduct Open-Loop Trials Using Flexible Binder and Lift Gate Tooling

Attempts by Erie Press to repair the malfunctioning binder control unit were not successful. The problem has been identified as a lack of control of pressure within the hydraulic cylinders in the binder control unit. The lack of control was caused by non-linearity of the mechanical press punch speed. Control of pressure within the hydraulic cylinder in the binder unit could not be achieved with a simple proportional integral derivative (PID) controller. The project steering committee decided to hire another supplier (Pathway Technologies) to solve the problem. Pathway presented a systematic approach to addressing and fixing the problem. Its strategy is based on evaluating a single cylinder and then proceeding to analyze the more complicated 26-cylinder system. A summary of Pathway's approach includes the following steps:

1. Mathematically model the interaction between the press punch and the hydraulic system dynamics to obtain a differential equation that relates the pressure rate to the various system states and inputs.
2. Obtain the parameters associated with this mathematical model from system specifications and/or experimental tests.
3. Simulate and analyze the system using the Matlab/Simulink system simulation and analysis environment.
4. Design and implement a nonlinear controller based on this analysis.
5. Simulate the closed-loop system to assess the controller's performance and ability to tolerate errors in parameters, noise in signals, and other real-world effects.

Since this controller is not a standard PID controller, the best platform for implementation would be a real-time rapid control prototyping system such as that offered by dSPACE. These systems allow for rapid implementation of any controller structure through an interface to Simulink (used in Step 3) and for real-time parameter tuning and data acquisition, which will be very important in accounting for variations from the simulation-based design.

Simulation

Based on basic information obtained from Erie Press, a preliminary mathematical model was derived and model parameters were adjusted to fit some experimental data provided by Erie Press. The mechanical press drive and the hydraulic cylinder are modeled in Simulink in block diagram form as subsystems. (The complete simulation block diagram is shown in Figure 1.) The model was then simulated in Simulink; the results for constant servo valve commands are shown in Figures 2 and 3. It can be seen that the mathematical model captures many of the significant effects observed experimentally; and with more accurate specification and/or experimental data, the models can be refined to sufficient accuracy for controller design.

Analysis of the model gives insight into the nature of the problems associated with closed-loop control of the flexible binder system, particularly with respect to its nonlinear nature and the adverse effect of having very little hydraulic fluid in the cylinder near BDC. This model will be used for

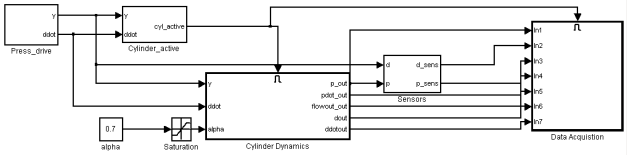

Figure 1. Open-loop Simulink simulation model.

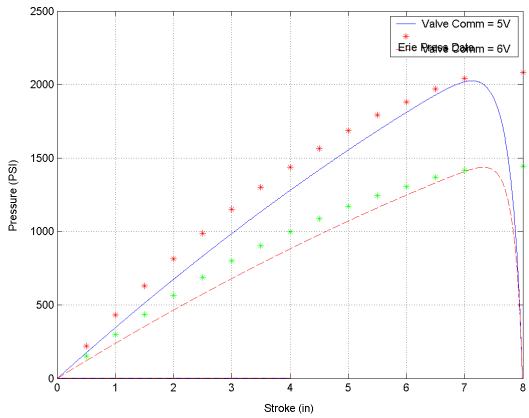

Figure 2. Pressure vs stroke.

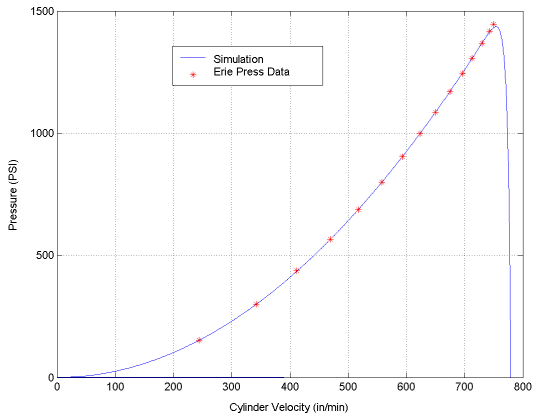

Figure 3. Pressure vs velocity.

designing feedback controllers and for simulating the closed-loop system.

Closed-loop simulation studies were conducted to test the performance of the non-linear controller in achieving pressure profile tracking. Feedback linearization (FBL) technique was used to design the controller based on the nonlinear model developed in the open-loop simulation study. The closed-loop system was simulated using the graphical simulation software package Simulink.

Figure 4 shows the Simulink representation of the closed-loop system. The performance of the closed-loop system was analyzed with respect to the parameters of the hydraulic force actuation unit, controller structure, servo-valve dynamics, and sensor noise.

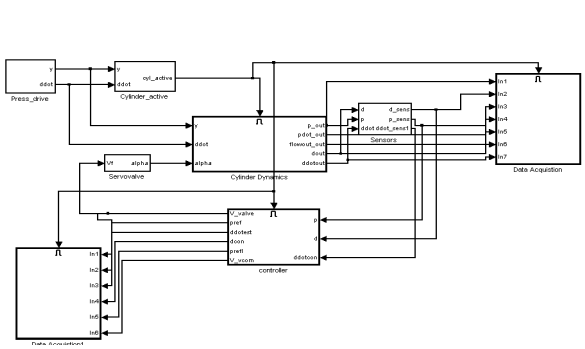

Figure 4. Closed-loop Simulink simulation model.

Figure 5 shows a comparison between pressure profiles using linear and nonlinear controllers. The good tracking performance of the non-linear FBL P controller is evident.

Experiments

A test stand for validating the simulation results was designed, fabricated, and installed in the Active Vibration Control Laboratory of the Department of Aerospace Engineering at The University of Michigan, Ann Arbor. The test stand is a hydraulic cylinder mounted under a shaker table with sensors (Figure 6).

Open-loop tests were conducted to validate simulation models and to identify problems in components. The open-loop models were modified to include an experimentally observed nonlinear relationship between voltage command to the servo valve and the effective flow area through the valve. In addition, the damping effect of the hydraulic fluid on velocity perturbations was considered. These modified models were validated against experimental data from the test stand and will be used to develop controllers to achieve pressure control in this test system.

Figure 7 shows the measured experimental data compared with the simulation model output. Results indicate that the model provides reasonable estimates of the cylinder pressure.

A schematic of the hydraulic test system for a closed-loop control system consisting of reservoir, servo valve, and other hydraulic components is shown in Figure 8.

Experimental closed-loop testing of the feedback linearized PI controller was conducted on the test stand. Figure 9 shows the commanded versus actual pressure curves and the corresponding valve control signals generated by the controller. The figure shows that the closed-loop system remained stable and tracked the pressure commands reasonably well, although their performance was limited by flow-rate limitations on the valve. The controller, however, did exactly what was necessary. It commanded the valve to open fully in order to drop the pressure, but the valve could not release enough fluid to reduce the pressure to the commanded value.

Conclusion

The nonlinear controller described has been experimentally shown to be a viable control strategy for pressure control in the hydraulic force actuation system for the binder force control unit. As

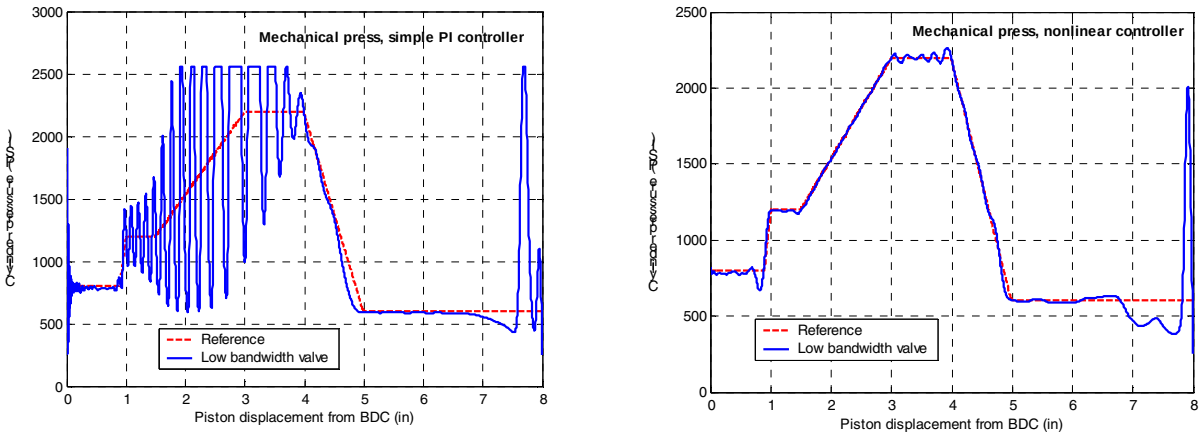

Figure 5. Closed-loop control simulation showing pressure response to ramp-step command using linear (left) and nonlinear FBL P controller.

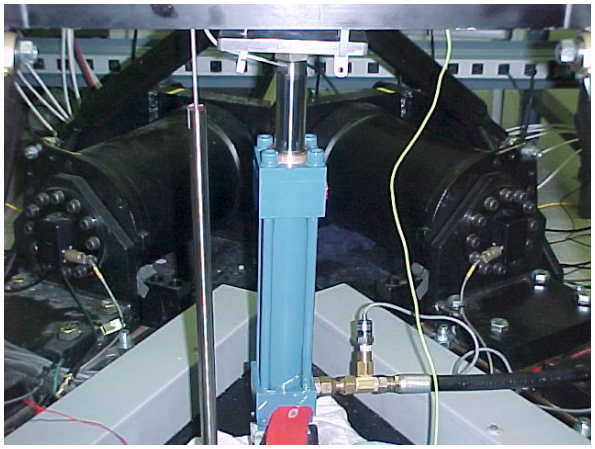

Figure 6. Hydraulic system test stand for single-cylinder test.

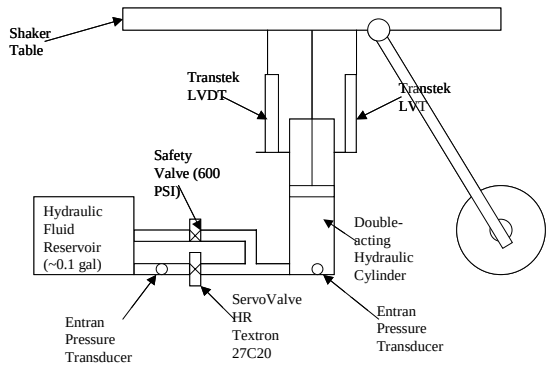

Figure 8. Schematic of the hydraulic test system for closed-loop control.

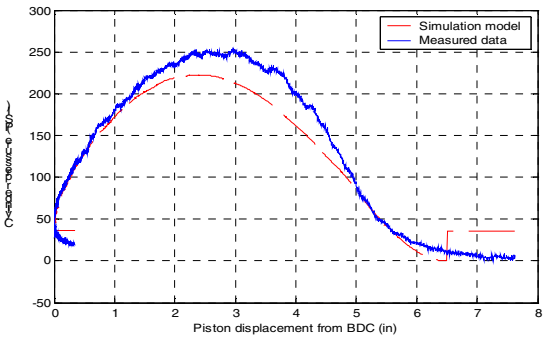

Figure 7. Experimental and model pressure-displacement profile with valve open 100%.

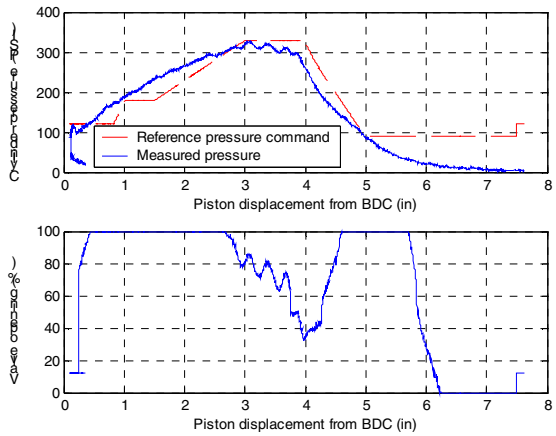

Figure 9. Closed-loop performances for ramp-step pressure profile.

mentioned in earlier simulation studies, the valve may have to be reconfigured to avoid leakage through the tank port and to allow sufficient flow rates to be achieved. Once controller specifications are clearly defined (e.g., acceptable overshoots, error tolerances) for various phases of the stamping cycle, the control parameters can be optimized for best performance.

Task 2: Develop Guidelines for Designing and Building Flexible Binders

Task 2 objectives are to develop guidelines for designing and building flexible binders. Specific areas of development include

- Binder segmentation
- Cone shape, numbers, and size
- Lower and upper binder material
- Effect of stress concentration and fatigue on flexible binders
- Allowable stresses and strains in flexible binders
- Computer-aided designs for flexible binder tools
- Hydraulic cylinder and pin sizes, capacity, and characteristics

IFU developed an 18-step procedure for designing and building flexible binders. Details of the procedure were given in an interim report. A brief description of each step follows. Sketches of the 18 steps are shown on the following pages.

1. In step1, the reference plane, F1, of the blank holder is defined.
2. In step 2, the inner contour of the blank holder K3 is built up. The contours, K6, which connect the surfaces, B, with the projected contours of the pins, P, are defined.
3. In step 3, two contour lines, K4 and K5, are generated, which tangentially connect pin areas P.
4. In step 4, the size of the surfaces B, on which the guiding plates are fixed, are defined. Contours K6 that connect the surfaces B with the projected contours of the pins P are defined.
5. In step 5, contour K4 is modified so that it includes the surfaces B.
6. Step 6 contains the generation of the cover plate of the blank holder.
7. In step 7, the contours K1 and K3, as well as the splitting lines T, are projected in the vertical direction onto the plane F2.
8. Step 8 is the generation of the cover plate of the blank holder V1 by extending the contours K1* and K3* in the vertical direction up to the bottom plane of the blank holder F1.
9. In step 9, the contours K1* and K3* are split.
10. In step 10, the peripheral of the pyramidal blank holder segment S is generated.
11. In step 11, the contact planes, pin–blank holder, named G, are generated.
12. In step 12, the pyramidal blank holder segments V2 are generated.
13. In step 13, guiding devices V3 are generated by extending contours K6 in the vertical direction.
14. In step 14, the blank holder segments with the surfaces on which the guides are fixed, V4, are generated.
15. In step 15, the bottom plate of the blank holder is generated.
16. In step 16, the body V6 of the blank holder is defined by adding the segments V4 and the bottom plate V5 to the cover plate V1 of the blank holder.
17. Step 17 contains the design of several devices, such as lifting and transportation.
18. In step 18, the devices are added to the body V6. This completes the design of the flexible blank holder.

Task 3: Develop Computer Simulation and Process Optimization Capabilities for Flexible Binders

The objectives of this part of Task 3 are

1. Develop an optimization program that can produce optimal BHF curves for stampings.
2. Apply adaptive simulation and optimization techniques to determine variable BHF profiles for the conical cup drawing process. This process simulates a single cushion pin operation for axi-symmetric parts. The program will produce optimal BHF trajectories, thereby reducing metal thinning and preventing part failure by wrinkling or splitting.

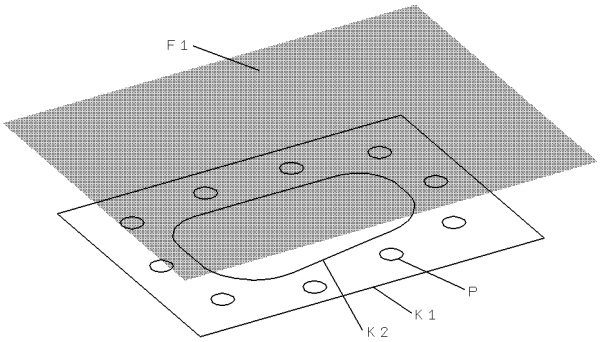

1. Providing the boundary conditions.

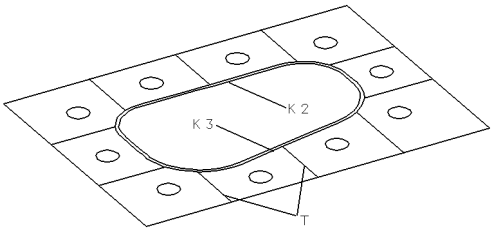

2. Generating inner contour- and splitting-lines.

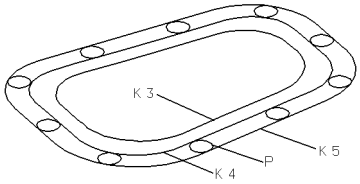

3. Generating the contour of the base plate.

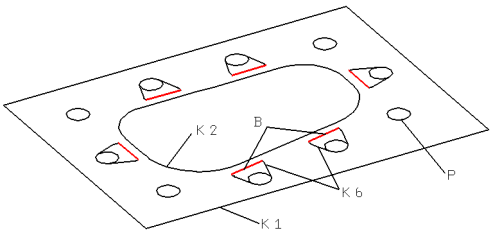

4. Generating the contours of the guides.

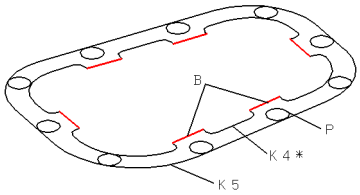

5. Adapting the contour of the base plate.

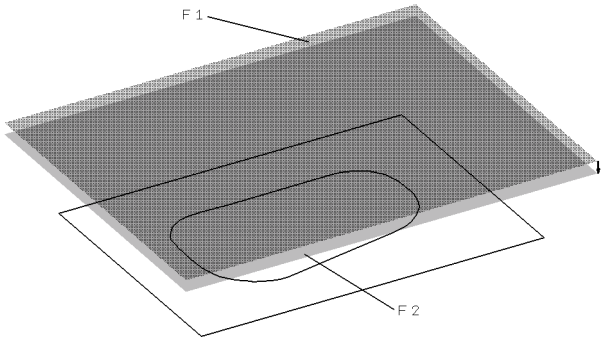

6. Generating the offset face.

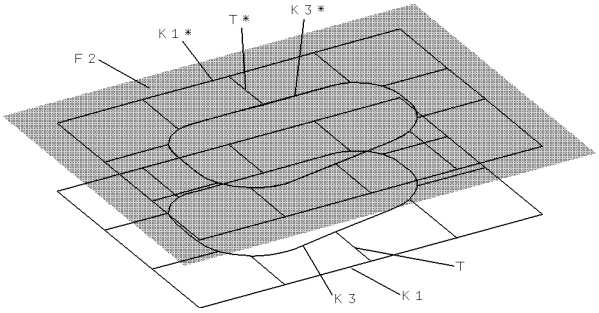

7. Projection of the segment boundaries.

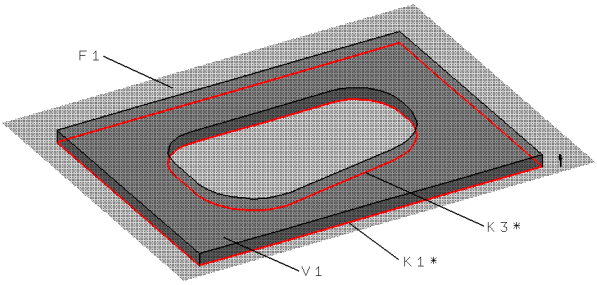

8. Generating the cover plate.

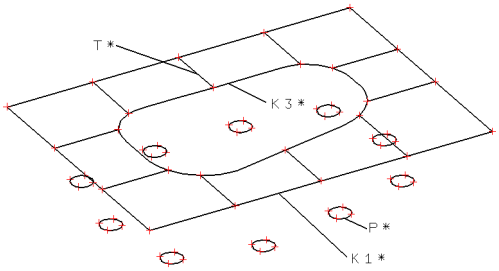

9. Splitting of the contours.

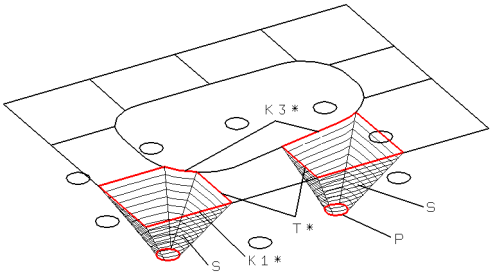

10. Generating the peripheral of the pyramid.

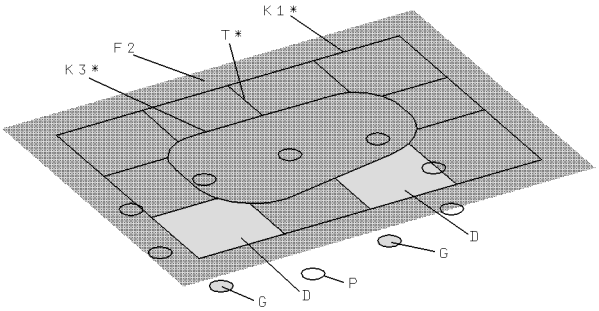

11. Generating the base and cover faces.

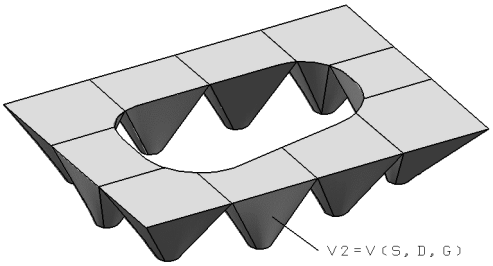

12. Generating the segments.

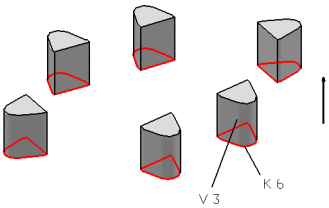

13. Generating the guiding devices.

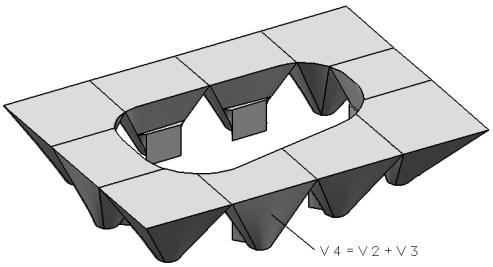

14. Adding the guiding devices.

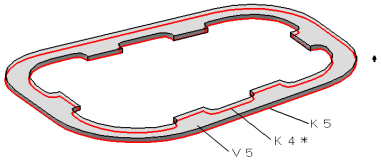

15. Generating the base plate.

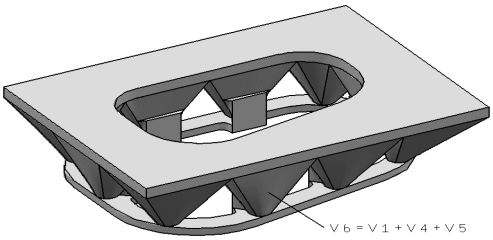

16. Adding the parts.

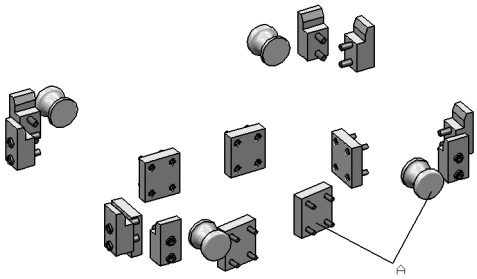

17. Generating guiding and lifting devices.

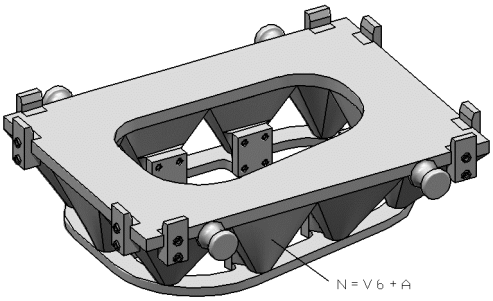

18. Adding the devices.

Simulation/Optimization

Four cases of BHF optimization were conducted and, in all four cases, cup drawing is simulated to a depth of 50 mm. Optimization is conducted by evaluating an objective function and comparing it with a constraint function value for thinning and wrinkling. The four cases are

1. One control point is used to define the BHF curve. This means that the BHF curve is constant.
2. Two control points are used. In this case, the BHF curve is a straight line, which can be increasing or decreasing.
3. Three control points are used. In this case, the BHF curve becomes a quadratic function.
4. Four control points are used for the BHF curve.

Figure 10 shows the initial and optimal BHF curves for different numbers of control points. The values of all optimal BHF curves are lower than the initial BHF value of 21 kN, and all optimal BHF curves except for the constant optimal curve are decreasing from 12 kN to 2 kN.

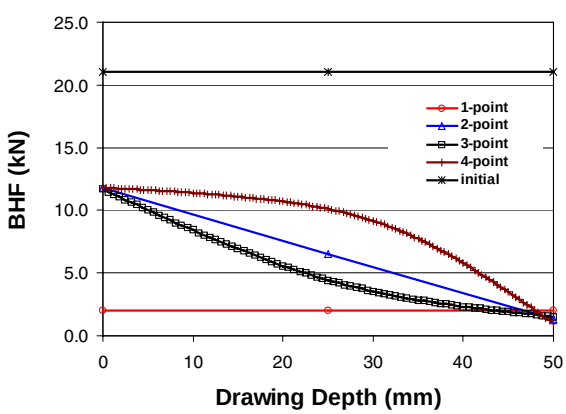

Figure 10. Optimal BHF curve versus drawing depth for different numbers of control points.

Experiments

A conical cup tooling was designed and manufactured at Ohio State University to conduct experiments to develop limit criteria for wrinkling and thinning and to verify simulation and optimization results. A schematic of the tooling is shown in Figure 11.

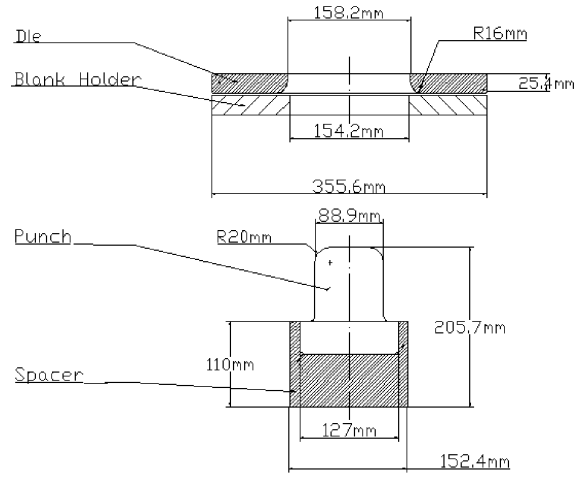

Figure 11. Schematic of the conical cup drawing tooling.

Figure 12 shows a comparison of measured thickness distribution for optimum constant and optimum variable BHF profiles at a draw depth of 57 mm. Results show that cups formed with the optimum variable BHF have less thinning (a 19% improvement) than that formed by the optimum constant BHF profile.

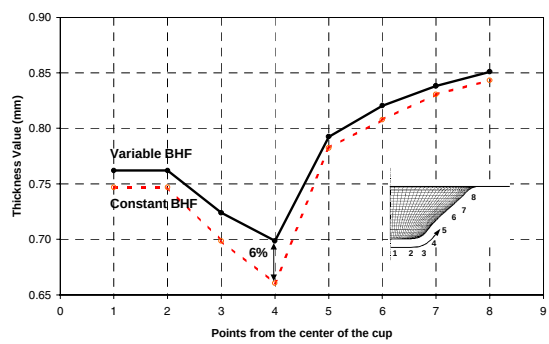

Figure 12. Schematic of the conical cup drawing tooling.

Accomplishments

1. Wrinkle and fracture criteria for sheet forming were developed.
2. Two optimization approaches were pursued:
   — Simulation based on classical optimization
   — Simulation based on feedback control
3. The two optimization approaches were implemented in PAM-STAMP.
4. The two optimization approaches were used successfully to determine optimum BHF profiles for conical cup drawing.

Participants

Ford Motor Company	Lead project and determine its direction and benefits
General Motors	Co-lead project and determine its direction and benefits
DaimlerChrysler	Co-lead project and determine its direction and benefits
US Steel	Provide steels and technical support
Rouge Steel	Provide steels and technical support
ALCOA	Provide aluminum and technical support
Pathway Technologies	Provide control expertise
Ohio State University	Provide simulation and optimization expertise
University of Stuttgart	Provide flexible binder technology expertise
University of Michigan	Provide control and feedback systems expertise
NIST	Support forming and friction activities
Troy Design & Manufacturing	Tooling and equipment for tryouts
Erie Press Systems	Tool building and equipment
FormSys	Project administration

B. Warm Forming of Aluminum—Phase 2

Project Leader: Suresh Rama
DaimlerChrysler Corporation
2730 Research Drive
CIMS 463-00-00
Rochester Hills, MI 48309
(248) 838-5356; fax: (248) 838-5338; e-mail: scr4@daimlerchrysler.com

Project Administrator: Constance J.S. Philips
National Center for Manufacturing Sciences
3025 Boardwalk
Ann Arbor, MI 48108-3266
(734) 995-7051; fax: (734) 995-1150; e-mail: conniep@ncms.org

Technology Development Manager: Joseph Carpenter
(202) 586-1022; fax: (202) 586-1600; e-mail: joseph.carpenter@ee.doe.gov
Field Technical Manager: Philip S. Sklad
(865) 574-5069; fax: (865) 576-4963; e-mail: skladps@ornl.gov

---

Contractor: U.S. Automotive Materials Partnership
Contract No.: DE-FC05-02OR22910

Objective

- Develop and demonstrate a warm-forming process including the materials, equipment, and heating processes to cost-effectively expand the forming limits of aluminum sheet.
- Develop a technical cost model of the warm-forming process that will enable cost comparisons of similar part geometries warm formed in aluminum with those formed through conventional processes in steel and aluminum.

Approach

- Establish a warm-forming process in a laboratory environment with the application of new processes on a variety of aluminum sheet alloys. Balance alloy and lubricant development with continuing evaluation of commercial alloys, along with process modeling, design, and demonstration.
- Develop a full-size demonstration of the warm-forming process and run tests in a production environment. Integrate a blank pre-heater, blank transfer mechanism, lubricant application system, and warm-forming press with a modified thermal profile controller and lubricant removal station into production trials. Conduct production feasibility tests of the warm-forming process at standard rates for current forming processes.
- Create a technical cost model that can generate cost comparisons between a warm-formed aluminum door inner and a same or similar door inner manufactured using conventional forming processes in steel and aluminum.

Accomplishments

- Funded Phase 2 statements of work and initiated process development including alloy studies, lubricant development, blank heater build, alloy fabrication, and cost model development.
- Completed formability tests using various lubricants (Fuchs LN1184 and LN1169 lubricants at 215, 260, and 315°C) and examined various performance variables. Compared these test results with results from dry forming.

- Completed evaluation of the heater controls on the existing die and estimated the costs of constructing and operating infrared- (IR-) heated dies for the warm-forming technical cost model. Conducted heating tests on aluminum material for different power densities and began fabrication of laboratory-sized IR heaters.
- Completed evaluations of five new alloy formations cold-rolled from 8-mm-thick to 1-mm-thick hot band and recrystallized at 450°C/60 min.

Future Direction

- Complete process studies and models including the effects of an IR heater, expanded effects of formability enhancements, etc.
- Complete lubricant studies and select the lubricant formulation for use in production demonstrations.
- Investigate a variety of aluminum materials suitable for warm forming, including pre-qualified commercial alloys, aluminum tailor welded blanks, and new alloy formulations, and select an alloy for use in production demonstrations.
- Establish process cost feasibility using the technical cost model comparing the cost of a warm-formed aluminum door inner with the cost of a similar door inner or geometry manufactured using conventional forming processes in steel and aluminum.
- Initiate the building of a production-ready system for use in a production demonstration.

Introduction

Using aluminum in automobiles reduces vehicle weight, thereby increasing fuel economy. However, automakers have found that current automotive-grade aluminum alloys generally have limited formability, and a cost penalty is associated with their use. The challenges include

- Mitigating the cost of aluminum by reducing the costs associated with the process used to form the material through part consolidation
- Lower formability of aluminum compared with steel
- Difficulty in forming sharp-edge contours
- Hard-to-achieve deeper draws
- Appearance problems in 5000-series aluminum

To overcome these challenges, significant improvements in the formability of aluminum need to be made through the development of enabling advances in process technologies, including

- Lubrication without loss of washability and paintability
- Temperature management for forming dies
- Blank preheating
- Alloy chemistry and metallurgical properties, if required

Warm Forming of Aluminum, Phase 2, is a 4-year development and demonstration program to establish the "production" feasibility of warm forming aluminum alloy blanks into automotive panels and to fully demonstrate a warm-forming process for cost-effectively manufacturing aluminum automotive panels with deep draw.

Phase 2 Detail

Phase 2 team formation and contractor selection is complete. Awards to contractors for first-stage tasks are complete.

The following tasks summarize the entirety of Phase 2:

- ***Alloy selection*** through laboratory evaluation and testing of candidate alloy compositions and their respective formability properties is being performed at the University of Michigan (UM). Evaluation and testing will include examination of microstructures after rolling and heating, tensile tests, warm-forming tests, and analysis of results.
- ***Lubricant selection*** through evaluation and testing of numerous lubricant formulations from Fuchs Lubricants during formability tests is being conducted by GM under various

temperature conditions, with a focus on easy application and removal.

- ***Thermal analyses***, including development of die and sheet models, predictive models for die temperature and distortion, and predictive models for estimating sheet temperature and distortion after forming, are being performed at UM.
- ***Blank heating*** using IR technology built by Infrared Heating Technologies includes a laboratory heater to first evaluate blank heating in the laboratory, and then the design, construction, and validation of a production-ready heater to be installed at Sekely Industries.
- ***Alloy fabrication*** of candidate materials for laboratory testing and full-scale production pilot runs is being done by Pechiney Rolled Products.
- ***Full-scale process demonstration***, from blank heating through cleaning, is to be conducted at Sekely Industries.
- ***Post-process inspection and material analyses*** will include panel and material inspection for strength, distortion, corrosion, etc.
- ***Continuous technology cost evaluation*** through application of the technology cost model developed by Camanoe Associates will compare the technical cost of warm forming the Dodge Neon door inner vs. manufacturing the same door inner or similar geometries using conventional forming processes in steel and aluminum.

Phase 2 Accomplishments

Pechiney Rolled Products produced and provided aluminum alloys for laboratory formability tests. Five different alloys composed of varying formulations containing magnesium, manganese, chromium, zirconium, copper, or scandium were provided for small laboratory heats. Five additional alloy formulations containing these additives were also provided for large laboratory heats.

UM completed the evaluation of four small heats. Alloys were cold rolled from 8-mm-thick to 1-mm-thick hot band and recrystallized at a set temperature and time. Findings indicate that grain size is critical to formability and that while some additives are beneficial to grain size, some promote or retard recrystallization. Additionally, higher temperatures are required with some additives, necessitating longer time periods for recrystallization to complete.

Results of initial warm-forming tests using rectangular cups indicate isothermal cup depth and the degree of recrystallization appear to be directly related. At 450°C/60 min, there is a relationship between additive particle content, recrystallization, and cup depth. Additionally, there is a relationship between recrystallization and particle content. The depths achieved in these trials are superior to isothermal cup depth for 5754 and 5182+Mn alloys studied under Phase 1.

GM and Fuchs completed formability tests using Fuchs LN1184 and LN1169 lubricants at 215, 260, and 315°C—examining the lubricant layer after forming, drawing behavior due to lubricant/ temperature effectiveness, and length of the wear scar—and compared these test results with results of dry forming. Findings confirm that cup depths are a function of temperature and lubricant. Higher formability is found with some lubricants at certain temperatures, but cleanability can be worsened at increased temperatures (Figures 1 and 2).

Sekely Industries evaluated heater controls on the Phase 1 die, estimated costs to construct and operate IR-heated dies for use in the warm-forming technology cost model, conducted heating tests on aluminum material for different watt densities, and has completed more than 50% of the IR laboratory heater fabrication.

Camanoe Associates completed the strawman technology cost model, which will continue to undergo further refinement to incorporate process

Figure 1. Test specimens showing formability effects of lubricant type and temperature.

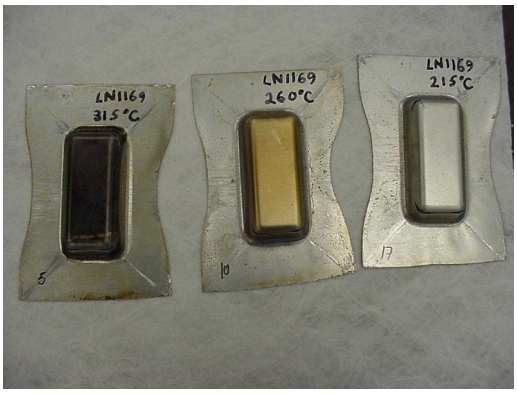

Figure 2. Test specimens showing marked formability effects of lubricant type and temperature.

changes, original equipment manufacturer or project bogey cost elements, the IR heater, die cost elements, etc., as the project progresses.

Future Work

Future work is planned in four areas:

- Alloy selection: Evaluate the uniaxial tensile behavior of these alloys to determine their formability characteristics and possible sources of formability enhancement. Study the IR heating technology to determine the effects of flash annealing. Evaluation of larger heats is under way.
- Lubricant development: Rerun the lubricant studies under different blank holding pressures and preheats. Conduct thermal studies to determine die overheat requirements to yield optimum temperature at forming. Study the coefficient of boron nitride compounds behavior at various temperatures and the benefits of adding a die-release compound.
- IR heater: Infrared Heating Technologies will deliver the laboratory heater to UM in the first quarter of FY 2003.
- Technical cost model: Camanoe Associates will continue to refine the technical cost model and present it to the team for evaluation.
- Thermal analysis: UM will conduct the thermal analyses required during the course of the program.

C. Hydroformed Aluminum Tubes

Project Chairman: Michael L. Wenner
General Motors Corporation
Mail Code 480-106-359
30500 Mound Road
Warren MI, 48090-9055
(586) 986-1108; fax: (586) 986-0574; e-mail: michael.l.wenner@gm.com

Technology Development Manager: Joseph A. Carpenter
(202) 586-1022; fax: (202) 586-1600; e-mail: joseph.carpenter@ee.doe.gov
Field Technical Manager: Philip S. Sklad
(865) 574-5069; fax: (865) 576-4963; e-mail: skladps@ornl.gov

---

Contractor: U.S. Automotive Materials Partnership
Contract No.: DE-FC05-02OR22910

Objective

- Develop material data, design rules, and computer modeling capability to enable the design and manufacture of hydroformed aluminum tubes for mass reduction in automotive bodies.

Approach

- Identify the most appropriate aluminum alloys for prospective automotive applications and obtain tubes, both welded and extruded.
- Design and carry out an experimental program to determine the basic material and frictional properties of the tube materials.
- Carry out simple laboratory experiments to determine the mechanical behavior in bending and hydroforming under a wide range of conditions.
- Use the measured data to determine forming limits during hydroforming and to devise empirical design rules to be used by product and process engineers.
- Using the material and frictional properties measured in the laboratory, carry out computer simulations in order to evaluate and improve our ability to model bending and hydroforming of aluminum tubes. This activity includes damage modeling to improve our ability to predict failure.
- Obtain and fully instrument a rotary draw bender to allow measurement of the actual forces exerted on the tube and to explore the effects of process parameters on bending and on subsequent formability.
- Use the bender to explore ways to enhance subsequent formability in hydroforming by push assists.

Accomplishments

- Conducted studies to measure the effect of friction in the hydroforming operation.
- Constructed an analytical expression relating burst pressure and achievable corner radii for a given lubricant and material.
- Conducted pre-bent corner fill tests to investigate the influence of bending on the subsequent formability of the tubes in hydroforming.

- Performed experiments with various levels of push assist using the rotary draw bender at the University of Waterloo.
- Constructed models to simulate the experiments on friction, straight tube corner fill, and pre-bent tube corner fill.
- Began damage modeling of the experiments.

Future Direction

- Carry out bending for smaller bend radii using push assists and determine the subsequent formability in hydroforming.
- Carry out simulation to further develop formability criteria based on these experiments.
- Identify a production die set (an engine cradle, for example) and carry out experiments and modeling to validate our understanding of the technology as applied to an automotive part.

Introduction

Many automotive structural parts can be made from hydroformed tubes. The tubes are first bent to shape in a rotary draw bender and are then put into a die and expanded by fluid pressure to the die configuration. Such parts have many advantages over the stamped and welded sheet metal parts that they replace. They enable reduced manufacturing costs (decreased part count, welding, and scrap) and can improve performance (reduced mass and increased stiffness). Steel hydroformed tubes are finding increased application in the automotive industry, but the behavior of aluminum in the bending and hydroforming operations is not well understood and is not yet used in the U.S. automobile industry. Figure 1 shows the bent tube and the hydroformed tube for an engine cradle.

This project includes participants from the automobile producers General Motors, Ford, and DaimlerChrysler; material suppliers Alcoa, Alcan, and VAW; research institutions IRDI and the University of Waterloo; and hydroforming equipment and product suppliers Eagle Manufacturing and F&P Manufacturing.

Measuring the Effect of Friction

Friction between the die and work piece is a critical factor in tube bending and hydroforming, as it is in most metal forming operations. To investigate friction in the hydroforming operation, a correlation study was carried out among a laboratory bench test, the twist-compression test, and the straight tube corner fill test, illustrated in Figure 2.

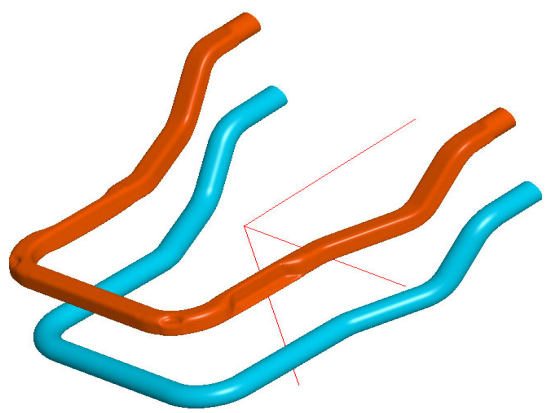

Figure 1. An engine cradle. The lower tube in the figure has been bent. The upper tube has been bent and hydroformed.

Friction measurements were made using two aluminum alloys and five lubricants. Coefficients of friction measurements were extracted from the data for all of the test conditions. To determine whether these coefficients of friction correlated with performance in the hydroforming die, tubes were expanded in the die, as shown in Figure 2, until they burst. During the test, the internal pressure, axial load, corner expansion, and axial displacement were measured. It was found, as expected, that there is a general trend for the axial displacement, corner expansion, and burst pressure to increase with a decrease in the friction coefficient. In other words, the tube's formability

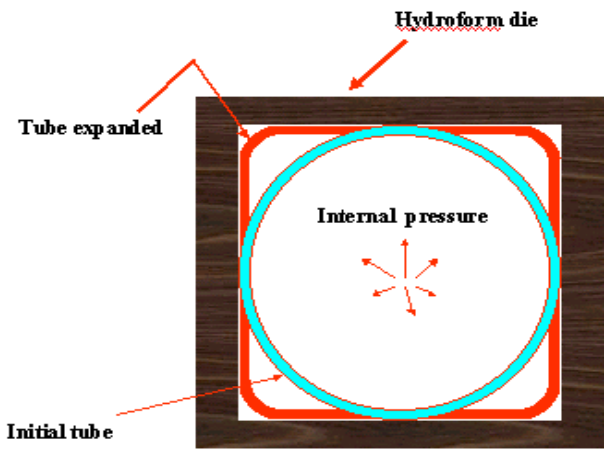

Figure 2. Schematic of the straight tube hydroforming die.

improved as the lubricant did. These are encouraging results, since they imply that frictional behavior can be characterized by a simple laboratory test.

Empirical Design Rules

Another project completed this year was the construction of an analytical expression relating burst pressure and achievable corner radii for a given lubricant and material. Estimating the minimum corner radius for no friction and then modifying the results to account for friction, as measured in the twist compression test, yielded a simple analytical relationship. The correlation between this formula and test results was reasonable. This work may prove useful to part designers, who will be able to estimate how sharp the corner radii of hydroformed parts can be made. (Part designers almost always want to make the radii very small, for both structural and aesthetic reasons.) Although these designs will still need to be checked by a full computer simulation, they should be more robust than those determined using no rational rules.

Pre-bent Corner Fill Tests

In pre-bent corner fill tests, straight tubes are bent to a given radius and angle before hydroforming. The goal of these tests is to investigate the influence of bending on the subsequent formability of the tubes in hydroforming. The strain and thickness distributions of the bent tubes are measured, as is the initial wall thickness of every tube (in order to get reliable data to compare with the wall thickness after bending).

The bend ratio (the ratio of the centerline radius of the bent tubes to their initial diameter) was fixed at 2.5 for these bends. The bend angle was 90°. Figure 3 illustrates the geometry after the tube (not shown) has been bent to 90°. After the tubes were bent, they were hydroformed in a die that has nearly the same shape as the bent tube, but with a cavity on either the outside or the inside of the tube. Hence the tube is permitted to expand in only one area. Figure 4 illustrates the inside corner fill test.

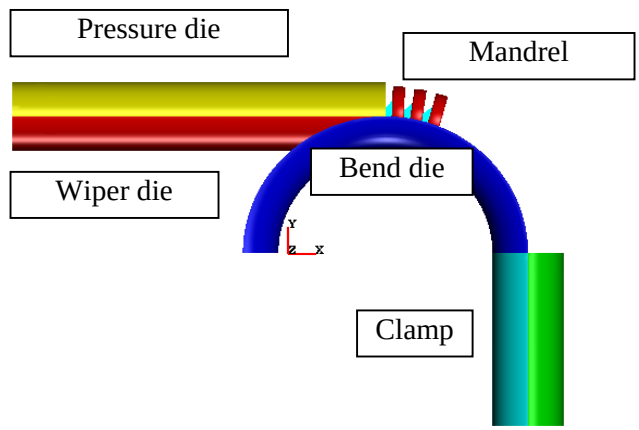

Figure 3. Geometry and nomenclature of the bend die.

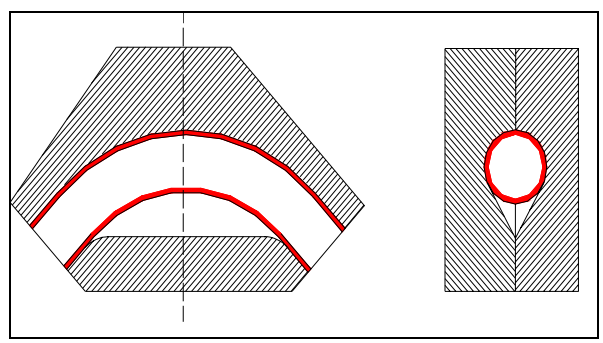

Figure 4. Geometry of the inside bent corner fill test.

The tubes typically burst at the tangent point where the tubes ceased to contact the dies (this failure location is common in hydroforming). As expected, the thicker material on the inside of the bend supported more deformation than the thinner material on the outside. Relatively little additional strain (typically less than 10%) was found after hydroforming, indicating that the bending

operation consumed much of the material's formability.

Bending Trials

The University of Waterloo has installed and instrumented a rotary draw bender on campus. The instrumentation includes displacement controls on the bend die and mandrel and load controls on the clamp die. There are also load cells on the pressure die clamp force and mandrel. This machine also has a unique fully instrumented method for push assist. That is, an additional force can be exerted along the tube axis behind the pressure die. This force can be used to reduce the thinning on the outside of the tube as it is bent. We used this capability to try to increase the subsequent formability during hydroforming. This machine is fully computer controlled.

Experiments with various levels of push assist have been carried out on 2.0-mm and 3.5-mm Al3.5Mg tubes. The push levels were 95, 100 and 102% of normal push force. The 2.0-mm tubes were also run at 104%. It was found that a very good lubricant (a solid film wax lube), was needed to prevent scratching by the mandrel. Springback varied considerably with the level of push assist, ranging from 2.0 to 3.7°. The strain on the outside of the bend also varied by up to 7%. We plan to evaluate the effects of these strain changes in the next phase of the program.

Computer Simulation

Modeling work by the University of Waterloo has also progressed this year. Models were constructed to simulate the friction and straight tube corner fill experiments described previously. The models showed the correct trends, but further work is needed to quantitatively match the results when using the measured coefficients of friction. Models were also constructed for the pre-bent tube corner fill tests. Figure 5 shows a comparison of

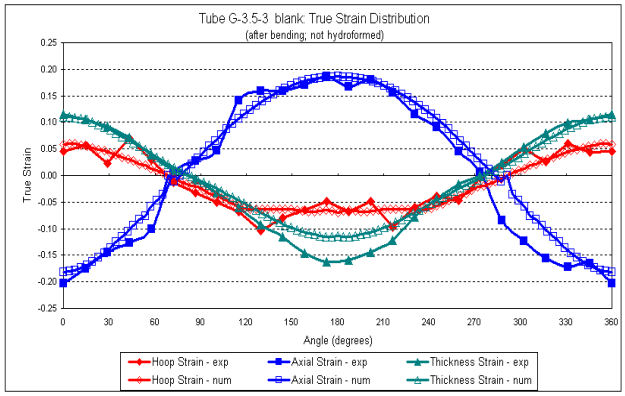

Figure 5. Calculated and measured strains in a bent tube.

predicted and measured strains around the circumference of the tubes at the middle of the bend. The model results are quite good.

Damage modeling of the experiments has also begun. We hope to be able to track the microstructural damage in the tube material as deformation proceeds in both bending and hydroforming. This work, if successful, would enable an analyst to track the tube formability as a forming simulation is carried out.

Project Benefits

Tube hydroforming has many benefits compared with making parts in several stampings. These include mass reduction, reduction of assembly operations, and enhanced structural performance. Use of aluminum in tube hydroforming would magnify the mass reduction obtainable from hydroformed tubes. The benefits of mass reduction are reduced fuel consumption and emissions. In addition, aluminum has greater recycling value than steel. It is one of the aims of this project to enhance our understanding of aluminum tube hydroforming to such an extent that product and process design for these parts are robust and accurate in a math-based system.

D. Electromagnetic Forming of Aluminum Sheet

Principal Investigator: Richard W. Davies
Pacific Northwest National Laboratory
P.O. Box 999, Richland, WA 99352
(509) 376-5035; fax:(509) 376-6034; e-mail: rich.davies@pnl.gov

Technical Coordinator: Sergey Golovashchenko
Ford Motor Company
Ford Research Laboratory, Dearborn, MI 48121-2053
(313) 337-3738; fax: (313) 390-051; e-mail: sgolovas@ford.com

Technology Development Manager: Joseph A. Carpenter
(202) 586-1022; fax:(202) 586-1600; e-mail: joseph.carpenter@ee.doe.gov
Field Technical Manager: Philip S. Sklad
(865) 574-5069; fax:(865) 576-4963; e-mail: skladps@ornl.gov

Participants
Dwight Rickel, EMF System Development, Los Alamos National Laboratory
James Sims, Coil Durability, Materials, and Design, Los Alamos National Laboratory
Andy Sherman, EMF R&D, Ford Motor Company
Jeffrey Johnson, EMF System and Control, Pacific Northwest National Laboratory
Gary Van Arsdale, EMF System Design and Metal Forming, Pacific Northwest National Laboratory
Nick Klymyshyn, Computational Mechanics, Pacific Northwest National Laboratory
Dick Klimisch, Project Coordinator and Material Supply, Aluminum Association
Derek Hunter, Oxford Automotive Company, EMF Industrial Embodiment

---

Contractor: Pacific Northwest National Laboratory
Contract No.: DE-AC06-76RL01830

Objective

- Develop electromagnetic forming (EMF) technology that will enable the economical manufacture of automotive parts made from aluminum sheet. EMF is a desirable process because the dynamic nature of the deformation results in benefits including increased forming limits and reduced springback.

Approach

- Establish analysis methods for forming system design.
- Develop durable actuators (coils).
- Develop industrial embodiment of the EMF process.

Accomplishments

- Completed a literature search for information on EMF, coil materials, and coil design/durability.
- Completed design and assembly of a 150-kJ pulsed power unit at Los Alamos National Laboratory.
- Designed an integrated forming coil system for high-volume automotive stamping
- Completed a literature review of patents, relevant coil materials, and the design of durable EMF coils.

- Created a conceptual design-forming coil intended for versatile positioning and stress resistance.
- Installed the 150-kJ pulsed power supply at Pacific Northwest National Laboratory (PNNL), demonstrated its operation, and installed an automated computer control system capable of automated cyclic testing and sheet metal forming.
- Completed fabrication of an experimental apparatus to evaluate coil durability.
- Established a cooperative research and development agreement that includes Ford, PNNL, and Oxford Automotive.

Future Direction

- Experimentally test the coil designs for durability during aluminum sheet forming.
- Complete fabrication of the coil durability testing apparatus.
- Develop concepts/designs for test systems suitable to generate hybrid forming (combined static and dynamic deformation) biaxial formability data.
- Explore and develop modeling capabilities that can assist in the design of EMF systems.
- Investigate the industrial embodiment of EMF systems for automotive manufacturing

---

Introduction

In the EMF process, a transient electrical pulse of high magnitude is sent through a specially designed forming coil by a low-inductance electric circuit. During the current pulse, the coil is surrounded by a strong transient magnetic field. The transient nature of the magnetic field induces current in a nearby conductive work piece that flows opposite to the current in the coil. The coil and the work piece act as parallel currents through two conductors to repel one another. The force of repulsion can be very high, equivalent to surface pressures on the order of tens of thousands of pounds per square inch. Thin sheets of material can be accelerated to high velocity under this applied loading in a fraction of a millisecond.

The desire to use more aluminum in automobiles has stimulated a recent interest in understanding EMF of metals. The high work piece velocities achievable using this forming method enhance the formability of materials such as aluminum. Also, the dynamics of contact with the forming die can help reduce or mitigate springback, an undesired effect that cannot be avoided in other forming techniques such as stamping. This process has been applied commercially since the 1960s. The large majority of applications have involved either the expansion or compression of cylinders (tubes). The forming of sheet materials is considerably more complex and has received relatively little attention.

Project Deliverables

At the end of this program, methods and data to assist the economical design of EMF sheet forming systems will be documented. These will include materials information and design methods for durable coils, coil durability test data for selected materials and design concepts, dynamic and hybrid formability data, methods for modeling the forming process, and concepts for the industrial implementation of the technology in an automotive manufacturing environment.

Approach

This project will address three main technical areas. The first area involves establishing analysis methods for designing forming systems. These methods will be based on developed knowledge of forming limits and relations between electrical system characteristics and deformation responses for specific aluminum alloys of interest. The second area of technical challenge is coil durability. Existing knowledge of EMF and relevant knowledge from pulsed power physics studies will be combined with thermo-mechanical analyses to develop durable coil designs that will be tested experimentally. Until we reach a more thorough understanding of economic factors that determine the required durability, a nominal 100,000-cycle coil life will be the goal for this project. The third technical area

involves the industrial embodiment of the EMF process. In this project, EMF is expected to be hybridized with conventional sheet metal stamping. Different approaches to hybridization will be analyzed for issues affecting economical implementation in a modern stamping plant. Different system concepts will be developed and studied. Existing knowledge of the EMF process and technical achievements in this project will be combined to establish a methodology for designing hybrid forming systems that can be readily integrated into modern manufacturing facilities for the economical production of automotive sheet aluminum components.

EMF System Commissioning

The initial testing and trials of the new EMF system at PNNL were conducted in September and October 2001. The trials consisted of assembling the new EMF power supply system, load cables, and inductive load coil. The apparatus used to conduct the experiments is illustrated in Figure 1. The figure

Figure 1. The capacitor bank and load cables connected to the forming coil.

shows the four parallel coaxial conductors connected between the power supply and the EMF coil. Figure 2 is an enlarged view of the single-turn coil. The coil used was a single-turn, low-inductance aluminum alloy coil made from AA6061-T6. Also shown in Figure 2 are multiple sheets of Mylar sheeting and G10 (glass fiber composite) insulating materials. Not shown in the figure is the coil containment shroud and associated supports. The experiments involved multiple cycles of charging and discharging of the capacitor bank through the load coil at various known energy levels. The

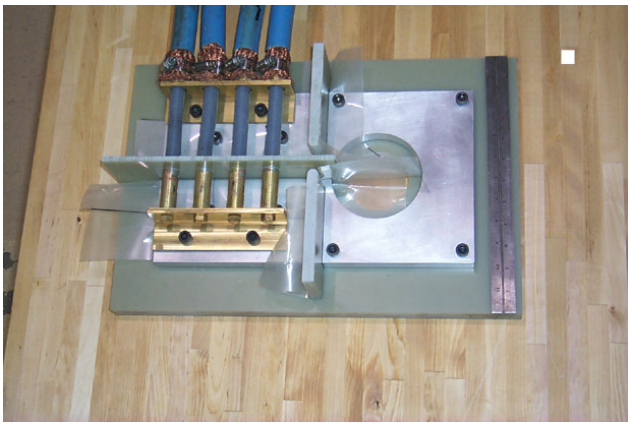

Figure 2. The single-turn forming coil and the load cable connections.

capacitor bank was controlled via the custom system developed for the unit. The sequence of testing consisted of charging the capacitor bank, isolating the charging power supply, triggering (releasing) the capacitor charge, and monitoring the response of the system. The system response was recorded using a high-speed digital oscilloscope.

Figure 3 illustrates the typical response of the system during a 15-kJ discharge of the capacitor bank. This figure shows that the half-current of the system (measuring half the total system current) is approximately 86 kA, so that a total current of approximately 172 kA passed through the load coil. The system rise time was shown to be approximately 26 microseconds. This EMF system received an automated computer control system capable of automated cyclic testing and sheet metal forming. The system has been commissioned and demonstrated.

Coil Design Concepts and Durability

In EMF, the large forces that deform the workpiece are mirrored in the coil. The coil, insulators, and support structure must resist these forces, as well as related thermal cycles, without significant permanent deformation or material failure. In contrast to typical cylindrical coils, sheet forming will require coils with general three-dimensional shapes that are inherently less resistant to forces induced during forming. The key issues involve materials selection and design. Materials must be selected for both electrical conductivity and mechanical properties. They must be capable of being joined or bonded and compatible with any necessary coil coolants, with coil manufacturing,

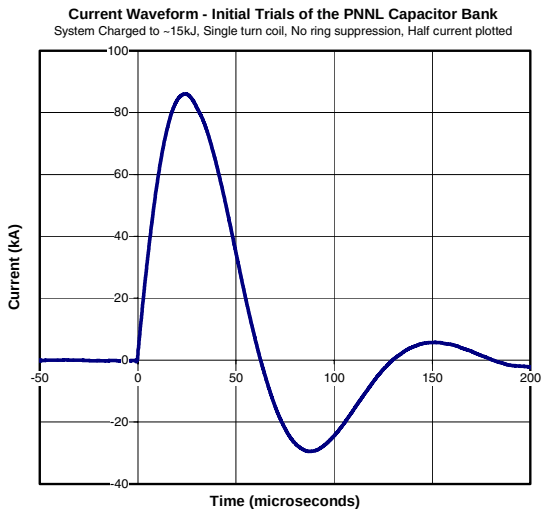

Figure 3. The current waveform that resulted during the initial system trials at PNNL.

and with integration into hybrid forming systems that combine conventional stamping and EMF. The design must integrate these elements while delivering the primary function of a spatial and temporal load distribution that achieves the desired deformations. Coil systems will have to be low-cost, modular, and highly durable (nominally 100,000 cycles) if they are to be relevant to automotive manufacturing.

During the second quarter of FY 2002, Los Alamos National Laboratory generated a technical report containing a conceptual coil design for use in a high-volume manufacturing system. This particular design is considered modular, and it would likely require multiple coils to execute any singular forming operation. This modular coil approach may require further study of coil-to-coil interaction and durability before it can be commercially implemented. In contrast, Ford Motor Company recently designed an integrated forming coil system for high-volume automotive stamping of complex components. This Ford-designed system is currently being tested for high-cycle forming trials at PNNL.

Beyond these trials on the Ford-designed coil system, PNNL has developed a system to evaluate these potential coil materials under high-cycle EMF conditions. PNNL has designed and fabricated a coil durability test apparatus. Figure 4 is a photograph of the coil configuration that is part of the apparatus (copper alloy shown). Removed from this coil photograph (for clarity) are insulating sheets of

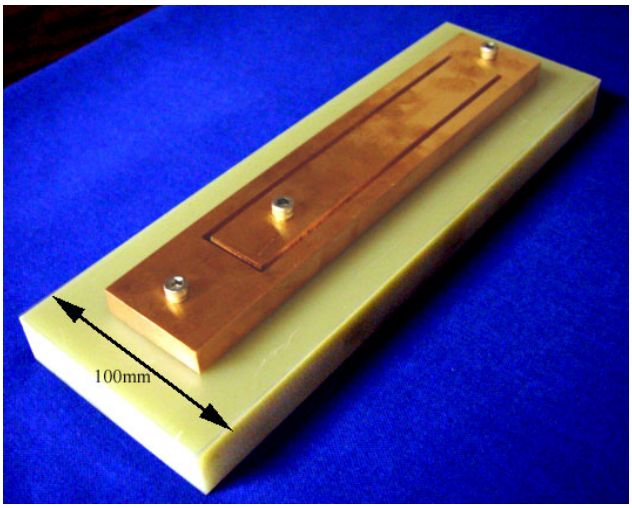

Figure 4. The coil system used for durability testing of different candidate coil materials.

Mylar that retard cross-coil sparking. This coil is connected to the EMF capacitor bank and control system via cables that connect on the bottom side of the coil shown. This coil is designed to be placed in close proximity to a stationary aluminum alloy plate and to be subject to cyclic pulse loading at different power levels and frequencies to determine the number of cycles to failure. The objectives are to make coils from multiple materials and to compare the coil durability across several samples from each population. PNNL is currently evaluating the performance of materials using this system.

Industrial Embodiment

Oxford Automotive is conducting an ongoing study of the industrial embodiment of the EMF process, which is designed to analyze potential methods to incorporate EMF into the highly integrated manufacturing of automobiles. This study is investigating integration into conventional sheet metal stamping production facilities and the potential to create an entirely new and separate production line based on EMF technology for aluminum alloy sheet. To date, several variations have been identified and are currently undergoing detailed study.

Conclusions

The technical feasibility of EMF for aluminum sheet in an automotive application has been demonstrated, during both this project and prior U.S. Council for Automotive Research projects.

However, the durability of relevant coil systems and methods for the economical design, construction, and implementation of forming systems have yet to be demonstrated. There is also a need for dynamic formability data for relevant aluminum alloys. This project targets these issues. Progress has been made in assessing the current state of knowledge for materials, coil design, formability, and system design. Also, a pulsed power system has been designed and fabricated to serve in experimental testing of coil systems. As this project progresses, a balanced combination of analysis and experiment will be applied to develop durable coil systems that meet the performance requirements of automotive manufacturing.

E. Aluminum Automotive Closure Panel Corrosion Test Program

Project Co-Chair: Tracie Piscopink
General Motors Corporation
Mail Code 483-370-101
3300 General Motors Road
Milford, MI 48380-3726
(248) 676-7014; fax: (248) 685-5279; e-mail: tracie.l.piscopink@gm.com

Project Co-Chair: Greg Courval
Alcan International
P.O. Box 8400
Kingston, Ontario K7L 5L9
(613) 541-2233; fax: (613) 541-2134; e-mail:greg.courval@alcan.com

Technology Development Manager: Joseph A. Carpenter
(202) 586-1022; fax: (202) 586-1600; e-mail: joseph.carpenter@ee.doe.gov
Field Technical Manager: Philip S. Sklad
(865) 574-5069; fax: (865) 576-4963; e-mail: skladps@ornl.gov

---

Contractor: U.S. Automotive Materials Partnership
Contract No.: DE-FC05-020R22910

Objective

- Develop a cosmetic corrosion test for finished aluminum auto body panels that correlates well with lab testing and field performance.

Approach

- Define a test matrix.
- Specify and obtain materials.
- Specify the phosphate and paint system.
- Pretreat and paint test specimens.
- Conduct laboratory corrosion testing.
- Conduct outdoor exposure, test track, and in-service testing.
- Evaluate test data according to defined procedures.
- Revise the second iteration of testing based upon initial data.

Accomplishments

- Defined laboratory test matrix.
- Defined outdoor exposure, test track, and in-service testing.
- Secured materials and prepared test panels according to agreed-upon specifications.
- Initiated laboratory, test track, and outdoor exposure tests.
- Started in-service exposure.

Future Direction

- Complete first iteration of all tests.
- Establish corrosion product analysis study.
- Analyze data and prepare second iteration of laboratory tests.

Introduction

The use of aluminum closure panels such as hoods, deck lids, and lift gates has increased greatly in recent years. This trend is expected to continue and indeed accelerate as the need to lower overall vehicle weight and hence improve fuel economy increases. One of the key requirements for closure panel materials is a very high degree of corrosion resistance and excellent paint durability. Although aluminum closures have been used for many years on a limited number of vehicles with satisfactory performance, the general level of confidence and ability to predict corrosion lifetimes in service remains uncertain.

Over the years, many laboratory corrosion test environments have been developed to determine the performance of painted closure panels in service. Although the results of these tests are useful for simple comparisons of alloys or paint systems, the correlation of the lab test results with in-service performance is often very poor. Many extensive studies have been carried out to establish this correlation for finished cold-rolled and galvanized steel substrates[1] through cooperative efforts among the automotive companies and steel, pretreatment, and paint suppliers. With the increased use of aluminum, it has been recognized that a program is required to establish the correlation between lab test results and in-service performance for finished aluminum closure panels.

In response to this need, a group composed of representatives from the auto companies, the aluminum industry, and associated suppliers was established in June 2000 to formulate a program to provide the needed correlation. The goals of this effort were to accelerate the adoption of lightweight aluminum materials to lower overall vehicle weight, and to reduce manufacturing costs by eliminating multiple test programs. A single corrosion test accepted throughout the industry could also be used to allow rapid selection and verification of alloy, pretreatment, and paint performance. This report, an outline of the test program, presents evaluation procedures and a preliminary discussion of the corrosion mechanisms.

SAE J2334—Cosmetic Corrosion Lab Test

Society of Automotive Engineers (SAE) J2334 was developed for steel and galvanized steel substrates. It therefore formed a basis for the start of this effort on aluminum corrosion testing. Published in June 1998, this laboratory corrosion test was the result of extensive, long-term studies by the North American automobile and steel industries and other interested parties. Because of its correlation with on-vehicle tests, and its rapidly-growing use in the automotive industry, it was selected as an important test to be included in the study of available accelerated laboratory corrosion tests.

SAE J2334 can be run in either manual or automatic conditions. Tests run manually can be conducted with a simple salt solution immersion tank, a humidity chamber capable of operating at 100% humidity, and an environmental chamber capable of controlling humidity at 50%. Although more labor-intensive, it allows the laboratory to conduct the test with minimal equipment investment. Fully automatic chambers are now available that will perform the test without the need for repeated sample transfer. Test durations of 60, 80, and 120 cycles are currently in use.

Reservoir of Standard Materials for Cosmetic Corrosion Testing.

In 2001, the first step in the development of a new cosmetic corrosion test occurred with the establishment of a reservoir of standard automotive sheet materials. These same materials will be used in the subsequent evaluation of all test methods. As listed in Table 1, the materials were selected to give a significant range of substrate compositions and performance characteristics. They include several aluminum alloys, both current and historical, used in the United States and in Europe. Electro-zinc-coated steel and uncoated cold rolled steel were included as

Table 1. Substrates

Alloy	Metal finish
AA6111-T4PD	No
AA6111-T4PD	Yes
AA6016	No
AA6022-T4E29	No
AA2036	Yes
Cold-rolled steel	No
Electro-Zinc 60 gram	No

reference materials. Two aluminum alloys were processed to simulate metal finishing in an automotive assembly plant body shop.

The materials were painted with a full automotive paint system by PPG Industries, Inc. This included phosphating, medium-build cathodic electrophoretic priming (e-coating), and spray painting with a primer surfacer and white basecoat-clear topcoat system for a total paint film thickness of approximately 100 µm. Panels were prepared with a single scribe penetrating through the coatings to the substrate by National Exposure Testing, Inc. The painted and scribed samples were then sent to laboratories for testing in a variety of environments, including laboratory, static outdoor exposure, proving ground, and on-vehicle tests.

Evaluation of Existing Cosmetic Corrosion Test Methods

To evaluate existing cosmetic corrosion test methods, the Task Force decided to use triplicate sets of the standard materials chosen for evaluation. These materials will be provided to testing laboratories as shown in Table 2. Ten laboratories, three automotive proving grounds, and three static outdoor tests will be included in these evaluations.

As used in previous SAE ACAP task force corrosion tests, these results will be quantitatively compared using scribe-creep results. The scribe-creep results will be compared with real-world standard results using two methods: (a) coefficient of variation (COV) and (b) R^2 + C- ratio. A detailed description of these methods will be described in subsequent presentations when actual test data are available.

Table 2. Cosmetic corrosion tests evaluated by the corrosion task force

Test	Test conducted by
Accelerated laboratory	
SAE J2334	General Motors
SAE J2334	Auto Technology Co.
GM9540—40 and 80 cycles	General Motors
GM9540—40 and 80 cycles	National Exposure Testing
Ford APEGE—30 and 60 cycles	Ford Motor Company
Ford APEGE—30 and 60 cycles	ACT
ASTM 2803	Alcan
ASTM 2803	Alcoa
ASTM G85	ACT
ASTM G85	Singleton Corporation
VDA 621-415	ACT
VDA 621-415	Alcan
ASTM B117	National Exposure Testing
ASTM B117	Auto Technology Co.
CCT 4	PPG
CCT 4	Singleton Corporation
HCL dip	Southwest Research
HCL dip	Alcoa
Volvo	Volvo
Volvo	Ford Motor Company
OEM test Track	
Chrysler Proving Ground	Daimler-Chrysler Corporation
Ford Proving Ground	Ford Motor Company
GM Proving Ground	General Motors
Outdoor exposure site	
South Florida Test Service	
Pittsburgh	
Cape Canaveral	
In service exposure	
Florida	
Detroit	
Montreal	
St. John's	
Alcoa truck route	Cleveland, Ohio to Massena, NY
Europe	Volvo

Designed Experiments to Determine Effects of Cyclic-Test Parameters

Once the initial test results are evaluated, the Task Force will evaluate the effects of certain cyclic test parameters that may further refine an in-laboratory test. Once parameters are established, the Task Force will conduct a statistically designed group of experiments aimed at identifying the effects of particular variables on the performance of certain corrosion test cycles.

Corrosion Mechanisms

Cosmetic or filiform corrosion can occur on both aluminum and steel automotive body panels. In both cases the corrosion is an aesthetic problem, propagating along the substrate-coating interface with minimal penetration into the metal substrate. Because the morphology of this under-film corrosion often has the appearance of "worm-track" filaments, the term filiform corrosion was coined. In reality, the morphology of cosmetic corrosion can vary from true filiform to minute micro-blisters to large blister-like delamination of the coating, depending on the substrate, the coating system, and/or the environmental exposure.[2,3]

The generally accepted mechanisms for filiform corrosion of aluminum and steel are parallel, but the physical and electrochemical differences between the two substrates lead to some differences in how and when this type of corrosion is observed. In general, filiform corrosion initiates at breaks in the coating, such as scratches or cut edges, which expose the bare metal. The worm-track-like filaments consist of an actively corroding head and a corrosion product-filled tail. The active corrosion at the head consumes the available oxygen and results in differential aeration from head to tail of the filament. Also, hydrolysis of the metal ions causes local acidification at the head of the filament. In the tail of the filiform track, the corrosion products precipitate and free the chloride anions, which return to the head of the track to repeat the cycle. These processes, which are schematically illustrated in Figure 1, serve to accelerate and self-perpetuate the propagation of the filament.[2,3]

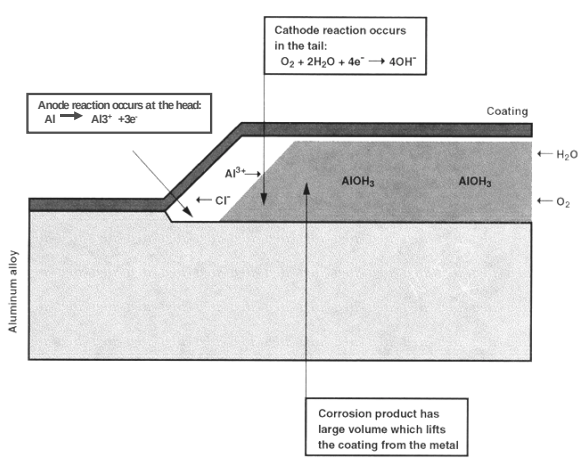

Figure 1. Schematic of filiform corrosion.

Many factors can impact the cosmetic corrosion performance of an organically coated metal substrate, including substrate composition and surface condition, cleaning and coating processes, and environmental exposure factors. The influence of the substrate is determined by its electrochemical and physical properties. In a differential aeration electrochemical cell, the corrosion rate is generally controlled by the diffusion-limited reduction of dissolved oxygen at the cathode. Therefore, the influence of the substrate on filiform corrosion performance is largely related to the efficiency of the substrate material as the surface for the cathodic electronation reaction. For example, the addition of copper to aluminum alloys increases susceptibility to filiform corrosion primarily because of the effects the copper has on the cathodic reaction kinetics of the alloy.[4,5] In addition to the effects of substrate composition, the condition of the surface can have a significant impact on filiform corrosion performance. It has been reported, for instance, that sanding of the metal substrate surface—as often occurs in base metal repair operations—is detrimental to the cosmetic corrosion performance of aluminum alloys.[6]

The cleaning and coating process variables are also significant factors in the performance of the coated system.[6,7] The importance of effective cleaning and optimized coating systems in minimizing the susceptibility to cosmetic corrosion is well documented. The weight and crystal size of the zinc phosphate coating, rinse conditioners, and organic coating type are a few parameters that have been cited as influential in cosmetic corrosion performance of automotive body sheet materials.

Finally, environmental exposure conditions can have a significant impact on cosmetic corrosion performance. Exposure conditions such as pH, ion concentrations, time of wetness, and relative humidity can significantly affect the morphology and extent of cosmetic corrosion attack. For example filiform corrosion is typically observed with exposure to high relative humidity (60–95% RH), whereas there is a general tendency for blisters to form at 100% RH or full immersion conditions.[2] The goal of this program is to identify environmental exposure conditions in an accelerated lab test that simulates the morphology and extent of cosmetic corrosion observed in long-term service-relevant outdoor exposures.

References

1. SAE J2334, Society of Automotive Engineers Surface Vehicle Standard, 1998.
2. H. H. Uhlig and R. W. Revie, *Corrosion and Corrosion Control*, John Wiley and Sons, New York, 1985.
3. D. A. Jones, *Principles and Prevention of Corrosion*, Macmillan Publishing, New York, 1992.
4. R. Bleeker and C. Lahaije, "Filiform Corrosion of Painted Automotive Body Sheet with Special Attention to the Alloying Element Copper", EUROCORR 2000, September 11–14, 2000.
5. L. F. Vega et al., "Filiform Corrosion of Aluminum Alloys: Influence of Alloy Composition," Corrosion 2000, March 27–31, 2000.
6. L. F. Vega et al., "Influence of Surface Treatments on the Durability of Painted Aluminum Alloys," Society of Automotive Engineers, 1997.
7. G. Courval and J. Allin, "Effects of Phosphating Systems on the Corrosion Resistance of Aluminum Body Sheet," ATA Conference on Surface Finishing and Anti-Corrosion, 1991.

3. ADVANCED MATERIALS DEVELOPMENT

A. Low-Cost Powder Metallurgy for Particle-Reinforced Aluminum Composites

Project Leader: Dr. Jean C. Lynn
DaimlerChrysler Corporation
800 Chrysler Drive
CIMS 484-01-13
Auburn Hills, MI 48326-2757
(248) 576-3192; fax: (248) 576-2176; e-mail: jcl6@daimlerchrysler.com

Project Administrator: Dr. Manish Mehta
National Center for Manufacturing Sciences/TRC
3025 Boardwalk
Ann Arbor, MI 48108-3266
(734) 995-4938; fax: (734) 995-1150; e-mail: manishm@ncms.org

Technology Development Manager: Joseph Carpenter
(202) 586-1022; fax: (202) 586-1600; e-mail: Joseph.Carpenter@ee.doe.gov
Field Technical Manager: Philip S. Sklad
(865) 574-5069; fax: (865) 576-4963; e-mail: skladps@ornl.gov

---

Contractor: U.S. Automotive Materials Partnership
Contract No.: DE-FC05-02OR22910
DOE CRADA No.: 96-Mult-AMP-0444

Objectives

- Develop low-cost powder metallurgy (PM) manufacturing methods for particle-reinforced aluminum (PRA) composite components.
- Advance PRA machining technology and PRA composite design methodologies.
- Provide sufficient information that U.S. Automotive Materials Partnership (USAMP) members and suppliers can make sound commercialization decisions regarding PMPRA technologies.
- Through participation by leading suppliers, establish (enhance) technical and manufacturing capabilities in North America to provide low-cost PMPRA components to the automotive industry through the USAMP partners.

Approach

During this 6.5-year project, execute the following tasks in two sub-projects, press and sintering (P&S) and direct powder forging (DPF):

- Establish property requirements and cost targets.
- Develop and assess low-cost PM processes for PRA components.
- Develop and apply process models for PM PRA technologies.
- Develop mechanical behavior and wear database for PM PRA materials.

- Develop PRA composite design optimization methodologies.
- Combine new process, machining technology, and composite design methodologies to optimize and fabricate PRA materials for at least two components
- Conduct bench and engine tests for at least three PM PRA components
- Develop and continuously update cost models for PM PRA materials and fabrication processes and PRA machining processes.

Accomplishments

P&S sub-project to develop moderate-strength aluminum composites:

- Completed in-plant test cell evaluations by suppliers of all candidate new coatings (polymer, non-polymer organic, and hard anodized) and the testing of compacted gears to meet more stringent wear and durability test regimes defined with the original equipment manufacturer (OEM) pump test engineers. (See Figure 1.)
- Obtained recommendation from supplier for two polymeric coatings based on wear performance and cost criteria.
- Received from a supplier several aluminum alloy gear-sets in OEM-provided aluminum gear housings for further OEM evaluation, along with a recommended process flow chart for aluminum gear testing.

DPF sub-project to develop high-strength, high-temperature aluminum metal matrix composite (MMC) applications:

- Established the powder premix alloy of aluminum and silicon carbide based on sizing, processability, ease of handling, strength, and fatigue performance criteria for the PM PRA connecting rod.
- Finalized the connecting rod design for aluminum alloy MMC, based on finite element modeling and simulation. Comparison of the current machined ferrous connecting rod design and Al–SiC design indicated that the Al–SiC connecting rod weighs 56% less. (See Figure 2.)
- Designed and procured tooling for compaction of preforms and forging.
- Evaluated several commercial powder blending methods with suppliers to optimize the processability and ease of handling of the down-selected premix alloy candidates.
- Obtained a demonstration by an agglomeration supplier of a commercially feasible, binderless process for powder agglomeration using granulator technology.
- Conducted room temperature tensile and fatigue property tests and microstructure studies that indicate it is possible to use sinter-forging methods to develop composites that perform as well in fatigue as would extruded components.

Future Direction

- Direct the DPF team to fabricate up to 150 prototype connecting rods for OEM evaluation using the new tooling and agglomerated powder.
- Complete a composite material/process design database for both P&S and DPF projects.
- Identify and explore additional opportunities for cost reduction and new powertrain applications of aluminum powder blends.

Major Project Deliverables

The PM PRA project management team directed an effort to develop an interactive CD-ROM–based design, processing, properties, and testing database for the P&S and DPF projects. Significant progress was made to complete the P&S database, and version 1.0 was released. When fully populated, this database will ensure that technical information from

the project is available in a form appropriate for future use by powertrain product designers and process engineers.

In FY 2002, the P&S and DPF teams delivered the following items to USAMP:

A set of compaction, sintering, and coining process conditions and dimensional capability data for aluminum alloy inner and outer transmission pump gears made by the P&S process were completed. These were based on microstructural analysis and wear analyses. Figure 1 illustrates a test cell setup. The data have been incorporated in the interactive design database, which has been released to the PM PRA team for evaluation.

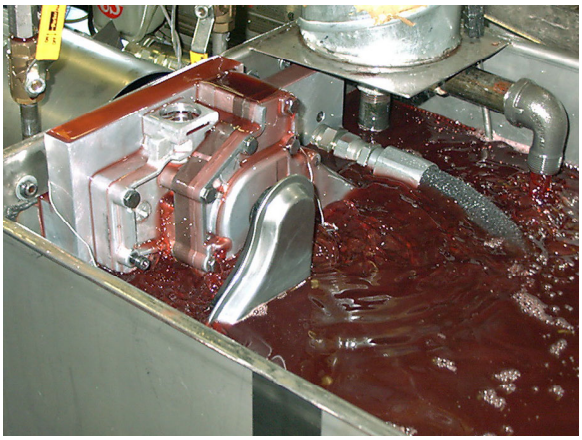

Figure 1. Test fixture used to test entire PM PRA transmission oil pump gear set.

For the DPF program, an alternative powder shape consolidation process (that does not require a binder or lubricant additive) for fabrication of forging preforms was demonstrated for the model test shape. Ames Laboratory evaluated compaction quality and inter-particle bonding.

The commercial potential for adapting the DPF process to a connecting rod manufacturing line was investigated by the DPF supplier lead. Figure 2 shows the final geometry and shape of the component.

Additional specimen fatigue tests at high temperature and mechanical property and cluster modeling data were developed for the quantitative assessment of material alloy and blend characteristics in DPF PM PRA.

Commercially viable powder blending technologies and an agglomeration process for handling of Al/SiC composite alloy powders were demonstrated.

Figure 2. Three-dimensional solid model of PM PRA connecting rod.

Conclusions

This DOE-funded program is nearing completion with the significant developmental milestones achieved during FY 2002. The P&S project has demonstrated a high potential for using powder metallurgy aluminum composite materials for moderate-strength lightweight transmission oil pump gear applications in high-volume production. The pump design is intended to address the worst-case operating condition, a hot idle, which can cause significant thermal expansion. Aluminum gears have the potential to improve performance during the hot idle condition and to improve engine efficiency. The insights gained from project experience in materials development, processing, and handling thus far suggest that design rules applicable to ferrous-based materials may need to be revised to completely exploit the benefits of using aluminum PM composites.

The USAMP team is committed to achieving its DPF component manufacturing technology milestones in early FY 2003 for further OEM testing and evaluation.

B. Low-Cost Cast Aluminum Metal Matrix Composites

Principal Investigator: Darrell R. Herling
Pacific Northwest National Laboratory
(509) 376-3892; fax: (509) 376-6034; e-mail: darrell.herling@pnl.gov

Technology Development Manager: Joseph A. Carpenter
(202) 586-1022; fax: (202) 586-1600; e-mail: joseph.carpenter@ee.doe.gov
Field Technical Manager: Philip S. Sklad
(865) 574-5069; fax: (865) 576-4963; e-mail: skladps@ornl.gov

USCAR Project Steering Committee:
Bruce Cox—DaimlerChrysler
(248) 576-0235; fax: (248) 576-7288; e-mail: bmc8@daimlerchrysler.com
Rena Hetcsh—Ford Mo. Co.
(313) 322-9079; fax: (313) 390-0514; e-mail: rhecht@ford.com
James Quinn— General Motors
(586) 986-6712; fax: (586) 986-9204; e-mail: james.f.quinn@gm.com

---

Contractor: Pacific Northwest National Laboratory
Contract No.: DE-AC06-76RL01830

Objective

- Develop low-cost aluminum (Al) metal matrix composite (MMC) materials that are cost-competitive with typical Al alloys used in the automotive industry to provide lightweight, cost-effective Al-MMC options for future hybrid and hydrogen-powered vehicles, with an initial focus on braking system components.
- Develop a modular mixing and holding system for low-cost Al-MMC materials under a cost-shared contract with MC-21.
- Develop economical innovative casting technologies to produce Al-MMC automotive braking systems and powertrain components.

Approach

- Develop rapid MMC mixing process and lower-cost, castable Al-MMC material.
- Conduct a foundry evaluation of castability.
- Evaluate mechanical and physical properties.
- Conduct friction and wear testing of sample products.
- Explore innovative casting and finishing options.
- Develop innovative brake system designs to use Al-MMC materials.

Accomplishments

- Completed wear and friction testing of seven combinations of candidate Al-based MMC materials and innovative casting methods at Rockwell Science Center using an instrumented test system. This information, coupled with the updated cost models, led to the down-selection of two processing routes on which to focus full-scale prototype testing.

- Completed the materials property evaluation of squeeze-cast Al-MMC samples prepared by Case Western Reserve University.
- Established a collaboration with Visteon Chassis Systems to model and subsequently design a brake rotor geometry appropriate for the properties of Al-MMC materials.
- Conducted a design review at THT Presses in Dayton, Ohio, of the Visteon-designed prototype brake rotor. THT Presses will be producing 80+ prototype rotor units for dynotesting at Visteon.

Future Direction

- Make the innovative brake rotor design available to the project participants for evaluation of this design using the low-cost Al-MMC material (Visteon).
- Cast prototype brake rotors of two types: (1) fully reinforced by squeeze casting (FY 2002 activity) and (2) selectively reinforced by centrifugal casting (FY 2003 activity) (THT Presses and the Casting and Composite Technology Center).
- Use prototype rotors for dynamometer brake testing at Visteon in FY 2002 and 2003.
- Investigate the use of centrifugal casting to demonstrate the production of a selectively reinforced brake rotor caliper with the reinforcement located in the bridge region of the caliper [Pacific Northwest National Laboratory (PNNL)].

Introduction

The initial goal of the project is to develop the next-generation mixing process for producing low-cost Al-MMC materials for casting applications. The concept is to use a modular melting-mixing-holding unit designed to be placed on the foundry floor, where the MMC material can be mixed for various products and delivered directly to the casting line on demand. The rapid mixing process, combined with the use of lower-cost SiC reinforcement feedstock, was selected to reduce the overall cost of particulate-reinforced Al-MMC materials. The target material cost, established by the domestic automotive industry, is to produce a range of aluminum MMC products for approximately $1/lb. In an effort led by MC-21, Inc., such a mixing technology was developed and demonstrated in previous years at the MC-21 facility in Carson City, Nevada. Cost modeling of the process and raw material costs has shown that an aluminum-SiC MMC product can be produced for a composite cost of $1/lb.

The ultimate goal of the project is to demonstrate that the cost of cast MMC powertrain and braking system components can be reduced to the cost of a comparable system consisting of cast iron components in an automobile application. In addition to reducing the cost of the feedstock Al-MMC material, a reduction in the downstream manufacturing costs is necessary to produce a component at a cost-effective price. Therefore, to further reduce the cost of Al-MMC components, the development and evaluation of innovative casting technologies is the second goal of the project. This phase of the project scope has now been completed, and two casting methods have been chosen to proceed with the final phase of the project—prototyping and evaluation of an Al-MMC brake rotor.

Innovative Casting Technology Development

The goals of the project depend significantly on the ability to achieve weight reductions cost-effectively. One area that has been targeted to demonstrate this weight reduction is the brake system, in which replacement of cast iron with an Al-MMC is desired. While current lightweight prototype and concept vehicles employ Al-MMC brake rotors, they are considered too expensive for high-volume use; therefore, the domestic automotive industry is not currently considering the widespread application of such a composite material. The target is to achieve the weight reduction at cost parity with cast iron.

It is recognized that meeting the goal of a low-cost brake rotor, at a manufacturing cost target of $15/rotor, will require more than just a lower-cost Al-MMC material. There are opportunities to be realized in the reduction of costs for brake system

components through the application of innovative casting methods and rotor designs. Therefore, work was performed in the previous year to identify and evaluate innovative casting technologies to address downstream processing methods and costs related to the production of an automotive brake rotor.

During FY 2001, contracts were placed with BFD, MMCC, Eck Industries, THT Presses, and Case Western Reserve University to produce Al-MMC test specimens for the evaluation of material properties and comparison with the property needs of aluminum brake rotors. In addition, PNNL produced test specimens manufactured by a process called centrifugal casting, which allows axisymmetric MMC parts to be selectively reinforced. This approach has the benefit of placing the reinforcement only where it is needed for wear resistance and other qualities, which subsequently decreases the time-consuming and costly machining requirements by leaving the rest of the part free of ceramic. The unreinforced regions of the part can be finished with conventional low-cost machining practices. The innovative casting methods evaluated are

- BFD—ONNEX process to produce a complex cermet structure part
- CWRU—direct squeeze casting
- Eck Industries—conventional permanent mold castings
- MMCC—pressure infiltration of a ceramic preform with aluminum
- PNNL—centrifugal casting of low-cost Al-MMC material
- THT Presses—subliquidus casting (SLC®) using a semi-indirect squeeze casting

In addition to specimens for obtaining property data and microstructural characterization, BFD, MMCC, and PNNL produced disks for wear testing. These wear specimens were a combination of selectively reinforced and fully reinforced disks produced by the methods listed earlier. Samples of each material set were machined into 200-mm-diameter, 12.5-mm-thick test specimens and delivered to Rockwell Science Center for wear testing. Wear and friction tests were conducted last year and completed in the first part of FY 2002. In this testing, three different commercially available brake pad materials were used.

The standard pads used for current limited production of Al-MMC brake rotors, such as those in the Plymouth Prowler, were not effective at temperatures above ~250°C because of an excessive and high rate of pad wear. The final pad material tested with the Al-MMC friction couples was a pad recommended by Ford R&D engineers, used on the Toyota Camry, that is formulated for cast iron brake rotor applications. This pad was able to handle temperatures of up to 400°C, a capability that was desirable during the wear testing to differentiate between the various Al-MMC materials and casting methods. Friction and wear test results for the 400°C case are shown in Figure 1. The data are an average of four test runs on RSC-instrumented wear test equipment.

The data suggest that the most appropriate material to use for a brake rotor application is the low-cost Al-MMC (MC21LC20) produced by centrifugal casting. Based on these data and the cost modeling information, it was decided to down-select two casting methods for future full-scale prototyping and dynamometer brake testing. The two innovative casting methods selected are (1) THT's SLC squeeze-casting process, which will produce a fully reinforced brake rotor, and (2) centrifugal casting, which will produce a selectively reinforced brake rotor with the ceramic particles placed only in the rubbing/friction region of the rotor. The latter processing route will allow for better wear resistance and improved higher-temperature friction as a result of the increased level of ceramic particles in the rubbing region of the rotor. It also will allow for easier and cheaper machining practices to be used in the center of the rotor, where the holes are drilled through which the wheel lugs pass when the rotor is installed on the vehicle.

Based on the cost modeling performed to date by Warren Hunt, Aluminum Consultants Group, the squeeze-cast fully reinforced Al-MMC rotor will cost about $13.50/rotor to produce, while the selectively reinforced centrifugally cast rotor will cost approximately $15.00/rotor to produce. These cost data also include the cost of capital, based on the best information currently available. Though it is expected that the selectively reinforced rotor will

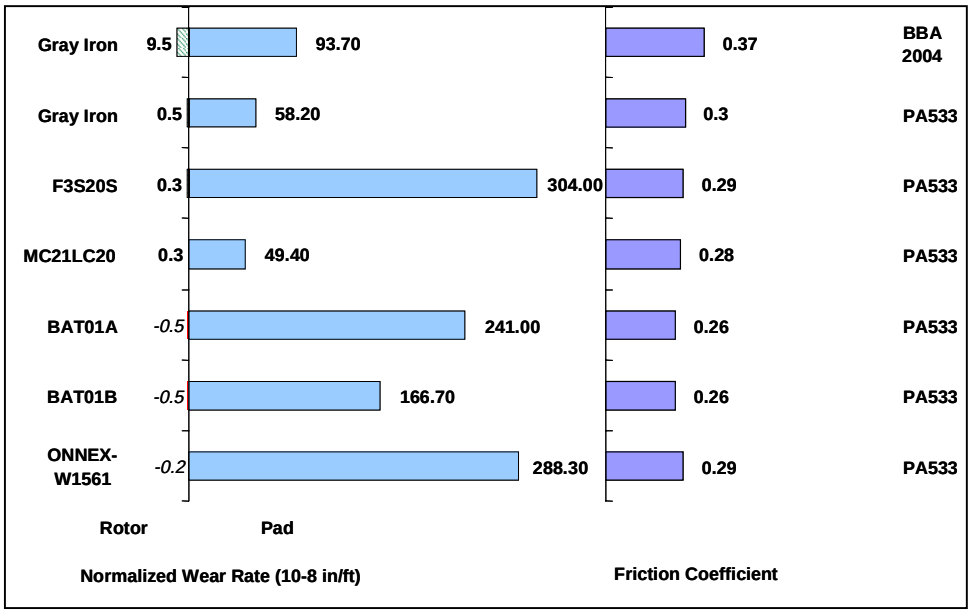

Figure 1. Aluminum MMC rotors tested against PA533 (Camry pad material) at 400°C.

have better wear resistance, the lower production cost of the fully reinforced rotor produced by squeeze casting warrants further investigation.

Innovative Brake Rotor Design, Prototyping, and Testing

Collaboration with Visteon Chassis Systems in Dearborn, Michigan, was initiated under a no-cost nondisclosure agreement to design an appropriate brake rotor geometry. Instead of using a common cast-iron brake rotor design and direct material substitution with Al-MMC, which has been tried in the past with poor results, the goal is to design from scratch a geometry that can exploit the properties of an Al-MMC material with good performance. With this approach, Visteon and the project team believe that a functional Al-MMC brake rotor can be produced and used on a typical mid-size passenger vehicle.

In the first half of FY 2002, Visteon provided an appropriate and novel brake rotor design to the project team, which will be used for prototyping and evaluation purposes. Based on the two casting methods selected for prototyping of Al-MMC brake rotors (squeeze casting and centrifugal casting), a cost-shared contract with THT Presses was established for the design and fabrication of the appropriate casting dies. Furthermore, THT will cast the prototype brake rotors at its Casting and Composite Technology Center. A review of the innovative brake rotor design was scheduled for May 2002 at THT Presses in Dayton, Ohio.

MC-21 MMC Rapid Mixing Technology

In the first phase of the project, MC-21 developed an evolutionary compositing process to mix MMC materials. The design of the mixer incorporates a rapid mixing process that significantly shortens compositing time and therefore reduces labor costs associated with production of the MMC material. The concept of the rapid mixing process calls for in-plant placement of the system so that the MMC material can be produced as needed and supplied directly to the casting line without the solidification, transporting, and remelting cycle required by other commercial Al-MMC products. The system is modular in design so that it can be scaled according to the casting foundries' business needs and hence provide a cost-effective, flexible compositing method. A U.S. patent (6,106,588) was issued to MC-21 in 2000 that covers the rapid mixing concept and the details of the process.

During FY 2001, MC-21 completed the scale-up of the modular mixing process from the previous 60-kg capacity to 600 kg. The larger equipment was demonstrated at MC-21's facility by producing 1200 kg of material, which is now being used for

casting trials and for producing the prototyping brake rotors at THT Presses' Casting and Composite Technology Center in Dayton, Ohio. A representative sample of this material was evaluated by PNNL during late FY 2001, and testing of the material was completed during the first part of FY 2002. The material property data are consistent with those for the material produced with the pilot-scale 60-kg unit, and it is comparable to other commercially available stir-cast materials (Duralcan).

The final step in developing the MMC rapid mixing technology is the deployment of the equipment to industry, where it can be linked to a casting line, to demonstrate the entire compositing/casting concept. However, at this time, MC-21 is hesitant to take this step because of concerns about losing control of the technology, the equipment, and its intellectual property rights. Currently, we are discussing options with MC-21 regarding how best to make this technology available to industry and demonstrate a mixing unit at THT Presses placed in-line with one of its squeeze-casting demonstration lines.

Future Work

During the last half of FY 2002, participation by Visteon's Chassis Systems Division and THT Presses was established to execute the final phase of the project. The scope of this final phase will focus on producing prototype brake rotors with an innovative design using the economical casting methods selected. During FY 2003, fully reinforced brake rotors will be produced by THT's SLC method and subsequently tested on a brake dynamometer at Visteon's facility. THT Presses will design and fabricate the casting tooling using the rotor design created by Visteon. PNNL will provide supplemental modeling support for further rotor design and casting mold design work as necessary. In addition, PNNL will characterize the microstructure and properties of the prototype brake rotors. It is anticipated that approximately 80 prototype rotors will be produced for testing and evaluation.

Also in FY 2003, PNNL and THT will work together to develop the design of a commercial centrifugal casting center, which can be used to manufacture Al-MMC brake rotors. These initial design data will be used to better model the capital costs associated with centrifugal casting of brake rotors and associated components. PNNL and the Aluminum Consultants Group will (1) update cost models for the new rotor and brake system designs based on data from the prototyping study and (2) compare them with the baseline cast-iron system currently available.

The scope of work for FY 2003 will also focus on prototyping and demonstrating the performance of selectively reinforced Al-MMC disk brake rotors, instead of the fully reinforced rotors that were the focus for FY 2002.

C. Exploratory Study into Improved Formability and Strength of Automotive Aluminum Sheet Alloys with an Electric Field

Principal Investigators: Hans Conrad and Charles R. Manning, Jr.
Accident Reconstruction Analysis
5801 Lease Lane
Raleigh, NC 27613
(919) 787-9675; fax: (919) 881-8112; e-mail: hans_conrad@ncsu.edu

Technology Development Manager: Joseph A. Carpenter
(202) 586-1022; fax: (202) 586-1600; e-mail: joseph.carpenter@ee.doe.gov
Field Technical Manager: Philip S. Sklad
(865) 574-5069; fax: (865) 576-4963; e-mail: skladps@ornl.gov

---

Contractor: U.S. Automotive Materials Partnership
Contract No.: DE-AC05-02OR22910

Objective

- Investigate the potential benefits of an electric field on the formability and strength of automotive aluminum sheet alloys.

Approach

- Determine the effects of an electric field applied during the solution heat treatment (SHT) of 6000-series aluminum alloys on the subsequent resistivity, hardness, and tensile test properties with natural aging.
- Determine the effects of an electric field applied during a pre-aging treatment of 6000-series aluminum alloys at room temperature on the subsequent resistivity, hardness, and tensile test properties with natural aging.
- Determine the effects of an electric field applied during both the SHT and the pre-aging treatment on the subsequent resistivity, hardness, and tensile test properties with natural aging.
- Determine the influence of an electric field applied during the tensile straining of the non–heat-treatable 5182 aluminum alloy on the corresponding flow stress and elongation.
- Determine the influence of an electric field applied during SHT and/or room temperature aging plus straining on the properties resulting from aging at elevated temperature.
- Compare the effect of the field on elongation with bend tests to evaluate its influence on folding and hemming.
- Determine the effects of the electric field on the corresponding microstructure, employing advanced techniques.
- Analyze and correlate the data for predicting behavior and determining the governing physical mechanisms.
- Transfer the technology to industry.

Accomplishments

- Determined that the effect of an electric field applied during SHT varies with the SHT temperature. The maximum effect for 6061 occurred for a SHT temperature of 525°C.
- Determined that the application of an electric field during SHT of 6061 at 525°C gave an increase in elongation by a factor of 36% and a corresponding increase in the hardness and tensile strength by 8%.

- Determined that the application of an electric field only during the pre-aging treatment of 6063 gave an increase in the elongation by a factor of 15–17%, with a marginal, if any, increase in strength.
- Established that the effect of a field appears to be through its influence on the number of aluminum-magnesium-silicon-vacancy clusters.
- Established correlations between resistivity, hardness, and tensile properties.

Future Direction

- Determine the role of alloy composition on the effects of an electric field.
- Determine the microstructure corresponding to the effects of the field.
- Determine the effect of an electric field applied during tensile testing of the non–heat-treatable 5182 aluminum alloy.
- Evaluate the effects of electric field on formability in bending.
- Determine the effect of an electric field applied during SHT and/or pre-aging at room temperature on the properties that result from subsequent artificial aging.

Introduction

To reduce weight and thereby improve fuel economy, auto makers are considering the use of aluminum in automotive body panels. Aluminum sheet, however, has lower formability than mild steel. Prior work had found that an electric field can have a significant effect on the microstructure and mechanical properties of aluminum alloys. The objective of the present investigation was to make an exploratory study of the potential for improving the formability and strength of automotive aluminum sheet alloys by applying an electric field during prior processing or during forming. The aluminum alloys investigated to date are 6061 and a modified 6063. The electric fields were applied during SHT and/or during a pre-aging treatment at room temperature. The electrical arrangements consisted of electrostatic (condenser-type) conditions illustrated in Figure 1. The electric currents were only of the order of mA at the SHT temperature and μA during the pre-aging treatment at room temperature.

Secondary goals of the investigation were to determine correlations that may exist between resistivity, hardness, and tensile properties and to determine the physical mechanisms governing the effects of an electric field.

Accomplishments: Milestones

It has been established that an electric field of 5 kV/cm applied only during SHT gives an increase in the tensile elongation of 6061 by a factor of 36% with a gain of 8% in tensile strength [Figure 2(a)]. The application of an electric field of 5 kV/cm during a pre-aging treatment of 2 minutes at room temperature gave an increase of 15–17% without loss in tensile strength [Figure 2(b)]. Similar effects were obtained for the “non-contacting” and the “contacting” electrical conditions Also, there were no clear effects of polarity for the “contacting” condition.

Correlations were established between resistivity, hardness, and tensile strength (Figure 3).

Project Benefits

The expected benefits to DOE and U.S. industry include the following.

The reduction in weight in transportation systems by the use of aluminum compared with steel will lead to improved fuel economy and lower emissions and make the United States less dependent on foreign oil.

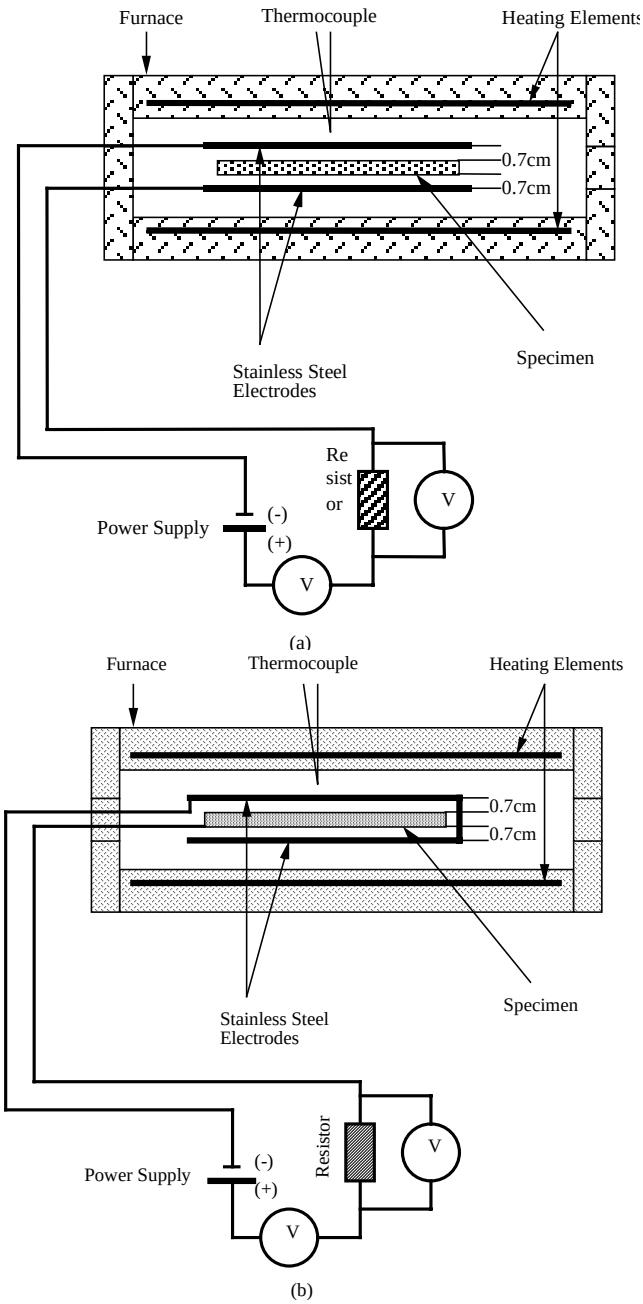

Figure 1. Electrical arrangement for: (a) non-contacting condition and (b) contacting condition.

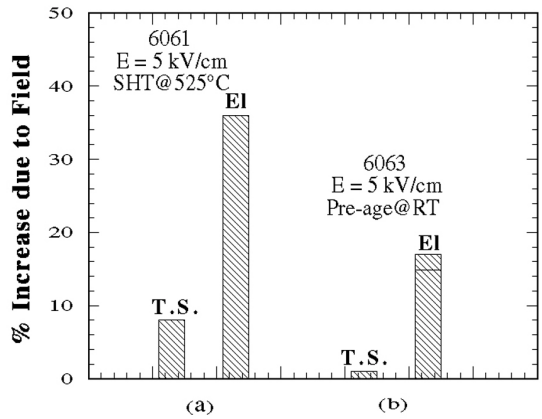

Figure 2. Percentage increase in tensile strength and elongation for the T4 temper with application of an electric field: (a) For field E = 5 kV/cm applied only during the solution heat treatment of 6061 and (b) for field E = 5 kV/cm applied only during pre-aging of 6063 at room temperature.

Applying electric fields during SHT of aluminum alloys offers the potential for performing this processing step at lower temperatures than are conventionally employed, thereby reducing the energy and costs pertaining to this process.

The increase in tensile strength along with the increase in elongation of the aluminum sheet during application of an electric field during SHT provides for an increase in the energy absorbed during a crash, thereby giving an additional safety factor when aluminum is used.

The correlations between resistivity, hardness, and tensile properties offer the potential for employing time-saving and lower-cost non-destructive tests for measuring and predicting behavior.

The application of an electric field as illustrated in Figure 1 is expected to be technologically feasible at a relatively low cost.

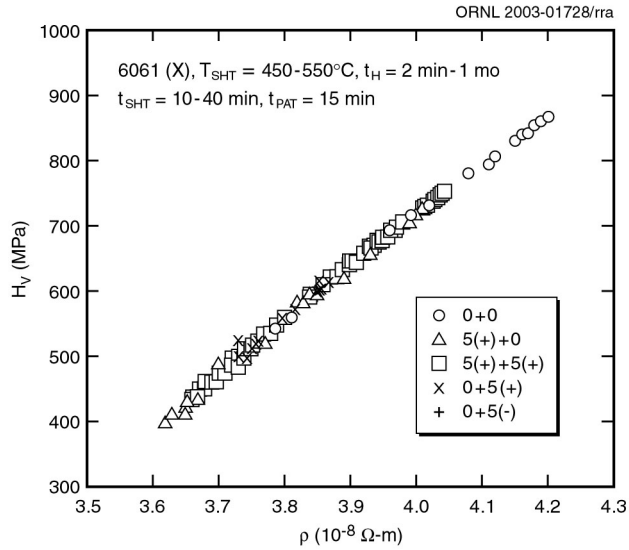

(a)

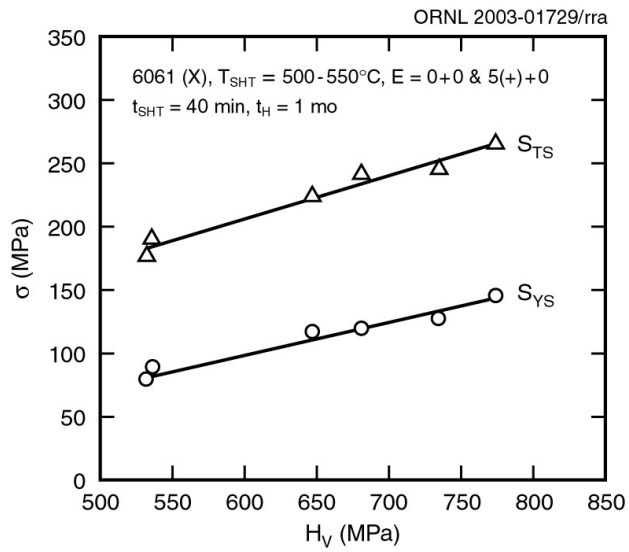

(b)

Figure 3. Correlation between the Vickers hardness and resistivity of 6061 for various processing conditions without and with electric field (a) and correlation between yield stress and tensile strength vs. Vickers hardness (b).

D. Magnesium Powertrain Cast Components

Project Manager: Bob R. Powell
GM Research & Development Center
MC 480-106-212, 30500 Mound Road, Warren, MI 48090-9055
(586) 986-1293; fax: (586) 986-9204; e-mail: bob.r.powell@gm.com

Project Administrator: Peter Ried
Ried & Associates, LLC
6381 Village Green Circle, Suite 10, Portage, MI 49024
(616) 327-3097; fax: (616) 321-0904; e-mail: pried_imagineer@netzero.net

Technology Development Manager: Joseph Carpenter
(202) 586-1022; fax: (202) 586-1600; e-mail: joseph.carpenter@ee.doe.gov
Field Technical Manager: Philip S. Sklad
(865) 574-5069; fax: (865) 576-4963; e-mail: skladps@ornl.gov

---

Contractor: U.S. Automotive Materials Partnership
Contract No.: DE-FC05-02OR22910

Objectives

- Demonstrate and enhance the feasibility and benefits of using magnesium alloys in engine components.
- Design an ultra-low-weight, cost-effective performance engine containing four components (block, bedplate, structural oil pan, and front cover) using the best low-cost, recyclable, creep- and corrosion-resistant magnesium alloys.
- Compare and select the alloys on the basis of common-protocol casting and testing. (The resulting cast specimen database will provide the necessary design data for the components.)
- Design and build the component dies.
- Cast and test the components in operating engines (dynamometer or vehicle).
- Validate the performance benefits, component durability, and system costs.
- Create a material specification for magnesium powertrain alloys common to original equipment manufacturers.
- Identify critical challenges for future magnesium alloy and component development and use this information to promote scientific research in the United States.

Approach

- Conduct the Magnesium Powertrain Cast Components (MPCC) project in two phases, each containing three tasks. A decision gate separates the two phases.
- Phase I: Produce the finite element analysis (FEA) engine design, the alloy property requirements for the engine, the comparison of the alloys in a cast-specimen material property design database, a cost model of the engine, and a set of scientific challenges to serve as the basis for requests for proposals for fundamental research programs to be conducted in the United States.

- Phase II: Produce test results for the magnesium-intensive engine using cast components, assembled and tested engines to validate Phase I predictions, an extensive design database using alloy specimens excised from cast components, the common magnesium materials specification, and the results of the fundamental research programs, the need for which were identified in Phase I.

Accomplishments

- Achieved participation of 44 companies and organizations that have joined or will join the MPCC project. The project team comprises the key magnesium alloy producers and casters, as well as a full complement of industrial partners, to enable a comprehensive execution of the project objectives.
- Selected seven high-pressure die casting alloys and three sand casting alloys for inclusion in the Task 1 alloy evaluation database. The die casting trials have been completed, and the specimens are at the testing laboratories.
- Completed the castability trials of the die casting alloys. The assessment documentation is nearly done. One die-casting alloy was eliminated from further consideration because of its very poor castability. The sand casting alloy trials are nearly complete.
- Completed computer-assisted design (CAD) files for the engine components and began the FEA analysis. Computation fluid dynamics and heat transfer analyses were completed, and structural analysis and design are progressing rapidly.
- Assembled a modeling team to design dies and patterns for the magnesium engine components to be cast in Phase II and formed a cost modeling team.

Future Direction

- Complete Task 1 alloy comparison database and select alloys for use in engine components in Phase II.
- Complete engine component design and cost model.
- Publish a review of scientific research needs to support future advances in magnesium alloys, casting processes, and powertrain applications and solicit research proposals to be considered for funding in Phase II.

Introduction

The MPCC project will provide comprehensive answers to questions regarding the feasibility and cost-benefit ratio of using magnesium in powertrain components. Although magnesium has been demonstrated to significantly reduce weight at acceptable cost in many areas of the vehicle, structural powertrain components have not benefited from this material. The reasons for this are as follows:

- The high cost of alloys that can withstand the operating temperatures of the engine without deforming under load (creeping)
- Limited powertrain design experience with magnesium alloys
- Lack of long-term field validation or controlled-fleet testing data for magnesium powertrain components
- The limited scientific infrastructure in the United States that is directed toward acquiring a fundamental understanding of magnesium alloys and casting processes.

The project is increasing interest in magnesium powertrains and promoting greater competition for and development of magnesium sources, manufacturing capability, and engineering expertise. It will encourage scientific research into the properties, processing, and behavior of magnesium by universities and national laboratories in the United States. The project began in 2001. It is being conducted in two phases separated by a decision gate, at which point the predicted feasibility and cost-effective performance benefits will be evaluated prior to entering Phase II. The decision gate for entry into Phase II will be in the first quarter of CY 2003.

The engine chosen for the MPCC project is the Ford Duratec (Figure 1). The components of this V-6 engine to be designed for magnesium are the block, the bedplate, the structural oil pan, and the front cover. The bedplate, oil pan, and cover will be high-pressure die cast, and the block will be sand cast.

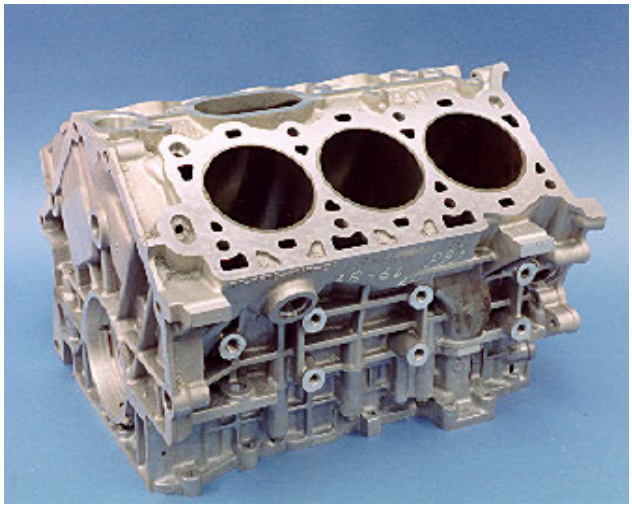

Figure 1. The Ford 2.5L Duratec engine block.

Details of Phase I

The first-phase goals of the project comprise three tasks: (1) evaluation of the alloys, (2) FEA design of the magnesium engine components, and (3) identification of the critical scientific knowledge necessary for future magnesium powertrain materials.

Task 1

Task 1 is the evaluation of the new creep-resistant alloys based on cast specimens using a common die and standardized mechanical property and corrosion tests to yield a short list of suitable alloys. Evaluation will be based on tensile and fatigue properties, creep and corrosion resistance, castability, recyclability, and estimated alloy costs.

On the basis of previously published data and properties data provided by alloy suppliers, the seven candidate alloys were identified, their producers agreed to participate in the program, and the test matrix was defined. The alloys were cast into the test specimens for evaluation. The specimen shot is shown in Figure 2.

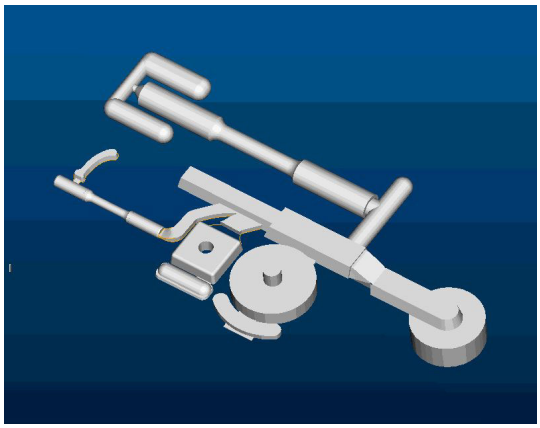

Figure 2. The specimen die shot from the four-cavity GM die used at Lunt Manufacturing.

Nearly 500 shots of each alloy were made to support the requirements of the test matrix development. Testing has begun. The test result documentation will be based on the same database structure and format developed in the project on design and production optimization for cast light metals that was completed for aluminum and launched for magnesium [structural cast magnesium development (SCMD)] in 2001 (see report 3I). MPCC and SCMD will have a common database of non-powertrain magnesium alloys, benefiting both groups of potential magnesium alloy users.

Castability is also an evaluation criterion for the alloys. Two castability trials were planned, a thin-wall part and a thick-wall part that will be used for the most promising alloys. The parts are shown in Figures 3 and 4. The transfer case simulates the oil pan and the front cover. Six alloys were cast into the transfer case die. One alloy was not cast because it showed poor castability in the specimen die trials and was subsequently dropped from further consideration.

The bedplate will be used to assess the potential of the downselected alloys for use in the analogous part in the Duratec engine block.

The database specimens for three sand casting alloys have been cast. The castability trials of the alloys will be done prior to the decision gate.

Task 2

Task 2 is the FEA design and cost model of the engine and its magnesium components. The initial designs will be based on the property data for the

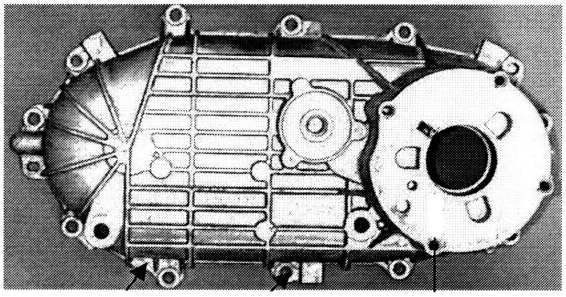

Figure 3. The Ford transfer case used at Meridian.

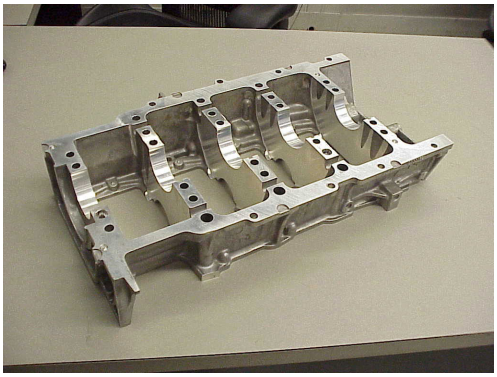

Figure 4. The General Motors Northstar bedplate that will be used at Gibbs Die Casting.

alloys that came from the literature evaluation in Task 1. As casting and test results are acquired, the model will be refined to achieve ultra-lightweight, cost-effective performance. The design and cost model results using the best alloys from Task 1 will form the basis for the decision gate for entry into Phase II of the project.

The aluminum 2.5-L Duratec V6 engine shown in Figure 1 was chosen as the starting point for the magnesium-intensive engine. Ford provided the CAD files for this aluminum production engine to Magna Steyr, the organization that is designing the magnesium version. Ford, General Motors (GM), and DaimlerChrysler powertrain engineers reached consensus on the design approach, the design criteria, and the alloy requirements. There will be a complete FEA design of four magnesium engine components, a durability analysis of those components, and a cost/benefit analysis of the resulting engine.

Working with Magna Steyr, the Ford, DaimlerChrysler, and GM powertrain engineers participated in developing the design approach and materials assumptions and identifying the various technology options for the engine. Several members of the project team who are not original equipment manufacturers also contributed to these activities. During the reporting period, the CAD files were assembled and delivered to Magna Steyr and computational fluid dynamics and heat transfer analyses were completed. Structural analysis including consideration of fatigue and creep of the magnesium alloys was accomplished. An image of the starting point is shown in Figure 5.

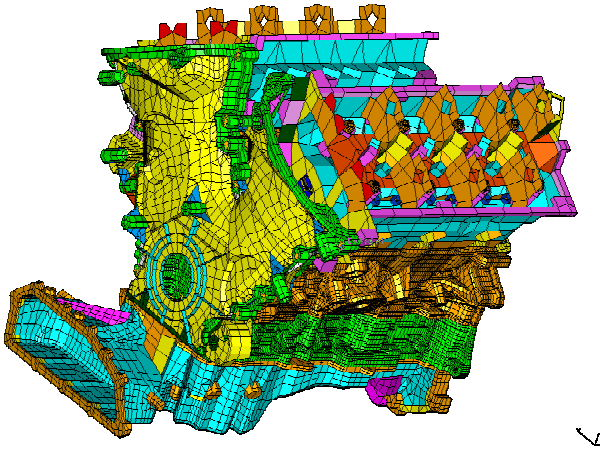

Figure 5. The finite element mesh of the aluminum version of the Duratec engine.

Several task teams under the Task 2 umbrella were formed to facilitate the design effort:

- Task 2.1: Engine Block, Bore, and Journals—identify and prioritize the technical options for the FEA design and cost modeling teams
- Task 2.2: Fasteners, Gaskets, and Sealing—address the mechanical design aspects of fastener systems and gaskets for the block and ancillary structures
- Task 2.3: Coolants and Corrosion—assess the state of the technology for coolant strategies; identify the best coolant system; and address the general and galvanic corrosion issues for magnesium in under-hood locations and in contact with internal materials such as gaskets, pumps, and other dissimilar materials.

Four major coolant manufacturers are participating the MPCC project. Each of them has developed an anti-corrosion coolant/additive formulation for use with magnesium. During the reporting period, the coolants and corrosion team worked with the manufacturers and the magnesium alloy suppliers to define a coolant evaluation protocol and to establish a common platform for testing the alloys and the coolant/additive packages. Three ASTM test procedures were adopted for the evaluation:

- ASTM B117-97: Standard Practice for Operating Salt Spray (Fog) Apparatus
- ASTM D1384-01: Standard Test Method for Corrosion Test of Engine Coolants in Glassware
- ASTM D4340-96: Standard Test Method for Corrosion of Test Aluminum Alloys in Engine Coolants Under Heat-Rejecting Conditions

The Task 2.3 team also identified an independent testing house to evaluate each of the alloys in each test condition. A "double blind" test protocol will be used.

Three other Task 2 teams were chartered:

- Task 2.4—Design Integration and Analysis
- Task 2.5—Casting and Casting Analysis
- Task 2.6—Cost Modeling

The Design Integration and Analysis team is responsible for coordinating the Task 2 input to Magna Steyr and for participating in design reviews during the development of the FEA model. As noted earlier, the Ford CAD files for the engine were delivered to Magna Steyr. The parts were meshed, and CFD and heat transfer analyses were begun. When complete, these will be coupled with a complete structural analysis of the engine, which considers assembly, bolt loads, primary and secondary creep behavior of the magnesium, and the cylinder gas forces, as well as the mass forces of the connecting rods. Fatigue analysis of the block is also being done. Multiple iterations will be allowed within the timetable of the project. Powertrain bending analysis and acoustic analysis will also be part of the Phase I deliverables. The baseline for comparison in bending and acoustic analysis will be assemblies using the aluminum components.

The Casting and Casting Analysis team will be responsible for the design of the dies and mold tooling for casting the components in Phase II of the project. During the reporting period, this team made valuable contributions to the modification of the GM die for trials of die cast specimens. Knowledge acquired as a result of that effort will benefit the project in Phase II when the actual component dies and patterns are designed.

The Cost Modeling team will work with an external modeling organization to develop a cost model that contains

- The cost impact of the alloy based on both intrinsic alloy costs and manufacturing costs, such as furnace and die life predictions and environmental and recycling considerations
- The cost of engine technologies required for successful operation with magnesium components, such as coolant costs and unique fastening and gasket requirements
- The benefits of reduced weight and design advantages that are enabled by the use of magnesium

Task 3

Task 3 identifies the fundamental scientific challenges of using magnesium alloys and casting processes in powertrain components. While alloy development is not within the scope of this project directly, the purpose of Task 3 is to promote new and strengthen existing scientific research in the United States, specifically for future magnesium alloy and component development (e.g., determining detailed mechanisms of creep and fatigue of magnesium alloys at elevated temperatures and establishing thermodynamic and phase equilibrium databases). Several such needs have already been identified in the project, and these will be presented in appropriate forums in the near future.

Details of Phase II

The second-phase goals of the project also comprise three tasks: (4) casting the engine components, (5) completing the magnesium alloy property database, and (6) conducting validation tests of the assembled engines. Upon entry into this phase of the project, its specific goals and objectives will be reconsidered and altered as necessary to best

serve the overall goals of the MPCC project. In addition, the identification and promotion of scientific research projects will continue.

Task 4

Task 4 will accomplish the casting of the engine components, which will ultimately be validation-tested in Task 6. The dies for the bedplate and structural oil pan and patterns for the engine block will be designed from fill and solidification models and fabricated. Components will be cast, inspected, and approved for assembly. Allowances for up to three iterations of casting trials and subsequent die and pattern modification have been included in the project schedule.

Task 5

Task 5 will complete the magnesium alloy database and will use alloy specimens excised from cast components obtained in Task 4. This database will not comprise all the alloys initially considered; rather, only those selected at the end of Tasks 1 and 2 will be included. Validation of "actual" properties may result in the identification of additional areas of technical challenge and the need for further scientific research, thereby furthering the objective of Task 3.

Task 6

Task 6 will achieve the completion of the project: the cast components assembled into complete engines and tested on dynamometers or vehicles to validate the design, performance, and durability of the components. All tested engines will be torn down for inspection; the final report will contain the test and teardown results, the FEA designs, the fill and solidification models, the alloy property databases, the final cost model, a common magnesium materials specification for powertrain components, and recommendations for future work.

Summary

The MPCC project is an aggressive attempt to address key concerns regarding the future prospects for a magnesium-intensive powertrain. Upon its completion, in addition to addressing these concerns, the project will have identified any additional scientific and economic implementation barriers, and programs to overcome the scientific barriers will have been undertaken by qualified U.S. universities and laboratories.

E. Solid Oxygen-ion-conducting Membrane Technology for Direct Reduction of Magnesium from Its Oxide at High Temperatures

Principal Investigator: Uday Pal
Department of Manufacturing Engineering
Boston University
Brookline, MA 02446
(617) 353-7708; fax: (617) 353-5548; e-mail: upal@bu.edu

Technology Development Manager: Joseph A. Carpenter
(202) 586-1022; fax: (202) 586-1600; e-mail: joseph.carpenter@ee.doe.gov
Field Technical Manager: Philip S. Sklad
(865) 574-5069; fax: (865) 576-4963; e-mail: skladps@ornl.gov

Participants
Timothy Keenan, Masters Candidate, Boston University
Ajay Krishnan, Masters Candidate, Boston University
Christopher Manning, Research Associate, Boston University

Contractor: Boston University
Contract No.: C#407200-ANS

Objective

- Demonstrate the technical and commercial viability of the solid oxygen ion-conducting membrane (SOM) process for production of magnesium directly from its oxide.

Approach

- Identify molten flux systems to operate the SOM process at 1300–1400°C.
- Examine the long-term stability of the SOM [yttria-stabilized zirconia (YSZ)] membrane in the candidate flux systems under static and dynamic conditions.
- Determine key physical properties of the candidate flux systems: volatilization rate, ionic conductivity, and mass transfer characteristics.
- Conduct laboratory-scale experiments with various anode-electrolyte-cathode configurations to determine the dissociation potential and the I-V characteristics for magnesium production from its oxide in the selected flux systems.
- Evaluate various methods of magnesium collection during the SOM process.
- Operate the SOM cell between 1300 and 1400ºC at current density on the order of 1 A/cm^2 and maintain low overall ohmic and polarization losses in the system so that the applied electric potential does not exceed 5 V. This arrangement will keep the power consumption at less than 13 KWh per kilogram of magnesium produced.
- Perform a cost-benefit analysis for a proposed scale-up design of the SOM process for next-stage development.

Accomplishments

- Conducted experiments to examine potential interactions between the yttria stabilized zirconia (YSZ) membrane material and two candidate flux compositions that were based on the SiO_2-MgF_2-MgO and MgF_2-

MgO systems. Based upon these results, the flux based on the MgF_2-MgO system was selected for the SOM process.

- Conducted thermogravimetric experiments to determine the volatility rate of the MgF_2-MgO flux at temperatures of interest for the SOM process.
- Assembled the experimental apparatus to study molten flux/YSZ interactions using impedance spectroscopy.
- Determined the molten flux/YSZ interaction mechanism and identified the means for limiting the interaction.
- Determined the electrical conductivity of the molten flux.
- Assembled a SOM cell incorporating the MgF_2-MgO flux, the YSZ membrane, and a magnesium vapor collection apparatus and demonstrated laboratory-scale electrolysis of magnesium between 1300 and 1400ºC. The apparatus is capable of producing and collecting 200 g of magnesium.
- Achieved high magnesium production rates (Faradaic current densities in excess of 1 amp/cm^2) without damaging the YSZ membrane or other components of the electrolytic cell. The applied electric potential was below 5 V.
- Successfully operated the SOM cell at 1300ºC for 5 hours with a steady-state current density of 800 mA/cm^2, producing 16 g of magnesium. The applied electric potential was 4.0 V, and the power consumption was estimated to be 10 KWh per kilogram of magnesium produced; these figures are clearly much superior to those for the state-of-the-art processes for magnesium production and for the Hall cell for aluminum production. Magnesium metal vapor that was produced was condensed both as a liquid and as crystals in the condenser.

Future Direction

- Determine the dynamic long-term stability of the stabilized zirconia membrane as a function of magnesium oxide content in the MgF_2-MgO flux (2–10 w%) and of the flux flow patterns while the SOM cell is operated at 1300ºC and current densities between 0.8–1 A/cm^2.
- Determine the stability of the key materials of construction of the SOM reactor (cathode and condenser) while performing the experiments to determine long-term membrane stability.
- Perform a cost-benefit analysis of the SOM system for primary magnesium production with input from the Magnesium Corporation of America.

Introduction

The SOM process employs YSZ as the membrane to separate the anode and cathode of a high-temperature electrolytic cell. This process exhibits several advantages over existing magnesium production routes, including improved economics and reduced environmental impact.

The SOM process is a generic, environmentally sound, energy-efficient alternative for oxide electrolysis using an inert-oxygen-ion-conducting membrane-based anode. The process can be an attractive alternative for the synthesis of high-energy-content metals such as aluminum, magnesium, titanium, tantalum, high-purity silicon, chromium, and value-added ferroalloys. This project focuses on the synthesis of magnesium metal using this technology.

The current production methods for magnesium are either electrolysis from a halide electrolyte bath, which requires extensive and expensive feed-material preparation, or metallothermic reduction (magnetherm process) at high temperatures (1200–1400ºC) involving expensive metal reductant (FeSi). The electrolytic magnesium process is based on an anhydrous chloride feed material that is recovered from brines via an elaborate and expensive front-end dehydration process. This feed preparation process step can represent 80% of the plant footprint and 30% of its capital cost. This process also generates a chlorine by-product at the graphite anode, an environmental concern that requires additional capital and operating resources.

The alternative metallothermic process for producing magnesium is based on the thermal reduction of calcined dolomite or magnesite with ferrosilicon to form a magnesium vapor that is

collected in an attached condenser. The ferrosilicon reductant represents 12 KWh/kg, or roughly 40% of the total energy required to produce magnesium; it also represents roughly one-third of its total production cost. Furthermore, this batch process generates about 4–5 tons of slag per ton of magnesium that must be properly disposed of.

In the SOM process, the oxide reduction is electrochemical, but it dramatically alters the existing electrolytic magnesium process flowsheet. It replaces the magnesium chloride dehydration process with a simple magnesium oxide calcining operation, thereby significantly reducing its front-end capital and operating costs. It also reduces the overall energy consumption of magnesium production by roughly 25%. In addition, eliminating the magnesium chloride feed also eliminates the production of chlorine and chlorinated hydrocarbons. Compared with the current metallothermic and electrolytic processes, the SOM process has the potential to be more economical, less energy-intensive, and more environmentally sound.

The configuration of the SOM process (Figure 1) consists of a solid-oxygen-ion-conducting, stabilized-zirconia electrolyte (membrane) that separates the anode from the melt containing the oxide of the metal to be reduced.

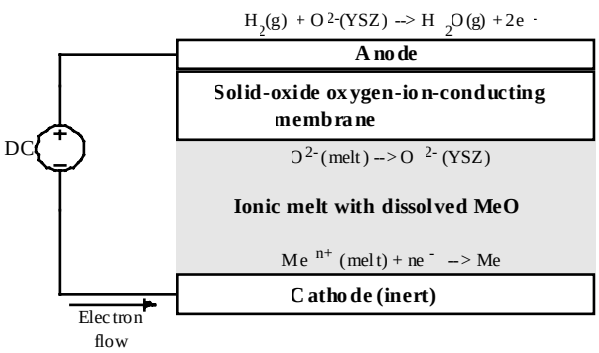

Figure 1. SOM process for metal (Me) production by direct reduction of its oxide.

An inert cathode is placed in the melt. When the applied electric potential between the anode and the cathode exceeds the dissociation potential of the oxide to be reduced, the desired metal cations are reduced at the cathode; oxygen ions migrate through the membrane and are oxidized at the anode. The applied electric potential between the electrodes can be increased as long as the potential at the melt-zirconia interface does not exceed the potential required for the dissociation of the solid zirconia and undesired oxides are not reduced at the cathode. This allows for larger potentials to be applied between the electrodes to increase the rate of production of the desired metal. The full benefit of the SOM process can be realized if the process is conducted at temperatures between 1200 and 1400°C.[1,2] At these temperatures, the overall resistance drop across the stabilized zirconia membrane and the melt are expected to be sufficiently low to allow high current densities on the order of 1 A/cm^2 or greater to be obtained. In addition, at these temperatures, the process efficiency can be further increased by directly reforming hydrocarbon fuel over the anode. It should be noted that several attempts have been made to employ SOMs at temperatures below 1000°C. However, these efforts have not been successful in developing a commercially viable process, mainly because sufficiently high current densities could not be obtained through the membrane.[3–8]

Work in Progress

Keeping commercial viability in mind, the present research is aimed at developing a stable SOM cell capable of producing and collecting magnesium with near 100% current efficiency at steady-state current density on the order of 1 A/cm^2 or greater with applied electric potentials not exceeding 5 V. This would result in a magnesium production rate that is at least 1.33 times the current aluminum mass production rate in Hall cells at comparable power consumption. The following sections summarize the various components of current research efforts toward this goal.

Molten Flux Selection

Two melt systems were selected as candidate fluxes for the SOM process for magnesium production. Selection criteria include low volatility at the temperatures of interest, viscosity of less than 10 poise, electrical conductivity of greater than 1 (ohm-cm)$^{-1}$, and MgO solubility of at least 5 wt%, at temperatures from 1300 to 1400°C. These requirements are expected to provide kinetically favorable conditions suitable for scale-up.[7–11] The first flux considered was based on the binary MgF_2-MgO system. The second flux investigated was

based on the eutectic composition of the ternary MgO-MgF_2-SiO_2 system.

For the proposed SOM technology to be technically feasible on a commercial scale, it is critical that the YSZ membrane be reasonably stable in the molten flux. Therefore, to identify a single best candidate flux composition for the SOM electrolytic cell, preliminary experiments were conducted to evaluate the stability of the SOM material, YSZ, in the two melts described earlier. In these experiments, YSZ crucibles containing the respective candidate fluxes were heated to the proposed operating temperature of the cell (1300°C). The flux-containing crucibles were held at temperature for periods of 10 and 30 hours and then cooled to room temperature. After cooling, the interfaces between the YSZ crucible and candidate fluxes were examined using optical and scanning electron microscopy for signs of dissolution, erosion, or general reaction. Chemical analysis of the region near the slag-crucible interface was performed using an electron microprobe equipped with a wavelength-dispersive X-ray spectrometer.

Examination of the solidified samples indicated that YSZ is relatively stable in contact with both slags. However, it was found that some pitting of the YSZ crucible occurred in the vicinity of the free surface of the silica-containing ternary slag. This phenomenon was not observed for the binary MgO-MgF_2 slag. Based on these observations, it was concluded that YSZ is more stable in contact with the binary MgO-MgF_2 slag, so this flux composition was selected for further experimentation.

Characterization of MgF_2—8mol%MgO Flux

Certain key properties of the binary magnesium oxy-fluoride slag, which has been selected for use in the SOM electrolytic cell at temperatures from 1300 to 1400ºC, have been determined. They include

- precise erosion/corrosion rate of YSZ by this flux
- its volatility
- its ionic conductivity
- its mass transfer properties

The first parameter listed is critical. The feasibility and design of a large-scale SOM-type reactor for the electrolysis of magnesium are extremely dependent upon the long-term stability of YSZ in the proposed flux. Therefore, laboratory experiments are being conducted to investigate the rate of YSZ attack as a function of the composition of the magnesium oxy-fluoride slag. For these experiments, impedance spectroscopy techniques are being employed to make the measurements.[11,12] One such experimental set-up is shown in Figure 2, and some current results are shown in Figure 3. Figure 3 indicates that even after 70–80 hours, the slag does not penetrate the membrane crucible, and hence its level and impedance do not change. Impedance data regarding stability of YSZ in the MgO-MgF_2 flux as a function of MgO content and fluid slow conditions for longer periods are being gathered using more sophisticated experimental techniques and will be presented later.

The electrical conductivity of the MgO-MgF_2 flux was measured by comparing its impedance with that of the standard calcium fluoride flux for a given cell geometry (cell constant). These measurements indicated that the ionic conductivity of the MgO-MgF_2 flux at 1300°C is 3.8 S/cm.

The specific rate of volatilization of the MgO-MgF_2 flux is also an important process parameter. Significant flux losses due to volatilization will not only complicate the laboratory experiments in progress but also decrease the attractiveness of a commercial-scale process based on this flux. Therefore, thermo-gravimetric (TGA) experiments have been performed using a high-temperature

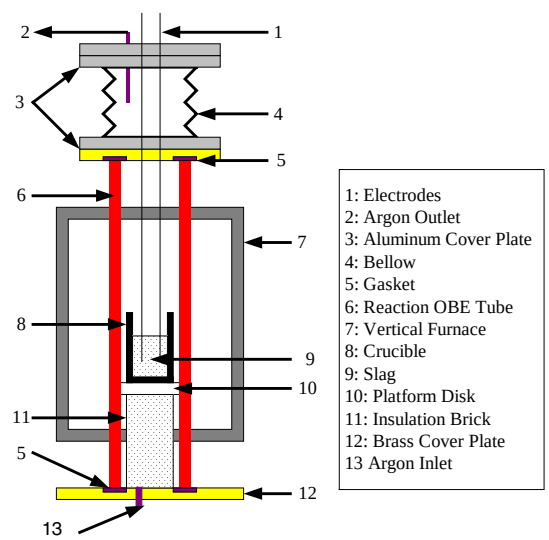

Figure 2. Experimental set-up for impedance measurement.

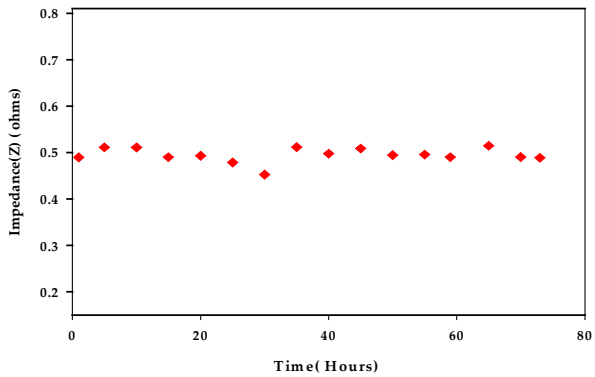

Figure 3. Impedance for a given electrode-immersion depth is stable over time.

D101-02 AT Cahn Balance to accurately determine the rate of volatilization of the flux at the proposed operating temperatures for the SOM process. For these experiments, approximately 20 g of slag were contained in a 2.2-cm ID graphite crucible and suspended from the microbalance using a mullite rod. All experiments were conducted in an inert atmosphere with a purging flow of argon gas. Volatilization experiments have been conducted at temperatures from 1300 to 1550°C. At these temperatures, the rate of volatilization has been found to be in the range of 10^{-7} to 10^{-6} g/cm^2·sec. This rate is relatively low and will not be a problem for either the laboratory experiments or the eventual commercial process. Based upon these experiments, the temperature dependence of the volatilization rate, *R*, was calculated in g/cm^2·sec (Figure 4) as

$$R = -3.96\times10^{-4}\exp\left(\frac{-14281}{T}\right)$$

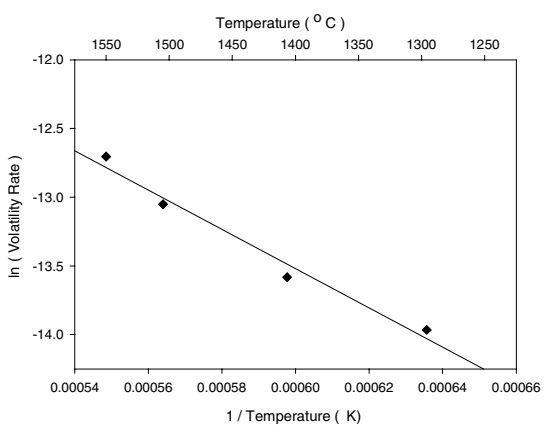

Figure 4. Volatilization rate of MgO-MgF$_2$ flux as a function of temperature.

Laboratory-Scale Electrolysis and Collection of Magnesium

Previous electrolytic cell designs for the production of magnesium via the SOM process have been presented in earlier progress reports and publications.[13, 14] These electrolytic cell designs were intended to produce and collect a small amount of magnesium metal (less than 3 g) to demonstrate the technical viability of this process and to evaluate fundamental electrochemical characteristics of the cell. A more advanced electrolytic cell and magnesium collection apparatus has been designed that allows for the production of much larger quantities of magnesium metal (several hundred grams) over an extended period of operation. This apparatus is shown schematically in Figure 5.

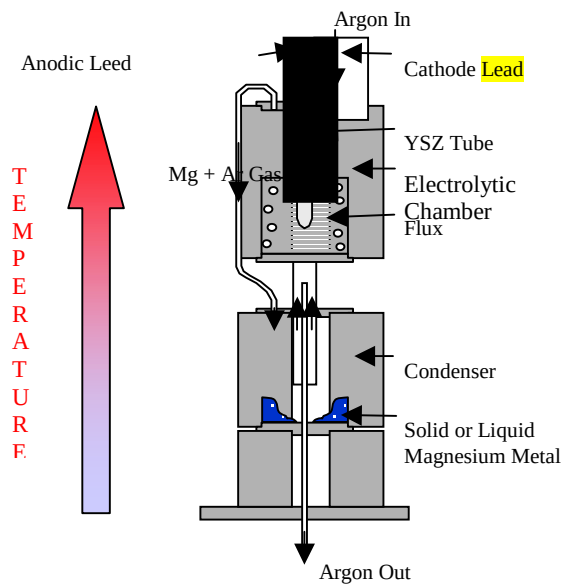

Figure 5. Apparatus for the laboratory-scale electrolysis and collection of magnesium metal using the SOM technology.

Nearly all of the apparatus shown in Figure 5, with the notable exception of the YSZ membrane and extended anode, is constructed of 304 stainless steel. The entire apparatus is contained and heated within the mullite reaction tube of a high-temperature resistance furnace. The upper electrolysis chamber shown in Figure 5 is approximately 6 in. in length, which is also the length of the hot zone of the resistance furnace. This electrolysis chamber can also be used in the membrane-flux stability investigation.

The apparatus in Figure 5 takes advantage of the natural temperature gradient of the resistance furnace, so that the electrolysis chamber is maintained at 1300°C while the lower condensation chamber can be positioned so that the temperature is anywhere from 1000 to 500°C. To protect the YSZ membrane above the flux from the extremely reducing magnesium vapor that is produced along the wall of the stainless steel container/cathode, argon gas is introduced into the chamber as a carrier gas and dilutant. The argon-magnesium gas mixture passes out of the electrolysis chamber to the lower condensation chamber, which can be maintained at a temperature such that magnesium is collected as either a liquid or solid. The remaining argon gas then passes through a baffle and exits the condensation chamber through the bottom of the furnace.

The electrolytic cell shown can reduce approximately 15 g of magnesium per hour when operated at an anode current density of 1 A/cm^2. In the configuration shown, the maximum capacity of the condensation chamber is approximately 200 g of magnesium if the metal is collected as a liquid. In an early trial of this apparatus, the cell was held at a constant voltage of approximately 4 V for 5.25 hours. Figure 6 shows the cell current as a function of time during this period.

Subsequent evaluation of the resistances of the component parts of the electrolytic cell indicated that the combined resistance of the anode and cathode electrical leads was on the order of 0.27 to 0.29 ohms. Therefore, at the currents depicted in Figure 6, the voltage drop within the electrical leads to the cell was on the order of 1.9 to 2 V, and the actual potential applied to between the electrodes was on the order of 2 V. This point is critical in evaluating the energy efficiency of the process and will be compensated for in future experiments.

The drop in current during this potentiostatic hold is due to the fact that the MgO content in the flux is decreasing as it is being electrolyzed. If continuous MgO feed to the reactor could be maintained, then one would obtain a steady-state current. During the experiment depicted in Figure 6, approximately 35 amp-hours of charge were passed through the system, theoretically reducing 15 to 16 g of magnesium. Following the completion of this experiment, the condensation chamber was disassembled for inspection. Although the precise weight of the metal produced (shown in Figure 7) was not determined, the approximate weight was found to correspond well with the theoretical prediction, thus indicating that the Faradayic efficiency of the process is high. The low cell potential and high current efficiency of the process suggests that the specific power requirements of a commercial process based upon the SOM technology will be low. A goal of future electrolysis experiments using this apparatus is to accurately quantify both the current efficiency and specific power consumption of the SOM process.

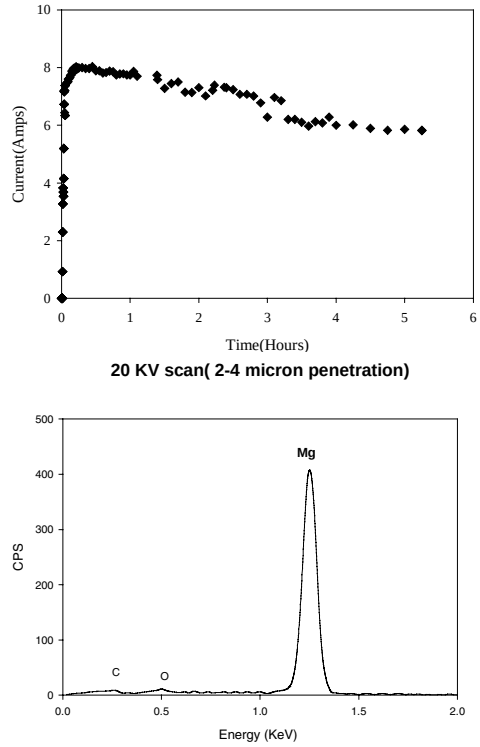

Figure 6. Cell current of the electrolytic cell shown in Figure 5 as a function of time during a potentiostatic hold at 4 V.

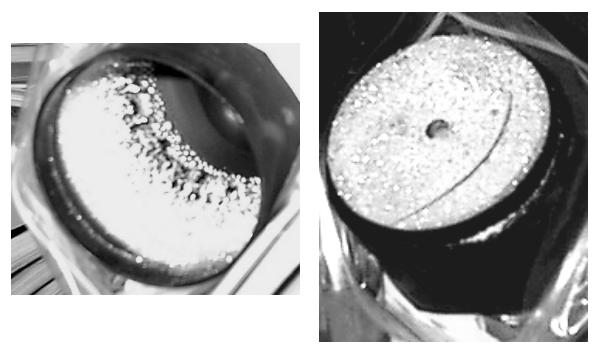

Figure 7. Condensed magnesium and its analysis.

Future Program Tasks

1. Modify the existing SOM test-reactor to accommodate continuous feeding of MgO source material for long-term operation of the SOM system. It will be used to determine and model the long-term stability of the stabilized zirconia membrane and the materials of construction of the scalable SOM reactor.
2. Conduct 150-hour static experiments to determine the effect of MgO content (2–10 w%) in the flux on the membrane and its influence on mass-transfer properties through impedance spectroscopy and post-experiment micro-structural evaluation. This information will be used to identify the optimum MgO content to study membrane stability under dynamic conditions.
3. Conduct 400-hour dynamic experiments by exposing 1 cm^2 of the membrane at 1300ºC and current densities on the order of 0.8-1A/cm^2 as a function of varying fluid-flow pattern around the exposed membrane in the SOM cell. These experiments will involve real-time impedance measurements and post-experiment micro-structural evaluation. The results will be used to determine and model the long-term membrane stability as a function of fluid-flow conditions in the flux.
4. At the end of the Task 3 experiments, micro-structurally evaluate the cathode and the condenser materials to determine viability for long-term use of these materials in the SOM reactor.
5. Use results obtained from the preceding tasks to formulate a detailed cost model to determine the competitive advantages of the SOM process for industrial-scale magnesium production over existing processes. This task will be performed in consultation with our industrial partner, Magnesium Corporation of America.

References

1. U. B. Pal and S. C. Britten, U.S. Patent 5,976,345, November 2, 1999, Boston University, Boston.
2. U. B. Pal and S. C. Britten, U.S. Patent 6,299,742, October 9, 2001, Boston University, Boston.
3. R. W. Minck, U.S. Patent 4,108,743, August 22, 1978, Ford Motor Company, Detroit.
4. D. S. Poa, L. Burris, R. K. Steunenberg, and Z. Tomczuk, U.S. Patent 4,995,948, February 26, 1991, U.S. Department of Energy, Washington, D.C.
5. A. F. Sammuels, U.S. Patent 4,804,448, February 14, 1989, Eltron Research, Aurora, Ill.
6. B. Marincek, U.S. Patent 3,692,645, September 19, 1972, Swiss Aluminum Ltd., Chippis, Switzerland.
7. D. E. Woolley, U. B. Pal, and G. B. Kenney, "Electrowinning Magnesium Metal from $MgCl_2$-NdOCl Melt Using SOM Technology," in *Proc. of the International Symposium on Molten Salts, Slags and Fluxes*, ed. S. Seetharaman, Stockholm, Sweden, ISS-TMS Publication, 2000 (CD-ROM).
8. D. E. Woolley, U. B. Pal, and G. B. Kenney, "Emerging SOM Technology for the Green Synthesis of Metals from Oxides," *Journal of Metals*, October 2001, 32–35.
9. S. Yuan, U. B. Pal, and K. C. Chou, "Modeling and Scaleup of Galvanic Deoxidation of Molten Metals Using Solid Electrolyte Cells," *J. of American Ceramic Society*, **79**(3), 641–650 (1996).
10. P. Soral, U. B. Pal, and H. R. Larson, "A Pilot Scale Trial of Improved Galvanic Deoxidation Process for Refining Molten Copper," *Metallurgical and Materials Transactions*, **30B**(2), 307–321 (1999).
11. S. B. Britten and U. B. Pal, "Solid State Amperometric Sensor for the In-Situ Monitoring of Slag Composition and Transport Properties," *Metallurgical and Materials Transactions*, **31B**(4), 733–753 (2000).
12. U.B. Pal et al., "Behavior of Ceria as an Actinide Surrogate in Electroslag Remelting and Refining Slags," *Metallurgical and Materials Transactions*, **32B**(6), 1119–1131 (2001).
13. T. Kennan, C. P. Manning, U. B. Pal, D. E. Woolley, A. Krishnan, and G. B. Kenney, "Solid-Oxide-Oxygen-Ion-Conducting Membrane (SOM) Technology for Green Synthesis of Magnesium from Its Oxides," *Magnesium Technology 2002*, TMS, 19–24, 2002.
14. U. B. Pal, A. Krishnan, T. Keenan, C. P. Manning, "Solid-Oxide-Oxygen-Ion-Conducting Membrane (SOM) Technology for Green Synthesis of Metals from Their Oxides," in *Proc. of the High Temperature Materials Symposium in Honor of the 65th Birthday of Professor Wayne L. Worrell*, ECS, 94–101, 2002.

F. Understanding the Economics of Emerging Titanium Production Processes

Principal Investigator: Randolph E. Kirchain
Camanoe Associates
P.O. Box 425242, Cambridge, MA 02142
(617) 253-4258; fax: (617) 258-7471; e-mail: kirchain@mit.edu

Principal Investigator: Richard Roth
Camanoe Associates
P.O. Box 425242, Cambridge, MA 02142
(617) 253-6487; fax: (617) 258-7471; e-mail: rroth@mit.edu

Jacqueline Isaacs
Northeastern University
305 Snell Engineering Center
Boston, MA 02115
e-mail: jaisaacs@coe.neu.edu

PNNL Contract Manager: Russell H. Jones
(509) 376-4276; fax: (509) 376-0418; e-mail: rh.jones@pnl.gov

Technology Development Manager: Joseph A. Carpenter
(202) 586-1022; fax: (202) 586-1600; e-mail: joseph.carpenter@ee.doe.gov
Field Technical Manager: Philip S. Sklad
(865) 574-5069; fax: (865) 576-4963; e-mail: skladps@ornl.gov

Participants
Professor Joel P. Clark, Department of Materials Science and Engineering, Massachusetts Institute of Technology
Frank R. Field III, Center for Technology Policy and Industrial Development, Massachusetts Institute of Technology

---

Contractor: Camanoe Associates
Contract No.: 406372-AU7

Objective

- Explore the potential for the widespread adoption of titanium in automobile structures by understanding the manufacturing economics of emerging processes for its production and of forming it into parts.

Approach

- Identify promising titanium production processes. These include
  - Plasma quench process being developed by Plasma Quench Titanium, Inc.
  - Armstrong process being developed by International Titanium Powders (ITP)
  - FCC (Cambridge) process being developed by British Titanium
- Catalog the technical fundamentals of processes of interest and their potential for technological development.
- Develop process-based cost models for each of the titanium production processes.

- Use the cost models to explore the behavior of the manufacturing economics of each process.
- Identify a probable potential lowest production cost for each process.
- Develop a process-based cost model of automotive parts production using titanium.
- Use the cost model to reveal the cost drivers associated with titanium parts production.

Accomplishments

- Constructed cost models of plasma quench, Armstrong, and FCC processes.
- Analyzed the economic behavior of each process, including quantifying parametric sensitivity and identifying key cost drivers.
- Assessed titanium production cost under likely current, pessimistic, and optimistic development of each technology.
- Constructed a cost model of hot isostatic pressing.
- Analyzed the sensitivity of part production cost to key cost drivers.
- Generated and delivered a report summarizing these results.

Introduction

An automobile design trend receiving much attention is the reduction of vehicle mass. Reducing mass can improve both performance and fuel economy. Although design changes can play a large role in reducing mass, large reductions ultimately will require the substitution of higher-specific-strength/stiffness materials in place of the now universal carbon steel. Primary contenders in this race are high-strength steels, aluminum, and fiber-reinforced polymer composites. One material that is not on this short list but that could provide even greater reductions is titanium. Although titanium is light and strong, its role in the automobile has been almost nonexistent because of its exorbitant price. The high price is a direct result of the current production route, the Kroll process, which is time-consuming; energy-, capital-, and labor-intensive; and batch-based.

However, new technologies are emerging that may change the characteristics of the titanium market. In particular, these technologies may reduce the price of titanium sufficiently to allow it to compete in high-volume markets, possibly even automotive markets. This project examines the production costs for three of these technologies in detail.

Project Deliverables

Three processes have been identified by the Northwest Alliance for Transportation Technologies Program as having the potential to significantly reduce the cost of producing titanium:

- Plasma quench
- Armstrong
- FCC

Process-based cost models were created for each of these processes to aid understanding of the economics of the processes. To understand how changes in raw material price ultimately impact part cost, a model of a part-forming process, hot isostatic pressing, was developed.

Planned Approach

Because all three processes represent technologies that are not yet implemented at full manufacturing scale, traditional accounting-based approaches to costs are ineffective. However, a set of methods, collectively referred to as technical cost modeling, has been developed for addressing just such questions. Technical cost models (TCMs) derive manufacturing costs by building up from the engineering realities of a process. Specifically, TCMs combine engineering process models, operational models, and an economic framework to map from details of product and process to operating

costs. Because TCMs are built around technical details, they allow an exploration of how costs evolve as a technology changes. The TCM approach was adopted for this project because of its obvious applicability.

Analysis Summary

Cost analyses of these processes proved to be very promising. Figures 1, 2, and 3 give a summary look at these costs for the baseline scenarios considered. In these charts, the label "Dense" indicates producing briquettes by lightly sintering powders. As the diagrams show, all three processes can deliver titanium powder well below the prevailing market price. Under a range of operating conditions, these processes could in fact manufacture powder for less than the selling price of sponge today.

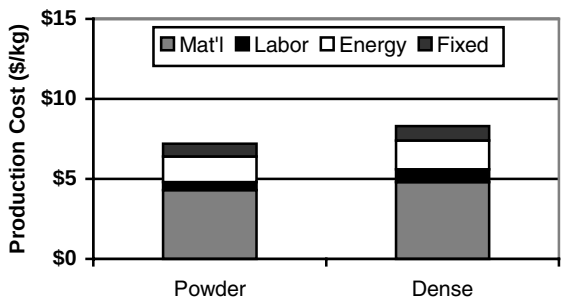

Figure 1. Baseline cost breakdown by major elements for plasma quench process.

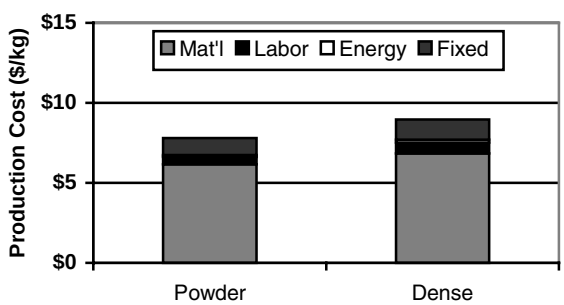

Figure 2. Baseline cost breakdown by major elements for Armstrong process.

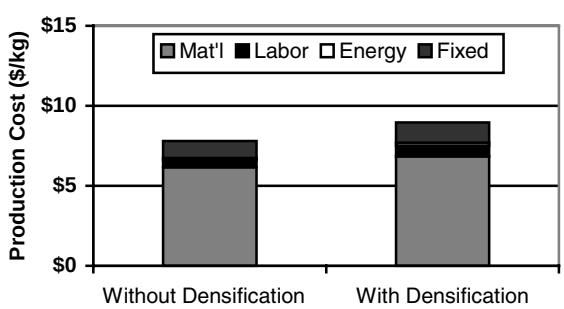

Figure 3. Baseline cost breakdown by major elements for FCC (Cambridge) process.

Plasma Quench Process

The plasma quench process involves the thermal dissociation and reduction of titanium tetrachloride ($TiCl_4$). This is accomplished by passing these reactants through an electric arc. The resulting plasma is drawn through a Delaval nozzle. The nozzle accelerates and expands the gas, quenching it rapidly enough to prevent significant back-reaction. The actual output from the plasma quench process is in fact titanium hydride (TiH_{1-2}), which contains ~97% titanium (by weight) and HCl.

The principal costs for the plasma quench process are

- $TiCl_4$
- electricity
- quench gas
- capital expenditures

In addition to the sale of titanium powder, HCl can provide a significant source of revenue.

In addition to a number of specific analyses, the economic performance of the plasma quench process was investigated under three development scenarios: (1) optimistic development, (2) likely current implementation, and (3) pessimistic development.

Figure 4 shows the production costs associated with each of these scenarios. Notably, using optimistic assumptions, the cost of titanium powder production falls nearly to half of the current price of sponge. Furthermore, although the range from "Optimistic" to "Pessimistic" cost covers nearly a factor of three, the "Pessimistic" result is still well below prevailing prices for titanium powder.

Armstrong Process

The process used at ITP, referred to as the Armstrong process, involves the reaction of gaseous $TiCl_4$ with sodium to produce titanium. In realizing this process, ITP's clear breakthroughs are permitting continuous operation of the process and the capability to produce powder directly. Since the product is in powder form, ITP can much more readily and effectively extract the titanium from the

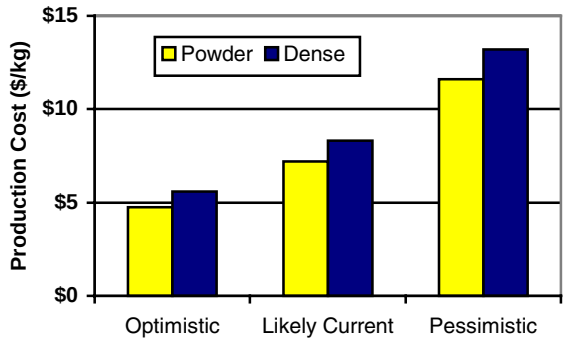

Figure 4. Plasma quench process costs across development scenarios.

byproduct NaCl and any remaining sodium. Because of the strong exothermic nature of the reaction, the primary energy demands derive not from initiating the process, but rather from cooling its products.

The principal costs for the Armstrong process are

- $TiCl_4$
- sodium
- capital expenditures

In addition to the sale of Ti powder, NaCl can provide a source of revenue, albeit a small one.

Figure 5 shows production costs for the Armstrong process across the scenarios investigated. Again, all cases represent notable decreases in titanium production cost, with the optimistic scenario coming in below current Kroll sponge production costs.

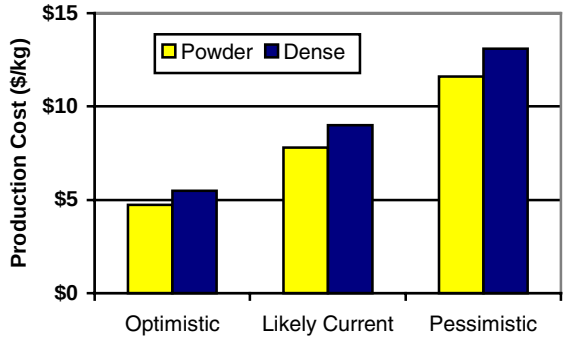

Figure 5. Armstrong process costs across development scenarios.

FCC Process

The FCC process involves the electrochemical reduction of titanium dioxide (TiO_2) in a molten salt bath. From the perspective of this analysis, the FCC process is the least developed and, therefore, the most speculative. The novelty of this process lies in its ability to produce titanium directly from native oxides, potentially affording significant savings in feedstock costs. To enable the maximum economic benefit from this feature of the process, lower-cost oxide ores must be used. Because impurities within the feedstock remain entrained in the metal product in this process, alloys produced from these ores (although much less costly to produce) may not be suitable for all applications. Another disadvantage of this process is the additional equipment and processing required to prepare the solid oxides for convenient electrochemical processing.

Preliminary analysis suggests that the principal costs for the FCC process are:

- TiO_2
- electricity
- capital expenditures

The significance of capital expenditures remains a great uncertainty for this process because of its early stage of development. Despite these concerns, as Figure 6 reveals, the FCC process offers great promise for delivery of powder or solid material at prices much below today's market.

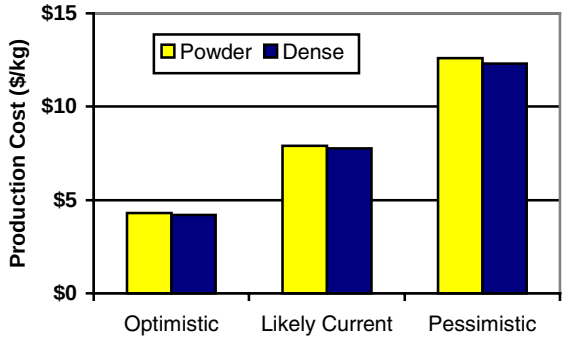

Figure 6. FCC (Cambridge) process costs across development scenarios.

G. Preparation of Closed Metal Cell Composites

Gerhard E. Welsch
Case Western Reserve University
10900 Euclid Avenue, Cleveland, OH 44106
(216) 368-4236; fax: (216) 368-3209; e-mail: gxw2@po.cwru.edu

E. Lidong
Case Western Reserve University
10900 Euclid Avenue, Cleveland, OH 44106
(216) 368-6492; e-mail: lxe10@po.cwru.edu

Technology Development Manager: Joseph A. Carpenter
(202) 586-1022; fax: (202) 586-1600; e-mail: joseph.carpenter@ee.doe.gov
Field Technical Manager: Philip S. Sklad
(865) 574-5069; fax: (865) 576-4963; e-mail: skladps@ornl.gov

Contractor: ORNL, Case Western Reserve University
Contract No.: DE-AC05-00OR22725, 4000017402

Objective

- Determine the feasibility of synthesizing cells from graphite and iron oxide and demonstrate that graphite/iron cells can be fabricated economically.

Approach

- Prepare slurry—fine-ground hematite ore powder mixed with binder (polyethylene glycol solution 400NF).
- Coat slurry onto graphite pellets approximately 5 mm diameter.
- Remove binder and dry the coated pellets at 250°C for 0.5 hours.
- Reduce the dried pellets in a retort with carbon powder at 900°C for 6 or 24 hours. Sintering occurs at the same time.

Accomplishments

- Determined the feasibility and parameters of synthesizing cells by coating iron oxide onto graphite pellets followed by reduction. Characterized the cell wall in terms of morphology, composition, wall thickness, and density, using metallography, scattering electron microscopy (SEM) and energy-dispersive spectroscopy (EDS).

Future Direction

- Consider experimental methods to reduce cracks that appear in the iron cell walls after reduction for 24 hours at 900°C, probably as a result of shrinkage during sintering.
- Form composite by hot compaction of cells.

Background

As a major component of the Department of Energy's Office of FreedomCAR and Vehicle Technologies, Automotive Lightweighting Materials focuses on the development and validation of advanced lightweight materials technologies to

significantly reduce automotive body and chassis weight without compromising other attributes such as safety, performance, recyclability, and cost. A specific class of engineered materials—which includes sandwich materials, metal foams, and honeycombs—offers the potential for ultra-lightweight components. In addition, these materials can offer improved energy management capabilities for crashworthiness.

Closed metal cell composites that have a lightweight core and a metallic wall have potential as lightweight structural materials that can compete with cast iron, powder metallurgical composites, and lightweight honeycomb-stiffened structures, as well as with foamed metals. The cells can be used as a filler in hollow components for their light weight, flexural and torsional rigidity, and vibration damping. Cell composites could also be used in parts that need tailored functional and mechanical properties. These composites are distinguished from honeycombs or foams because they contain a filler substance in the cells that imparts compressive strength and crushing resistance, which may enhance their ability to absorb energy. The constituent materials of the cell cores and cell walls control the physical, thermo-physical, and mechanical properties of the materials. The volume fraction, shape, packing arrangement, and degree of compaction can be varied to produce cell composites with densities of as low as 2.5 g/cm^3 and as high as 7 g/cm^3. Understanding how the constituent materials and their geometric arrangements control the properties of the composite would enable tailoring of the "architecture" of such composites to meet specific performance targets.

This activity will focus on determining the feasibility of synthesizing cells from graphite and iron. The study will demonstrate the fabrication of cell cores and the deposition of metallic cell walls. It will enable an assessment of the cost of fabrication. On a commercial scale, the cost may be as low as $0.49 per kilogram or $1.25 per liter of cells. This cost compares with $0.40 per kilogram or $3.12 per liter of solid steel. In addition, the properties of the cell materials produced will be used to gage the potential of the process for further development.

Cells of graphite and iron will be synthesized in the study. First, graphite pellets will be formed. Hematite (Fe_2O_3) or magnetite (Fe_3O_4) powder will then be mixed with a binder (Figures. 1 and 2) and painted; or applied onto graphite particles (the cell cores) by dipping, spraying, or another method (Figures 3 and 4) and then dried (Figure 5) and reduced at an elevated temperature (Figure 6). Reduction of the oxide will result in spongy iron, the density of which is determined by the Pilling-Bedworth ratio (2.15 and 2.10 for hematite and magnetite, respectively) and by the degree of densification of fine-grained iron sponge during sintering. The resulting cell wall is spongy iron. Further densification would occur during

Figure 1. Hematite ore powder (M ≈ 1X).

Figure 2. Slurry of hematite powder and binder (M ≈ 1X).

Figure 3. Graphite pellets (M ≈ 1X).

Figure 4. Coated pellets (M ≈ 1X).

Figure 5. Pellets after removal of binder (M ≈ 1X).

Figure 6. Sintered and reduced pellets (M ≈ 1X).

compaction and hot compression of cells into a composite. The demonstration is focused on proving the technology of fabricating graphite/iron cells from low-cost materials.

Morphology Analysis of Cell Wall

Cells were made by coating and reducing iron oxide on 5-mm diameter carbon cores (Figure 7). The cell walls had a thickness of between 0.5 and 0.9 mm. Figures 8 and Figure 9 show the external surfaces of cell walls after reduction with carbon at 900°C for 6 and 24 hours, respectively. The cell wall consists of spongy iron. The density of the sponge iron increases with increasing reduction time.

Figures 10 and 11 show optical images of cross-sections through the sponge-iron cell walls in Figures 8 and 9. In addition to densification, they show increased degree of reduction after a prolonged (24-h) reduction time.

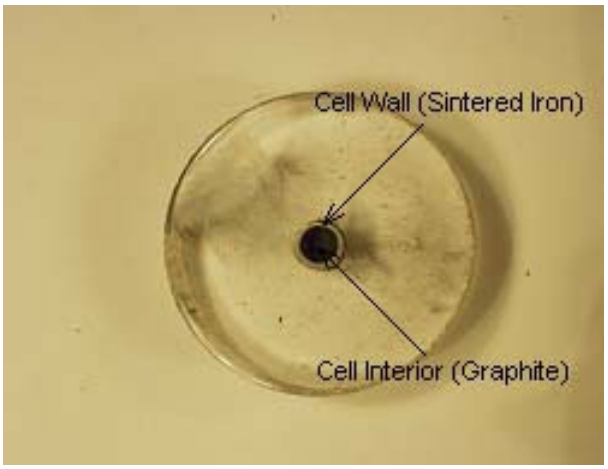

Figure 7. A cross-section through a metallographically mounted pellet, showing the cell interior (graphite) and cell wall (sintered iron).

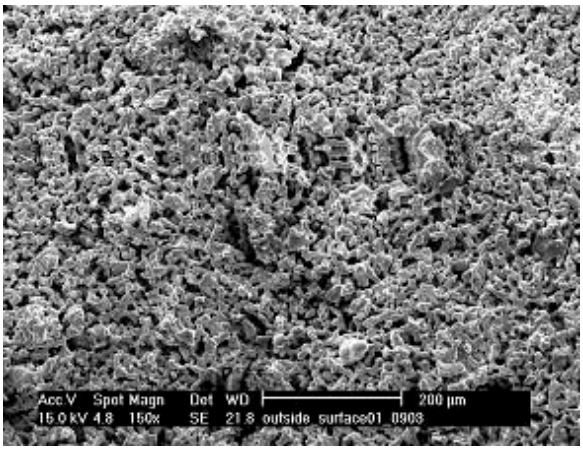

Figure 8. SEM micrograph of porous outer surface of iron cell wall. Reduction treatment: 6 h at 900°C (M = 200X).

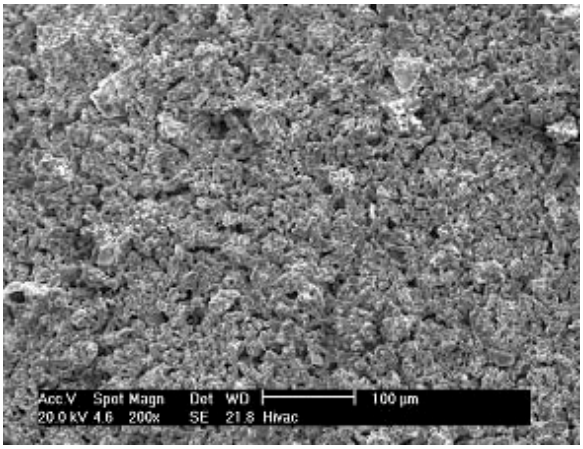

Figure 9. SEM micrograph of outer surface of an iron cell wall. Reduction treatment: 24 h at 900°C with CO (M = 200X).

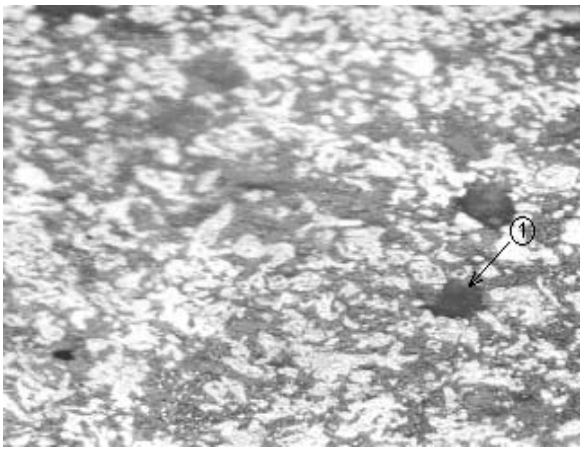

Figure 10. Optical micrograph of as-polished cross-section of cell wall. Reduction for 6 h at 900°C (M = 500X)

Figure 11. Optical micrograph of as-polished cross-section of cell wall. Reduction for 24 h at 900°C (M = 500X).

Composition Analysis of Cell Wall

An EDS analysis of the composition of hematite ore powder is shown in Figure 12. Silicon exists as an impurity in the powder. Most of the silicon is in the form of SiO_2, according to the analysis.

EDS analyses of the sponge-iron cell wall after 6 and 24 hours of reduction are shown in Figures 13 and 14, respectively. After reduction for 6 hours at 900°C in a bed of graphite powder, a significant amount of the iron oxide is still unreduced. After reduction for 24 hours, most of the iron oxide is reduced to metal.

The dark area labeled ① in Figure 10 consists of a silicon compound, according to the EDS analysis in Figure 15. Gray areas are mixtures of non-reduced iron oxide and a silicon compound. The silicon compound may be SiO_2 and/or SiC (grinding particles) that could have been smeared into the pores during grinding and polishing.

Conclusions

Work conducted so far has demonstrated the feasibility of synthesizing metallic closed cells by reduction of iron-oxide-coated graphite pellets. The cells can serve as building blocks of lightweight composites. The cell wall is spongy iron. The density of the spongy iron and degree of reduction increase with increasing reduction time. After reduction at 900°C in CO gas for 24 hours, most of the iron oxide is reduced.

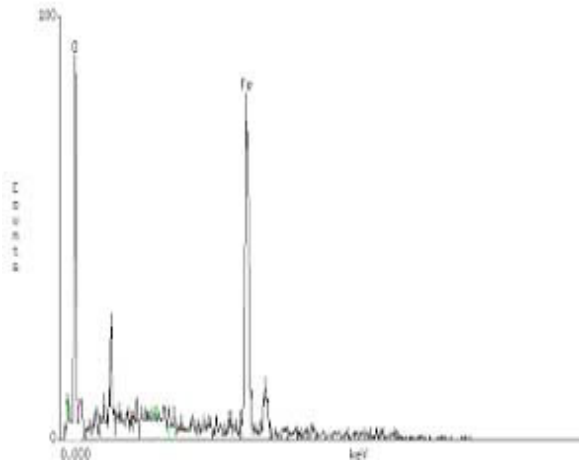

Element	k-ratio (calc.)	ZAF	Atom %
C-K	0.0093	3.055	8.00
O-K	0.1399	1.457	43.25
Ti-K	0.0082	0.982	0.57
Si-K	0.0152	1.346	2.47
P-K	0.0017	1.246	0.23
Cl-K	0.0049	1.100	0.52
Ca-K	0.0017	0.964	0.13
Fe-K	0.6734	1.076	44.02
Mg-K	0.0028	2.068	0.80
Total			100.00

Figure 12. An energy-dispersive spectroscopy analysis of the composition of hematite ore powder.

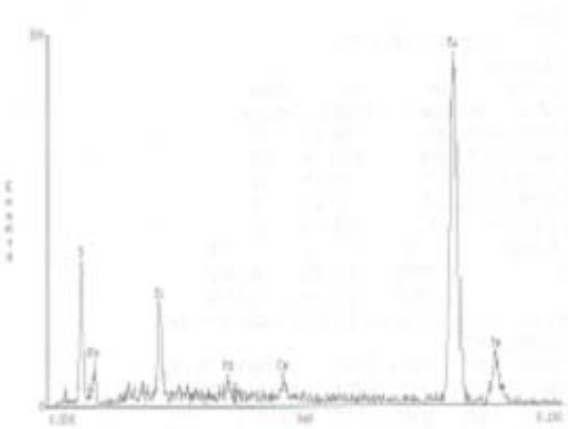

Element	k-ratio (calc.)	ZAF	Atom %
O-K	0.076	2.104	35.83
Fe-K	0.7029	1.106	47.88
Si-K	0.0305	1.796	7.00
C-K	0.0060	4.522	8.17
Ca-K	0.0125	0.992	1.11
Total			100.00

Figure 13. Energy-dispersive spectroscopy analysis of the sponge-iron cell wall after 6 hours of reduction.

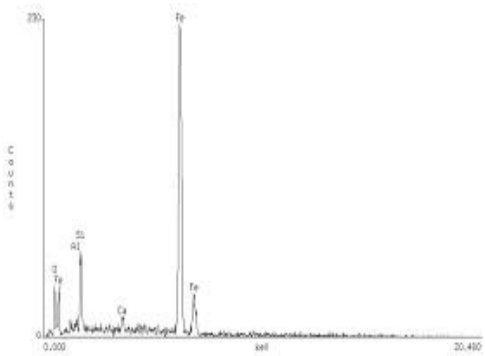

Element	k-ratio (calc.)	ZAF	Atom %
C-K	0.0044	4.650	7.16
O-K	0.0340	2.065	18.32
Si-K	0.0339	1.739	8.77
Ca-K	0.0140	0.973	1.41
Fe-K	0.7841	1.041	60.98
Mg-K	0.0040	3.143	2.18
Al-K	0.0032	2.323	1.16
Total			100.00

Figure 14. Energy-dispersive spectroscopy analysis of the sponge-iron cell wall after 24 hours of reduction.

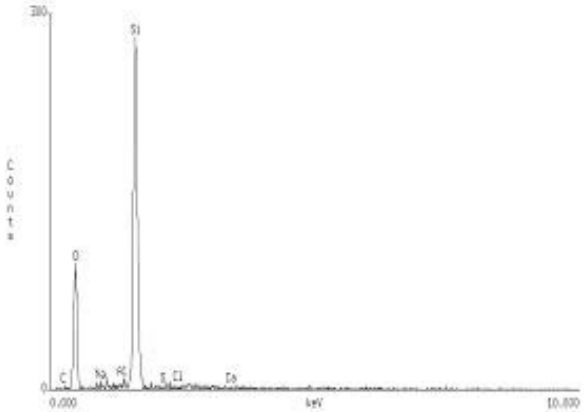

Element	k-ratio (calc.)	ZAF	Atom %
O-K	0.2496	2.161	67.28
Si-K	0.3898	1.182	32.72
Fe-L	0.0000	2.335	0.00
C-K	0.0000	9.051	0.00
Total			100.00

Figure 15. Energy-dispersive spectroscopy analysis showing that the dark area in Figure 10 consists of a silicon compound.

H. Structural Reliability of Lightweight Glazing Alternatives

Principal Investigator: Moe Khaleel
Pacific Northwest National Laboratory
(509) 375-2438; fax: (509) 375-6605; e-mail: moe.khaleel@pnl.gov

PPG Project Manager: Rick Rueter
(412) 820-8731; fax: (412) 820-8705; e-mail: rueter@ppg.com

Visteon Project Manager: Mike Brennan
(313) 755-1879; fax: (313) 755-7485; e-mail: mbrenna1@visteon.com

Technology Development Manager: Joseph Carpenter
(202) 586-1022; fax: (202) 586-1600; e-mail: joseph.carpenter@ee.doe.gov
Field Technical Manager: Philip S. Sklad
(865) 574-5069; fax: (865) 576-4963; e-mail: skladps@ornl.gov

---

Contractor: Pacific Northwest National Laboratory
Contract No.: DE-AC06-76RL01830

Objectives

- Optimize glazing systems for cars of the future by decreasing sound transmission while maintaining structural rigidity.
  - Reduce sound transmitted through sidelights by 6 db by determining the effect of sidelight shape on sound transmittance, investigating sound-dampening materials for operating sidelight glazing, and quantifying the influence of alternate materials (e.g., laminated glass, bi-layer glass) on sound attenuation.
  - Maintain the level of structural integrity while reducing glass thickness by validating the structural rigidity model for various types of urethane used in fixed glazing systems and by expanding/ combining existing models to test various alternative constructions and glazing systems for side, rear, and roof windows.
- Reduce vehicle weight through alternate or thinner vision panels and/or by reducing the heat load transmitted through the glass. The goal is to improve the fuel economy of a car by requiring 30% less glass weight.
- Reduce side, rear, and potentially roof window glass weight while maintaining acoustics and minimizing price increases.
  - Consider several material options, including laminated glass, cast-in-place pseudo-laminated glass, and bi-layer materials.
  - Enhance fuel economy from reduced solar energy transmission.
  - Reduce solar energy transmission through glass by using absorbing substrates and reflective coatings.
  - Quantify gas mileage improvement opportunities from improvement in solar energy transmission.

Accomplishments

- Fabricated new lightweight windshield and side-body glasses that are 30% lighter than conventional glazing systems.
- Fabricated new glass with polyvinyl butyral (PVB) thickness ranging from 0.5 to 0.76 mm.
- Determined the contribution of the glazing system to overall car rigidity.
- Developed new tests for measuring bending and edge strength of finished windshield specimens and measuring stone impact.
- Determined the tin/air side strength and the effect of temperature on glazing strength.

- Developed models to simulate the through-thickness damage evolution in monolithic and layered glass subjected to blunt and sharp indentors.
- Designed a new computational tool for design of lightweight glass.

Future Direction

- Develop lightweight side-door glass.
- Study asymmetric glass construction and/or the use of coatings to harden the outer surface of glass for weight reduction.
- Investigate the effect of strength and thickness of PVB on overall windshield/side-door strength and performance.
- Investigate the overall thermal behavior based on the new lightweight glass, including the effect of the laminated side-door glass.
- Characterize the strength of the new lightweight glass.
- Verify and extend the predictive stone impact models to investigate the effect of the impact of sharp indenters on glass.
- Enhance and extend the numerical tool for design of lightweight glass to include stresses encountered during fabrication of glass.
- Develop a methodology for modeling acoustical response of glass.

Introduction

This project is a cooperative research and development agreement (CRADA) between the U.S. Department of Energy, Pacific Northwest National Laboratory (PNNL), Visteon Automotive Systems (Glass Division), and PPG, Inc. It started in June 2002.

The project will evaluate designs for optimized glazing systems to be used in cars of the future and will work to achieve the goals of FreedomCAR. The primary objective of the project is to reduce vehicle weight, improve fuel economy, and reduce vehicle emissions. However, to achieve these goals, it is necessary to consider the needs for high levels of structural reliability, competitive manufacturing costs, and passenger comfort from the standpoints of minimal acoustical noise levels and controlled interior temperatures. Energy savings will come from reducing weight by using thinner glazing; prior studies at PNNL have shown a potential for 30% reductions in weight from thinner glazing. Energy savings will also come from reducing interior heat loads; that, in turn, will reduce the demand for air conditioning. The evaluation of alternative glazing concepts will also seek means to improve acoustical characteristics that will minimize interior noise levels while maintaining glazing at minimal thickness and weight levels.

Lightweight Glass Manufacturing

New lightweight windshield glass was fabricated using 1.6-, 1.8-, 2.0-, and 2.1-mm glass plies (a conventional automotive glass ply has a thickness of between 2.4 and 2.6 mm; total windshield thickness is usually over 5.2 mm). The new glass was formed and laminated at the Visteon Tulsa Plant. The new glass constructions were

- 2.1-mm glass, 0.76 mm PVB, and 1.6 mm glass (29% weight reduction)
- 1.8-mm glass, 0.76 mm PVB, and 1.8 mm glass (31% weight reduction)
- 2.0-mm glass, 0.76 mm PVB, and 1.8 mm glass (27% weight reduction)

New lightweight laminated side glass was fabricated using 1.6-mm, 2.1-mm, and 2.6-mm plies. The new side glass constructions were

- 1.6-mm glass, 0.76 PVB, and 1.6-mm glass
- 2.1-mm glass, 0.76-mm PVB, and 2.1-mm glass
- 2.6-mm glass, 0.76-mm PVB, and 2.6-mm glass (see Figure 1)

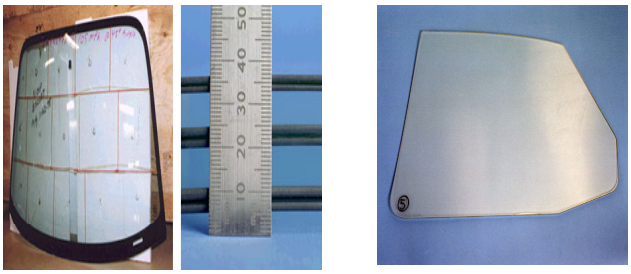

Figure 1. Lightweight glass materials windshield and sidelight.

Studies on other asymmetric glass constructions, coatings to harden the outer surface, and tempering will continue during FY 2003 and FY 2004. We will continue to seek more weight reduction while maintaining or enhancing side glass performance.

During the fourth quarter of FY 2002, researchers completed the initial conceptual design for injection molding of cast-in-place pseudo-laminates. We are currently fabricating a system to conduct the initial studies on the feasibility of resin injection between glass plates. A database on PVB alternatives for the injection molding process has been established by collecting information on clear polymer systems that could be used as potential interlayer materials. The database is based on commercially available materials. The evaluation of properties and cost is being addressed and documented in the database. These commercially available materials can be altered to specific characteristics once the core properties have been established. A table listing specific critical properties was created, and the properties were ranked by relative importance, such as impact, tear resistance, and optical transmission. The database of materials will then be compared with PVB as the baseline material. Since the optical requirements for the sidelight are not as stringent as those for the windshield, other materials may prove to be more attractive and cost-effective. The weighted comparison approach will help determine the direction in which PVB side lamination needs to go relative to the critical properties.

Contribution of Glass to Structural Rigidity

Experiments and models were conducted to determine the contribution of glass to overall car rigidity and the stresses transferred to the glass. The work focused on the 200 CW 170 Focus and the P2000 vehicles. Visteon Glass Division investigated strain induced in the windshield when it is subjected to road load vibration, body flex, and mechanical loading for a 200 CW 170 Focus. The vehicle was instrumented for strain and acceleration data acquisition. Three tests were performed consisting of road load data acquisition, direct mechanical loading of windshield, and torsional body flexure. Based on the observed strain, it does not appear that the loading methods produced significant strains in the windshield.

A finite element model of the P2000 body-in-white has been obtained from the Vehicle Safety Research Department at Ford. The model was obtained to study the contribution of the front windshield and back-glass to the P2000 overall rigidity, as well as the effect of the glass thickness and molding stiffness on both the glass contribution to overall rigidity and the loads transferred to the glass.

The analyses showed that the torsional rigidity of the P2000 is 24.29 kNm/deg with windshield and backlight glass and 16.44 kNm/deg without glass (i.e., the glass contributes about 30% to overall car rigidity). Reducing the glass thickness by 40% resulted in a minor reduction in the rigidity, which was 23.26kNm/deg .

Additional analyses were conducted to investigate the effect of glazing molding stiffness on the glazing system's contribution to the P2000's torsional rigidity. The results show that increasing the glazing molding stiffness results in a marginal gain in torsional rigidity, but decreasing the glazing molding stiffness results in a significant loss in torsional rigidity.

Strength Characterization

PNNL built unique experimental tools to measure (1) bending strength of finished windshield specimens, (2) edge strength of windshields, and (3) impact resistance with blunt and sharp indentors. The bending strength apparatus is similar to a standard ring-on-ring apparatus that produces a uniform bending stress in flat glass; however, the new device accommodates the radii of finished manufactured windshields. Extensive strain gage data and experimental windshield strength results have been made to validate the apparatus. Researchers measured the strength and flaw measurements for conventional automotive windshields in new and used conditions. They also

examined the effect of high-speed impact damage on windshield strength. The strength of single-glass plies, notably in the edge region, was also examined. The data were used to design lightweight glazing systems for future vehicles. These are some of the conclusions from the experiments on conventional used and new windshields:

1. The maximum strength of carefully handled new windshields approaches 30,000 psi.
2. The minimum strength of production-quality new windshields is 7500 psi, or 25% of maximum strength. This is comparable to the strength of used windshields with 53,000 road miles, indicating the severe handling damage during manufacturing.
3. The adhesion of the PVB layer is critical not only for containment of glass fragments during an accident but also for maximizing the load-bearing capacity of laminated windshields.
4. The well-bonded PVB layer transmits a membrane stress of as much as 21% of maximum tensile stress in each of the glass plies during ring-on-ring flexure tests.

Figure 2 shows the flexible ring-on-ring apparatus, and Figure 3 shows the edge strength test. Figure 4 shows the edge strength of single plies. We obtained minimum strength estimates of 29, 23 and 19 MPa at failure probabilities of 1×10^{-4}, 1×10^{-5}, and 1×10^{-6}, respectively. These are only 20 to 30% of the maximum edge strength of 86 Mpa, indicating the need for better control of edge quality during finishing and handling. The combination of edge

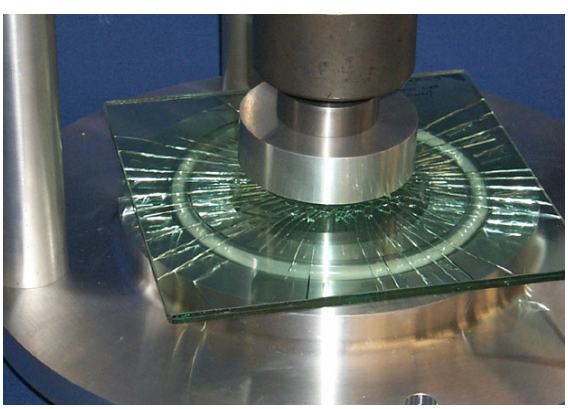

Figure 2. Photograph of the ring-on-ring apparatus during a test.

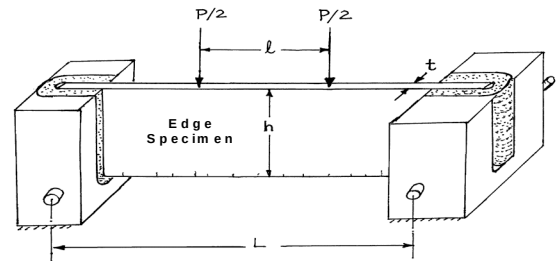

Figure 3. Edge strength test setup.

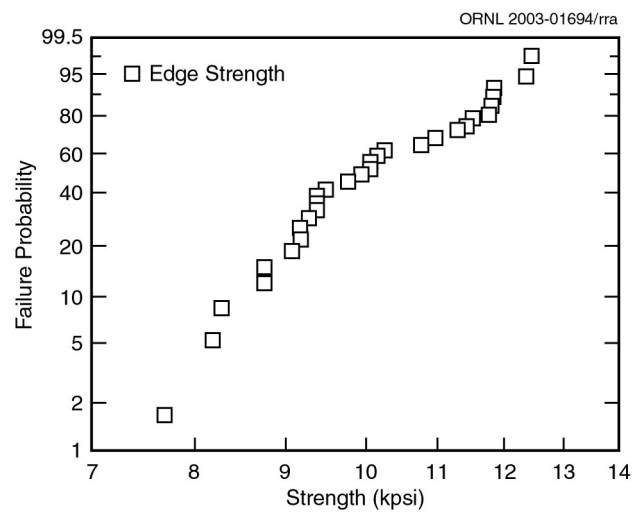

Figure 4. Weibull distribution of edge strength of single glass plies.

flaws, inner band residual tension, and bending stress induced by lamination can initiate premature cracking from the edge and undermine the long-term durability of the windshield. Such premature cracking is generally minimized by improving edge quality through diamond grinding and/or by introducing moderate levels of compression in the edge region by convective cooling following sag-bending of individual plies. Figure 5 shows the bending strength of square plate-glass specimens as determined using a concentric ring-on-ring test apparatus. These tests were conducted on single-ply sheets of soda-lime float glass (measuring $300 \times 300 \times 2$ mm thick) in ambient conditions at a crosshead speed of 1.27 mm/min. The key message conveyed by Figure 5 is that the air side is consistently stronger than the tin side. This may be helpful for manufacturing side-door glass because of the less restrictive optical requirements for side-door glass.

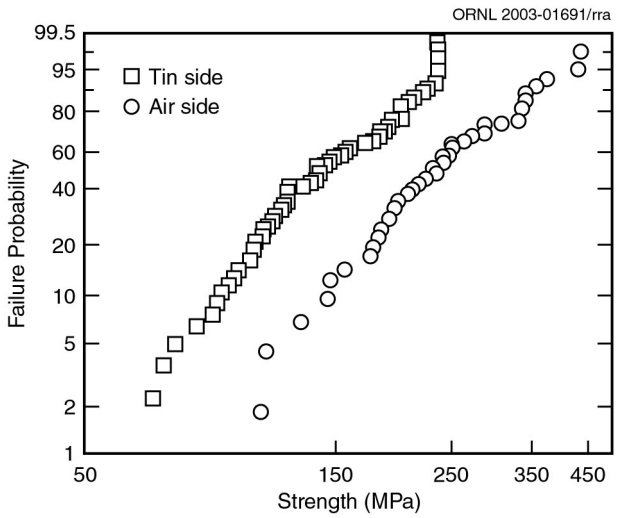

Figure 5. Weibull plot of strength distribution of tin vs air side of single plies.

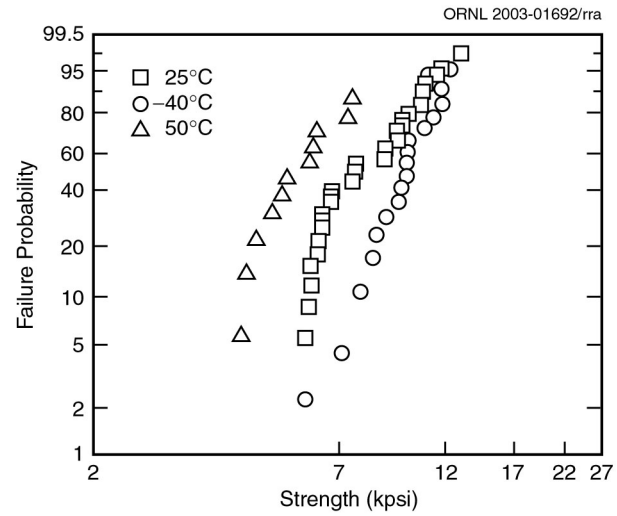

Figure 6. Weibull plot of strength distribution of new windshields.

Future windshield designs are required to be safer and more economical without compromising performance. In this regard, it is critical to understand the strength behavior of conventional laminated windshields under various operating conditions—notably temperature and relative humidity. All of the strength measurements were carried out in controlled-temperature environments and ambient humidity. The data in Figure 6, as might be expected, show that the biaxial strength is 28% lower at 50°C and 21% higher at –40°C than at room temperature. In addition, the scatter in strength data at 50°C is significantly higher than at 25°C and –40°C. Figure 7 shows the experimental setup for precision impact of glass (at up to 70 mph) and a representative result. PNNL has built this apparatus to experimentally investigate the response of automotive glazing to impact events. The apparatus uses a spring-loaded projectile launch system capable of firing symmetric or asymmetric projectiles. The system measures the speed of the projectile immediately prior to impact via two pairs of infrared beam sensors. The system precisely positions a strain-gage–instrumented single-ply or laminated glass sheet in the impact system and measures the dynamic response of the glass to the impact. The preliminary results show that a single-ply sheet of 3.6-mm glass develops 4000 psi of tensile stress on the glass sheet immediately opposite the impact event. The residual strength of an impact-damaged windshield was also measured using the ring-on-ring test. The residual strength distribution of a population made up of six impacted windshield specimens is shown in Figure 8.

A series of experiments were conducted with a ring-on-ring apparatus with variable loading rates to determine the influence of rate of loading and relative humidity on the strength of conventional automotive glass. The experiments consisted of applying loads at different speeds to glass specimens inside a ring-on-ring test system. The test conditions used for these experiments applied load on the ring-on-ring apparatus at load rates of 5000 lb/s, 10 lb/s, and 0.1 lb/s at ~17% relative humidity and room temperature. The results show that with increasing load rate, the apparent strength of the glass increases. Additionally, a second set of experiments was conducted at a 0.1 lb/s load rate, submerged in tap water, to determine the influence of humidity on the strength of glass under low rates of loading. The results for these submerged specimens show some degradation in the strength of the specimens due to the presence of water. A total of ~30 specimens from each sample population was tested; a statistical summary of all these populations is shown in Figure 9.

Windshield Resistance to Stone Impact

Axisymmetric finite element models were developed to simulate the windshield glass damage evolution when a windshield glass is subjected to impact loading of flying objects. The windshield glass consists of two glass layers laminated with a

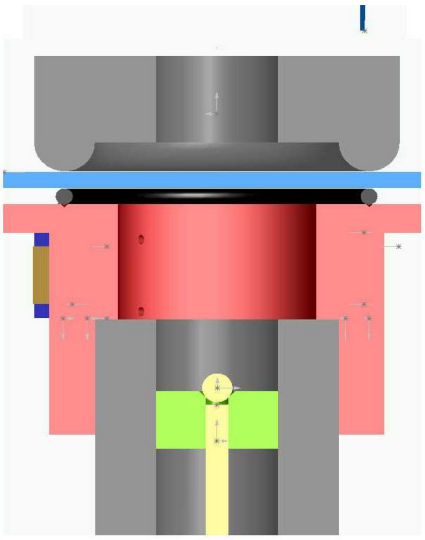

(a)

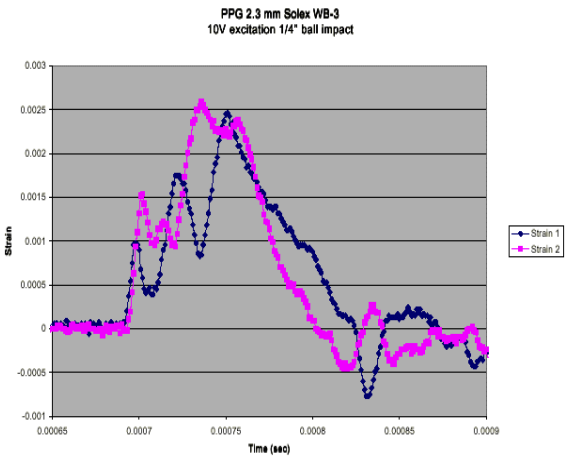

(b)

Figure 7. Impact apparatus (a) and measured strain histories (b).

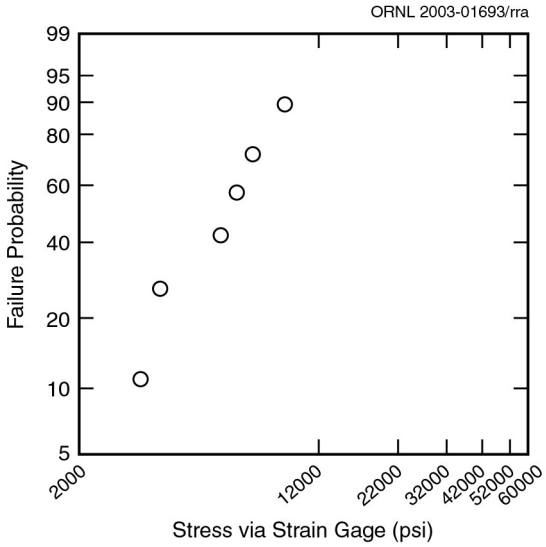

Figure 8. Residual strength distribution of impact-damaged windshield.

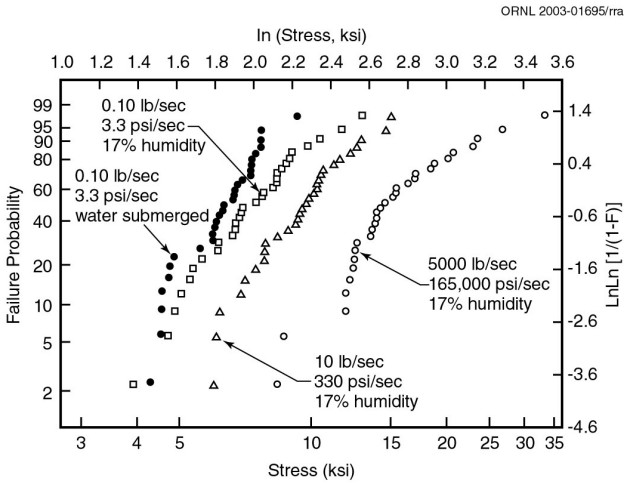

Figure 9. Effect of loading rate on the apparent strength of glass.

thin PVB layer. The model is used to predict and examine through-thickness damage evolution patterns on different glass surfaces and cracking patterns for different windshield designs, such as symmetric or asymmetric glass construction, thickness of glass plies, and curvature. These models are used to determine appropriate glass construction schemes that meet requirements such as strong resistance of the glazing to abrasion and impact of particles, while at the same time minimizing the weight of the glass.

Blunt Indentor

Stone impact experiments were performed for conventional and lightweight glass. The windshields were impacted with ¼-in.-diameter steel spheres to simulate windshield damage due to stone impact. These experiments were used to validate the models. Stair-stepping (threshold seeking) stone impact experiments were also performed to better determine values of parameters used in the models. Models were also validated using controlled experiments done at PNNL. Figure 10 shows a half-symmetry model, and Figure 11 shows the contour plots for web-shape damage for the tri-layered glass

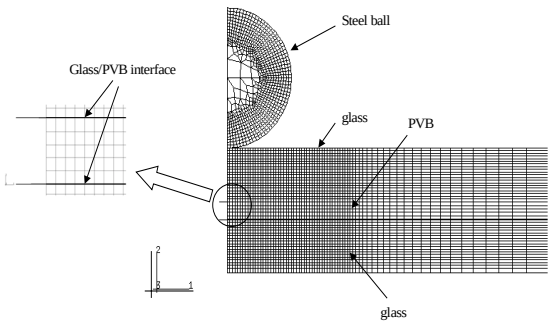

Figure 10. Half symmetry representation of the finite element model.

constructions under a ball-bearing impact of 60 mph. It was predicted that visible damage would be produced on surface 2 for all of the four tri-laminated cases. It is important to note that the least damage results when the thin piece of glass is used as the inside layer.

Sharp Indentor

A similar impact analysis procedure was used to study the impact resistance of different windshield constructions for sharp indentors, such as a diamond-tipped Vickers indentor. The angle of the indentor tip in the axisymmetric model was set to 68° to represent the face angles of 136° for a square-based pyramidal diamond. Impact velocity of the indentor was set to 12.5 mph. The outer glass ply was set to 2.3 mm. Two inner glass thicknesses are considered: 2.3 mm for symmetric construction and 1.3 mm for asymmetric construction. Figure 12 depicts the damage zone size and shape for the two thickness constructions. The conclusions for the sharp indentor were summarized as follows:

- The median crack forms right underneath the indentor during impact.
- No Hertzian cone is formed.
- There is no significant bending-induced damage.
- No significant differences of damage pattern and damage magnitude are observed if the inner layer thickness is reduced from 2.3 to 1.3 mm.
- Thinner, asymmetrical glazing systems sustain the impact slightly longer.

A Numerical Tool for Design of Lightweight Glass

A method for predicting structural failure probabilities for automotive windshields has been developed. The predictive model is supported by the data from strength tests performed on specimens of automotive glass. Inputs for stresses are based on finite element calculations or from measurements of the residual stresses that arise from fabrication. The failure probability for each surface or edge subregion of a windshield is calculated from the local state of stress, the surface area or length of the subregion, and the statistical distribution of glass strengths. Figure 13 shows failure probabilities for an entire windshield that result from residual stresses. This new tool will be used to design lightweight glass with reasonable reliability levels. Recent work has resolved concerns with the original probabilistic formulation and has validated the numerical results for cases of high failure probability. The work will now focus on applications of the failure prediction model. Data from PPG were obtained for measured edge strengths of laminated sidelight glass and for measured stresses induced by door slam tests. This information will be used as input to predict failure probabilities for the loading condition of concern. Results will be compared with results of similar calculations to be performed by PPG research staff.

Side Door Slam

A versatile door slam test fixture was constructed that is capable of applying realistic door slam loads using a fast-acting hydraulic actuator attached at the door latch. Figure 14 shows a Lincoln LS door mounted in the test fixture with the hydraulic ram attached at the latch point. The door hinges are bolted to a 3.5-in.-diameter steel post, and the hinge post is in turn bolted to a massive steel base plate that measures 3 ft × 5 ft × 4 in. thick. The hydraulic cylinder is supported between two additional posts, and it is attached to the latch assembly with a swivel coupling that allows bending and flexing during the door slam tests. The fast-acting cylinder is capable of accelerating the door to a velocity of 5 ft/sec. An extensometer was included in the system that allows recording of the displacement history of the latch mechanism.

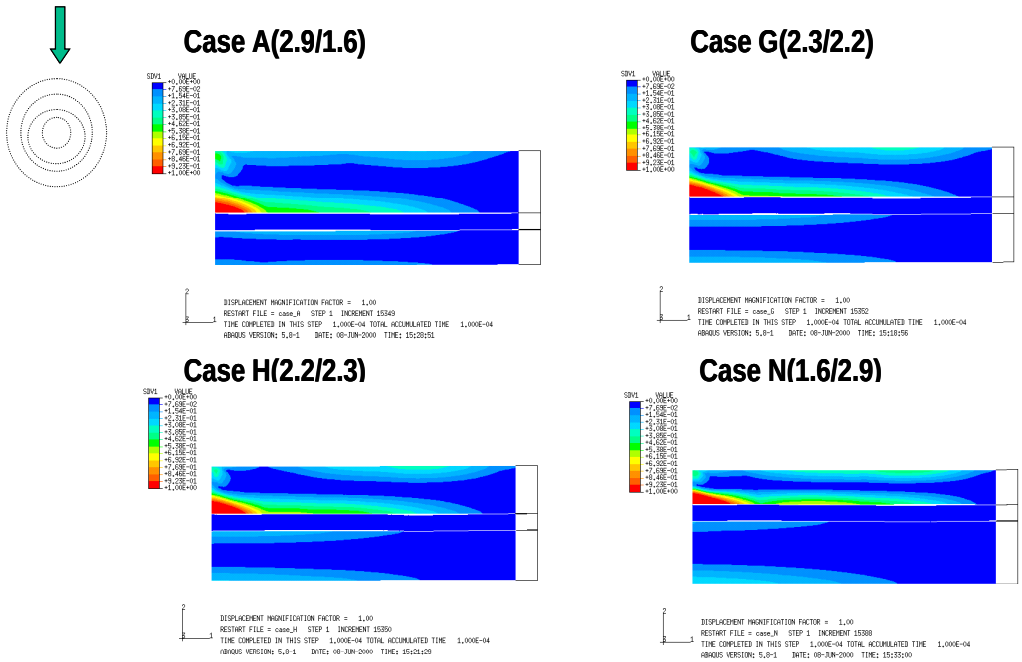

Figure 11. Contour plots of predicted damage for total thickness of 5.2 mm (web shape).

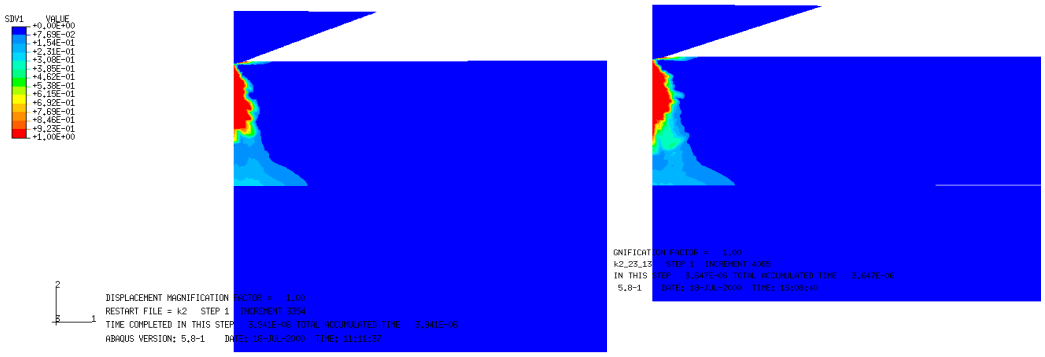

Figure 12. Contour plots of predicted circumferential damage for two windshield constructions subject to impact loading of a sharp, dart-type indentor.

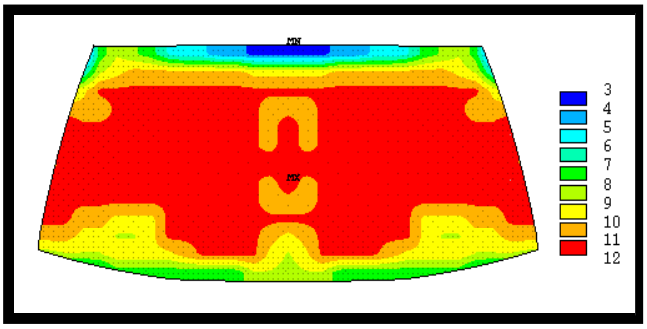

Figure 13. Predicted failure probabilities as a result of residual stresses (failure probability is 4.2E-05 because of edge flaws and 2.0E-07 because of surface flaws).

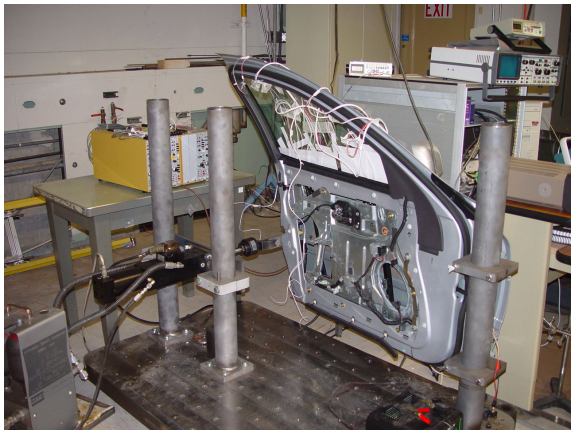

Figure 14. The door slam testing assembly.

Strain gages were attached to the inside surface of the sidelight before it was installed in the car door. Figure 15 shows the placement of the strain gages on the glass. A finite element model of the window was constructed to help strategically place the strain gages where stresses were predicted to be high. For conditions where the clips are held rigidly in the raising mechanism, high stresses were predicted near the corners of the attachment clips. Therefore, the location of the strain gages in the door slam test was determined accordingly (see Figure 15). Figure 16 shows the typical strain measurements.

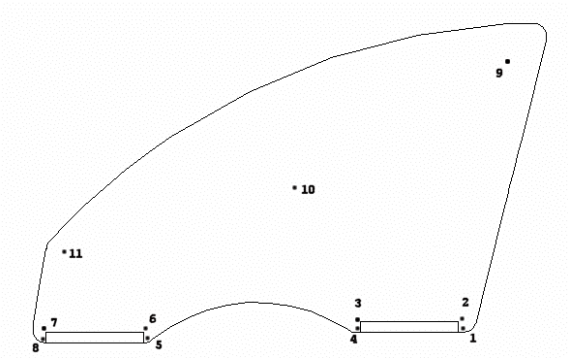

Figure 15. Placement of strain gages on the sidelight (convex side shown, gages are placed on concave side).

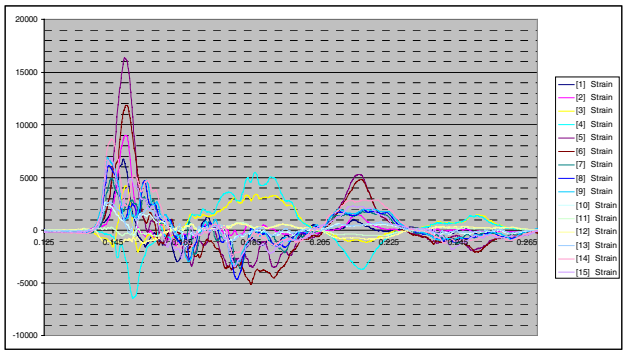

Figure 16. Measured strains from door slam test.

Future Work

Future work will focus on fabrication of lightweight glass using cost-effective manufacturing technologies. Researchers will continue to seek more weight reduction while maintaining or enhancing glass performance. The static and dynamic strength of the glass will be characterized and the computational models verified. The overall mechanical, thermal, and acoustical behavior of the new lightweight glass will be evaluated using both experimental and analytical procedures. Modeling efforts will continue to focus on stone-impact studies and acoustics. Work will also be conducted to enhance and extend the numerical tool for design of lightweight glass to include stresses encountered during the glass fabrication process.

I. Structural Cast Magnesium Development

Structural Cast Magnesium Development Project Chairman: Richard J. Osborne
General Motors Corporation
Mail Code 480-205-314
30007 Van Dyke Road
Warren MI 81033-57039
(586) 575-7039; fax: (586) 492-5115; e-mail: richard.osborne@gm.com

SCMD Project Administrator: D. E. Penrod
Manufacturing Services and Development, Inc.
4655 Arlington Drive
Cape Haze, Florida, 33946
Phone/fax: (941) 697-5764; e-mail: DEP@gls3c.com

Technology Development Manager: Joseph Carpenter
(202) 586-1022; fax (202) 586-1600; e-mail: joseph.carpenter@ee.doe.gov
Field Technical Manager: Philip S. Sklad
(865) 574-5069: fax: (865) 576-4963; e-mail: skladps@ornl.gov

---

Contractor: U.S. Automotive Materials Partnership
Contract No.: DE-FC05-02OR22910

Objective

- Develop the science and technology necessary to cast structural cast magnesium components (a magnesium front cradle cast by two distinctively different processes). The technology that is developed will be shared with other concurrent magnesium programs.

Approach

- Investigate various methods of casting and techniques used.
- Develop mold fill parameters.
- Develop/investigate corrosion factors and methods of protection.
- Develop nondestructive evaluation (NDE) and sensor applications.
- Enhance the current design guideline.
- Develop and continue the existing database.
- Develop joining best practices.
- Develop a business case, cost model, and cradle validation casting for Corvette testing.
- Transfer technology for all project items to industry.

Accomplishments

- Issued two iterations of the database CD for evaluation by the project participants.
- Increased the collection of magnesium production castings for development of the material property database.
- Selected an additional magnesium casting process for development and evaluation.

- Involved the steering committees in working actively with the core team to carry out the project tasks.
- Continued the collection and evaluation of modeling software for later use in the development of the final model.
- Continued the casting and corrosion mitigation investigations at Natural Resources Canada (CANMET).
- Continued the quantitative characterization of cast microstructures for the magnesium production castings.

Future Direction

- Award all major purchase orders for tooling and project support work on time.
- Complete on time the tasks outlined in the statement of work.
- Continue solicitating additional project industrial (equipment) participants.

Introduction

The structural cast magnesium development (SCMD) project focuses on resolving critical issues that now limit the large-scale use of magnesium castings in automotive components. This project will develop the science and technology necessary to implement a front structural cradle (and other magnesium castings) that will interface with other concurrent magnesium programs proposed for the U.S. automotive industry (see report 3D). The development of this component involves all of the difficult manufacturing issues, including casting processes (e.g., high-pressure die casting and semisolid, low-pressure, and squeeze casting) and joining, along with harsh service environment challenges such as corrosion, fatigue, and stress relaxation associated with fasteners.

- The project team includes personnel from
- The Big Three automotive companies
- 34 companies from the casting supply base
- Academic personnel
- American Foundry Society (AFS)
- Technical associations
- Oak Ridge National Laboratory (ORNL)
- Sandia National Laboratories (SNL)
- Lawrence Livermore National Laboratory (LLNL)
- CANMET

Figure 1 illustrates the technology that will be developed to help engineers and product designers reduce cast component variation, resulting in lower component cost and weight.

Figure 2 illustrates a generated database that uses an entirely different architecture for comparing

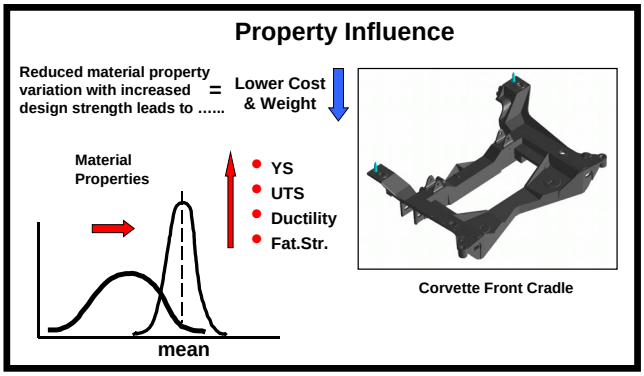

Figure 1. The technology being developed to help reduce cast component variation.

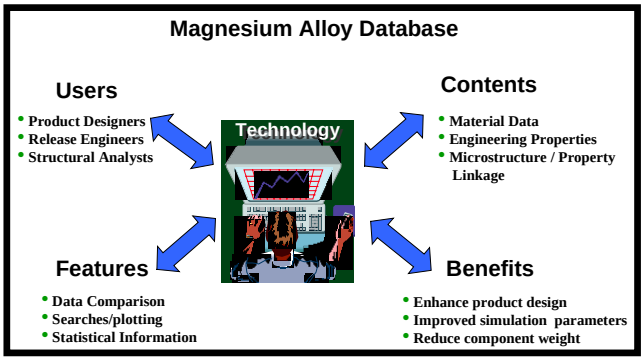

Figure 2. Comprehensive material database

magnesium. It includes historical literature data and comprehensive mechanical property data derived from samples excised from actual production magnesium castings. Castings included in the database were manufactured by high-pressure die-casting and gravity, permanent-mold, semisolid, low-pressure, and squeeze casting processes.

Figure 3 indicates the development of on-line process monitoring, feedback control, and NDE techniques. These items and work were used for the

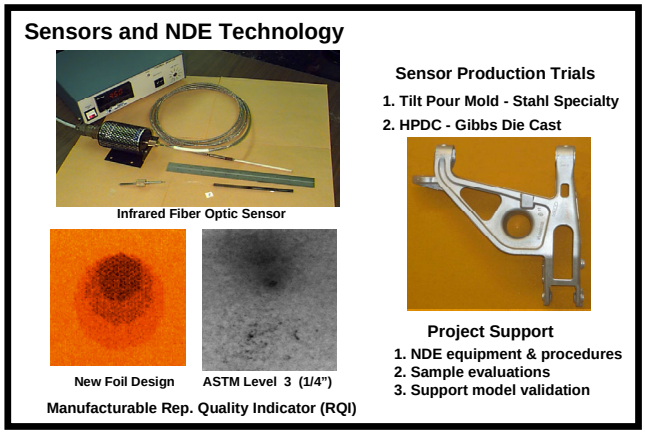

Figure 3. Process sensors, radioscopic quality indicators, and nondestructive evaluation project support.

cast light metals (CLM) project and further expanded for the SCMD project by LLNL. Continued development will ensure cast component consistency and quality. LLNL has begun evaluating quality assurance methodologies and equipment and will further develop a new radioscopic standard for magnesium castings, based on improving ASTM standards, that was provided by the previous CLM project

Figure 4 indicates the evaluation and development of numerical modeling techniques to predict cast microstructure and subsequent mechanical properties throughout cast component sections. A major goal of the SCMD project is to develop math-based models that predict the microstructure and subsequently the mechanical (tensile and cyclic) properties of cast components from the mold, casting, and component function criteria (Figures 4 and 5). The results of this work will be a joint effort of industrial participants, national laboratories, and academia.

The material property simulation model (Figure 5) indicates the use of microstructure in the modeling techniques, as the study of variability in ductility and ultimate tensile strength (UTS) in production casting of magnesium alloys continues. Samples have been successfully correlated with the presence of defects through careful qualitative and quantitative fractographic observations, and quantitative microstructural data have been obtained through digital image analysis and stereological techniques. Quantitative correlation between tensile elongation and total area fraction of defects (e.g., oxides, pores, flux residues) of the fracture surface has been demonstrated for various groups of

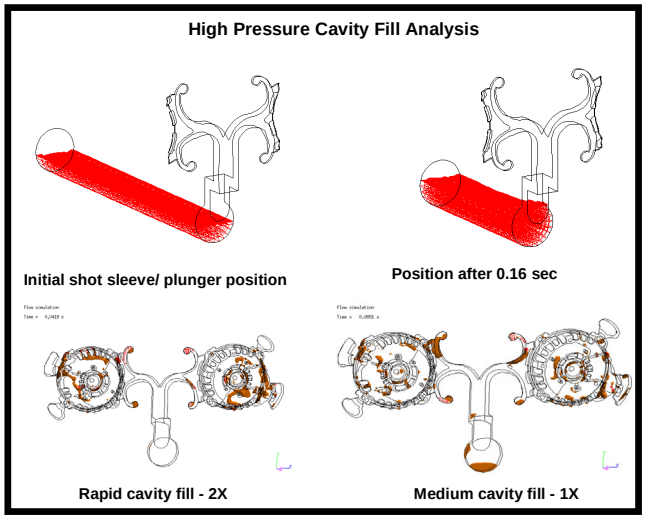

Figure 4. Evaluation and development of numerical modeling techniques to predict cast microstructure and subsequent mechanical properties throughout cast component sections.

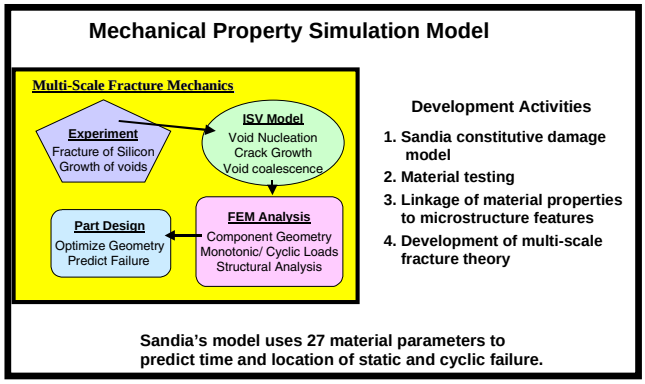

Figure 5. Material property simulation model.

production castings on the previous project and already completed for the SCMD project. Fractographic analysis work continues for tensile test specimens of various magnesium alloy specimens from several production castings. Georgia Tech continues this investigative work, and it is being used for the modeling work performed by ORNL and SNL.

Milestones

Cooperative Agreement

- A front cradle has been chosen for conversion from aluminum to magnesium.
- A purchase order has been issued for the magnesium cradle tooling.
- Additional magnesium castings have been chosen for evaluation by the project team.

- Detailed quantitative microstructural characterization has been completed for production components cast with AM 60 and AZ 91 magnesium alloys.
- Steering committees are actively working with the project team and all industrial participants on major task issues.

Cooperative Research and Development Agreement

- **LLNL:** Radiographic analysis of validation mule castings has started in order to determine discontinuity types and grades at predicted high-stress locations. Implementation tests of a fiber optics in-mold thermal monitoring system for high-pressure die casting will be initiated in several high-volume production facilities. Laboratory personnel initiated computed tomography of notched tensile bar magnesium samples to measure porosity void nucleation and growth for constitutive equation modeling parameters.
- **ORNL:** ORNL has received modeling software from three members of the supply team and started the evaluation review. The end result will be the use of the ORNL models in current and future commercial software.
- **SNL:** Finite element simulations of AM60B notch tensile tests were performed to corroborate experimental load-displacement curves with porosity data from the interrupted X-ray tomography. Comparisons are encouraging, considering that no coalescence is yet included in the magnesium model, which considers only void growth. We expect to include more about pore–pore coalescence as the project continues. We have also quantified some microstructural property relations for fatigue based upon some microstructural evaluations of AM60B and AZ91D magnesium alloys. This information will be used for our multi-scale fatigue model.

Project Benefits

The benefits that DOE and U.S. industry are expected to derive from successful completion of this research include the following:

- Vehicle mass savings for ground and air transportation vehicles will lead to reductions in fuel consumption, emissions, and dependence on foreign oil.
- Automakers are under increasing pressure to reduce carbon dioxide emissions and increase corporate average fuel economy (CAFE). The North American auto industry currently uses approximately 70,000 MT of magnesium per year, equivalent to about 3.5 Kg per vehicle. The ability to significantly increase magnesium usage will help the industry meet future federal CAFE targets and reduce exposure to CAFE penalties. Cast magnesium structures have the potential to reduce vehicle mass by 100 Kg, which could reduce emissions by 5% and fuel consumption by approximately 1.0 mpg (ignoring secondary mass savings).
- Light metal alloys have greater recycling value and reduce the energy required for recycling compared with plastics (including melting, machining, handling, and transportation energy requirements).
- The competitive global postures of the Big Three U.S. automakers will improve if they can design and manufacture vehicles offering greater consumer value. This could improve the U.S. trade balance with countries that market more fuel-efficient vehicles than those produced in North America.
- Light metal casting operations present fewer health and environmental issues for workers than do ferrous foundries and polymer molding operations.
- The national laboratories will gain valuable experience in manufacturing development and product application.
- The national laboratories will gain an opportunity to develop math-based simulation models and NDE technologies that benefit both the auto industry and federal technology programs.

Future Direction

- We will work with the tooling company toward the development and on-time delivery of the magnesium cradle (Figure 6).
- Solicitation of additional industrial (equipment) participants will continue.
- The tasks listed in the project statement of work will be followed to complete the project on time. The project has been somewhat curtailed by

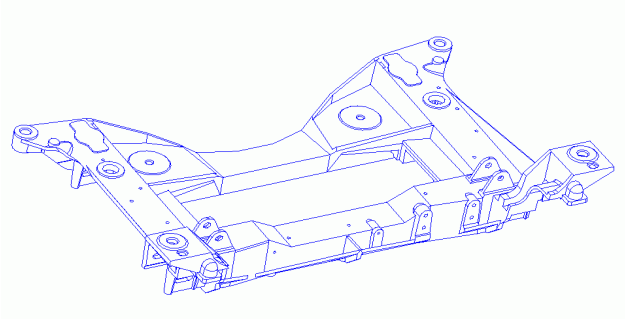

Figure 6. Magnesium cradle.

delays on the part of the Big Three automakers in signing the cooperative research and development agreement, revising the original work agreement, and approving key purchase order documents. All U.S. Automotive Materials Partnership/Automotive Metals Division and SCMD personnel are aware of the problems and are working to correct them, to help the SCMD core team meet Corvette's Job 1 date for the magnesium cradle, and to comply with all milestone and deliverable tasks.

Two elements are essential to the SCMD project:

- Research institutions participating in the project—universities, national laboratories, industry, and CANMET—must work together to carry out the required scientific research (e.g., microstructure, effects of modeling, corrosion and fastening properties, NDE methods.
- Industry needs a "fast-track" effort to convert an existing aluminum cradle to magnesium and have a part ready for testing on an actual vehicle in 3 years. Therefore, the industrial participants cannot wait for all intricate scientific issues to be understood before a process is chosen, tooling built, parts cast, and validation tests run.

Participants on each side of the project, researchers and industry, must be constantly aware of the needs and progress of the other.

4. POLYMER COMPOSITES R&D

A. Development of Manufacturing Methods for Fiber Preforms

Program Manager: Jeff Dahl
Ford Motor Company, Scientific Research Laboratory
P.O. Box 2053, MD 3135 SR
Dearborn MI 48121-2053
(313) 845-1039; fax: (313) 390-0514; e-mail: jdahl@ford.com

Composite Materials Research Engineer: Thomas Hoseck
Oak Ridge National Laboratory (at the National Composite Center)
National Composite Center
2000 Composite Drive
Kettering OH 45420
(937) 297-9431; fax: (937) 297-9543; e-mail: hosecktm@ornl.gov

Field Project Manager, Composites: C. David Warren
Oak Ridge National Laboratory
P.O. Box 2009, Oak Ridge, TN 37831-8050
(865) 574-5069; fax: (865) 574-4963; e-mail: warrencd@ornl.gov

Technology Development Manager: Joseph Carpenter
(202) 586-1022; fax: (202) 586-1600; e-mail: josephcarpenter@ee.doe.gov
Field Technical Manager: Philip S. Sklad
(865) 574-5069; fax: (865) 576-4963; e-mail: skladps@ornl.gov

---

Contractor: DOE Cooperative Agreement
Contract No.: DE-FC05-02OR22910

Objectives

- Develop and demonstrate new fiber preforming processes to decrease cost, increase manufacturing rates, and improve reproducibility of large preforms for composite molding.
- Provide process development support to Automotive Composites Consortium (ACC) Focal Project 3 (FP3) (see report 4B).

Approach

- Identify carbon fiber properties required to permit rapid processing and achieve desired performance levels.
- Explore the extension of automated preforming technology to make preforms with a thermoplastic matrix.
- Investigate methods to achieve rapid orientation of reinforcing fibers.

Accomplishments

- Developed a ROBCAD model of the ACC programmable powdered performing process (P4) machine and successfully implemented the offline programming robotic software on the ACC's FP3 B-pillar test section.
- Characterized the in-plane permeability of both glass and carbon fiber preforms.

- Developed a test method and procedure to quantify preform light transmission and analyzed carbon fiber preforms using this method.
- Conducted preform compressibility testing on various glass and carbon fiber preforms.
- Fabricated carbon fiber flat panel preforms for structural reaction injection molding (SRIM) to support the Oak Ridge National Laboratory (ORNL) carbon fiber durability program with the ACC.
- Fabricated carbon fiber flat panel preforms to support fundamental SRIM research and mechanical property evaluation within the ACC.

Introduction

This project has focused on the development of P4, a fully-automated robotic process, and its demonstration in the ACC FP2 pickup truck box program. A prototype two-station manufacturing cell was designed, fabricated, and installed at the National Composite Center in Kettering, Ohio. Optimized spray patterns for pickup box preforms, areal density consistency, net-edge quality, and desired cycle times were demonstrated. Several generations of improved glass fiber and binder products have been identified. The need for an integrated binder and reinforcing fiber system was identified, and development work on such a product was initiated with a material supplier.

Preforming and molding technology related to the use of chopped, random glass fiber composites is relatively mature; and the associated weight savings (20–30% compared with steel) have been demonstrated in the past through several research programs, including the ACC's FP2 pickup truck box program. Additionally, similar technology has been applied to current production vehicles, including the Aston Martin Vanquish and the GM Silverado pickup truck. However, to obtain higher mass savings with composites relative to steel (50–70%) and to compete with aluminum for similar mass savings, carbon fiber must be used as the reinforcing fiber.

The extension of this technology to manufacturing carbon fiber preforms is now in progress to support the development of ultra-lightweight structures. This project will identify the carbon fiber properties required to permit rapid processing and achieve the desired composite performance levels. This will provide guidance for fiber manufacturers to develop new products. Opportunities to extend automated preforming technology to make preforms containing a thermoplastic matrix, which can be consolidated to form the final part, will be explored. Methods to achieve rapid orientation of reinforcing fibers will be investigated. Advances in preforming technology will be demonstrated in the structural automotive parts designed and prototyped as part of the ACC FP3.

ROBCAD Offline Programming

To enhance preform tooling design capabilities and reduce preform lead times, ROBCAD offline programming software was used to develop a ROBCAD model for the ACC's preforming equipment (Figure 1).

Figure 1. ROBCAD offline programming model.

First, the machine model and software were used to design the B-pillar preforming tool to optimize the location of the inner and outer halves. The model and software were then used to develop offline robotic paths of the FP3 B-pillar test tool, and these programs were successfully implemented, allowing fabrication of preforms. It is estimated that using ROBCAD, rather than teach-mode programming, reduced preform lead-time by 4 weeks. The ROBCAD model is completed and

will be used for offline programming of future components on the ACC's preforming machine.

In-Plane Permeability Characterization

The use of chopped carbon fiber for liquid molding processes such as resin transfer molding (RTM) and structural reaction injection molding (SRIM) is an immature technology; therefore, data for the in-plane permeability for chopped-carbon-fiber preforms are not yet well understood or reported. Based on this fact, a program was initiated with Michigan State University to investigate the in-plane permeability of glass and carbon fiber preforms. A brief summary of the results is highlighted in Table 1.

Based on the experimental permeability data, it is believed that as carbon fiber rovings approach bundle geometries comparable to those of glass fiber rovings, which are necessary for uniform surface dispersion, the permeability of carbon fiber preforms will be substantially lower than those of glass fiber preforms. This can potentially be an issue in the molding process for several reasons, one of which is that higher injection pressures will be present when carbon fiber preforms are used, increasing the risk of fiber wash. Further permeability characterization will be required as new carbon fiber rovings are developed in order to identify potential molding issues.

Carbon Fiber Preform Light Transmission

Large regions of zero fiber content were identified within chopped-carbon-fiber preforms fabricated via P4. This issue was deemed an unacceptable characteristic of chopped-fiber performs, and the phenomenon was investigated further. Exploratory experiments were performed to determine the contributing factors of localized material variation within chopped-carbon-fiber preforms (Figure 2).

These experiments were successful in identifying the major cause of zero fiber regions within preforms—the particular carbon fiber roving used in manufacturing the preforms. Furthermore, these experiments determined that specific preform processing parameters were not a significant contributing factor to zero-fiber regions, based upon the qualitative analysis that was performed. In order to provide a quantifiable measure of the light transmission characteristics of chopped-carbon-fiber preforms, an experimental test method and analysis technique was developed and successfully demonstrated using image analysis software.

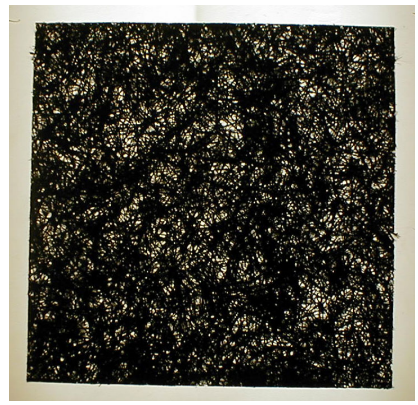

Figure 2. Preform light transmission issues.

Experimental results (Figure 3) obtained using the quantitative test method identified large differences among particular carbon fiber rovings. Based upon the quantitative test results, the method can be used to characterize future experimental carbon fiber rovings.

Preform Compressibility Testing

Preform compressibility is an important characteristic, as it affects several items in the RTM and/or SRIM processes. As a rule of thumb, all chopped-fiber preforms are fabricated to a thickness 25–50% larger than that of the final molded component to ensure some degree of compaction force on the preform in the molding tool. This

Table 1. In-plane permeability results.

Preform type	Material type	Thickness (mm)	Fiber volume fraction (%)	Wetted in-plane permeability (Darcy)	COV (%)
Random chopped carbon fiber	Carbon roving A	3.0	40	145	27
Random chopped carbon Fiber	Carbon roving B	3.0	40	59	25
Random chopped glass fiber	Glass roving	3.0	40	125	21
Continuous filament material (glass)	CSM	3.0	24	1032	14

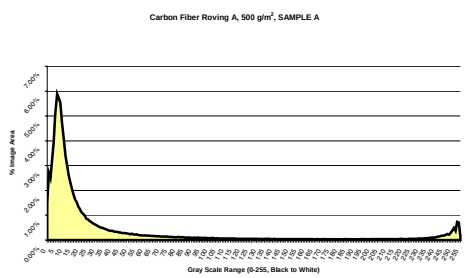

Figure 3. Quantitative light transmission graph.

allows the molding tool to "hold" the material in place during the injection process and can help reduce fiber wash at high injection rates/pressures. However, the amount of compaction force exhibited by a particular preform depends upon the areal density, specified fiber volume fraction, and final molded part thickness. In the same way, the amount of force required to compress a particular preform will affect the size of press necessary to the molding process, as the press will need not only to react the compaction force of the preform, but also to react internal mold pressures during resin injection. A total of 75 preform samples were tested to determine the compressibility response of various glass fiber and carbon fiber preforms to determine these characteristics.

The compressibility responses for preforms manufactured at a fiber volume fraction of 40% for a 3.0-mm molded part thickness using carbon roving A, carbon roving B and glass roving A are shown in Figure 4. Note that for this particular areal density, the glass fiber preform exhibits a compressibility response different from that of the carbon preforms manufactured using either carbon roving A or B.

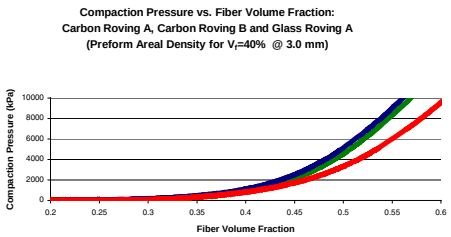

Figure 4. Compaction pressure vs. fiber volume fraction.

This response may be attributed to the increased number of bundles and reduced bundle cross-sectional area relative to carbon fiber. Those characteristics would enable more efficient packing of the material in a random-fiber perform, leading to a decreased required compaction pressure for fiber volume fractions greater than approximately 35–40%. Additional analyses were conducted for the remaining tests performed within this testing program. Similar conclusions can also be drawn from examining the compressibility responses throughout the range of areal densities tested during this experiment.

Carbon Fiber Roving Development

The use of random, chopped carbon fiber for automotive structures is currently an immature technology; consequently, carbon fiber roving technology is still in its infancy. Current carbon fiber materials for chopped-fiber preforming are, in most cases, slightly modified versions of carbon fibers developed for other manufacturing processes and are not suitable for chopped-fiber preforming. But more important, carbon fiber rovings are normally single-ended materials. These carbon fiber tows have traditionally been used in fiber conversion processes such as weaving, braiding, stitch-bonded fabrics, and pre-preg manufacturing; or in composite fabrication processes such as pultrusion and filament winding; but not in chopped-fiber applications. Glass fiber is also available in a single-ended product form and is used in the same processes as mentioned for carbon fiber. However, an entirely different product form is used for chopping applications. Glass fiber fabrication processes such as traditional spray-up, conventional directed fiber preforming, sheet molding compound, and P4 use a multi-ended glass roving specifically designed for that type of processing, not a single-ended roving.

Although several carbon fiber roving variants have been and currently are under development by several carbon fiber manufacturers, they all seem to fall short of the optimum compared with glass fiber rovings designed for chopped-fiber applications. Carbon fiber rovings have not been designed for use in chopped-fiber preforming applications; therefore, a myriad of processing issues exist in attempting to fabricate performs, such as fiber fuzzing, substantial fiber "fly," and excessive filamentization of the deposited material. Fabrication of material to preliminary ACC specifications remains a critical obstacle to developing carbon rovings suitable for

use in chopped-fiber performing processes such as P4.

Carbon fiber rovings supplied by all manufacturers to date are unsuitable for high-volume chopped-fiber preforming applications. These rovings will allow prototype preform manufacturing and component testing but could not be applied successfully to high-volume commercial chopped-fiber applications. All carbon fiber manufacturers have yet to make fundamental modifications to their carbon fiber rovings that have been suggested by the ACC. It is believed that such modifications would enhance the chopped-fiber preforming characteristics of the roving, making it more suitable for P4 and other chopped-fiber processing methods. It is felt that a stand-alone program with a carbon fiber manufacturer is necessary to bring carbon fiber rovings to a usable state in commercial chopped-fiber applications.

In an effort to develop a roving development program with various carbon fiber manufacturers, meetings were held with Zoltek, Hexcel and Fortafil. At this time, no official program is under way with any carbon fiber supplier to manufacture a roving suitable for chopped-fiber applications. Despite this issue, efforts are ongoing to develop a carbon fiber roving development program with a carbon fiber manufacturer. As materials are made available, new and improved carbon fiber rovings will continue to be tested in P4 to evaluate chopped-fiber material processing and performance.

B. Composites-Intensive Body Structure Development for Focal Project 3

Nancy Johnson
GM Research & Development
MC 480-106-256
30500 Mound Road
Warren, MI 48090-9055
(586) 986-0468; fax: (586) 986-0446; e-mail: nancy.l.johnson@gm.com

Raymond G. Boeman
Oak Ridge National Laboratory
(248) 452-0336; fax: (248) 452-8992; e-mail: boemanrg@ornl.gov

Field Project Manager, Composites: C. David Warren
Oak Ridge National Laboratory
P.O. Box 2009, Oak Ridge, TN 37831-8050
(865) 574-9693; fax: (865) 574-4963; e-mail: warrencd@ornl.gov

Technology Development Manager: Joseph Carpenter
(202) 586-1022; fax: (202) 586-1600; e-mail: joseph.carpenter@ee.doe.gov
Field Technical Manager: Philip S. Sklad
(865) 574-5069; fax: (865) 576-4963; e-mail: skladps@ornl.gov

---

Contractor: U.S. Automotive Materials Partnership
Contract No.: DE-FC-02OR22910

Objectives

- Design, analyze, and develop the technology to build a composite-intensive body-in-white (BIW), offering a minimum of 60% weight savings over steel at a cost close to that of steel, while meeting manufacturing, assembly, and performance targets.
- Provide a focus for bringing together technology developed by each of the Automotive Composites Consortium (ACC) working groups through emphasis on carbon-fiber-reinforced composites and the use of hybrid materials, faster manufacturing processes, design optimization including crashworthiness, and rapid joining methods.

Approach

- Optimize the design and complete the finite element analysis (Phase 1).
- Build one part of the BIW to demonstrate high-volume processing methods, including the component as well as the needed assembly fixtures (Phase 2). Test the component before continuing with the construction of the complete BIW.
- Build the complete BIW (Phase 3). To reduce cost, not all parts will be made from production tooling; however, care will be taken to ensure that the properties of each part are consistent with those that will be obtained from production tools.

Accomplishments

- Completed BIW design files and converted them to files that each company could use.
- Completed the learning tool preform screens and molds.

- Initiated molding of parts from the learning tool to conduct the research necessary to build a complete body side.
- Completed a preliminary assessment of the cost for the body side parts using the P4 method with structural reaction injection molding (SRIM).

Introduction

All of the materials, manufacturing processes, and fabrication and assembly methods to be considered in this project are to be consistent with the following overall objectives:

- High-volume production techniques (>100,000 units per year)
- Cost parity with equivalent steel structures
- Overall 60% mass reduction relative to steel BIW structure
- Structural performance equivalent to or better than that of a steel structure
- Dimensional tolerance equal to or better than that of steel

Much of FY 2002 was devoted to developing the manufacturing processes necessary to build the body side. Research areas were identified that must be completed before the full body side is fabricated.

The complete BIW design files were reviewed for accuracy and converted to files that each of the companies could use.

Details of Phase 2

Throughout the year, work has been ongoing for Phase 2 of the project. The fabrication of the learning tool and perform screens was completed. This work was required so that the necessary preforming and molding research for chopped carbon materials could begin prior to the attempt to build a complete body side as the demonstration part.

Learning Tool

A learning tool was designed to conduct the processing and materials research necessary to enable production of the body side. A section representative of the B-pillar portion of the design for the body side was selected for the learning tool, which had many of the features of the final part. The tool was made to be versatile for use with SRIM, FiberRim, and sheet molding compound. It has a polished surface so that it can be used to develop class A surface techniques later if desired. The tool incorporates many challenging features not yet addressed by the composites industry, including liquid molding of variable-thickness sections at high volume fractions.

The steel tools were completed. During this time, the plaque molding study was being done at the National Composites Center (NCC) (report 4D). The results of the plaque molding study will be used to continue the work for this project.

The tool was completed and shipped to NCC in Dayton, Ohio, to begin molding trials. The necessary modifications were made to the press at NCC to allow the molding to be done.

The corresponding preform screens for the B-pillar section were completed and shipped to NCC. The first set of preforms was made using glass to verify the conformability of the hammer-formed screens. At the end of June, the first carbon preforms were made. Analyses will be done to check the uniformity of the aerial density throughout the preform.

Fiberglass materials were used for the initial mold tryouts. Figure 1 shows the mold with molded fiberglass inner and outer B-pillars lying in the mold cavity.

Figure 1. Mold with molded fiberglass inner and outer B-pillars lying in the cavity.

Cost Modeling

ORNL continued developing a cost model geared specifically toward the comparison of costs for different processes. A preliminary assessment was completed of the cost for the body side parts using the P4 preforming method with SRIM. Cost models were also developed by the Massachusetts Institute of Technology to investigate the full BIW cost. Meetings were held to review input for the models to provide the best data possible at the time. It was recognized that we do not have a complete set of data to provide all the information needed to get a single cost number.

C. Thermoplastic Composite Sheet Manufacturing

Principal Investigator: Mark T. Smith
Pacific Northwest National Laboratory
P.O. Box 999, Richland, WA 99352
(509) 376-2847; fax: (509) 376-6034; e-mail mark.smith@pnl.gov

James Grutta and Larry Stanley
Delphi Automotive Systems
8385 South Allen Street, No. 140, Sandy, UT 84070-6434
(801) 568-0170; e-mail itgrutta@hotmail.com

Technology Development Manager: Joseph A. Carpenter
(202) 586-1022; fax (202) 586-1600; e-mail: joseph.carpenter@ee.doe.gov
Field Technical Manager: Philip S. Sklad
(865) 574-5069; fax: (865) 576-4963; e-mail:skladps@ornl.gov

Contractor: Pacific Northwest National Laboratory
Contract No.: DE-AC06-76RL01830

Objectives

- Demonstrate and develop processing methods for carbon-fiber-reinforced thermoplastic matrix composites at rates consistent with large-volume automotive structural applications.
- Investigate and develop methods for shortening process cycle times and improving materials performance.
- Develop methods for achieving a Class A surface finish requirement, consistent with outer body panels for automotive use.
- Investigate the potential for cored (sandwich) structure composites with thin-walled thermoplastic matrix composite skins.
- Determine the cost-effectiveness of thermoplastic matrix composites in production volumes consistent with automotive applications and having the potential to achieve cost targets in the future.

Approach

- Use data from previously completed parametric studies of time, temperature, and pressure to optimize properties for structural automotive composites and determine the combinations of processing factors that will accelerate process cycle time.
- Develop heating and cooling methods and process operations to achieve consistent cycle times.
- Analyze alternative methods of melt processing for the various operations required for consolidation, including experimental evaluation of cored structures.
- Apply a multiscale materials modeling approach to develop predictive numerical models for thermal and structural responses for constituent materials and architectures and apply it to processing conditions for cycle optimization, material property prediction, and end-use performance prediction.
- Use data to influence materials suppliers to modify base material feeds in ways that support increased cycle times.
- Use complex-shaped components to determine process limitations and factors for economic evaluation.

- Evaluate methods to achieve a Class A surface finish with reinforced thermoplastic matrices and analyze them in production cycles on complex tooling.

Accomplishments

- Completed a two-press system installation and demonstrated its operation using a single modified cone mold.
- Began investigating alternate thermoplastic composite materials that either require shorter consolidation times or are pre-consolidated.
- Developed a new processing method for continuous processing with multiple tooling sets and optimized heat/cooling methods. Delphi has filed a record of invention for the process.
- Partially automated the two-press system to simplify it and ensure its proper operation. (Safety-critical operations, such as closing the press, are still controlled manually.)
- Investigated infrared (IR) heating as a way of pre-heating the tool surface.
- Created a finite-difference model of the effects of IR heating to explore and determine the feasibility of using IR energy as a means of rapid preheating and reducing thermal momentum.
- Designed a new seven-sided forming tool with flat sections at 0°, 30°, 60°, and 87° from perpendicular to the loading direction.
- Completed significant compression testing using curved specimens and began correlating results with molding process parameters.
- Continued to analyze materials production and materials forms with suppliers to determine cost and volume potential and material supply limitations.
- Determined cost/volume scenarios for thermoplastic components for different processing methods.
- Completed microscale models for simulating the behavior of unidirectional reinforced-fiber composites. The primary model is based on assumed hexagonal packing of fibers, and it is parameterized to allow any possible volume fraction of fiber and any desired finite element mesh refinement to be applied.
- Developed a numerical model of a consolidated 4-harness satin fabric-reinforced composite.
- Developed a numerical model that predicts 2×2 twill unconsolidated fabric shear behavior to simulate properties useful for macro models of stamp-forming process modeling.
- Developed relations between fabric openness, in-plane shear locking angle, and effective normal strains for better understanding of fabric formability characteristics.
- Constructed four different fabric (mesoscale) models: a consolidated plain weave lamina, a consolidated 2×2 twill weave, 2×2 twill, and a 4-harness satin.
- Developed a complex set of boundary conditions for a fabric shear model for the 2×2 twill material. The final issue of contact conditions during shear locking is being resolved.
- Developed a number of variations on macro-modeling of the forming process.

Future Direction

- Develop novel process methods to determine whether they can be implemented into higher-volume production using multiple tool and press system approaches.
- Work with materials supplier to adapt other materials forms that not only are more cost effective but also can increase production cycle times.
- Complete material-specific models, including the three structural fabric models that are all well developed and near completion.

- Formally document the procedures for constructing and applying the various models for future reference and technology transfer. In particular, the complex periodic boundary conditions for simulating the various fabric-reinforced lamina have not been previously documented (to our knowledge).

Introduction

Polymer matrix composites are a class of materials that have a combination of properties required to achieve significant reductions in vehicle mass, compared with conventional materials. Although widely regarded as having the most potential for future weight savings, their application is severely restricted by fundamental issues in achieving required production volumes and by the cost of basic materials. These issues have been studied and analyzed based primarily on liquid thermosetting matrix composites, such as those used in the Automotive Composites Consortium (ACC) focal projects. The cost and availability of fiber materials, especially for carbon fibers, are being addressed by the low-cost carbon fiber projects by ALM (see Section 5). This project has identified carbon fiber thermoplastic matrix composites as having significant potential to meet structural property requirements and to achieve rapid processing cycles similar to stamping of metal components. Automotive applications will be most widespread if two other fundamental issues can be addressed: cored, thin-walled structures (for optimum structural performance and minimum weight) and Class A surface finish in a semi-structural component. Developing the thermoplastic composites to meet these requirements will require a combination of experimental approaches, materials and process modeling, and modification of materials forms and processing methods to achieve an optimum manufacturing process.

Project Deliverables

This multi-year project will develop and demonstrate knowledge in four areas related to forming processes for thermoplastic composites: (1) effects of process cycle time and materials properties at high forming rates; (2) results of Class A surface finish trials; (3) methods for manufacturing thin face-sheet cored structures; and (4) modeling tools for predicting and optimizing the thermal and structural materials behavior of fiber-reinforced thermoplastics.

Planned Approach

Experimental and analytical methods are being used and developed for high-rate forming of thermoplastic composite sheet and cored structures. The team is focusing on processing methods for achieving production rates comparable to those of automotive metal stamping operations and on materials modifications to enable rapid flow and consolidation. By integrating these two approaches, we are able to determine where difficulties occur in the process and materials form and can suggest methods to overcome these barriers. Several significant invention disclosures have resulted, and further focus on the process and materials kinetics will allow the bench-scale demonstration of high-rate stamping. Recent experiments using complex 3-dimensional molds indicate that longer dwell times are required to consolidate materials in draw and draft angle portions of the dies. This finding points to the need to explore alternate material forms in future work, including pre-consolidated thermoplastic sheet materials.

Experimental Methods—Manufacturing Tasks

The initial experimentation used flat plate molds and developed a process diagram based on achieving a pre-defined “acceptable” quality of consolidation, as measured by compressive strength of the coupons. These process conditions were used as a basis for processing a conical mold that had varying angles of fabric shear (deformation) and varying forming radii (both convex and concave) to provide an understanding of the forming limits under different process conditions. Coupons have been taken from the conical mold and tested in compression to match the consolidation results to the results from the basis flat plate mold. Methods for achieving rapid process cycles were developed as an ongoing part of the conical mold trials. A two-press system (Figure 1) was developed over the past year to simulate a newly developed continuous cycle process. However, with the use of more-complex 3-dimensional molds, experimental results indicate the need for increased dwell time to achieve

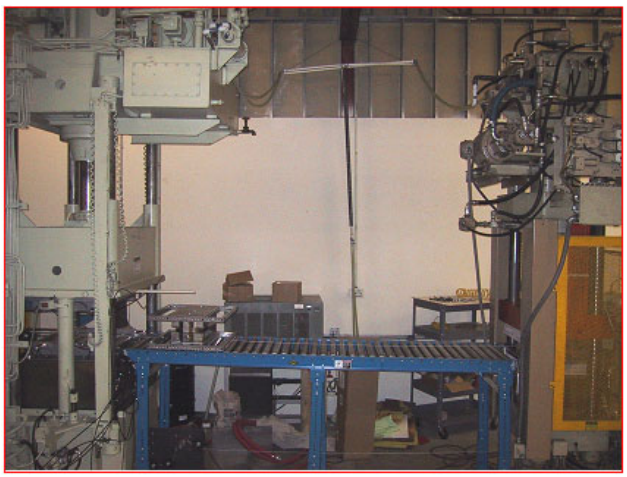

Figure 1. Two-press system with tool shuttle.

consistent, full consolidation of the powder-impregnated materials. As a result, additional attention will be focused on the application of pre-consolidated thermoplastic composite materials, as well as the use of a new mold design that incorporates multiple entrance angles so that the influence of die geometry on cycle dwell times can be quantified.

Approaches using combined hot stamping and consolidation as a single step have indicated that a long dwell time is necessary for fiber wetting and optimum resin distribution when trial parts are fabricated under realistic processing conditions. Although the materials properties can be developed for simple sections—where conditions of combined temperature, pressure, and time meet our original process map—we find that in working on areas with other high draft angles and lack of directly applied pressures, there is a longer dwell time requirement. Although this is still consistent with the process map, it is further out on the boundaries of allowed conditions and leads to a longer process cycle. This is a significant issue in dealing with the powder-impregnated materials, since it could make it necessary either to pre-form the material into a partially consolidated near-net shape preform in a separate step or to start with flat pre-consolidated sheet stock.

Although this approach is not inconsistent with traditional composite molding—such as the pre-form and molding multi-step approach developed for SRIM pick-up truck boxes by the ACC (see report 4A)—it is a significant departure from what we would like to accomplish: one-step stamping to rapidly form structural thermoplastic composites. The costing and production parameters required for this dual-step approach will be investigated, and we will investigate potential ways to work around this problem, such as molding with higher internal cavity pressures. New demonstration tooling, which has more easily modeled faces and the capability to hold face pressures and contour, has been designed for continuing process development.

Modeling Task—Analytical Methods

A multiscale modeling approach is being applied to develop modeling tools with long-term value to the technology of fabric-reinforced thermoplastic composites. As illustrated in Figure 2, three important material scales have been addressed. A description of and motivation for the multiscale approach is available in the FY 2001 annual report for this project. Here, we will describe progress made during the past year and present some representative results from modeling activities.

The microscale models were developed in previous years. In addition, some mesoscale models were developed previously to predict thermal and structural behavior for the 2×2 twill woven fabric material in a consolidated form. Process (macro) models have been developed to initially study the effect of in-plane shear stiffness on formability and drape characteristics for the cone-shaped mold. In addition, macro-models were applied to predict in-mold pressure distributions during forming.

Efforts during the past year have focused primarily on two challenging tasks. One was to model a consolidated 4-harness satin weave material for comparison with previous modeling results for 2×2 twill weaves. The second was to explicitly model the in-plane shear behavior of the unconsolidated 2×2 twill fabric and develop insight as to the kinematics of fabric shear as it relates to drapability/formability. This model can ultimately provide shear properties for macro-models such as the cone-mold model developed under this project.

An image of the 4-harness satin weave unit cell model is shown in Figure 3. The stress plot in Figure 3 indicates the complex stress field developed as a result of heterogeneity and anisotropy of the weave-reinforced material under the action of simple (uniaxial) far-field stress boundary conditions. The 4-harness satin and 2×2 twill fabrics are of particular interest for drape

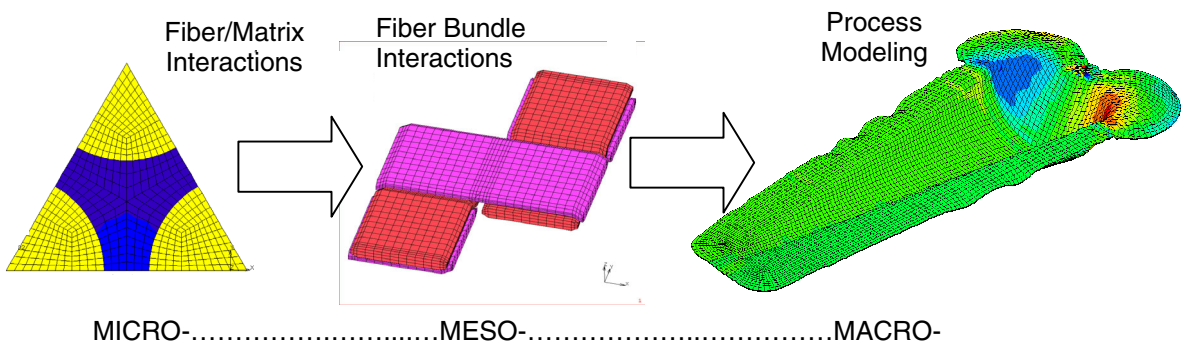

Figure 2. Multiscale modeling of fabric-reinforced composites. Shown are a hexagonal fiber pack unit cell for micro-scale modeling, a 2×2 twill fabric unit cell for meso-scale modeling, and cone forming process model results at the macro-scale.

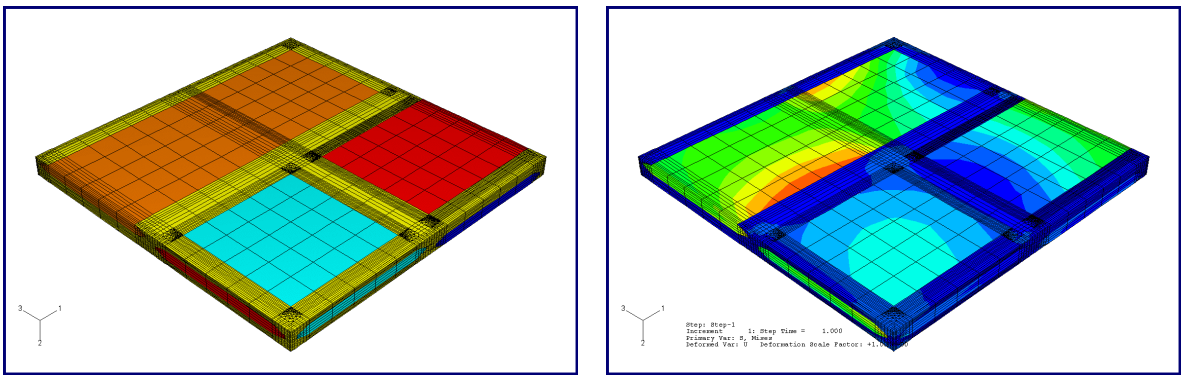

Figure 3. One-quarter periodic unit cell model for a consolidated 4-harness satin weave-reinforced composite (left) with shading indicating separate tows in the weave. Stress contours due to uniaxial global stress boundary conditions (right).

forming because they exhibit better drapability than plain weaves, while maintaining good handling and forming characteristics (such as minimal tow separation during forming).

The fabric shear model and three deformed configurations of the model are shown in Figure 4. Notice that for computational economy, this model has one-half the volume of the previous 2×2 twill models (see Figure 2), as it exploits a plane of rotational symmetry. In the second image, the model has been loaded to simulate the geometry and stresses due to weaving. In the third image, fabric shear is simulated where the shear angle is less than the initial locking angle so that contact between adjacent tows has not yet occurred. In contrast, the last image shows the deformation resulting from such contact. It is this contact between parallel tows that causes a dramatic rise in in-plane shear resistance, as indicated in Figure 5. This resistance limits the formability, since increased shear resistance causes in-plane stress and eventual buckling (wrinkling) of the sheet.

It is well known from sheet metal forming technology that the combined effects of "draw-in" and in-plane strain capacity dominate the formability of a flat sheet of material. Draw-in is the drawing of material from the periphery of the mold into the mold. In doubly curved molds, draw-in is immediately accompanied by wrinkling unless in-plane stretching occurs to accommodate the transition from planar to three-dimensional shape. In continuous fiber-reinforced composites, draw-in is required because the fibers are limited to elastic behavior. Therefore, a commensurate amount of stretching is required to avoid wrinkling. Since minimal stretching can occur in the fiber directions, it must come dominantly from the off-fiber directions as the result of fabric shear. As mentioned, the forces of contact between parallel tows in the fabric ultimately limit the total shear angle. This contact can be postponed by weaving a

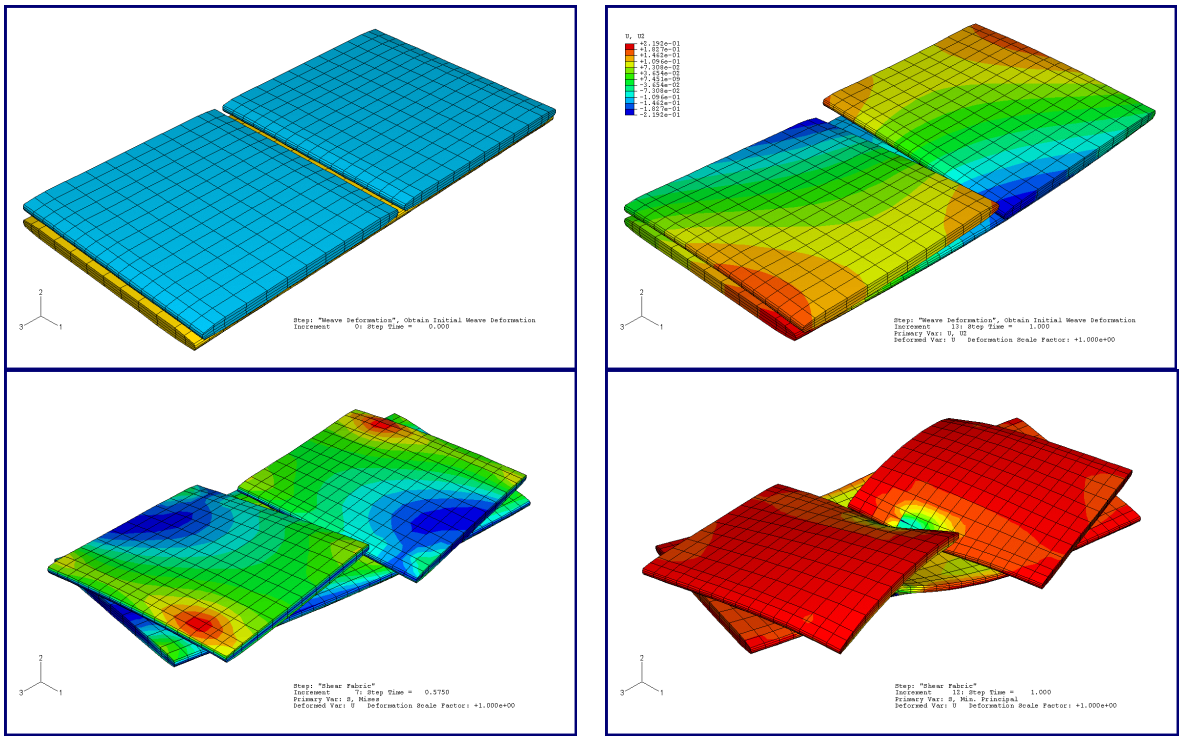

Figure 4. Fabric shear model for 2 × 2 twill weave. Initial model geometry and mesh (upper left). Model deformed into weave pattern (upper right). Shear deformation before tow edge contact (lower left). Shear deformations after tow edge contact (lower right).

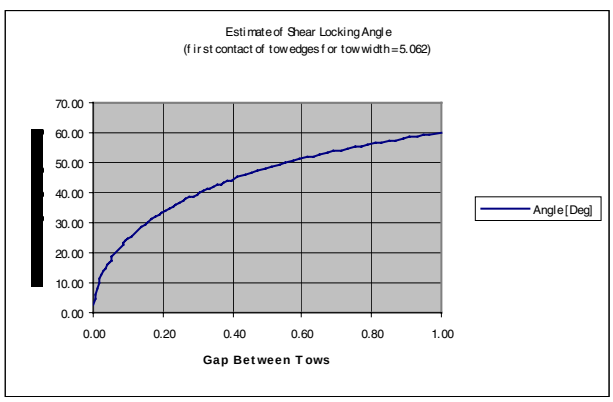

Figure 5. Shear force history showing sharp rise in shear resistance after tow-edge contact.

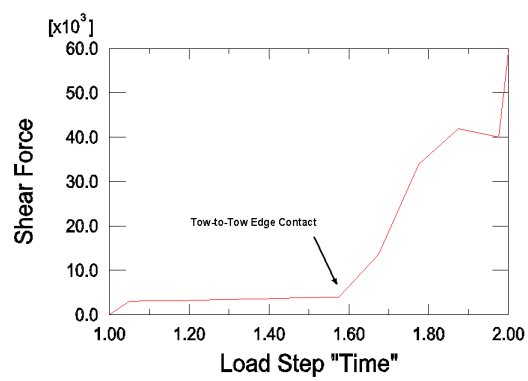

Figure 6. Fabric shear angle at initial tow-edge contact as a function of the normalized gap between the tows.

loose fabric with larger initial average gap between the tows.

If we normalize the gap as a fraction of the tow width, then the relation between the maximum shear angle before initial tow contact and the normalized gap is as shown in Figure 6. Notice that the slope of the curve is very large for small gaps. If we translate this shear angle into the equivalent maximum in-plane normal strains, which occur at ±45° from the initial tow axis, then the relations are as shown in Figure 7. Fairly large strains are available, especially considering that we can generally go beyond initial contact. However, loose weaves, say anything beyond a normalized gap of 0.10 to 0.20, are generally undesirable since they result in non-uniform product (variable gaps between tows) and low-volume fraction of reinforcement. Fortunately,

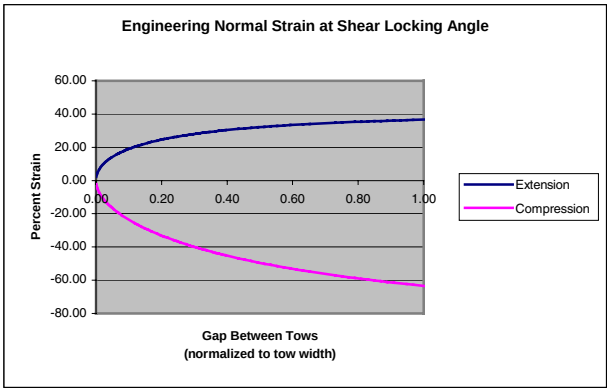

Figure 7. Equivalent normal strain at ± 45° from the initial tow axis as a function of the normalized gap between tows.

most of the benefit of an open weave comes before 0.20 where the tensile strain is 25% and the compressive strain is 33% at initial tow edge contact. Notice the contrast with sheet metal forming, where compressive strains are generally limited to little more than half the tensile strain in the orthogonal direction.

Finally, we must consider the anisotropy of strains available from fabric shear. These strains occur in specific directions relative to the fiber tows, whereas they can occur in any direction for isotropic materials. The relationship between strain and material orientation for a series of normalized gaps and associated shear angles is shown in Figure 8, where, again, the material angle is relative to an

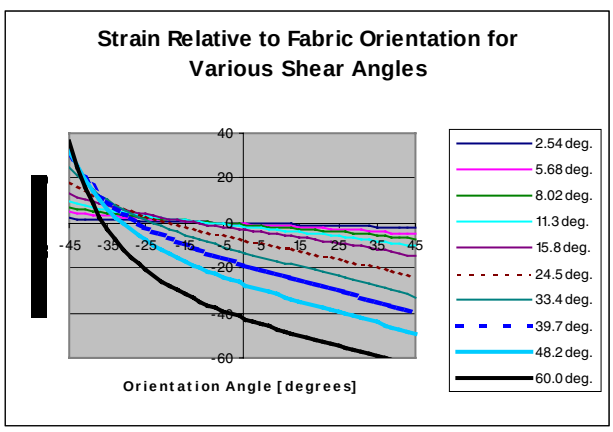

Figure 8. Equivalent in-plane normal strain as a function of orientation relative to original tow axis for various in-plane shear angles.

initial tow axis. Notice the rotation of the zero normal strain orientation with increasing shear angle and the associated domination of compressive normal strains at large shear angles.

Future work will be directed at exercising the models as needed for the project and consolidating/documenting the various models for future reference.

Conclusion

The technical demonstration of stamp-forming of thermoplastic carbon/nylon composites for automotive applications has revealed significant process barriers to the consolidation of powder-impregnated carbon fiber thermoplastics into realistic component shapes. Initial demonstration work performed on flat panels indicated that process cycle times of between 1 and 3 minutes are achievable. However, for 3-dimensional component shapes with near-vertical draft angles, it appears that a significant increase in dwell time is required to fully wet fibers. For this reason, the future work scope for the project will include the evaluation of pre-consolidated preform materials that can subsequently be heated and formed into final part shapes. With this approach, the process dwell time associated with consolidation and flow of resin can be significantly reduced. Along with examining alternate processing approaches, the project will perform a more detailed cost and process model evaluation of pre-consolidated materials. Significant challenges remain in optimizing the process and developing it into a commercially viable robust process, especially given the requirements for cored thin-walled structures and Class A surfaces for structural components. Materials costs and production volumes are within acceptable limits for large-scale automotive applications.

D. High-Volume Processing of Composites

Co-Principal Investigator: Stanley A. Iobst
General Motors R&D Center, MC 480-106-710
30500 Mound Rd, Warren, MI 48090-9055
(586) 986-1223; fax: (586) 986-1207; e-mail: stanley.a.iobst@gm.com

Co-Principal Investigator: Chao H. Mao
DaimlerChrysler Corporation, CIMS 482-00-13
800 Chrysler Drive, Auburn Hills, MI 48326-2757
(248) 576-7482; fax (248) 576-7490; e-mail: chm@daimlerchrysler.com

Field Project Manager, Composites: C. David Warren
Oak Ridge National Laboratory
P.O. Box 2009, Oak Ridge, TN 37831-8050
(865) 574-9693; fax: (865) 574-4963; e-mail: warrencd@ornl.gov

Technology Development Manager: Joseph Carpenter
(202) 586-1022; fax: (202) 586-1600; e-mail: joseph.carpenter@ee.doe.gov
Field Technical Manager: Philip S. Sklad
(865) 574-5069; fax: (865) 576-4963; e-mail: skladps@ornl.gov

---

Contractor: U.S. Automotive Materials Partnership
Contract No.: DE-FC-02OR22910

Objectives

- To develop and demonstrate high-volume manufacturing technology to produce lightweight composite automotive body structures.
- To achieve higher fiber volumes in thinner sections than were successfully achieved in the Automotive Composites Consortium (ACC) Focal Project 2 (FP2).
- To support the goals of ACC's Focal Project 3 (FP3) (see reports 4A and 4B).

Approach

- Investigate the structural reaction injection molding (SRIM) process at high fiber loadings using carbon fiber.
- Design and build a shape tool to investigate the complex preforming and molding processes required for the ACC FP3 program.
- Team with supplier partners to investigate alternative liquid molding processes.

Accomplishments

- Completed a plaque molding program designed to characterize the SRIM processing of carbon fiber preforms.
- Built the B-pillar mold and installed it in the 1000-ton press at the National Composites Center (NCC).

Introduction

The purpose of this project is to further develop liquid composite molding technology to encompass higher reinforcement volumes and the molding of carbon fiber preforms. This project will extend the liquid molding process into more structurally demanding applications and support the molding development needs of the ACC FP3. The earlier ACC programs used glass fiber reinforcement at 30% by volume. The new programs need 40% by volume carbon fiber reinforcement.

In this program, we expect to develop and demonstrate the high-volume liquid molding technology to produce lightweight composite automotive body structures and to achieve higher fiber volumes in thinner sections than were successfully achieved in FP2.

Two basic approaches will run in parallel. The first is the extension of conventional SRIM technology to carbon fiber preforms of reduced section thickness (the target is 1.5 mm) in support of the ACC FP3. The tools required for this project will be the current ACC plaque mold and a new B-pillar shaped mold. The moldability of the chopped carbon fiber is expected to differ from glass because of differences in density, fiber size and stiffness, bundle size, sizing, binder type, and higher fiber loading. This program is under the direction of and includes the direct participation of ACC personnel. The second approach will be to work with supplier-partners to adapt their liquid molding processes toward greater compatibility with the material property and processing requirements of FP3.

The project team includes personnel from the Big Three automotive companies and Oak Ridge National Laboratory. The support team includes personnel from the NCC and Visteon. Supplier-partners are Cyclics Corp. and Huntsman Chemical.

Plaque Molding Program

The plaque molding program was intended to characterize the SRIM injection/compression processing of chopped carbon fiber preforms with urethane resin. It was carried out with the ACC plaque mold in the 1000-ton press at NCC. The program was set up at NCC in anticipation that the B-pillar program would also be located there. This strategy also co-located the molding operations with the ACC programmable powered performing process (P4) preformer. This allowed the reactivation of the SRIM equipment at NCC, which had been idle since the completion of FP2, in anticipation of FP3 molding needs. Figure 1 shows the plaque mold installed in the NCC press.

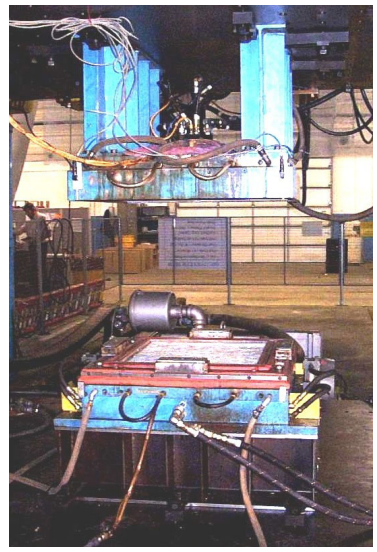

Figure 1. Plaque mold in the press at NCC.

The following table lists the experimental design variables for this program.

DESIGN VARIABLES	**—**	**0**	**+**
Reinforcement fiber type	Carbon		Glass
Reinforcement volume %	35	40	45
Target plaque, mm	1.5		3.0
Press tonnage	200	300	400
Injection gap, mm	8		25

Output data from this molding study included the molding pressure traces from the in-mold monitoring; the overall plaque quality, including observations on fiber wash, dry areas, and surface appearance; and plaque thickness. Mechanical properties testing is in progress on a selected number of plaques from this experiment.

The main findings to date are that the high-volume-fraction reinforcement required higher press tonnage than the FP2 style preforms (400 tons vs 150 tons) and the carbon fiber preforms required slightly higher tonnage than the glass. The in-mold pressures were slightly higher for the carbon fiber preforms, indicating a higher flow resistance and

lower permeability for the carbon fiber preforms. Direct permeability measurements are being made by the ACC preforming program. The lighter-weight preforms (thin, low volume content) were susceptible to fiber wash, but this was minimized by using the higher injection gap.

B-Pillar Molding Program

The B-pillar molding program is designed to bridge the gap between the plaque molding and the FP3 body side molding programs. The mold is a simplified version of the B-pillar section of the full body side. The mold contains the minimum (1.5 mm) and maximum (8 mm) thicknesses of the full part and the bonding flanges. It will be used to generate data on the molding characteristics of the high-volume carbon fiber preforms of complex shape and to assist in the final design of the body side molds. The mold contains both the inner and outer cavities in the same base and will be able to produce parts for bonding studies (Figure 2).

The mold was designed and built by Hi-Tech Mold and Engineering. It has been delivered and installed in the press at NCC (Figure 3).

Shakedown molding is under way with glass fiber preforms. Some additional refinements will be made in the preforming program using glass before the carbon fiber work begins.

Figure 2. B-pillar mold showing the inner (near) and outer (far) with glass reinforcement.

Figure 3. B-pillar mold being delivered to the NCC.

Supplier-Partner Liquid Molding Programs

Work is under way with two supplier partners, Huntsman Chemical and Cyclics Corporation, to develop alternate liquid molding processes.

The Huntsman process consists of co-spraying the urethane resin along with the chopped fiber reinforcement into an open mold, then closing the mold and curing. Huntsman has supplied plaques with its current technology to ACC for evaluation. An improved mix head has recently been installed that should produce higher reinforcement content at a thinner cross section.

The Cyclics resin is a thermoplastic polyester material that reacts by a ring opening polymerization. This offers the potential for a liquid molded thermoplastic matrix process, but a rapid production system is still to be developed. Evaluation plaques of the Cyclics material have also been supplied to the ACC.

Initial mechanical and DMA testing of these materials have determined both the Huntsman and Cyclics systems to be candidates for further processing development.

5. LOW-COST CARBON FIBER

A. Low-Cost Carbon Fibers from Renewable Resources

Project Contact: C. F. Leitten, Jr., W. L. Griffith, A. L Compere
Oak Ridge National Laboratory
Post Office Box 2009
Oak Ridge, TN 37831-8063
(865) 576-3785; fax: (865) 574-8257; e-mail: leittencfjr@ornl.gov

Field Project Manager: C. David Warren
Oak Ridge National Laboratory
Post Office Box 2009
Oak Ridge, TN 37831-8050
(865) 574-9693; fax: (865) 574-4963; e-mail: warrencd@ornl.gov

Technology Development Manager: Joseph Carpenter
(202) 586-1022; fax: (202) 586-1600; e-mail: joseph.carpenter@ee.doe.gov
Field Technical Manager: Philip S. Sklad
(865) 574-5069; fax: (865) 576-4963; e-mail: skladps@ornl.gov

---

Contractor: Oak Ridge National Laboratory
Contract No.: DE-AC05-00OR22725

Objective

- Investigate and establish proof-of-principle processing conditions for several types of low-cost carbon fiber precursor materials that are suitable—in properties, volume, and cost—for use by the automotive industry.

Approach

- Evaluate the spinning of fiber from high-volume renewable and recycled fiber streams.
- Evaluate the carbonization and graphitization of renewable and recyclable fibers using a variety of bench techniques (e.g., thermogravimetric analysis, micrography, resistance/conductance).
- Evaluate the effects of modern carbon fiber production technologies (e.g., hot stretching, controlled thermal and atmospheric environment) on selected fibers to improve properties.
- Focus on factors (e.g., feedstock availability, cost, and yield) critical to economic feasibility.
- Evaluate mechanical and composite properties of graphitized melt-spun fibers.

Accomplishments

- Established proof-of-concept demonstration for single lignin-based fibers:
  - Compositions
  - Processing methods
  - Evaluations
  - Fiber quality

- Obtained preliminary data indicating that yields of 50%, consistent with those obtained commercially for lignin-based activated carbon, are feasible.
- Successfully prepared lignin-blend fibers with a dominant graphitic content at a firing temperature of 2000°C.
- Successfully spun small amounts of multiple lignin-based fibers (4 strands) at the University of Tennessee. No sticking problems were apparent, and fiber diameter was reduced from ~80 microns to ~20 microns, with an apparent increase in mechanical properties. (To our knowledge, this is the first time that a multiple-filament lignin fiber has been spun.)
- Successfully produced 28-filament tow on the initial attempt after methods to remove lignin contaminants were developed.

Future Direction

- Working with MeadWestvaco, supply lignin that has been screened prior to precipitation and drying. (Based on results to date, this material will be melt-spinnable.)
- Emphasize work on multiple-filament spinning to produce smaller (10–15 micron) fiber in small tows (20–50 fibers).
- Perform multiple-fiber hot-stretching, stabilization, and carbonization/graphitization tests.
- Perform initial studies on fiber-resin interactions to provide a basis for systems used in small composite tests.
- To move program technology toward active commercialization, study economics and adaptation to existing lignin and polymer recycle lines and evaluate fiber processability using commercial technology. Also, actively seek increasing industrial partnership and participation.

Introduction

This project focuses on development of carbon fibers from high-volume, low-cost, renewable or recycled fiber sources to reduce precursor and processing costs. Use of these materials also decreases the sensitivity of cost to changes in petroleum production and in energy costs. Earlier literature reports indicate that a wide variety of fibers—Kevlar®, nylon, polyacetylene, polyethylene, polystyrene, and pitch—as well as natural and renewable products such as wool, rayon, and lignosulfonate were also used to make low-performance carbon fibers in the 1960s and 1970s. In quality, cost, and volume, kraft lignins and recycled petrochemical polymers are attractive in the United States. This project will evaluate the feasibility of preparing carbon fiber precursors from a variety of high-volume renewable and recycled polymers.

Project Deliverables

By the end of this multi-year project, the production of one or more environmentally-friendly, economically feasible carbon fiber precursors will be demonstrated.

Planned Approach

Producing low-cost, high-volume carbon fiber precursors requires the simultaneous development of processes for making the feedstock fibers and of downstream processing techniques that improve the properties of each type of fiber. Because of high levels of emissions and costs typically associated with spinning of fiber from liquids, first priority was placed on development of melt-spinning techniques for fiber. Using lignin and other non-nitrogenous feedstocks would eliminate cyanide emissions during furnacing. The use of modern furnacing techniques, such as hot-stretching and controlled atmosphere processing, is being evaluated to improve the properties and yield of carbon fiber precursors from feedstock.

Promising fiber blends will be prepared as precision, small-tow (25 to 50) fibers. In addition, they will be graphitized to permit evaluation of the finished fiber structure and of the mechanical properties of individual fibers and composites.

Blends and pre-fiber processing will be adjusted to facilitate spinning.

Carbon fiber for use in aerospace or recreational products is typically produced in three steps: (1) spinning, (2) stabilization/oxidation (with hot stretching, in the case of polyacrylonitrile), and (3) carbonization/graphitization under reduced oxygen or inert atmosphere to increase strength and stiffness. Systematic evaluation will be required to find appropriate conditions for spinning and furnacing melt-spun lignin-based fibers.

Precursor Evaluation

The U.S. automotive industry annually produces approximately 15 million cars and light trucks. In 1997, these vehicles averaged 985 kg of ferrous metals. Replacing ferrous metals in light transport with 60% carbon fiber resin composites would require ~4 million tonnes of carbon fiber. Use of carbon fiber would be a significant step in reducing life-cycle greenhouse gas emissions in that it would both sequester renewable carbon in a long-term storage form (carbon fiber) and decrease the fuel and emissions required to operate light transport. By doing so, carbon fiber technology could (1) decrease dependence on petroleum imports and (2) decrease tariffs levied against domestic vehicles by countries committed to greenhouse gas reduction.

Lignin is a ubiquitous polymer that typically constitutes 20–30% of wood and woody biomass. In pulping, lignin and lignin compounds are separated from cellulose and either burned, or recovered and sold as a byproduct. Detailed estimates place the volume of lignin in chemical pulping liquors at around 85,000 tonnes per day. Diversion of ~10% of this material to production of a melt-spun, 80% lignin/20% recycled polymer fiber would permit replacement of 50% of the ferrous materials in light passenger transport.

Gasification—which is being evaluated as an alternative to current pulp-mill lignin combustion processes—could provide significant amounts of lignin, as well as high-temperature process heat and low-cost electricity. This could greatly increase the availability and decrease the price of carbon fiber.

Fiber Spinning

Studies of melt-spun single lignin-blend fibers have continued. Because of its narrow melting point range, Westvaco hardwood kraft lignin has been used. As reported earlier, it was desalted prior to use to prevent void formation during graphitization.

Under a completed contract, single lignin-blend fibers were spun to our specifications by North Carolina State University staff from prepared lignin mixtures. Although the fiber diameters were somewhat variable, the quality was sufficient to demonstrate proof-of-concept for melt-spun lignin-blend carbon fiber feedstocks. The major difficulties with single fibers were inconsistent diameters among batches and a diameter higher than that appropriate for use in composites. However, the results from these stages of investigation indicated that the next step, production of melt-spun multifber tow, was likely to be successful.

Professors Petrovan and Collier of the University of Tennessee (UT) were contracted to provide multiple fiber spinning. Using a conventional twin-screw extruder equipped with a multifilament die, it was possible to produce non-sticking, drawable multiple kraft lignin-blend fiber. The fiber was strong enough to permit drawing from a 600-μ die to a <30-μ raw fiber. The Leistritz twin screw ZSE-27 extruder is a standard industrial extruder that can be readily scaled: the largest comparable Leistritz twin screw extruders can produce more than 100 tonnes of raw fiber per day, enough for half the current worldwide carbon fiber production.

This is believed to be the first successful melt-spinning of multiple kraft lignin-blend fibers.

The most significant difficulties encountered in melt-spinning the lignin-blend fiber were due to an unforeseen (and unusual) contaminant in the hardwood kraft lignin processed for this project. The primary constituent was a fibrous, non-melting cellulosic that blocked portions of the die. It appears to have been a residue from other types of processing performed in the same lignin production facility and was present at <1%.

Desalted lignin was successfully cleaned and processed using a 28-filament die with an average hole size of 225 microns. The resulting raw fibers were readily spooled, as shown in Figure 1, and relatively uniform, as shown in Figure 2.

The lignin manufacturer, MeadWestvaco, is preparing a fresh batch of hardwood lignin for this project.

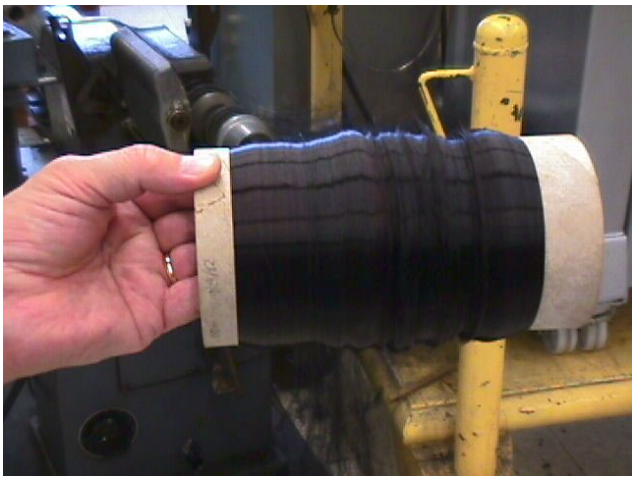

Figure 1. Spool of lignin-blend fiber spun through 28-filament die using UT Leistritz twin-screw extruder

Figure 2. Raw lignin-blend fiber spun through 28-filament die.

Stabilization, Carbonization, and Graphitization

Conditions that provide good stabilization of lignin fiber blends containing polyesters, polyolefins, and polyethers continue to be profiled. Computer-controlled furnacing and a novel technique for stretching single fibers are producing the dense, solid fibers shown with little or no inter-fiber adhesion or melting.

After stabilization, the lignin-blend fibers were carbonized in a reducing atmosphere, again with hot stretching. Carbonized lignin-blend single fibers are dense and compact with relatively few visible defects. Figures 3 and 4 show carbonized fibers spun through the 28-filament die at UT.

Figure 3. Carbonized fibers from 28-filament die tests.

Figure 4. Tip of carbonized fiber from 28-filament die showing dense fiber structure and smooth surface.

The carbonized fibers were then heat treated in an inert atmosphere to temperatures between 1400 and 2400°C. Fibers heated to 2400°C showed a pronounced graphitic structure with X-ray diffraction, while fibers processed at 1400 and 1600°C showed no graphitic structure. Cursory mechanical testing of single fibers indicated strength and stiffness similar to that of standard industrial fibers of comparable diameters and processing temperatures. Attempts were made to incorporate these fibers into resin and measure the resultant composite properties. The tests were unsuccessful because there was little to no fiber-resin adhesion. With an appropriate resin and sizing system, this type of composite testing can be successfully evaluated.

Future Direction

Proof-of-concept production of small amounts of 4- and 28-filament lignin-blend fiber tow has been established. Economic studies, coupled with strength and stiffness evaluations, indicate the potential for use of this material as a feedstock for industrial-grade carbon fibers.

The near-term goals center around development of methods for consistent production of small (25–50 filament) tows that produce even, dense carbon fibers with 10 to15-micron diameter. The studies involved in this will include melt-spinning, systematic evaluation of lignin-polyester blends and plasticizers, optimization of stabilization and carbonization profiles, and evaluation of fiber surface treatment to increase resin bonding.

Conclusions

This project has demonstrated the first multiple melt-spun lignin-blend fiber tow.

Several lignin-based-blend fibers that can be oxidized, carbonized, and graphitized have been demonstrated using equipment and techniques

developed during this project. Preliminary evaluation indicates that production of carbon fiber precursor from renewable and recycled materials is likely to be feasible. The yield of carbon fiber, ~50%, is consistent with data from lignin-based activated carbon.

Production of small tows from lignin-polyester blends by melt-spinning has been demonstrated. However, studies are needed to optimize and extend the production techniques to produce consistent, dense, defect-free carbon fiber in order to facilitate the ultimate transition of the technology to industrial use. Development of fiber surfacing and resin systems critical to production of strong, durable composites is also needed. The knowledge base for production of this exciting new fiber is being developed.

This technology could play an important part in reducing the weight, fuel consumption, and emissions of passenger vehicles because lignin from kraft pulp mills is available in large enough quantities to replace more than half of the steel used in such vehicles.

B. Low-Cost Carbon Fiber Development Program

Program Manager: Mohamed G. Abdallah
Hexcel Corporation
P.O. Box 18748, Salt Lake City, UT 84118
(801) 508-8083; fax: (801) 508-8103; e-mail: mohamed.abdallah@hexcel.com

Field Project Manager: C. David Warren
Oak Ridge National Laboratory
P.O. Box 2009, Oak Ridge, TN 37831-8050
(865) 574-9693; fax: (865) 574-4963; e-mail: warrencd@ornl.gov

Technology Development Manager: Joseph A. Carpenter
(202) 586-1022; fax: (202) 586-1600; e-mail: joseph.carpenter@ee.doe.gov
Field Technical Manager: Philip S. Sklad
(865) 574-5069; fax: (865) 576-4963; e-mail: skladps@ornl.gov

Principal Investigators:
Harini Dasarathy, Carlos Leon y Leon, Stephen Smith, and Brent Hansen

---

Contractor: Hexcel Corporation
Contract No.: 450001675

Objective

- Define technologies needed to produce a low-cost carbon fiber (LCCF) for automotive applications at a cost of $3 to $5 per pound in quantities greater than one million pounds per year. The required carbon fiber properties are a tensile strength greater than 400 ksi, a modulus greater than 25 Msi, and a strain-to-failure rate of greater than 1%.

Approach

- Develop new precursors that can be converted into carbon fiber at costs below the costs of current processes.
- Explore processing by methods other than thermal pyrolysis.
- Develop technologies leading to significant improvements in current production methods and equipment.
- Develop alternative methods for producing carbon fiber from pitch, polyacrylnitrile (PAN), or other precursors.
- Reduce precursor cost by the use of commercially available energy-efficient precursors and high conversion yields.
- Improve precursor production economics of scale and throughput.
- Introduce novel low-cost carbon fiber production methods.

Accomplishments

- Evaluated proposed research areas through laboratory trials and refinement of manufacturing cost analyses. These focused on:
  - PAN-based precursors: large-tow benchmark, commodity textile acrylic tow, chemical modification, acrylic fibers spun without solvents, and radiation and nitrogen pretreatment of PAN-based materials.

  - Precursors other than PAN: polyolefins—polypropylene (PP), linear low-density polyethylene (LLDPE) and high-density polyethylene (HDPE); polystyrene; and polyvinyl chloride (PVC) pitch.
- Scaled up promising technologies to pilot line trials.
- Assessed the technical and economic feasibility of the proposed research areas.
- Down-selected the most promising technologies to meet the program objectives:
  - Commodity textile acrylic tow with chemical modification or radiation pretreatment.
- Developed detailed manufacturing cost models for the down-selected technologies.
- Commenced the engineering feasibility studies for a large-scale production line.
- Proposed two follow-up programs;
  - A short-term (1-year) program to develop carbon fiber roving to meet the immediate needs of the Automotive Composites Consortium (ACC) development programs.
  - A long-term (3-year) program to build on the results of the LCCF program to produce production quantities of commodity textile acrylic–based carbon fiber for the ACC programs

Future Direction

- Complete the engineering feasibility study of the large-scale production line for commodity acrylic–based carbon fiber.
- Develop manufacturing project plans that include the configuration of facilities, sites, supply of raw materials, and economic feasibility studies for the selected technology(ies) for the large-scale production of LCCF for automotive applications.
- Revise the cost model to reflect the updated equipment, labor, materials, and energy cost of the commodity textile–based carbon fiber
  - Develop the program plans for the follow-up programs:
  - A short-term (1-year) program to develop carbon fiber roving to meet the immediate needs of the ACC development programs.
  - A long-term (3-year) program to build on the results of the LCCF program to produce production quantities of commodity textile acrylic–based carbon fiber for the ACC programs.

Introduction

The goal of this program is to define and demonstrate technologies needed for the commercialization of LCCFs to be used in automotive applications. Lighter-weight automotive composites made with carbon fibers can improve the fuel efficiency of vehicles and reduce pollution. In order for carbon fibers to compete more effectively with other materials in future vehicles, their cost must be reduced.[1–3] Specifically, this program targets the production of carbon fibers with adequate mechanical properties, in sufficiently large quantities, at a sustainable and competitive cost of $3 to $5 per pound.

Project Deliverables

At the end of this multi-year project, technologies for LCCF production will be defined. This definition will include the required materials and facilities and will be supported by detailed manufacturing cost analyses and processing cost models. Laboratory trials and pilot-scale demonstrations will be performed to support the defined technologies.

Planned Approach

This project was divided into two phases:

Phase 1: Critical review of existing and emerging technologies, divided into two tasks:

Task 1.1. Literature review and market analysis.

Task 1.2. Laboratory-scale trials and preliminary LCCF manufacturing cost assessments for the proposed

technologies. Phase 1 led to further refinement and down-selection of the most promising technologies for Phase 2.

Phase 2: Evaluation of selected technologies using pilot-scale equipment and cost models. Phase 2 was divided into three tasks:

Task 2.1. Pilot-scale design for the evaluation of selected LCCF technologies. This task included modification of a PAN-spinning pilot line (PL) and two different carbon fiber conversion lines [a single-tow research line (RL) and a multi-tow PL] and the construction of continuous sulfonation processing equipment

Task 2.2. Experimental evaluation of down-selected LCCF technologies, including commodity textile-tow PAN (with chemical modification and radiation and/or nitrogen pretreatment) and polyolefins (LLDPE and PP).

Task 2.3. Large-scale feasibility study of selected LCCF technologies.

The planned approach included decision points within each of the tasks in order to further down-select and define the most promising technology(ies) that will meet the program objectives, as indicated in the overall LCCF program timeline (Figure 1).

Conclusions of FY 2001 Results

The results of the laboratory trials of proposed technologies were as follows.

1. We halted further work on acrylic fibers spun without solvents, plasticized PAN, PVC, and polystyrene because of technical, environmental and cost issues.
2. We evaluated and selected the following most promising LCCF technologies for Phase 2: commodity textile PAN-based precursors (as-received and with pretreatment using chemical modification, radiation, and nitrogen pre-stabilization technologies) and polyolefin precursors (LLDPE and PP).
3. We used a large-tow PAN precursor technology benchmark as a metric to evaluate the proposed technologies in terms of their potential to meet the LCCF cost targets. The difference between commodity textile PAN and large-tow precursor, based on carbon fiber cost, is approximately $1.80 vs $3.10/lb.

Summary of the Results of FY 2002

Task 2.2.1.1. Chemical Modification of PAN Fibers[4]

Chemical modification of commodity acrylics was one of the down-selected technologies carried forward based on a successful proof of concept using standard PAN precursor. Cost projections for carbon fiber using this technology, in conjunction with commodity textile fiber and conversion technology information available at that time, had indicated a price range of from $5 to 5.25/lb. The task ahead for the third year was well defined: demonstrate the technology equivalence of commodity textile fiber and achieve the desired carbon fiber property targets.

The work plan for FY 2002 was as follows:

- Spin and modify textile polymer on the PAN PL.
- Optimize the oxidation/carbonization process to achieve LCCF target properties.
- Screen textile acrylic fiber candidates
- Perform in-line chemical modification of 28-K textile fibers.
- Carbonize chemically modified 28-K textile fibers.
- Reduce process cost.
- Define process recipe.
- Estimate cost.

The following sections summarize the work performed and results achieved during FY 2002.

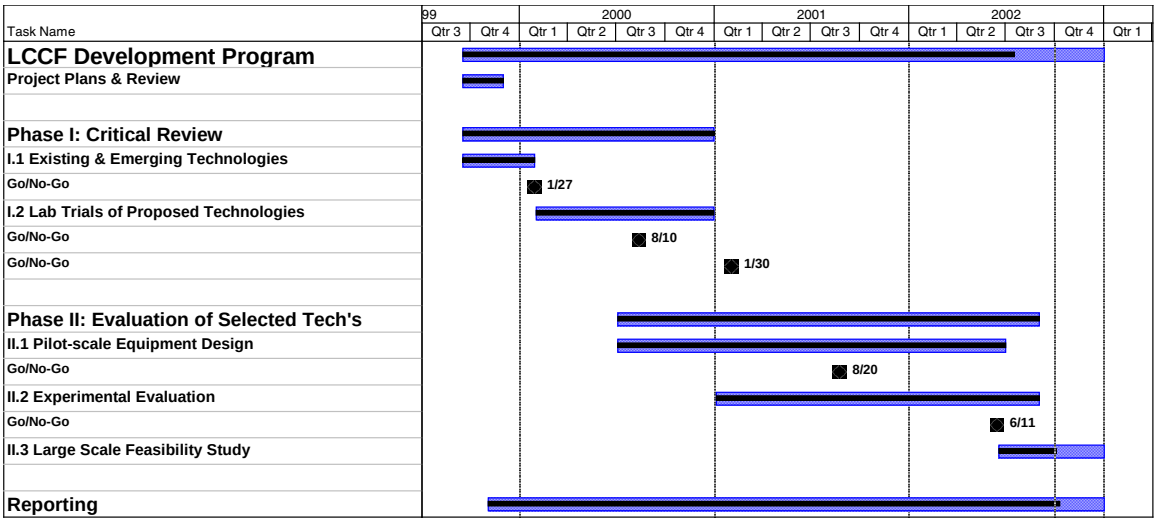

Figure 1. Low-cost carbon fiber development program timeline.

Spin and modify textile polymer on PAN pilot line

Sterling Fibers, Inc., was identified as a reliable textile polymer source. Sterling Fibers agreed to supply 500 lb of its commercially available textile polymer [IP-49] as 35% water slurry. This polymer was spun and modified in the Decatur PAN PL (trial PL056) using a modifier solution of 4% NaOH + 7.5% H_2O_2. One control spool (PL056-1-27) and three spools of modified fibers (PL056-1-28, 29, and 30) were collected. DSC spectra comparison (Figure 2) showed a slope change for the modified fiber of between 200 and 300°C. Since this is also the temperature range when the PAN precursor fibers are oxidized and stabilized, it was deemed possible to oxidize and stabilize the modified fiber by proper selection of time/temperature profile.

Optimize oxidation/carbonization process to achieve LCCF target properties

Batch oxidation of control and chemically modified fibers was performed to determine the temperature/time profile to obtain the highest oxidized fiber density without fiber failure. An oxidation profile with an average temperature of 240°C and a 75-min residence time was selected for continuous RL carbonization. Carbon fiber made from chemically modified fibers met the LCCF target properties of 400 ksi tensile strength,

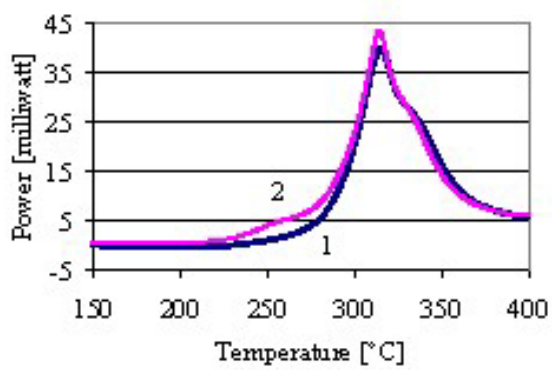

Figure 2. DSC spectra of PL056-1-27 [(1) control] and PL056-1-30 [(2) chemically modified] fibers.

25 Msi modulus, and >1% strain (Table 1). The control fiber could also be carbonized, but the carbon fiber properties were well below the LCCF target.

In the last run, the oxidation densities of control and modified fibers were matched. The modified and control fibers needed 58 and 75 min, respectively, to achieve the same oxidation density of 1.32 g/cm^3. The carbon fiber properties from modified fiber did not drop to the control fiber level. This indicated that chemical modification not only reduces the stabilization time but also contributes toward increasing the strength of the carbon fiber.

Once it was established that the fibers spun from textile polymer could achieve the desired properties, a set of screening experiments using

Table 1. Processing conditions and carbon fiber properties of textile polymer fiber (chemically modified) spun on the Hexcel PAN pilot line.

Processing conditions and fiber properties		PL056 fiber ID				
		1-27	1-27	1-29	1-30	1-29
Modifier composition	(%)	None	None	4% NaOH + 7.5% H_2O_2		
Oxidation residence time	(min)	75		75		58
CF density	(g/cm^3)	1.73	1.73	1.72	1.74	1.76
CF mass per unit length	(g/m)	0.195	0.198	0.217	0.202	0.207
CF tow tensile strength	(ksi)	275	250	420	412	443
CF tow tensile modulus	(Msi)	28.2	28.7	29.7	31.4	29.0
CF strain to failure (measure)	(%)	1.00	0.88	1.35	1.25	1.44

polymer films was performed to optimize the concentrations of sodium hydroxide and hydrogen peroxide in the modifier solution. Results suggested that it would be beneficial to increase the NaOH concentration from 4% to 6%.

Screening textile acrylic fibers

A second meeting was held with Sterling Fibers to explore the possibility of obtaining true textile fiber based on IP-49 polymer. Sterling agreed to supply 1000 lb of 28-K uncollapsed wet IP-49 fiber for chemical modification trials in the Decatur PAN PL.

DSC and Fourier transform infrared analysis data of the as-received IP-49 fibers matched those of PL056-1-27 spun in the Hexcel PAN PL. Lab-scale screening tests for chemical modification of the 28-K Sterling IP-49 were performed with various modifier solution compositions. Results indicated the following:

1. Modifier (4% NaOH + 7.5% H_2O_2) was effective on textile PAN fiber and was not specific only to Decatur spun fibers.
2. H_2O_2 in the modifier could be reduced to 3.5% and possibly even eliminated and still achieve the desired modification.

In-line chemical modification of 28-K textile fibers

The 28-K IP-49 based textile fiber was chemically modified on the PL. Modifier compositions for various runs and sodium levels in the modified fibers are shown in Table 2.

Batch oxidation of some of the modified fibers (PL065) was performed with a total residence time of 58 min. Based on DSC and FTIR analyses,

Table 2. Inline chemical modification of Sterling 28-K fibers.

Sample ID	Modifier		Na content in fiber (ppm)
	NaOH (%)	H_2O_2 (%)	
PL065-CM01	0.00	0.00	215
PL065-CM02	6.00	0.00	3366
PL065-CM04	6.00	3.50	2494
PL065-CM05	5.00	3.50	4069
PL065-CM06	4.10	3.50	2603
PL065-CM07	3.90	3.50	2595
PL065-CM08	3.35	3.50	3145
PL065-CM09	2.75	3.50	2071
PL065-CM11	2.25	3.50	1737

PL065 CM1 (control), PL065 CM2, and PL065 CM4 were selected for carbonization trials.

Carbonization of chemically modified 28-K textile fibers

PL065-CM1, CM2, and CM4 were oxidized on the RL and carbonized on the evaluation line. The carbon fiber properties are shown in Table 3. The data show that chemically modified textile fibers modified with one- and two-component systems meet all the carbon fiber target properties.

Process cost reduction

After achieving the desired carbon fiber properties, the work focused on minimizing the cost of the modification and carbonization processes. Since carbon fiber properties of 28-K fibers modified with only NaOH also met target properties (PL065 CM2), additional PL trials were run with the NaOH concentration at 3, 4, 6, 8, and 10%. DSC analysis confirmed a successful modification effect for all concentrations. Batch oxidation experiments showed that the fibers

Table 3. Processing conditions and carbon fiber properties of Sterling 28-K fibers (modified with one- and two-component modifiers).

Processing conditions and fiber properties		PL065 fiber ID		
		CM1	CM2	CM4
Modifier composition	(%)	None	6% NaOH	6% NaOH + 3.5% H_2O_2
Oxidation residence time	(min)	58	58	58
CF density	(g/cm^3)	1.69	1.74	1.74
CF mass per unit length	(g/m)	2.151	1.983	2.098
CF tow tensile strength	(ksi)	268	423	359
CF tow tensile modulus	(Msi)	20.0	27.1	25.2
CF strain to failure (measure)	(%)	1.31	1.38	1.41

modified with 3, 4, and 6 % NaOH could be stabilized when oxidized for a 50-min residence time. Fibers modified with 8 and 10 % NaOH showed uncontrolled exotherm and resulted in fiber failure. Several carbonization trials were run under various processing conditions. Processing conditions and the resulting carbon fiber properties are shown in Table 4. The data show

Table 4. Processing conditions and carbon fiber properties of Sterling 28-K fibers (modified with NaOH)

Processing conditions and fiber properties		PL067 fiber ID	
		CM1	CM3
Modifier composition	(%)	0	6
Oxidation residence time	(min)	60	50
CF density	(g/cm^3)	1.71	1.74
CF mass per unit length	(g/m)	2.070	2.037
CF tow tensile strength	(ksi)	279	403
CF tow tensile modulus	(Msi)	17.5	23.7
CF strain to failure (measure)	(%)	1.55	1.66

that the chemically modified textile fibers can be successfully made into carbon fiber with a tow tensile strength of ~400 ksi. However, the tow tensile modulus fell below 25 Msi. Additional carbonization trials were run with 50 min of oxidation time and varied stretch conditions in low-temperature (LT) and high-temperature (HT) furnaces. Applying a fiber tension that gave 8% stretch in an LT and 3% shrinkage in a HT furnace resulted in carbon fiber with a tow tensile strength of 400 ksi and modulus of >25 Msi (Table 5). Since carbon fiber properties after 50-min oxidation were above desired levels, one fiber process. Fiber properties from this trial also met the LCCF property target levels. Under similar LT and HT conditions, carbon fiber properties of the

Table 5. Processing conditions and carbon fiber properties of Sterling 28-K fibers (modified with NaOH).

Processing conditions and fiber properties		PL067 fiber ID	
		CM1	CM2
Modifier composition	(%)	0	6
Oxidation residence time	(min)	75	50
CF density	(g/cm^3)	1.71	1.74
CF mass per unit length	(g/m)	1.884	1.820
CF tow tensile strength	(ksi)	335	462
CF tow tensile modulus	(Msi)	24.0	28.3
CF strain to failure (measure)	(%)	1.46	1.55

control fiber also showed improvement when the oxidation residence time was increased to 85 min. experiment was run with 34 min of residence time in oxidation to further lower the cost of the carbon

Process recipe definition

A total process recipe for the chemical modification of textile acrylic fiber for LCCF has been established for standard textile acrylic fibers (500K+ tow) as shown in Table 6. Since no empirical data are available for large tow, this recipe gives suggested ranges for each processing parameter, rather than absolute numbers from the 28-K processing conditions. For example, although Tables 3 and 4 indicate 6% as the modifier concentration, the recipe shows a range of 4 to 6% because the main criterion for successful carbonization is to obtain modified fibers that have a sodium level of between 3000 and 5000 ppm. Similarly, although oxidation residence times of as low as 34 min for the modified fiber gave desired carbon fiber properties, the residence time in the recipe is given as approximately 50 min, allowing for more time that might be necessary because of large-tow thermal mass constraints.

Table 6. Recipe for chemical modification and carbonization processes.

Description		Specification
Feed fiber		Un-collapsed textile acrylic fiber
Modifier	(%)	4%–6% NaOH
Wash media		DI water
Finish		Precursor (textile) finish
Sodium level in the modified fiber	(ppm)	3000–5000
Oxidation/stabilization temperature	(°C)	240–250
Residence time in oxidation	(min)	≈50
LT temperature	(°C)	300–600
HT temperature	(°C)	1250–1400

Cost estimation

Using the parameters mentioned in the recipe and the cost model supplied by DOE, the cost of producing carbon fiber from textile acrylic fiber was estimated at $4.23/lb for mill cost and $5.83/lb, including a 20% return on investment.

Task 2.2.1.2. Radiation Treatment of Textile Acrylic Fiber[5]

The viability of using radiation pretreatment to reduce carbon fiber manufacturing costs was demonstrated in 2001. This work showed that using an E-beam radiation pretreatment step significantly increased the oxidation rate of textile-based acrylic fibers, which are typically much less reactive to thermal oxidation than specialty PAN precursor fibers. However, the resulting carbon fiber had mechanical properties that were lower than the requirements of this project. It was believed that using a modified textile acrylic composition containing slightly less vinyl acetate might result in improved carbon fiber tensile properties.

Work performed in 2001 used a textile polymer that was made into a small-tow (3-K filament) fiber on the Hexcel Decatur PL. Work in 2002 focused on obtaining a different composition textile acrylic fiber and demonstrating the ability to apply a radiation treatment to increase the oxidation rate and also meet the mechanical property requirements of this program.

Sterling Fibers of Pace, Florida, was asked to supply textile PAN polymer that could be used to produce small-tow (3-K) textile PAN at the Hexcel Decatur PAN PL. Spools of this spun fiber were taken to Energy Sciences (ESI) in Wilmington, Massachusetts, for continuous E-beam radiation treatment. The equipment was set up so that individual or combined 3-K tows of the PAN fiber could be passed continuously from a feed spool through the E-beam radiation chamber and then collected on a winder. Several trials were run with fibers irradiated to different dosage levels. In all of the trials, there was a visible color change in the PAN fiber following the radiation treatment. The PAN fiber that was white prior to radiation turned into a yellow-gold color afterward. As expected, the trials with higher radiation dosages resulted in darker fiber. These trials went very well, and irradiated PAN fibers were produced. The irradiated fiber samples were then sent back to Hexcel Decatur for oxidation and carbonization studies.

The reason for performing the radiation pre-treatment step was to controllably increase the oxidation rate of the textile PAN fibers. Accordingly, the irradiated fibers were then subjected to a series of oxidation trials to determine how much impact the radiation treatment had on the oxidation performance of these fibers. It was shown that the PAN fiber with the radiation pretreatment could be oxidized in less than 65% of the time required to oxidize the non-radiated control fiber. The irradiated fibers could be oxidized to a 1.34 g/cm³ density in a total time of 50 min, while the non-irradiated control fiber required at least 75 min to reach an oxidized density of only 1.32 g/cm³. An oxidation residence time of 50 min is comparable to that used today for the manufacture of aerospace-grade carbon fiber from specialty PAN precursor. These textile-PAN–based, E-beam-irradiated fibers were also converted into carbon fiber using the RL at Hexcel Decatur. The results from these carbonization trials are shown in Table 7.

These carbonization trials show that not only does the irradiated fiber oxidize at a faster rate but

Table 7. Properties of carbon fiber made from textile PAN polymer and spun in-house in a pilot-scale facility

Description		Control not radiated (3K)	E-beam radiated 30 Mrad (12K)	E-beam radiated 30 Mrad (12K)
Oxidation residence time	(min)	75	75	50
Oxidized fiber density	(g/cm^3)	1.32	1.38	1.34
Fiber density	(g/cm^3)	1.73	1.70	1.70
Fiber MPUL	(g/m)	0.196	0.870	0.790
Tow tensile strength	(ksi)	263	420	435
6-1 tow tensile modulus	(Msi)	28.4	29.3	25.1
Tow tensile elongation	(%)	0.94	1.38	1.63

also the resulting carbon fiber has significantly improved tensile strength (over 50% higher) compared with the control (non-irradiated) material. The carbon fiber properties of this irradiated material also exceed the requirements of the LCCF project for tensile strength and modulus.

This set of trials demonstrated that textile PAN polymer could be used to produce carbon fiber with mechanical properties that meet the targets. The next step in scaling up this approach was to obtain a true textile-grade fiber bundle that is small enough to be processed through standard oxidation and carbonization equipment. This requires a tow bundle of between about 20K and 80K filaments.

To continue the scale-up effort for this technology, Sterling Fibers was contacted about its ability to make a reduced-filament-count textile-grade PAN fiber. Sterling responded that it would be able to make fiber with a filament count of 28 K. This product would meet the objectives of this phase of the project: (1) it is a true textile fiber made at a commercial PAN manufacturing facility; and (2) it is a small enough tow bundle that it can still be handled and processed at the E-beam radiation facility and subsequently at the Hexcel Decatur conversion facilities.

Arrangements were made for Sterling to produce the 28-K PAN fiber. It was made from the same polymer used to spin the 3-K product at Hexcel Decatur described in the previous section. A total of about 60,000 m of the 28-K textile PAN fiber was produced.

A set of trials was conducted at ESI in April 2002 to irradiate the 28-K textile PAN fiber. The ESI equipment ran well, and tow spreading equipment made it possible to get the 28-K tow uniformly treated. The processing speeds used for these radiation treatments match up well with those used during carbon fiber manufacturing. This again suggests that the radiation equipment can be placed in-line at the beginning of the carbon fiber process to irradiate the fiber just prior to the oxidation step.

The spools of irradiated fiber were sent back to Hexcel Decatur for oxidation and carbonization trials. The DSC spectra for these fibers, shown in Figure 3, indicate advancement of the oxidation reactions for the irradiated fiber.

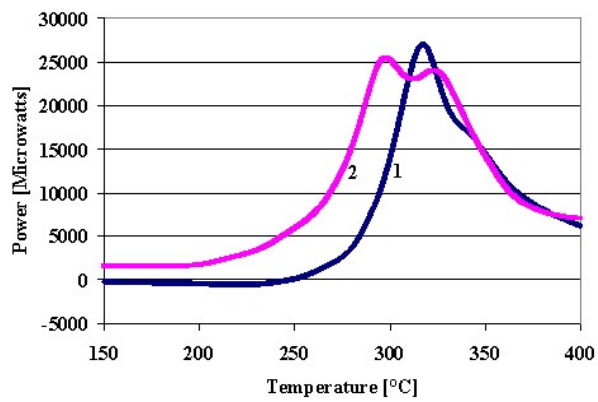

Figure 3. DSC spectra of control and E-beam irradiated 28-K textile PAN fiber (Sample 1: non-irradiated control. Sample 2: 30 Mrad radiation treatment).

As was shown with the 3-K textile-based fiber, the spools of 28-K fiber that had been irradiated underwent oxidation at a significantly faster rate than the non-irradiated samples. Using an oxidation residence time of 50 min, the fiber that had been irradiated at 30 Mrad reached an oxidized density of 1.36 g/cm^3. Using the same oxidation residence time, the non-irradiated control fiber reached an oxidized fiber density of

only 1.31 g/cm³. In this case, the radiation treatment reduced by about 40% the oxidation residence time needed to reach a typical oxidized fiber density of 1.35 to 1.36 g/cm³. The spools of 28-K fiber were then carbonized at the Hexcel Decatur facility. A summary of the processing conditions and test results is shown in Table 8. The data in this table represent average values of several spools that were oxidized and carbonized at the same processing conditions.

These trials have proved that a commercially available textile acrylic fiber made in a large-scale production facility can be pretreated with an E-beam radiation process and subsequently oxidized and carbonized at typical production rates to make carbon fiber that meets the mechanical property requirements of the LCCF development project (2760 MPa tensile strength and 172 GPa modulus). The radiation treatment step is key to both reducing the time required to complete the oxidation process and increasing the carbon fiber tensile strength from this textile acrylic fiber.

Task 2.2.2. Polyolefins

Polyolefins are bulk commodity polymers available at low cost, in fiber form, and with a high carbon content (~86% wt). These features clearly distinguish them from other non-acrylic-based materials as potential LCCF precursors.[1–3,6,7] Prior-art literature indicated that polyolefins (being thermoplastic) could be prevented from melting by crosslinking, but it offered limited information on practical LCCF conversion technologies and no evidence that polyolefin-based carbon fibers could be made with mechanical properties as high as needed to meet LCCF targets.[1,3] Work during FY 2002 focused on (a) developing continuous polyolefin fiber stabilization and carbonization processes and (b) demonstrating their ability to produce polyolefin-based carbon fibers that meet or exceed LCCF property targets.

Polypropylene

Earlier work in this project had demonstrated the feasibility of producing PP-based carbon fibers in a 2-step conversion process.[3] Preliminary trials yielded stabilized fibers the quality of which seemed to deteriorate with increasing degrees of sulfonation, and carbon fibers with relatively low mechanical properties. Many process improvements were made subsequently, but our attention was shifted to a polyolefin thought to be less prone to undergo destructive chain scission during stabilization: polyethylene (PE).

Polyethylene

LLDPE was selected over other types of PE because it provides a good compromise between spinnability and desirable structural features in a LCCF precursor.[3,6] Initial tests with LLDPE tows yielded carbon fibers with properties that fell below LCCF targets.[3] However, a systematic evaluation of process variables uncovered several pathways for improvement. In particular, the sulfonation process was found to be extremely sensitive to sulfuric acid concentration, reaction temperature, residence time, and line tension.[6] Optimum sulfonation parameters were determined through design-of-experiment trials. Optimization took into account the appearance of defects (grooves or cracks) in a small portion of sulfonated filaments, especially at conditions where high carbon yields (~80% wt) were

Table 8. Properties of carbon fiber made from 28-K filament textile PAN fiber

Description		Control not radiated (28K)		E-beam radiated 30 Mrad (28K)
Oxidation residence time	(min)	50	75	50
Oxidized fiber density	(g/cm^3)	1.31	1.34	1.36
Fiber density	(g/cm^3)	1.71	1.71	1.69
Fiber MPUL	(g/m)	2.070	1.884	1.903
Tow tensile strength	(ksi)	279	335	398
6-1 tow tensile modulus	(Msi)	17.4	24.0	26.0
Tow tensile elongation	(%)	1.55	1.40	1.46

attained. Optimum conditions (i.e., those leading to maximum carbon yield, maximum melting suppression, and minimum concentration of defective filaments) were found at (a) temperatures 5–10°C below the melting point of the precursor and (b) shorter residence times for higher acid concentrations.[6] Two-stage sulfonation was also explored as a means to reduce the concentration of filament defects. Fewer filament defects appeared at conditions that minimized the initial shock that LLDPE tows experience when plunged directly into hot sulfuric acid.

The continuous sulfonation reactor was redesigned to provide tight control of all key process variables.[6] Special challenges were posed by the need to maintain a constant concentration of sulfuric acid throughout the entire sulfonation process. Provisions were made to eliminate the influence of the slow dilution of sulfuric acid by ambient moisture, interactions with system components, and the addition of reaction byproducts (particularly water) to the reactor. These included minimizing the exposure of fresh acid to ambient air, working with excess sulfuric acid, and replenishing the reacting acid continuously with fresh preheated acid fed through a system of pumps and intermediate reservoirs. Several means to provide adequate line tension control were also tested.

Optimum conditions also depended on the properties of the starting LLDPE precursor employed. Lowering the precursor denier had a small effect on reaction rate, presumably because of a compensation effect between increased external surface area and restricted internal acid diffusion. On the other hand, increasing the LLDPE precursor melt index improved the processability and overall quality of the sulfonated tows.

Using the improved sulfonation reactor, small lengths (~ 100–300 ft) of sulfonated 3-K tows were produced from different LLDPE precursors. The sulfonated samples were continuously carbonized in N_2 under controlled tension in single-stage or two-stage tube furnaces. The latter provided better control of carbonization parameters. During continuous carbonization, it was noted that the sulfonated tows tended to exhibit an overall shrinkage. Most of the shrinkage occurred in the high-temperature furnace at 1350°C. At lower temperatures, the tows exhibited a tendency to stretch under constant tension, particularly at temperatures near where their major carbonization weight losses occur. This suggests that the LLDPE tows exhibit a plastic transition at low carbonization temperatures, which may be exploited to further improve fiber orientation.

The carbonized fibers were collected on cardboard cores and tested without further treatment. Impregnated tow strands were prepared for mechanical property testing using standard procedures, including tow cross-sectional areas calculated from density and weight-per-unit-length measurements. The results of selected LLDPE conversion trials are listed in Table 9.[7]

Table 9 shows that LLDPE fibers can be converted to carbon fibers that meet or exceed the LCCF mechanical property targets. Average tensile strengths and moduli as high as 395 ksi and 28.3 Msi were recorded, along with strain-to-failure values in the range 1.2 to 1.3%. X-ray diffraction analyses of selected samples showed their orientation, crystallinity and mechanical properties to be in line with those expected of PAN-based carbon fibers of comparable filament diameters.

Figure 4 provides a visual summary of the technical progress made in LCCF Task 2.2.2 since its inception. Preliminary manufacturing cost model projections suggest that the cost of LLDPE-based carbon fibers could be competitive with that of textile PAN-based alternatives. However, implementing the LLDPE conversion technology on a commercial scale would involve a significant departure from conventional carbon fiber manufacturing practices. This would require further investment in scale-up efforts and a novel infrastructure with long-term market potential. In this sense, and at their present stage of technological development, LLDPE-based carbon fibers are not ready to compete with textile PAN-based carbon fibers in potential LCCF markets.

Summary and Conclusions of FY 2002 Activities

These are the highlights of the progress made during FY 2002.

1. We demonstrated the technologies of chemical modification and radiation pre-treatments of commercial commodity textile (28 K) tow to produce LCCF that meets the project

Table 9. Selected results of LLDPE fiber sulfonation and carbonization trials

Acid conc. (%wt)	Shrinkage (%)		CF yield (%wt)	CF diameter (µm)	Fil. defects (%)	Hollow area (%)	Tensile strength (ksi)	Tensile modulus (Msi)
	Sulf.	Carb.						
96 (A)	23	12	61	9.8	5	11	129	15.3
96 (A)	12	10	68	9.9	4	0	220	NA
98 (A)	9	11	62	8.6	29	19	191	19.5
96 (B)	24	14	78	9.7	12	28	205	19.3
96 (B)	24	12	78	9.3	12	9	263	23.1
96 (B)	–32	12	77	9.2	24	0	338	25.8
96 (B)	–32	8	77	8.9	24	0	395	28.3

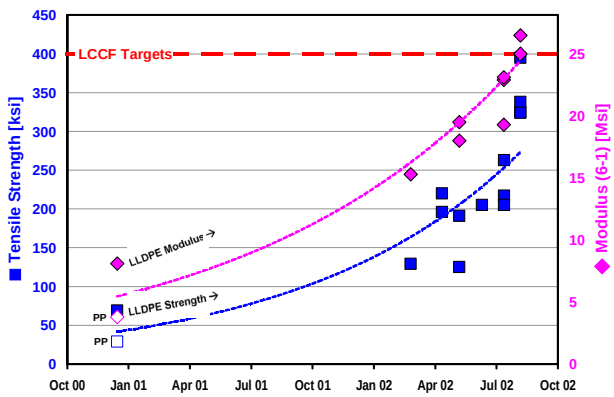

Figure 4. Low-cost carbon fiber task 2.2 (polyolefin conversion)

targeted properties and estimated cost predictions.

2. We developed manufacturing recipes for the conversion of commodity textile acrylic fibers into LCCF using the technologies of chemical modifications and radiation treatments.
3. Table 10 gives the estimated carbon fiber cost using chemical modification and radiation pre-treatment of commercial commodity textile acrylic fibers.
4. We demonstrated the conversion of LLDPE to LCCF that meet the targeted properties of the program and estimated cost predictions. Because of the issues of sulfuric acid recycling and the available precursor, we concluded that the LLDPE-based technology would need more development effort to compete with modified textile PAN-based technologies.
5. We commenced the engineering feasibility study of the production lines to produce LCCF based on commodity textile acrylic PAN using chemical modification and radiation pretreatment technologies.
6. We started the plans and statements of work for the long-term and short-term follow-up programs.
7. We updated and refined cost models to reflect the accomplishments in FY 2002.
8. We produced four papers (three published during SAMPE 2002, in Baltimore and one for the Global Outlook for Carbon Fiber 2002, in Raleigh, N.C.) and made a presentation during SAMPE 2002, in Long Beach, California.

Table 10. Estimated carbon fiber costs from commodity textile acrylic fibers

Hexcel proposed processes	Textile acrylic tow with			
	Chemical modification		Radiation treatment	
Process steps	Mill cost	With 20% ROI	Mill cost	With 20% ROI
Precursor	1.90	1.90	1.90	1.90
Pre-treatment	0.12	0.12	0.15	0.35
Stabilization/oxidation	0.71	1.51	0.71	1.51
Carbonization	0.69	1.19	0.69	1.19
Sizing, S.T., packaging, Q.C.	0.81	1.11	0.81	1.11
Total per pound of CF	$4.23	$5.83	$4.26	$6.06

References

1. C. A. Leon y Leon, R. A. O'Brien, H. Dasarathy, J. J. McHugh, and W. C. Schimpf, pp. 1–11 in M. Rokosz, R. B. Boeman, D. T. Buckley, and J. Jaranson, eds., *Development of Low Cost Carbon Fiber (LCCF) for Automotive and Non-Aerospace Applications. Part 1: Review of Existing and Emerging Technologies*, SAMPE-ACCE-DOE-SPE Midwest Advanced Materials and Processing Conference, Dearborn, Michigan, 2000.
2. S. Smith, pp. 12–23 in M. Rokosz, R. B. Boeman, D. T. Buckley, and J. Jaranson, eds., *Development of Low Cost Carbon Fiber (LCCF) for Automotive and Non-Aerospace Applications. Part 2: Precursor Processing Technologies, SAMPE-ACCE-DOE-SPE Midwest Advanced Materials and Processing Conference*, Dearborn, Michigan, 2000.
3. C. A. Leon y Leon, R. A. O'Brien, J. J. McHugh, H. Dasarathy, and W. C. Schimpf, *Polyethylene and Polypropylene as Low Cost Carbon Fiber (LCCF) Precursors*, 33rd International SAMPE Technical Conference, Seattle, Washington, 2001.
4. H. Dasarathy, T. Burleson, S. B. Smith, C. W. Herren, A. Frame, P. W. Heatherly, and W. C. Schimpf, *Low Cost Carbon Fiber from Chemically Modified Textile Acrylics*, SAMPE 2002, Baltimore, November 4–7, 2002.
5. H. Dasarathy, W. C. Schimpf, S. B. Smith, C. A. Leon y Leon, B. C. Hansen, C. W. Herren, A. Frame, and P. W. Heatherly, *Low Cost Carbon Fiber from Radiated Textile Acrylics*, SAMPE 2002, Baltimore, November 4–7, 2002.
6. C. A. Leon y Leon, W. C. Schimpf, C. W. Herren, A. Frame, P. W. Heatherly, and B. C. Hansen, *Low Cost Carbon Fiber from Non-Acrylic Based Precursors*, SAMPE 2002, Baltimore, November 4–7, 2002.
7. M. G. Abdallah, C. A. Leon y Leon, H. Dasarathy, B. C. Hansen, S. B. Smith, G. Jacobsen, and W. C. Schimpf, *Low Cost Carbon Fiber (LCCF) Program for Automotive Applications*, Global Outlook for Carbon Fibers 2002 Conference, Raleigh, N.C., October 22–23, 2002.

C. Low-Cost Carbon Fiber for Automotive Composite Materials

Principal Investigator: Donald G. Baird
Department of Chemical Engineering
Virginia Tech, Blacksburg, VA 24061
(540) 231-5998; fax: (540) 231-2732; e-mail: dbaird@vt.edu

Principal Investigator: Amod A. Ogale, Ph.D.
Clemson University

Co-Principal Investigator: James E. McGrath
Virginia Tech, Department of Chemistry
(540) 231-5976; e-mail: jmcgrath@vt.edu

Co-Principal Investigator: Dan D. Edie, Ph.D.
Clemson University

Technical Support: Michael Bortner, Ph.D. student; V. Bhanu, Post-doctoral associate
Virginia Tech

Technical Support: Conceicao Paiva, Ph.D., visiting assistant professor/research associate
Prajakta Kotasthane, Graduate research assistant
Keith Seal, Undergraduate research assistant
Clemson University

Field Project Manager: C. David Warren
Oak Ridge National Laboratory
P.O. Box 2009, Oak Ridge, TN 37831-8050
(865) 574-9693; fax: (865) 574-4963; e-mail: cdwarren@ornl.gov

Technology Development Manager: Joseph Carpenter
(202) 586-1022; fax: (202) 586-1600; e-mail: joseph.carpenter@ee.doe.gov
Field Technical Manager: Philip S. Sklad
(865) 574-5069; fax: (865) 576-4963; e-mail: skladps@ornl.gov

---

Contractor: Virginia Tech University
Contract No.: 4500011036

Objective

- Develop a cost-effective route to producing low-cost carbon fiber (<$5/lb) with a tensile strength of greater than 2.7 GPa, a modulus of >170 GPa, and a strain to failure rate of >1%. This range of carbon fiber properties has been deemed necessary for generating composite materials suitable for automotive applications.

Approach

- Develop melt-spinnable polyacrylonitrile (PAN) copolymers by controlling the copolymer ratio, molecular weight, and end-groups.
- Identify an alternate melt-spinnable precursor system containing a higher carbon content.

- Develop a new stabilization process based on ultraviolet (UV) irradiation to cross-link the fibers.
- Develop a thermal treatment for oxidative stabilization and carbonization of fibers made from different precursors to produce low-cost carbon fibers with desired mechanical properties.

Accomplishments

- Successfully synthesized melt-processable acrylonitrile (AN) copolymers using four different polymerization methods by copolymerizing methylacrylate (MA) with AN to produce a series of copolymers of controlled molecular weight but of variable MA content.
- Found that the best composition with sufficient stability for spinning on a laboratory system was 85/15 AN/MA with small amounts of chemical stabilizers (e.g., 1 wt% boric acid).
- Modified the AN/MA copolymer with 1 mole% photosensitive comonomer [acrylobenzophenone (ABP)] to yield a composition, 85/14/1 AN/MA/ABP, that was melt-processable and that could be subsequently stabilized (cross-linked and cyclized) by UV radiation.
- Successfully carbonized the stabilized fibers.
- Scaled up both the 85/15 AN/MA and 85/14/1 AN/MA/ABP compositions to 1-kg levels for further evaluation.

Future Direction

- Melt-spin multiple-filament bundles of fibers from the scaled-up copolymers to provide highly oriented precursors suitable for conversion to carbon fiber.
- Develop fundamental information on the scaled-up copolymers—concerning rheological properties as a function of temperature, time, and shear rate—that is needed to design a large-scale spinning system.
- Fine-tune the UV stabilization process and scale it up for handling multiple-filament bundles.
- Design a spinning pack to handle marginally stable precursor copolymers.
- Spin the 85/14/1 AN/MA/ABP terpolymers in a larger-scale spinning system to further establish the ability to melt-spin these materials.
- Explore the synthesis and study the rheology of terpolymers with higher AN content (~88%) to increase the rate of stabilization and carbon yield.
- Reduce the cost of the carbon fibers further by synthesizing AN/MA/epoxy terepolymers that can be photochemically stabilized in a matter of minutes, rather than hours.
- Continue to develop alternate methods of reducing oxidative stabilization time by introducing sites in the AN/MA copolymers that provide a site for cross-linking at lower temperatures.
- Continue to search for a lower-cost, higher-carbon-content precursor that can be photochemically rather than oxidatively stabilized.

Introduction

To use plastics in the manufacture of automobiles in order to reduce weight and thus improve energy consumption, it is necessary to reinforce them with glass or carbon fibers. Glass fibers are quite inexpensive (less than $1 per pound), but their reinforcing capabilities and density make them less desirable than carbon fiber. At present, carbon fibers suitable for use in automotive composites cost more than $7 per pound, making them prohibitively costly for general use. It has been determined that for carbon fiber to be used economically in the manufacture of automobiles, the price must be less than $5 per pound. Approximately half of the present cost for carbon fiber is associated with the production of the carbon fiber precursor. For automotive composites, the precursors at present are generated from PAN copolymers that are solution-spun using highly toxic solvents.

Considerable savings could be realized if these copolymers could be melt-spun without the use of the highly toxic solvents. Furthermore, as the PAN copolymers contain only about 50 wt% carbon, new precursors with higher carbon levels would reduce the cost even more.

Project Deliverables

At the end of this multi-year program, a melt-spinnable polymer system will have been developed and scaled up that is suitable for the production of carbon fiber precursors that can be stabilized more rapidly by means of radiation. This development will lead to a significant reduction in the cost of producing carbon fiber.

Planned Approach

To meet the target of generating carbon fiber that costs less than $5 per pound, the present approach using PAN copolymers must be significantly modified. These modifications include developing melt-spinnable PAN copolymers that can be stabilized and carbonized efficiently and economically and identifying a precursor system that contains higher carbon levels.

Melt-Spinnable PAN Copolymers

Melt-processable AN copolymers were successfully prepared by copolymerizing MA with AN to produce a series of copolymers of controlled molecular weight but variable MA content. In a significant departure from past procedures, copolymers were prepared with an azo-initiator, which produced non-associative end groups and thereby led to a significant reduction in melt viscosity. These materials were successfully extruded on a laboratory-scale spinning system (see Figure 1a) to produce carbon fiber precursors (Figure 1b).

Efforts must be continued to obtain the highest AN-to-MA ratio possible, while keeping the molecular weight at the highest level possible, to provide adequate melt strength for melt-spinning. The approach we are taking requires that a delicate balance be maintained between a copolymer that is sufficiently stable to be melt-spun, but eventually will become unstable so that cross-linking and cyclization can take place in a subsequent step. As a result, we are investigating other avenues for

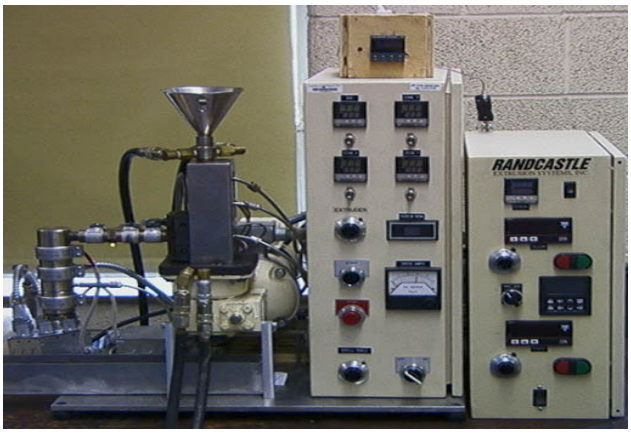

Figure 1a. Micro-spinline for producing carbon fiber precursors from small quantities of polymer (<50 g).

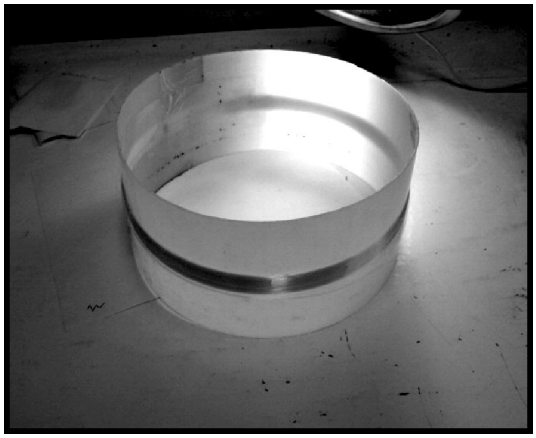

Figure 1b. Precursor fibers produced as a multi-filament tow from a batch-extruder.

stabilizing the fiber precursor besides direct thermal oxidative methods. One approach employs the use of a UV-sensitive coating applied to the fibers, which, when subjected to UV radiation, will initiate the cross-linking of the copolymer at the surface. The fiber can then be subjected to heating to promote thermal oxidative stabilization of the remainder of the fiber (Figure 2). It is desirable to make the whole fiber UV-sensitive by synthesizing an AN/MA/ABP terpolymer, where ABP is a photosensitive component. This polymer was successfully synthesized and melt-spun to form precursor fibers.

The procedure for UV cross-linking and further thermal stabilization is presently being evaluated. Significant reductions in cost can result from eliminating or reducing the time required for oxidative stabilization. At present, we have shown that fibers stabilized in this fashion can be converted

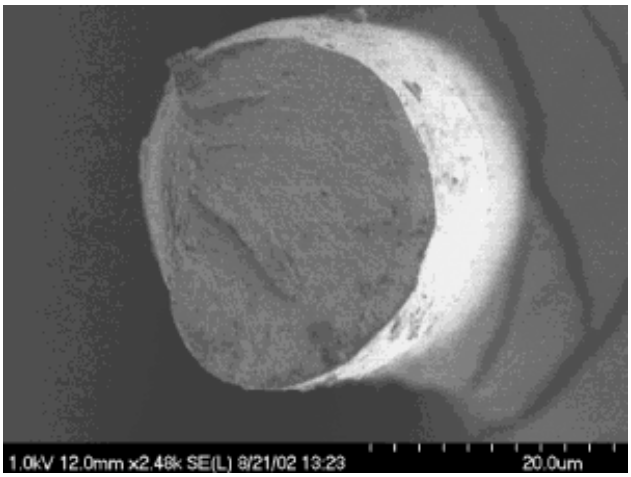

Figure 2. Scanning electron microscope micrographs of UV–oxidatively stabilized fibers (UV for 2.5 h at 150°C, 180–220°C).

to carbon fiber (Figure 3). This is the slowest step in the carbon fiber manufacturing process.

Another approach available as a backup in case we cannot produce a system that is sufficiently thermally stable is the use of CO_2 as a plasticizer for PAN copolymers. Carbon dioxide is a benign solvent that is obtained from air and can be released back to air. PAN copolymers that are currently solution-spun may be melt-spun in the presence of small amounts of CO_2 (~5 wt%). Although we will not actively pursue this approach in the coming year, it could be an important technique for handling the UV-sensitive terepolymers.

Higher-Carbon-Level Precursors

Another factor that must be considered in reducing the cost of carbon fiber is the use of a precursor material that contains a higher carbon content. Future efforts will involve adding a photosensitive group that would allow all the polymer to be cross-linked by means of UV radiation.

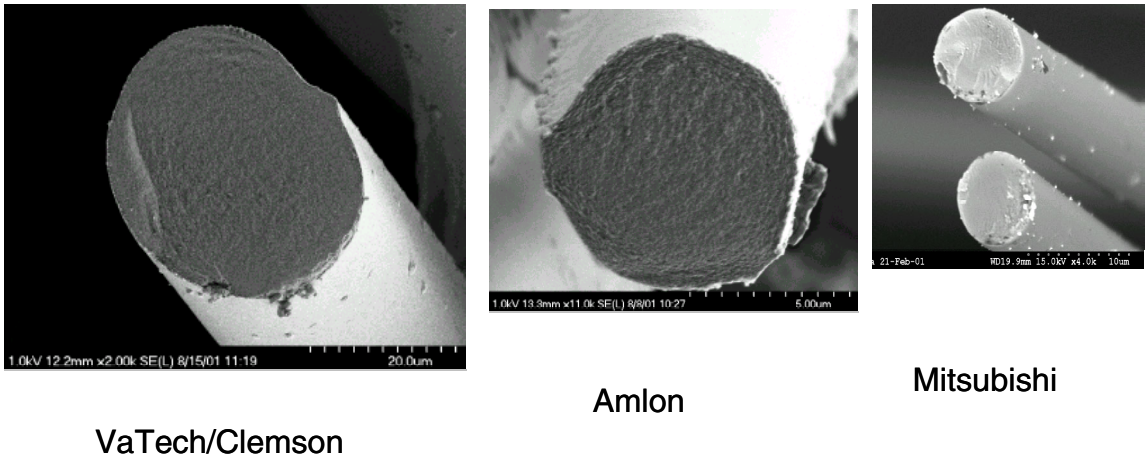

Figure 3. Scanning electron microscope micrographs of carbon fibers produced by UV–oxidative stabilization (2.5 h at150°C, 180–220°C) followed by carbonization (1500°C for 30 min).

D. Microwave-Assisted Manufacturing of Carbon Fibers

Principal Investigator: Felix L. Paulauskas
Oak Ridge National Laboratory
Oak Ridge, TN 37831-8048
(865) 576-3785; fax: (865) 574-8257; e-mail: paulauskasfl@ornl.gov

Field Project Manager: C. David Warren
Oak Ridge National Laboratory
P.O. Box 2009, Oak Ridge, TN 37831-8050
(865) 574-9693; fax: (865) 574-4963; e-mail: warrencd@ornl.gov

Technology Development Manager: Joseph A. Carpenter
(202) 586-1022; fax: (202) 586-1600; e-mail: joseph.carpenter@ee.doe.gov
Field Technical Manager: Philip S. Sklad
(865) 574-5068; fax: (865) 576-4963; e-mail: skladps@ornl.gov

Participants
Terry L. White, Oak Ridge National Laboratory
Kenneth D. Yarborough, Oak Ridge National Laboratory
Professor Roberto Benson and Matthew J. Williams
University of Tennessee, 434 Dougherty Engineering Building, Knoxville, TN 37996-2200

Contractor: Oak Ridge National Laboratory
Contract No.: DE-AC05-00OR22725

Objective

- Investigate and develop a microwave-assisted technical alternative to carbonize and graphitize polyacrylonitrile-based (PAN-based) precursor.
- Prove that carbon fiber with properties suitable for use by the automotive industry can be produced inexpensively using microwave-assisted processing.
- Demonstrate that microwave-assisted processing can produce acceptably uniform properties over the length of the fiber tow.
- Show that for specified microwave input parameters, fibers with specific properties may be controllably and predictably manufactured using microwave furnaces.
- Most important, demonstrate the economic feasibility of producing approximately 30-Msi-modulus fibers at a significant cost reduction compared with those produced conventionally.

Approach

- Conduct parametric studies with the existing single-tow, continuous pilot-unit carbon fiber processing unit. This evaluation will provide data about unit performance, energy balance, limitations, and thresholds.
- Characterize properties of microwave-assisted-plasma (MAP)–processed carbon fibers.
- Use the results of these parametric and fiber characterization studies to develop and incorporate modifications necessary to transform the single-tow processing unit from a low-production-speed line to a high-production-speed line.
- Continuously evaluate the underlying technology, hardware, and ideas required to transform this laboratory, uni-tow, high-production-speed line pilot unit to a multi-tow, moderate- to-high-production-speed line.

Accomplishments

- Successfully operated the continuous MAP carbon fiber pilot facility and carbonized/graphitized 50-K PAN fiber tows at processing line speeds of up to 110–120 in/min.
- Evaluated physical, mechanical, and morphological properties for fiber samples manufactured at line speeds of up to 110 in/min. Property results generally satisfied or exceeded specified requirements.
- Developed improved techniques for analyzing carbon fiber surface chemistry using X-ray photoelectron spectroscopy (XPS) and secondary ion mass spectroscopy (SIMS).
- Designed and manufactured an improved resonance cavity for a dielectric measurement system that can operate at >1000°C with kHz sampling rates and acquired the data acquisition system for it.
- Upgraded the instrumentation and control hardware, especially the infrared temperature measurement system.
- Made equipment and process modifications to reduce tow fouling; improve plasma discharge, heating uniformity, and control over the pressure and temperature profiles along the discharge tube; and reduce tow tensioning variability.
- Commenced design and construction of a multi-tow processing line.
- Had two patents formally issued, including the base technology patent for MAP carbonization and graphitization.

Future Direction

- Develop a scalable multiple-tow, high-speed continuous research line.
- Study process parameters, limitations, and threshold in this continuous pilot facility and incorporate modifications.
- Complete the required mechanical evaluation and characterization of MAP carbon fiber and comparison with conventionally processed, commercial-grade carbon fibers.
- Integrate with other carbon fiber technology developments, e.g., new precursors, rapid oxidation/stabilization processes, advanced surface treatment, and advanced downstream formatting and/or component manufacturing processes.
- Develop and demonstrate related technologies in the area of carbon fiber manufacturing (e.g., advanced characterization, surface treatment, sensing and control technology, recovery and reuse) as resources and time permit.
- Develop partnership(s) to commercialize the technology.

Introduction

The purpose of this project is to investigate and develop a microwave-assisted technical alternative to carbonize and graphitize PAN precursor. The project is to prove that carbon fiber with properties suitable for use by the automotive industry can be produced inexpensively using microwave-assisted processing. It is to be demonstrated that microwave-assisted processing can produce acceptably uniform properties over the length of the fiber tow. The project is also to show that, for specified microwave input parameters, fibers with specific properties may be controllably and predictably manufactured using microwave furnaces. Finally, but most important, this project is to demonstrate the economic feasibility of producing approximately 30-Msi-modulus fibers at a significantly reduced cost compared with those produced conventionally.

Project Deliverables

At the end of this multi-year project, a continuous, high-production-line-speed MAP carbon fiber prototype unit will have been developed, constructed and tested. A final report will be issued with the test results of the carbon fibers processed with this unit. Appropriate industry briefings will be

conducted to facilitate commercialization of this economically enabling technology.

Fiber Properties

A key goal of this project is to demonstrate that the MAP process can produce carbon fibers with satisfactory material properties. Project goals established for fiber properties are 25 Mpsi tensile modulus, 300 ksi ultimate tensile strength (UTS), and 1.0% elongation at break. During this reporting period, the project team evaluated the physical, mechanical, and morphological properties of carbon fiber samples that were carbonized and graphitized at line speeds of 35 to 110 in./min. Fiber test results are tabulated in Tables 1–3. Mechanical property results generally satisfied the specified requirements, except that the UTS still needs to be improved at higher line speeds. This is attributed to the observation that the fiber tensioning system was unable to respond rapidly enough to maintain constant tension at high line speeds. The fiber tensioning system will be upgraded in FY 2003 when the line is upgraded for multiple-tow processing; this change is expected to produce improved tensile strengths. Physical properties generally compared favorably with those of commercially available, large-tow commercial grade fibers. There were notable differences in electrical resistivity, but this may also be related to fiber tension during processing.

Key fiber morphology parameters are tabulated in Table 3 and compared with those of commercially available fibers. The MAP fiber morphology compares favorably with that of commercial-grade fibers, and even that of IM7, an intermediate-modulus fiber that is among the least costly aerospace-grade fibers. Thornel P120 morphology data are tabulated to show what can be achieved technically; however, this is a high-modulus, highly graphitized, and very expensive aerospace-grade fiber that is not targeted by this project. X-ray diffractograms are shown in Figures 1 and 2. The diffractograms also indicate that the MAP fiber morphology compares favorably with those of commercial fibers. One noteworthy feature of MAP processing is that fiber morphology can be adjusted (over a reasonable range) by changing controllable process parameters.

The researchers continued developing improved methodologies for characterizing elemental chemical composition and functional groups present on the surfaces of carbon fibers. This characterization was undertaken with conventionally produced PAN-based carbon fibers using XPS and SIMS. These techniques have been used to characterize plasma-activated surfaces of both fiber and particulate graphite forms and to show that the surface characteristics of these materials can be readily manipulated in plasma.

XPS is an analysis technique used to determine the elemental chemical composition at solid surfaces—in this case, on the surfaces of carbon fibers. It can also determine the functional groups with which the primary elements are associated (high-resolution mode). Elemental concentrations were found and compared for PAN-based carbon fiber manufactured conventionally and by MAP. Sputtering the carbon fiber samples with argon allowed a comparison of elemental chemical compositions at the surface and at discrete locations beneath the fiber surfaces. Figure 3 shows the oxygen/carbon ratio obtained by this method as a function of sputtering time for each sample. This information enables qualitative comparison of surface and bulk compositions among carbon fibers manufactured by different processes. For example, Figure 3 shows that the MAP fibers are similar/equivalent in composition to one low-cost commercial PAN fiber with no surface treatment. This demonstrates that the MAP fibers are

Table 1. Mechanical test data[a]

		MAP carbon fiber				Zoltek PANEX 33	Fortafil 3(C)	Project goal
Production line speed	in./min	35	60	80	110	–	–	–
Tensile modulus	Mpsi	29.0*	26.6	26.0	25.0	26.1	31.1	25
Ultimate strength	kpsi	342*	248	262	276	408	485	300
Elongation at break	%	1.25*	0.97	1.00	1.17	1.5	1.5	1.0

[a]PAN-based fibers, 50-K tows. MAP carbon fiber tests were performed immediately after processing, except for those marked by *, which were neither surface-treated nor sized and were tested 4 months after processing.

Table 2. Physical test data

Fiber type	Production line speed (in./min)	Tow linear electrical resistance (Ω/m)	Electrical resistivity (10^{-3} Ω-cm)	Calculated filament diameter (μm)	Calculated tow area (10^{-2} cm^2)	Density (pycnometer) (g/cm^3)
MAP	35	8.9	1.82	7.20	2.04	1.77
	45	11.8	2.30	7.18	2.03	1.84
	60	14.6	4.30	7.36	2.13	1.77
	80	14.9	4.35	7.44	2.17	1.83
	110	20.3	4.39	7.43	2.17	1.80
Zoltek PANEX 33	–	8.23	1.62	7.37	1.96	1.81
Fortafil 3(C)	–	7.80	1.67	7.43	2.17	1.77

Table 3. Comparison of MAP and commercial fiber morphologies

Sample description	Misorientation angle,[a] degrees	(002) d-spacing (Å)	Stack height,[b] L_c (Å)	In-plane crystal size,[c] L_a (Å)
MAP 7.5 in./min	19.3	3.465	16.4	39
MAP, 20 in./min	17.4	3.492	16.7	43
MAP 35 in./min	18.5	3.465	17.6	47
MAP, 45 in./min	18.0	3.485	15.2	39
MAP, 60 in./min	18.8	3.453	14.5	35
MAP, 80 in./min	18.9	3.455	14.2	36
MAP, 110 in./min	19.0	3.460	14.2	35
Fortafil 3(C)	19.9	3.503	17.1	45
Zoltek Panex 33	19.1	3.483	17.5	50
Hexcel IM7[d]	15.3	3.495	15.8	44
Thornel P120[d]	3.3	3.378	283	435

[a]Average angle of the graphene planes relative to the fiber axis, as measured by the half-width of the 002 planes in the azimuthal direction.
[b]Stack height of the graphene planes.
[c]Crystal size in the direction parallel to the graphene planes.
[d]Aerospace grade fibers.

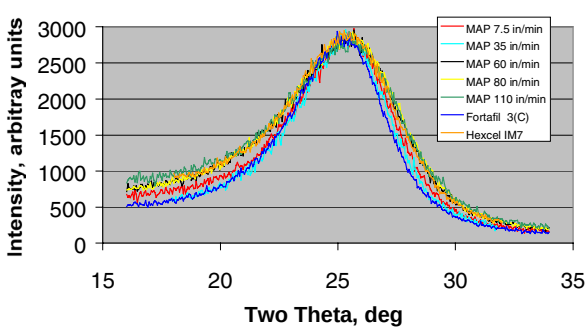

Figure 1. Profiles of the 002 reflection for selected carbon fibers. Data have been normalized to approximately the same maximum intensity.

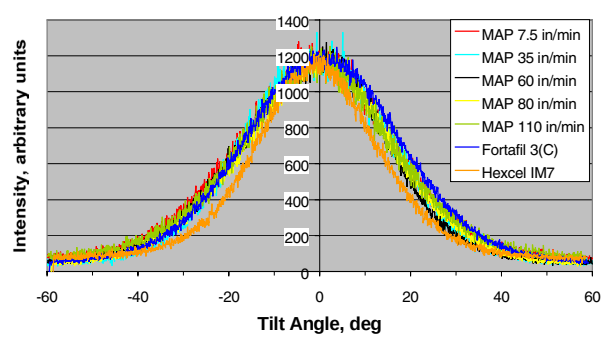

Figure 2. Azimuthal scans of the 002 reflection showing the relative scattering from the graphene planes as a function of their angle of tilt with respect to the fiber axis.

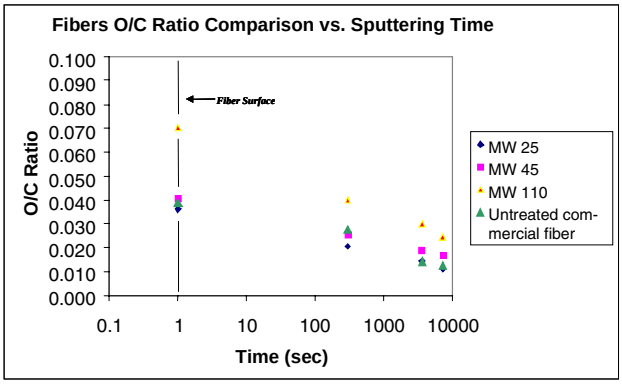

Figure 3. Photoelectron spectroscopy determination of carbon fiber surface and near-surface elemental composition by ion milling of the fiber surface.

chemically equivalent (at the surface and in the region immediately beneath the surface) to low-cost, commercial PAN-based carbon fibers.

Throughput

The economics "figure of merit" is cost per unit throughput. Increasing throughput usually reduces unit cost. Hence the MAP process must be operable at production line speeds and "bandwidths" (number of tows) comparable to or exceeding those of conventional fiber manufacturing lines if it is to realize the desired cost effect. Conventional large-tow carbon fiber manufacturing lines normally run at line speeds in the 90–120 in./min range with about 100 tows per line (a typical line is rated at nominally 1M lb/year when processing 50-K tows).

At the beginning of FY 2002, the researchers had demonstrated a MAP production line speed of 35 in./min. The hardware was upgraded during the year with a goal to achieve 100 in./min production line speed. Line speeds were continually increased throughout the year. The research line was operated successfully at 110 in./min in the third quarter of FY 2002. The line operated at approximately 120 in./min; however, at this speed, the tensioning system response was too slow.

All continuous line operation to date has been on a single-tow line. In the fourth fiscal quarter, design and construction of a multiple tow line commenced. This will be a three-tow line that is scalable to 100 tows.

Parametric Studies

The researchers conducted a number of parametric studies during FY 2002 to determine how various processing parameters and hardware configurations affect fiber properties and economics. The results of such parametric studies should enable process optimization to produce competent fibers and maximize production line speed.

At the beginning of the reporting period, the research line consisted entirely of a continuous plasma chamber, with power supplied from a 915-MHz microwave generator. A preheating section was added, consisting of two shorter, independent preheating stages in series, each powered by a 2.45-GHz microwave generator. Temperatures of several hundred degrees can be reached in the preheater. This addition improved the thermal and power profiles and enabled higher line speed.

Various sealing techniques were evaluated. The fiber must be transported from atmospheric conditions into the evacuated plasma chamber and vice versa. The seals must allow the tow to be tensioned and transported undamaged over the full range of line speeds and between atmospheric conditions and evacuated space, yet minimize gas leakage so that pump size, cost, and power demand are acceptable. Multiple seal designs were tested; the selected design provided the best combination of functionality, sealing, and fiber damage.

Methods for improving the plasma discharge and heating uniformity were evaluated. In the original MAP system, the plasma discharge in the carbonization and graphitization section was about 3 to 4 ft long. The system was modified to lengthen the discharge to about 5 to 6 ft, thereby achieving much improved heating uniformity.

Snapshots of tow electrical resistivity were obtained to map tow processing levels to position in the plasma chamber under various processing conditions. This was accomplished by simultaneously extinguishing the plasma and stopping tow transport, indexing the tow position in the plasma chamber, and then measuring tow electrical resistivity at various points along the partially processed tow. A "process profile" was created that will guide future modifications to enhance microwave energy/plasma distribution and line speed.

Instrumentation and Control

A patent was issued for the process monitoring technique that measures the tow dielectric properties and, by their correlation to fiber physical properties (based on network analysis), infers the fiber properties and process conditions. The researchers continued to improve this process monitoring technique in the laboratory. Previous designs were limited to operation at temperatures below 600°C. The system must be capable of processing fibers in nitrogen at temperatures exceeding 1000°C at kHz sampling rates. A fast data acquisition system was required to time-resolve the rapid changes that the fiber experiences during processing. The resonance cavity for dielectric measurement requires corrosion-resistant materials that are structurally competent and dimensionally stable at high temperature. Improved monitoring hardware was designed and fabricated and will be tested in FY 2003.

The infrared temperature measurement system was modified to obtain better focus and reliability in the temperature monitoring during processing. A two-color, infrared temperature system was acquired for low-temperature measurement.

The existing tow tensioning system responds so slowly that it cannot adequately adjust to changing conditions at high line speeds. The tow therefore tends to be alternately undertensioned or overtensioned. This is believed to be a major contributor to the observed degradation of fiber properties as line speed increases. An optical tachometer was added to the take-up winder to accurately measure the line speed independently of the take-up winder speed and line tension. Additionally, modifications are presently under way to improve the tensioning system's response time.

Patents and Publications

Two patents were issued during FY 2002:

- "Carbon Fiber Manufacturing via Plasma Technology," U.S. Patent 6,372,192 B1, April 16, 2002. This patent comprises the intellectual property foundation for the MAP carbonization technology and related discoveries.
- "Diagnostic Monitoring for Carbon Fiber Processing," U.S. Patent 6,375,875 B1, April 23, 2002.

The principal investigator was awarded a Battelle Science and Technology award for a carbon fiber business and research proposal that included elements derived from discoveries made in this project.

Summary

These are highlights of the progress during FY 2002.

1. Successfully operated the continuous MAP carbon fiber pilot facility and carbonized/ graphitized 50-K PAN fiber tows at processing line speeds of up to 110–120 in./min.
2. Evaluated physical, mechanical, and morphological properties for fiber samples manufactured at line speeds of up to 110 in./min. Property results generally satisfied or exceeded specified requirements.
3. Commenced design and construction of a multi-tow processing line.
4. Developed improved techniques for analyzing carbon fiber surface chemistry using XPS and SIMS.
5. Designed and manufactured an improved resonance cavity for a dielectric measurement system that can operate at >1000°C with kHz sampling rates, and acquired the data acquisition system for it.
6. Upgraded the instrumentation and control hardware.
7. Made equipment and process modifications to reduce tow fouling; improve plasma discharge, heating uniformity, and control over the pressure and temperature profiles along the discharge tube; and reduce tow tensioning variability.
8. Had two patents formally issued, including the base technology patent for MAP carbonization and graphitization.

Conclusions

The development of MAP carbonization and graphitization technology has progressed according to plan. All FY 2003 milestones were satisfied ahead of schedule. Construction of a multi-tow research line is now under way. MAP processing is generally considered to be an evolving "success story" with great potential for making an impact on carbon fiber technology and cost.

6. RECYCLING

A. Recycling of Polymer Matrix Composites

Principal Investigator: Bassam J. Jody
Argonne National Laboratory
9700 South Cass Avenue, Argonne, IL 60439
(630) 252-4206; fax: (630) 252-1342; e-mail: bjody@anl.gov

Project Manager: Edward Daniels
Argonne National Laboratory
9700 South Cass Avenue, Argonne, IL 60439
(630) 252-4206; fax: (630) 252-1342; e-mail: edaniels@anl.gov

Technology Development Manager: Joseph A. Carpenter
(202) 586-1022; fax: (202) 586-1600; e-mail: joseph.carpenter@ee.doe.gov
Field Technical Manager: Philip S. Sklad
(865) 574-5069; fax: (865) 576-4963; e-mail: skladps@ornl.gov

---

Contractor: Argonne National Laboratory
Contract No.: W-31-109-Eng-38

Objective

- Develop efficient and cost-effective processes for recovering carbon fibers from polymer matrix composites (PMCs).

Approach

- Work with a carbon fiber manufacturer to produce and test PMC panels made with recovered fibers and compare their properties with those of similar virgin-fiber panels.
- Recover carbon fibers for reuse in an automotive application.
- Investigate the technical feasibility and potential advantages of using the hybrid processes.

Accomplishments

- Evaluated three processes to separate carbon fibers from PMC scrap: thermal treatment, chemical treatment, and thermal shock. The thermal treatment method, a single-step process, recovered carbon fibers from PMCs made with different polymeric substrates. The recovered fibers had adequate properties for reuse in chopped fiber applications.
- Conducted an economic analysis of this method, which showed it to have a potential payback of less than 2 years. Therefore, its development was continued in FY 2002.
- Recovered carbon fibers from PMC panels supplied by Hexcel Carbon Fibers, Inc., that were made with known fibers and known substrates. The recovered fibers were evaluated by Hexcel and by Oak Ridge National Laboratory (ORNL). The recovered fibers have the following qualities:
  - High shear strength and high oxygen concentration on the fiber surfaces, indicate that the recovered fibers should adhere well to matrix resins without the need for additional surface treatment. Surprisingly, some of

the recovered fibers exhibited higher concentrations of elemental oxygen at and just beneath the fiber surface than the corresponding virgin "control" fibers.
— Within experimental error, the physical and morphological characteristics of the recovered fibers are nearly identical to those of the virgin fibers.

- Hexcel used the recovered fibers from the virgin panels to make new PMC panels of equivalent dimensions and substrate compositions and then compared the properties of these panels with those of the original panels from which the fibers were recovered. The data showed a reduction in stiffness of ~10% and a reduction in short beam strength of ~12%. The new panels also had an ~50% reduction in strength and elongation. These results demonstrate that the recovered fibers are suitable for use in chopped-fiber applications.
- Evaluated a combination of hybrid treatment processes (thermal treatment process followed by a chemical treatment process, and vice versa, and thermal treatment followed by ultrasonic separation).

Future Direction

- Complete production of recovered fibers for testing in an actual automotive application.
- Test the thermal treatment process on PMCs made with other substrates, such as polyester and nylons.
- Work with carbon fiber manufacturer to develop a plan for demonstrating the technology on a larger scale.
- Refine the economic analysis of the thermal treatment process.

Testing PMC Panels Made with Recovered PMC Fibers

Hexcel manufactured and supplied PMC panels with known properties for carbon fiber recovery tests. We processed these panels under different operating conditions and sent the recovered fibers back to Hexcel for a comparison of their properties before and after recovery. Samples of the recovered fibers were also sent to ORNL for additional evaluation and characterization. Figure 1 shows a typical panel before treatment and the recovered fibers after treatment. Based on the results of these tests, appropriate recovery conditions were established for the fibers from these panels. These conditions were then used to recover fibers from the panels. Hexcel used the recovered fibers to fabricate new panels. Properties of the panels fabricated from recovered fibers were then compared with properties of the virgin fiber panels.

Figure 1. A typical PMC panel before thermal treatment (left) and the recovered carbon fibers after treatment (right).

The recovered fibers had characteristics similar to those of the original virgin fibers. For example, as shown in Table 1, the density and diameter of the recovered fibers were essentially the same as those of the virgin fibers.

Table 1. Comparison of the density and diameter of the recovered fibers and virgin fibers

Sample	Density (g/cc)	Diameter (μm)
Virgin	1.8553	5.33
Recovered	1.8561	5.39

As shown in Table 2 and Figures 2 and 3, the morphology of the recovered fibers was also found to be nearly identical to that of the virgin fibers.

The 002 reflection and the azimuthal scans showing the orientation of the graphene planes were nearly identical for the virgin carbon fiber samples and the recovered carbon fibers. These data prove that at the appropriate processing conditions, the thermal treatment process does not degrade the morphology in the interior constituent material.

Table 2. Comparison of the morphological characteristics of the recovered fibers and virgin fibers

Fiber sample	Misorientation angle[a]	D_{002} (Aº)	L_c (Aº)[b]	La (Aº)[c]
Virgin[d]	16.3	3.489	15.2	43.9
Virgin[e]	15.3	3.493	15.8	44.3
Recovered	16.6	3.477	15.7	45.2

[a]Average angle the graphene planes make with the fiber axis as measured by the half-width of the 002 reflection in the azimuthal direction.
[b]Stack height of the graphene plane.
[c]Crystal size in the direction of parallel to the graphene planes.
[d]Untreated and unsized virgin fiber.
[e]Surface-treated and unsized virgin fiber.

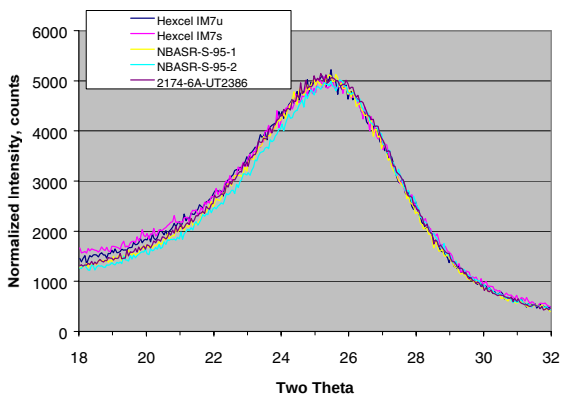

Figure 2. The 002 reflection from virgin and recovered fiber samples.

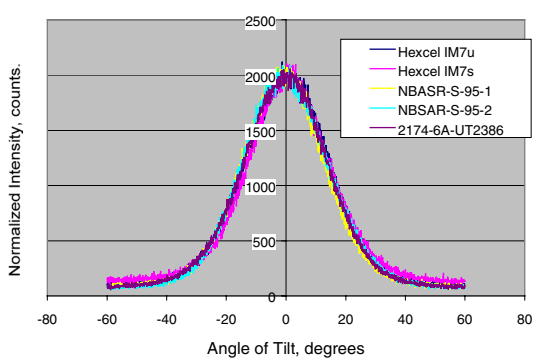

Figure 3. Azimuthal scans of the 002 reflection showing the orientation of the graphene planes. In this case, all curves superimpose.

The recovered fibers also exhibited high shear strength and high oxygen concentration on the fiber surface, indicating that the recovered fiber should adhere well to matrix resins without the need for additional surface treatment. Surprisingly, some of the recovered fibers exhibited higher concentrations of elemental oxygen at and just beneath the fiber surface than the corresponding virgin control fibers. A possible explanation is that at a specific temperature and residence time, the epoxy substrate may generate a favored combination of chemical compounds or groups that deposit oxygen on the fiber surface. This finding is significant because it about $0.40 per pound of carbon fiber could be saved if the fibers do not require surface treatment.

Hexcel used some of the recovered fibers as-is to make new panels of equivalent geometry and composition to the virgin panels and compared their properties with those of the panels from which the fibers were recovered. The data showed a reduction of only 10% in panel stiffness and ~12% in short beam strength. The panels also showed a reduction of ~50% reduction in strength and elongation. Obviously, during the treatment process and handling of the recovered fibers afterward in the hood, some of the fibers were lost; and some lost their original direction and place, as shown in Figure 4.

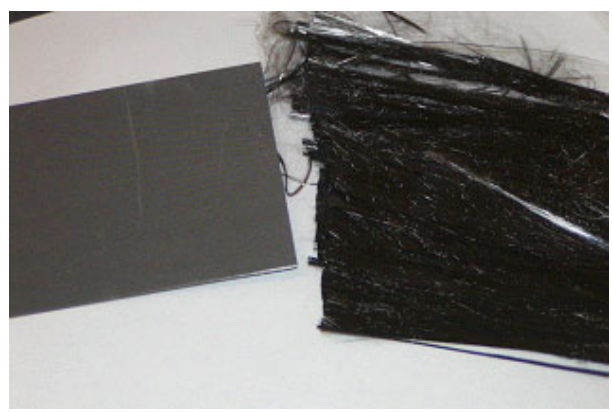

Figure 4. Recovered fibers from a thermally treated PMC panel. Individual fibers at the edge are being disturbed by the air flow in the hood.

Therefore, the recovered fibers could be used in many applications that require chopped fibers, such as sheet molding compounds or preform products like those made in the slurry process to manufacture automobile parts. Other applications include

batteries and fuel cells. Figure 5 is a magnified picture of recovered carbon fibers.

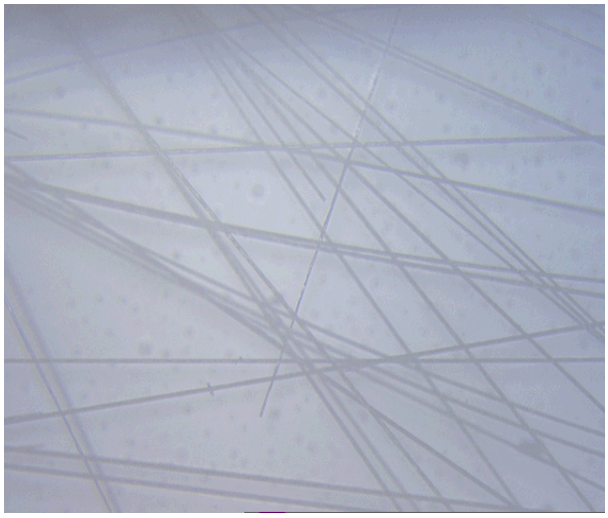

Figure 5. Magnified picture of recovered carbon fibers.

Recovery of Carbon Fibers for Reuse in an Automotive Application

Arrangements were made with Hexcel to provide ORNL with carbon fibers having known properties. At the time of this report, Hexcel had supplied ORNL with about 150 lb of fiber, and ORNL was making PMC scrap panels from the fibers. Argonne will process the panels and recover carbon fibers from them. We plan to process the panels and then send the recovered fibers to ORNL to use in manufacturing skid plates for sport utility vehicles using the Budd slurry process.

Argonne was scheduled to receive the PMC scrap panels from ORNL in late October 2002 and expected to complete processing them in December 2002.

Testing of Hybrid Treatment Processes

We also conducted experiments on the hybrid treatment processes. The thermal method can remove about 99% of the polymeric substrate and its breakdown by-products in a matter of minutes. In some cases, such as with epoxy resins, removing the remaining 1% or so takes much longer. We investigated a hybrid method in which the PMC sample is thermally processed for a few minutes and then chemically processed to remove the residual carbon-based material. We conducted preliminary experiments on this hybrid treatment process (thermal treatment followed by wet chemical treatment) with isocyanorate/urethane–based substrates. This hybrid method worked very well. However, with epoxy substrates, the wet chemical treatment was not very effective in removing the residual carbonaceous material from the fibers. In another process using chemical treatment followed by thermal treatment, the chemicals had to be washed off the PMC panels prior to the thermal treatment to avoid the emission of volatile organic compounds. This technique was effective with the PMCs made with isocyanorate/urethane substrates but was not effective with the PMCs that had an epoxy substrate.

In another hybrid process tested, an ultrasonic separator was used to remove residual materials from the carbon fibers after thermal treatment removes the bulk of the substrate. In these experiments, several sets with two equivalent PMC panels in each set were treated at different temperatures. Each set was thermally treated at the same temperature to remove the bulk of the epoxy substrate, and then one of the treated samples was deposited in the ultrasonic bath while the other was allowed to cool in the hood. A small amount of a solid residue collected in the bottom of the ultrasonic bath. However, results showed that this technique did not remove enough of the residual substrate to justify using it as a second step in the process.

Disposal and Treatment of the Effluent Gas Stream

The PMC waste stream will contain scrap made with various types of thermosets and perhaps thermoplastic substrates. The thermal treatment method will be capable of treating all of these substrates. However, different substrates generate different pyrolysis and oxidation products, including volatile and semi-volatile organic compounds. Previously, we analyzed the gases and vapors generated when we treated isocyanurate/urethane–based substrates. The gas/vapor products were cooled down to near ambient temperature, and the resulting gas and liquid samples were sent for chemical analysis. The gas sample contained N_2, O_2, CO_2, CO, and only trace amounts of hydrocarbons. The liquid sample was analyzed for volatile and semi-volatile compounds. It contained about 30 such

compounds. The major species identified, in descending order, were 2,2,6,6,tetramethyl-4-piperidinone, aniline, 4-methyl benzene amine, 4-methyl-3-penten-2-one, 4-amino-4-methyl-2-pentanone, and benzonitrile. Therefore, this waste stream will have to be incinerated at high temperatures in an afterburner.

During FY 2002, we analyzed the gases generated from epoxy-based substrates. We designed and constructed a gas sampling collection system, shown schematically in Figure 6. This system was fitted to the experimental apparatus and collected the gases that evolved, which were then analyzed.

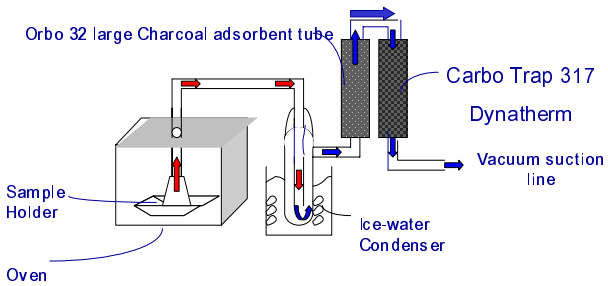

Figure 6. Schematic diagram of the gas sampling/ collection subsystem.

The evolved gases were first cooled in an ice/water condenser and then passed through two absorption tubes, as shown in Figure 6. The effluent gases and vapors included acetone, isopropyl alcohol, benzene, acrylonitrile, and toluene. These species need to be incinerated at high temperatures in an afterburner with heat recovery to reduce the heat duty of the process.

Based on the heating values of polymers used in PMCs, we estimated that at least 60% of the energy requirements of the process could be satisfied by the energy value of the generated gases and vapors. In most cases, the PMC panels are made with about 30 to 50% polymeric substrates that have a heating value of over 18,000 Btu/lb of substrate. The energy released upon combustion of the polymeric substrate is enough to maintain the thermal treatment reactor at the desired temperature; therefore, the system can be energy self-sufficient. An afterburner is required to destroy residual carbon monoxide and organic compounds. The process does not generate liquid or solid waste streams.

Updating of the Conceptual Design and Economic Analysis

The thermal treatment process conceptual design developed last year was reevaluated; included in the reevaluation were the subsystems for loading the PMC scrap and for collecting the recovered carbon fibers and treating the effluent gaseous stream. No changes to the design were necessary. We also reevaluated the economic analysis for a full-scale plant processing 1,000,000 lb/year of PMC scrap. The estimated payback of about 2 years is still valid.

Milestones

The following milestones of the proposed effort are to be conducted in FY 2003.

Test the process on new PMC materials made with different substrates, including polyester substrates.

Complete production of recovered carbon fibers for testing in an actual automotive application.

Develop a demonstration plan for the technology.

Conclusions

Work conducted so far has demonstrated that the recovery of carbon fibers from PMC scrap is technically feasible and potentially economical. The recovered fibers have properties that make them usable in chopped-fiber applications for making value-added products such as car, fuel cell, and battery parts.

B. Recycling Assessments and Planning

Principal Investigator and Project Manager: Edward J. Daniels
Argonne National Laboratory
9700 S. Cass Ave., Argonne, IL 60439
(630) 252-5279; fax: (630) 252-1342; e-mail: edaniels@anl.gov

Field Project Manager: C. David Warren
Oak Ridge National Laboratory
P.O. Box 2009, Oak Ridge, TN 37831-8050
(865) 574-9693; fax: (865) 574-4963; e-mail: warrencd@ornl.gov

Technology Development Manager: Joseph A. Carpenter
(202) 586-1022; fax: (202) 586-1600; e-mail: joseph.carpenter@ee.doe.gov
Field Technical Manager: Philip S. Sklad
(865) 574-5069; fax: (865) 576-4963; e-mail: skladps@ornl.gov

---

Contractor: Argonne National Laboratory
Contract No.: W-31-109-Eng-38

Objectives

- To establish priorities for cost-effective recycling of advanced automotive technology materials and components.
- To focus long-term efforts on enhanced recovery/sorting procedures and advanced recycling technologies that are enabling factors in a vision for 100% recyclability.

Approach

- Consult with automotive manufacturers and recycling industries, the U.S. Council on Automotive Research (USCAR) and its affiliates, national laboratories, universities, and other relevant organizations to assess critical recycling needs/barriers.
- Develop a recycling R&D program plan that will serve as a "working document" to guide DOE/FCVT in establishing priority goals, with an initial emphasis on lightweight body and chassis materials.
- Assist DOE in establishing advanced recycling R&D initiatives and provide technical oversight to ensure that priority objectives/goals are accomplished.

Accomplishments

- Organized the Recycle Roadmapping Workshop during the fourth quarter of FY 2000. The workshop was facilitated through a subcontract with Energetics. The Roadmap (*A Roadmap for Recycling End-of-Life Vehicles of the Future*) was completed in May 2001.
- Prepared a draft 5-year program plan based on the recommendations and priorities identified in the Roadmap and based on an initial planning meeting with the management council of the Vehicle Recycling Partnership (VRP) of USCAR. Follow-up meetings with the VRP and the American Plastics Council (APC) have provided the basis for structuring a cooperative research and development agreement among Argonne, VRP, and the APC to conduct the research that is the subject of the 5-year plan.

Future Direction

- Establish the formal working relationships with the key stakeholders to execute the major elements of the program plan and to finalize the 5-year plan.
- Continue development of the Recycling R&D Plan through collaboration with the USCAR VRP and associated USCAR affiliates, the APC, the Automotive Parts Rebuilders Association, remanufacturing industries, materials trade organizations, and other appropriate industries involved in automotive recycling.
- Continue evaluations of recycling technology progress in Europe and Japan, along with assessments of critical recycling technologies as new needs are identified.
- Continue to work with the Automotive Aluminum Alliance, which is working with Huron Valley Steel Corporation to demonstrate technology developed by Huron Valley Steel for separation of aluminum alloys.
- Continue ongoing project efforts to assist DOE in preparation of planning documents, priority recycling R&D needs, proposal reviews, and related tasks.

Summary

The objective is to establish priorities and develop cost-effective recycling technologies and strategies in support of the DOE FCVT long-term objectives and goals. Automobile recycling is the final productive use of end-of-life vehicles (ELVs). The obsolete car has been a valuable source of recycled raw materials and useable parts for repair since cars have been mass-produced. Today, cars that reach the end of their useful service life in the United States are profitably processed for materials and parts recovery by an existing recycling infrastructure. That infrastructure includes automotive dismantlers who recover useable parts for repair and reuse; automotive remanufacturers who remanufacture a full range of components, including starters, alternators, and engines to replace defective parts; and ultimately the scrap processor who recovers raw materials such as iron, steel, aluminum, and copper from the remaining auto "hulk" after components have been recovered for recycling. Each of these activities contributes to the recycling of obsolete vehicles.

Today, less than 25 wt% of obsolete cars is not profitably recoverable for recycling and is therefore landfilled. Over the past 10 years, the original equipment manufacturers—Ford, GM, and DaimlerChrysler—through the VRP and other organizations including the Aluminum Association, APC, the Institute of Scrap Recycling Industries, Automotive Recyclers Association, Automotive Parts Rebuilders Association, and the federal government have been working both collaboratively and independently to address technical, institutional, and economic issues that currently limit the recycling of ELVs. Progress has been made in understanding some of these issues, and technology has been developed that can impact the level of ELV recycling.

The recyclability of ELVs is presently limited by the lack of commercially proven technical capabilities to cost-effectively separate, identify, and sort materials and components and by the lack of profitable post-use markets. While nearly 75 wt% of ELVs is currently recycled in some form, the remaining 25% is sent to landfills each year. Over the next 20 years, both the number and complexity of ELVs are expected to increase, posing significant challenges to the existing recycling infrastructure. The automobile of the future will use significantly greater amounts of lightweight materials (e.g., ultra-light steels, aluminum, plastics, and composites) and more sophisticated/complex components.

New technology is and will continue to be needed to improve vehicle recyclability. Using the Roadmap as a framework, we will work with the key stakeholders over the next year to structure a suite of projects to be undertaken in this program area.

The Recycling Strategy

The following strategy outline was developed as part of the Roadmap to maximize the value recovered from ELVs.

- Come together as a unified recycling community to cost-share the development of required new technology.

- Incorporate reuse, remanufacturing, and recycling into the design phase for cars whenever possible.
- Recycle as early in the recycling stream as possible, while relying on the market to optimize the value and amount recycled at each step.
- Maintain a flexible recycling process that can adapt to diverse model lines fabricated with different techniques and materials from various suppliers.
- Develop automated ways to recover bulk materials.
- Emphasize R&D on post-shred material identification, sorting, and product recovery
- Focus R&D efforts on materials not recycled today by sorters (e.g., post-shred glass, rubber, fluids, textiles, plastics)
- Develop uses for recovered materials (whether in the same or different applications) and testing specifications.
- Encourage investment in the infrastructure needed to achieve the recyclability goal. Build on the existing infrastructure.
- Develop a means to prevent the entry of polychlorinated biphenyls and other hazardous materials into the recycling stream and promote acceptable limits in shredder residues.
- Consider the recycling requirements of new technologies entering fleets as early as possible.

The 5-Year R&D Plan

Based on the Roadmap and continuing discussions with key stakeholders, a 5-year R&D plan has been prepared. The plan includes the following three focus areas:

Area 1. Baseline Technology Assessment and Infrastructure Analysis

Understanding the state of the art is critical to moving forward. As stated in the Roadmap

> … the status of technologies used, existing process capabilities, and the mass balance flow of automobiles at end-of-life is not known with the level of confidence needed to assure that the industry is making the best choices to optimize recyclability. A better understanding of the interrelationships of all steps in the recycling process from a financial perspective will promote development of [the] infrastructure … analysis of data is needed to better understand the environmental and economic trade-offs.

The focus of the work under this activity will be to develop the tools and document the information necessary to make effective decisions relative to technology needs to facilitate sustainable future vehicle recycling, and to make effective decisions regarding allocation of R&D resources. Research conducted under this area generally addresses the broader priorities of "proactive industry wide-action" and "industry-wide analysis" for which a number of specific needs are identified in the Roadmap.

In FY 2003, the focus of this area will be on developing a catalogue of available and emerging automotive recycling technologies and preparing an updated assessment of the state of the art of the recycling industry.

Area 2. Materials Recovery Technology Development and Demonstration

Development of technology that can lower the cost of recycling and meet the financial and institutional requirements of the market is critical to improving the recycling rate of automotive materials. Technology development and demonstration is the cornerstone of this program and will serve as the program's focal point. Although research to be conducted in this area will initially focus on addressing technology needs for post-shred materials recovery, projects that enhance pre-shred recovery, including disassembly for materials recovery and direct reuse and remanufacturing of components, will also be included. In the long term, components such as fuel cells, advanced batteries, and hydrogen reformers are more likely to enter the recycle stream through pre-shred recovery for remanufacturing, repair, and materials recovery. Research will be undertaken to determine the technology needs to ensure the recyclability of these very advanced automotive components. This area of research generally supports the needs of the broad priorities of "lowering the risk of technology development and purchase," "pre-shred recovery," and "post-shred material identification and sorting" that are outlined in the Roadmap.

In FY 2003, the focus of this area will be to support development and demonstration of post-shred separation technology, building upon the technology development efforts previously undertaken by Argonne, the VRP, the APC, and others. Development of technology to cost-effectively sort post-shred material is a top priority need.

Area 3. Recovered Materials Performance and Market Evaluation

Understanding and enhancing recovered materials performance is an essential ingredient to a successful recycling program. This is especially true in automotive systems when the materials and components that are recovered have been in use for an average of from 10 to 15 years. This area will include projects to quantify the relative performance of recovered materials vis-à-vis new or virgin materials; research on compatibilization of recovered polymers to improve performance properties; development of technologies to upgrade the recovered materials, such as separation of fibers from polymeric substrates; and development of applications for other recovered materials, such as rubber and glass.

FCVT is currently funding two projects in this area: recycling of polymer matrix composites (see report 6A) and separation of scrap aluminum alloys. Both of these projects are expected to achieve their respective objectives in FY 2002–2003. In FY 2003, research will be initiated on understanding performance properties of recovered polymers and on determining compatibilization/compounding requirements. The work that will be done on compatibilization and compounding will be coordinated with the materials recovery technology development and demonstration effort outlined in Area 2. That is, compatibilization/compounding research will be conducted for the materials recovered as part of the technology demonstration of Area 2.

7. ENABLING TECHNOLOGIES

A. Durability of Lightweight Composite Structures

James M. Corum (Principal Investigator), R. L. Battiste, M. B. Ruggles-Wrenn, Y. J. Weitsman
Oak Ridge National Laboratory, P.O. Box 2009
Oak Ridge, TN 37831-8051
(865) 574-0718; fax: (865) 574-0740; e-mail: corumjm@ornl.gov

Automotive Composites Consortium Contact: Libby Berger
General Motors R&D, 30500 Mound Road 1-6
Warren, MI 48090-9055
(586) 986-1177; fax: (586) 986-1207; e-mail: libby.berger@gm.com

Field Project Manager: C. David Warren
Oak Ridge National Laboratory, P.O. Box 2008
Oak Ridge, TN 37831-6065
(865) 574-9693; fax: (865) 576-4963; e-mail: warrencd@ornl.gov

Technology Development Manager: Joseph A. Carpenter
(202) 586-1022; fax: (202) 586-1600; e-mail: joseph.carpenter@ee.doe.gov
Field Technical Manager: Philip S. Sklad
(865) 574-5069; fax: (865) 576-4963; e-mail: skladps@ornl.gov

---

Contractor: Oak Ridge National Laboratory
Contract No.: DE-AC05-00OR22725

Objective

- Develop experimentally-based, durability-driven design guidelines to ensure the long-term (15-year) integrity of representative carbon-fiber–based composite systems that can be used to produce large structural automotive components. Durability issues being considered include the potentially degrading effects—on structural strength, stiffness, and dimensional stability—of cyclic and sustained loadings, exposure to automotive fluids, temperature extremes, and low-energy impacts from such events as tool drops and kickups of roadway debris.

Approach

- Characterize and model the durability behavior of a progression of three representative carbon-fiber composites, each with the same thermoset urethane matrix but having a different reinforcement preform: (1) continuous fiber, ±45° crossply; (2) continuous fiber, quasi-isotropic; and (3) random chopped fiber.
- Replicate on-road conditions in laboratory tests of each composite to generate durability data and models.
- Develop and publish durability-based design criteria for each composite.
- Subsequently shift focus to suitable thermoplastic composites, for which durability issues are generally more significant.

Accomplishments

- Published a report providing durability-based design criteria, with supporting data and models, for quasi-isotropic carbon-fiber composite (ORNL/TM-2002-39).

- Submitted three technical papers that were accepted for presentation/publication.
- Successfully fabricated chopped-carbon-fiber plaques for durability studies [Automotive Composites Consortium (ACC)].
- Completed, with the exception of ongoing creep tests, planned durability tests of 3-mm-thick chopped-carbon-fiber thermoset composite plaques; a more limited test program is under way on 1.5-mm-thick chopped-carbon-fiber composite plaques.
- Fed chopped-carbon-fiber composite data directly into the planning and analysis for the Focal Project 3 (FP3) carbon fiber body-in-white (see report 4B).

Future Direction

- Prepare and publish a durability-based design criteria document for 3-mm-thick chopped-carbon-fiber composite; include 1.5-mm-thick chopped-fiber composite results as an addendum.
- Address the durability of thermoplastic carbon-fiber composites, with initial material being chosen by the ACC from existing formulations.
- Publish durability-based design criteria documents for representative thermoplastic composites suitable for automotive structural applications.

Chopped-Carbon-Fiber Material Development

The ultimate goal for the FP3 carbon-fiber composite body-in-white is to achieve a fiber-volume fraction of 40% and a minimum thickness of 1.5 mm over 70% of the structure.

The ACC successfully molded chopped-carbon-fiber plaques meeting these FP3 requirements. The carbon fiber, chopped by the programmable powdered preform process machine in 50-mm lengths, was Zoletek Panex 33, seven-split 46K. The urethane matrix was Bayer 420 IMR, the same as in previous composites addressed by the Durability Project. Unfortunately, although the average properties of the 1.5-mm-thick plaques satisfied FP3 design requirements, the variability was excessive. The plan originally was to use 1.5-mm-thick plaques for durability studies. However, because of the larger than expected variability in the 1.5-mm material, ACC instead fabricated and supplied 3-mm-thick plaques in March 2002. These 3-mm-thick plaques, which exhibit improved variability, have been adopted as the reference chopped-fiber material.

While tests of 1.5-mm plaques are being carried out for comparative purposes, the results will be presented only as an addendum to the final design criteria report on the 3-mm-thick material.

Figure 1 depicts, in the form of a probability density function, the distribution of the modulus of elasticity values measured on 419 individual specimens from the 3-mm-thick chopped-carbon-fiber composite. A 20.3-mm-wide specimen with an extensometer having a 25.4-mm gage length was used for the measurements. The Gaussian distribution implies that if enough specimens were tested, variations in stiffness approaching a factor of four would be observed.

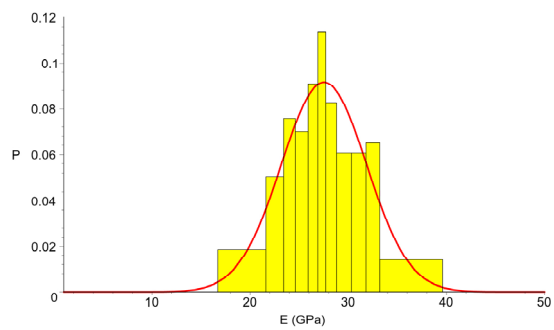

Figure 1. Distribution of modulus of elasticity values from 419 specimens from 3-mm-thick chopped-carbon-fiber composite.

Much of this observed variation is inherent in the random nature of the orientation and position of the fiber strands, or bundles. To illustrate this, a number of computer-generated plots showing randomly-oriented strands was developed. A typical plot is shown in Figure 2. Here, 50.8-mm-long fiber strands are randomly distributed over a 152-mm^2 area of a larger plaque. Both the coordinates and the

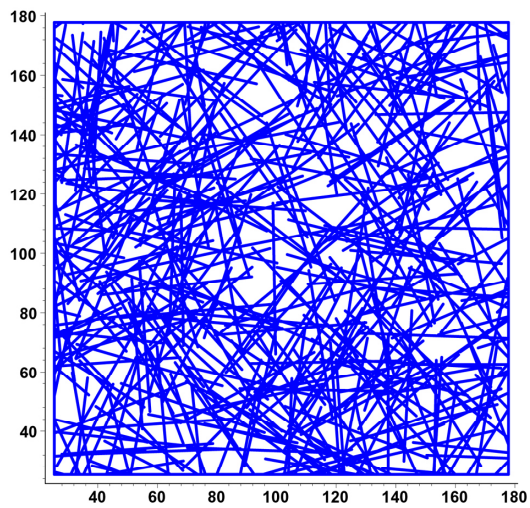

Figure 2. Computer-generated depiction of 50.8-mm-long random chopped-fiber strands.

angle of orientation of the strands were randomly generated. This plot illustrates that there are clearly areas of low and high fiber density, and there are other areas where many strands seem to be similarly aligned. By visualizing a 20.3-mm-wide by 25.4-mm-long element of a test specimen located at various points on the plot, a major source of property variation can be understood.

A second source of variation, especially in thinner plates, is also illustrated in Figure 2. Because the bundles of carbon fiber are so large (compared with glass strands), when several of them land on top of each other, the crossover points can cause a fiber pillar that is taller than the plaque is thick (see Figure 3 for an example). This area is tightly compressed in molding and is not wet with resin. Small flaws are thus formed, which lead to variability. These pillars are considerably reduced in thicker plaques, as are the property variations due to the random nature of the fiber strand locations and orientations.

More splits in the large-tow carbon fibers and a more uniform cross-sectional area of the resulting strands would lead to significantly improved 1.5-mm-thick material. The ACC is working with the carbon fiber manufacturers to achieve this goal.

Basic Short-Time Properties of 3-mm-Thick Chopped-Carbon-Fiber Composite

More than a thousand tests have been performed to characterize the durability of the reference

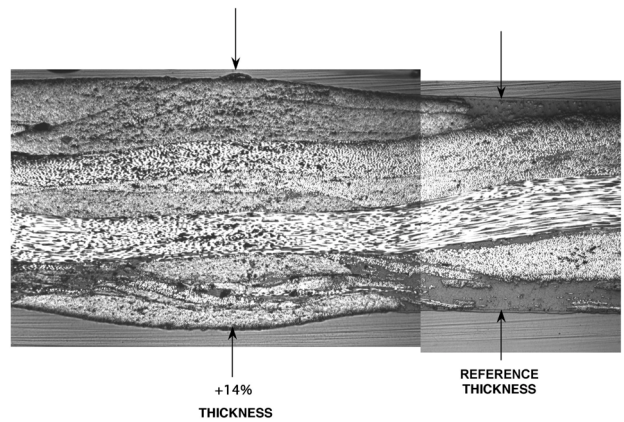

Figure 3. Photomicrograph of the edge of a 1.5-mm-thick specimen showing an example of a pillar of fibers across the thickness (courtesy of ACC).

chopped-fiber material. In addition to basic short-time properties (i.e., tensile, compressive, shear, and uniaxial and biaxial flexural), cyclic fatigue, time-dependent creep, impact, and post-impact strength properties have been established. In most cases, property characterization has included the effects of temperature, over the –40 to 120°C automotive design range, and two representative automotive fluids, distilled water and windshield washer fluid (70% methanol/30% distilled water). In the case of the basic properties, additional effects examined include loading rate, thermal cycling between −40 and 120°C, and prior loadings.

The room-temperature tensile properties of the chopped-carbon-fiber material are compared in Figure 4 with the properties of the quasi-isotropic and crossply carbon-fiber composites previously characterized, and with the properties of the chopped-glass-fiber composite that was also

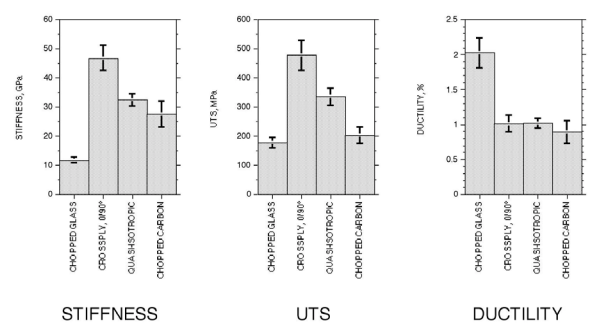

Figure 4. Comparison of tensile properties of four composites having the same urethane matrix.

previously characterized. All of these composites have the same Baydur 420 IMR urethane matrix. The significant improvement in stiffness of the chopped-carbon composite over that of the chopped-glass composite is apparent, although the stiffness and strength of the chopped-carbon-fiber composite are less than the values for the continuous-fiber composites, and the relative variability is seen to be larger.

Table 1 lists the in-air tensile, compressive, and shear properties of the chopped-carbon-fiber material over the temperature range of interest.

The design-allowable tensile stress, S_0—which is defined as two-thirds of the tensile strength—is 102, 104, and 72 MPa at –40°, 23°, and 120°C, respectively.

Figure 5 shows the measured weight gain of the chopped-fiber composite resulting from exposure to distilled water or 70% relative-humidity (RH) air.* The results of similar measurements on the quasi-isotropic continuous-fiber composite are also shown for comparison. Both appear to follow classical Fickian behavior. In general, 1000-h exposure to moisture reduces strength by about 11% and stiffness by about 4%.

In real structures, biaxial stress states exist. Also, bending is unavoidable at some locations. Both uniaxial and biaxial flexure tests have thus been performed at various temperatures and in both air and in representative fluids. In simple beam tests, the modulus of rupture (the maximum elastically-calculated stress determined from simple bending theory) varies from 2.0 times the ultimate tensile strength (UTS) at –40°C down to 1.2 times the UTS at 120°C. These factors will be incorporated into the final design criteria. Biaxial flexure tests use circular-plate specimens, as shown in Figure 6. Here, a 94-mm-diam specimen is simply supported at the outer edge and loaded with a concentric ring load (the nose of the loading ram in Figure 6 is toroidal in shape). The resulting failure data will be used in formulating a biaxial strength theory for the final design criteria.

Cyclic Fatigue Behavior

Fatigue S-N curves (stress vs number of cycles to failure) were established for the chopped-carbon-fiber composite for a number of loading conditions, e.g., tensile cycling, compressive cycling, and completely reversed stress cycling. Curves were established over the –40 to 120°C temperature range and for exposure in the two representative automotive fluids. The room-temperature curve for tensile cycling is shown in Figure 7, where the results are compared with similar results for the quasi-isotropic and crossply continuous-fiber composites.

The fatigue strength multiplication factors tabulated in Table 2 are intended for use with the curve in Figure 7 to account for typical environmental effects.

This and similar information for other conditions will be used to formulate cyclic-fatigue rules for the design criteria.

Time-Dependent Creep and Creep Rupture

Time-dependent creep tests are under way on the chopped-carbon-fiber material to establish (1) creep deformation curves with time and (2) creep-rupture curves, which show stress vs time to rupture. Some 56 tests have been completed or are under way at 23°, 120°C, in distilled water, or in windshield washer fluid. Most are tensile creep tests, but a few are compressive. The longest of these tests are approaching 4000 h of test time.

Figure 8 compares the time-dependent deformation response of four specimens subjected to identical tensile stresses of 101 MPa, which is 50% of the UTS. Also shown in Figure 8 are average curves at the same stress level for the quasi-isotropic carbon-fiber composite and for the chopped-glass-fiber composite. The magnitudes of the creep strains in Figure 8 are approximately inversely proportioned to the original modulus of elasticity of the respective specimens.

Once all tests are discontinued, a creep model will be developed for each set of test conditions. These will be incorporated into the design analysis guidance that will be part of the design criteria for the chopped-carbon-fiber composite. Likewise, creep-rupture curves will be developed for each set of conditions, and these will be used to derive the time-dependent allowable stresses that will be provided in the design criteria.

*The 70% RH is the approximate average daily value over most of the year in most cities in the United States.

Table 1. Tensile, compressive, and shear properties in an air environment

Temperature (°C)	Tensile		Compressive		Shear	
	Stiffness (GPa)	Strength (MPa)	Stiffness (GPa)	Strength (MPa)	Stiffness (GPa)	Strength (MPa)
–40	29.2	197	30.9	212	10.0	189
23	27.8[a]	201[b]	28.9	172	9.1	151
120	22.5	139	25.4	83	6.8	92

[a]Based on 525 stiffness tests on specimens from 23 plaques.
[b]Based on 112 strength tests.

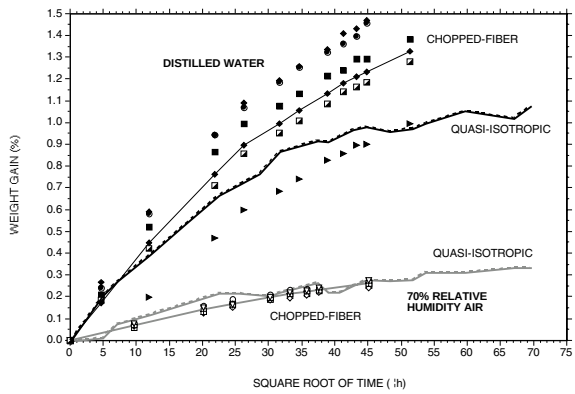

Figure 5. Weight gain due to moisture absorption.

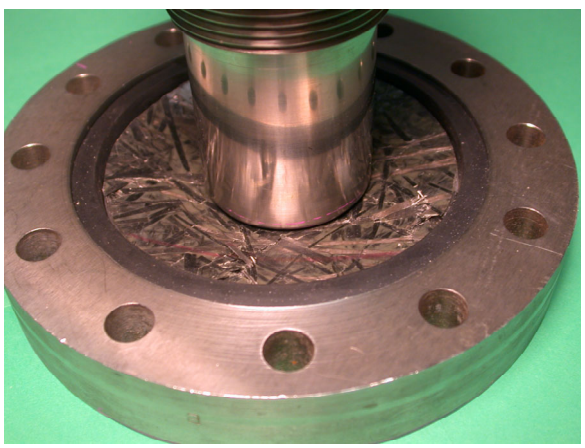

Figure 6. Failure test of a chopped-carbon-fiber disk subjected to biaxial flexural loading.

Table 2. Fatigue strength factors to account for environment

Environment	Cycles			
	10^2	10^4	10^6	10^8
23°C	1	1	1	1
120°C	0.79	0.73	0.66	0.60
Windshield washer fluid	0.91	0.89	0.87	0.85

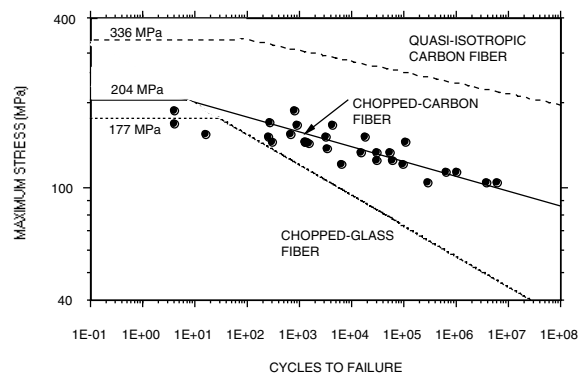

Figure 7. Room-temperature tensile fatigue strength compared with that of previous composites.

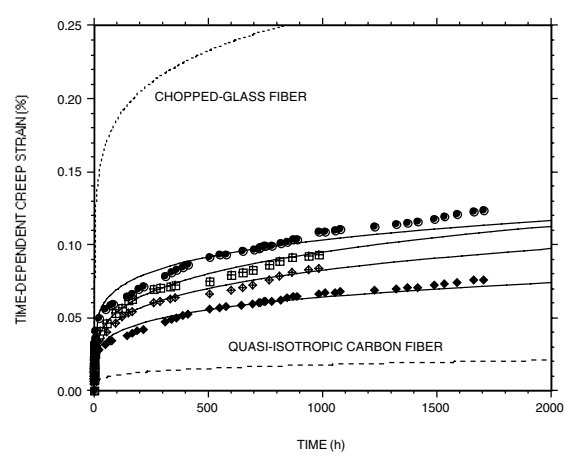

Figure 8. Time-dependent room-temperature creep strains vs time for four tests at a stress of 101 MPa. Curves for previous composites at the same stress level are shown for comparison.

Impact Damage

Impact tests using a pendulum to represent tool drops and an air gun projectile to represent roadway kickups have been performed on plates of the reference chopped-carbon-fiber composite, as well as on each previous composite addressed. Correlations between damage areas, as measured by ultrasonic C-scans, and impactor mass and velocity were developed in each case. Test specimens were then cut from the impacted plates to determine strength degradation due to the impact-induced damage. Similar specimens containing circular holes and slits of various sizes were also tested for the chopped-fiber material. Collectively, the test results provide a measure of the damage tolerance of the chopped-fiber composite.

The impact damage susceptibility of the chopped-carbon-fiber composite compared with that of previous composites is depicted in Figure 9,

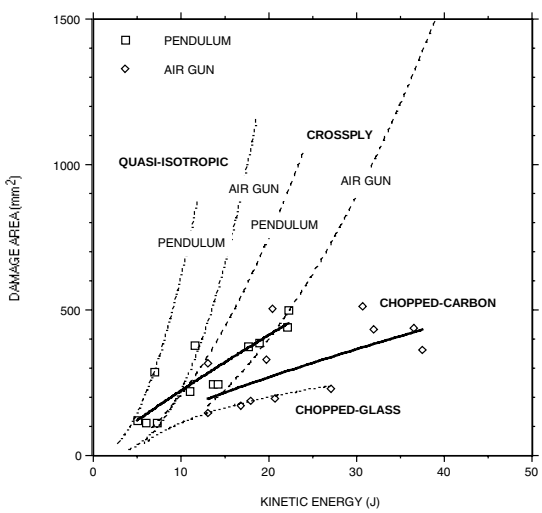

Figure 9. Impact damage area vs kinetic energy of impactor for chopped-carbon-fiber composite. Correlations for other composites are shown for comparison.

where measured damage area is plotted as a function of impactor kinetic energy. In all cases except that of the chopped-glass-fiber composite, the pendulum and air-gun tests gave different levels of damage; therefore, two correlations are shown. Each of the materials represented in Figure 9 had the same urethane matrix and, with the exception of the quasi-isotropic carbon-fiber composite, each was 3 mm thick; the quasi-isotropic material was 2 mm thick. The chopped-carbon-fiber material shows relatively good damage resistance.

To determine how the damage resistance of the molded carbon/urethane composites compares with that of the more familiar and well-studied aerospace carbon/epoxy composites, 13 references that report the results of impact tests on carbon/epoxy composites were reviewed. Most used cross-ply on quasi-isotropic layups. The studies used a variety of ply numbers, tup sizes, impact velocities, specimen sizes and shapes, and specimen boundary conditions. Not surprisingly, none of the sets of conditions exactly matched those used to generate the results in Figure 9. Nonetheless, it could be concluded that the damage resistance of the molded carbon/urethane automotive-type composites is at least as good as that of many aerospace-type carbon/epoxy composites.

Publications

J. M. Corum, et al., *Durability-Based Design Criterial for a Quasi-Istropic Carbon-Fiber Automotive Composite*, ORNL/TM-2002/39, Oak Ridge National Laboratory, March 2002.

J. M. Corum, R. L. Battiste, and M. B. Ruggles-Wrenn, "Durability-Based Design Criteria for a Quasi-Isotropic Carbon Fiber Automotive Composite," in *Proceedings of 34th International SAMPE Technical Conference*, Baltimore, November 2002.

J. M. Corum, R. L. Battiste, and M. B. Ruggles-Wrenn, "Low-Energy Impact Effects on Candidate Automotive Structural Composites," accepted for publication in *Composites Science and Technology*.

S. Deng, X. Li, and Y. J. Weitsman, "Time-Dependent Deformation of Stitched T300 Mat/Urethane 4-20IMR Crossply Composite Laminates," accepted for publication in *Time Dependent Materials*.

B. Creep, Creep Rupture, and Environment-Induced Degradation of Carbon-Reinforced and Glass-Reinforced Automotive Composites

John M. Henshaw
The University of Tulsa
600 South College
Tulsa, OK 74104
(918) 631-3002; fax: (918) 631-2397; e-mail: john-henshaw@utulsa.edu

Ian K. Lisko
The University of Tulsa
e-mail: ian-lisko@utulsa.edu

ACC Project Contact: Dan Houston
Ford Motor Co.
20000 Rotunda Dr., MD 3182 SRL, P.O Box 2053
Dearborn, MI 48121-2053
(313) 323-2879, fax: (313) 323-0514; e-mail: dhousto2@ford.com

Field Project Manager: C. David Warren
Oak Ridge National Laboratory
P.O. Box 2009, Oak Ridge, TN 37831-8050
(865) 574-9693; fax: (865) 574-4963; e-mail: warrencd@ornl.gov

Technology Development Manager: Joseph Carpenter
(202) 586-1022; fax: (202) 586-1600; e-mail: joseph.carpenter@ee.doe.gov
Field Technical Manager: Philip S. Sklad
(865) 574-5069; fax: (865) 576-4963; e-mail: skladps@ornl.gov

---

Contractor: U.S. Automotive Materials Partnership (cooperative agreement)
Contract No.: DE-FC05-02OR22910

Objectives

- Design and develop low-cost, reliable fixtures and methods for the characterization of creep rupture behavior of automotive composites with and without environmental exposure. Confirm the results generated by the new fixtures with those from conventional testing systems.
- Incorporate these fixtures and methods into industry-standard test methods for automotive composites.
- Using the results of short-term-tests, develop predictive models for lifetime property degradation.
- Investigate the fundamental damage mechanisms in polymer-matrix, E-glass, and carbon fiber composites as a function of specific, varied mechanical loading with concurrent environmental exposure.

Approach

- Design and develop a compact creep rupture test fixture system and confirm its performance.
- Use the new fixture system to develop a creep rupture database.

- Develop a standard procedure for creep rupture testing using the new system.
- Develop and verify damage and creep rupture models for structural automotive composites.

Accomplishments

- Developed a final concept prototype that continues to meet or exceed nearly all original design specifications.
- Verified fixture multiplication ratio.
- Performed cyclic and environmental testing.
- Analyzed creep rupture and creep compliance data for Bayer programmable powered performing process (P4) material.
- Performed polycarbonate testing.
- Modified the data acquisition system and laptop (see Figure 7).

Future Direction

- Continue environmental testing.
- Conduct further testing of P4 material (with normalization of data).
- Develop creep rupture fixture test standard.

Introduction

Because of insufficient information on the long-term durability of lightweight composite materials, reliable methods and models requiring relatively short-term tests are essential if composites are to achieve their full potential in the automotive industry. The purpose of this project is to develop simple low-cost fixtures and methods for the creep and creep rupture characterization of automotive composites and to confirm the in-situ creep test fixture results by comparing them with results obtained using conventional testing methods.

Final Concept of the Creep Rupture Fixture

Based on the results obtained from the first prototypes, some improvements were made and a final concept was produced. This later prototype consists of two pulleys, two sprockets, and a lever arm (Figure 1). It is designed to achieve a ratio of up to 216:1. Verification of the multiplication ratio is discussed later in this report.

A series of tests were performed on Bayer P4 composite specimens. These tests verified successfully the ability to creep and to rupture, therefore proving the feasibility of the concept selected. Also, test data showed encouraging results and compared well with ORNL results generated on standard dead-weight machines.

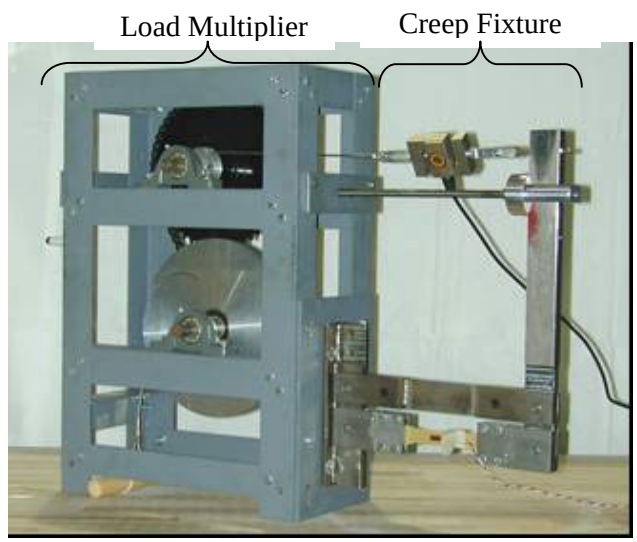

Figure 1. Final creep rupture prototype.

A series of improvements were implemented on the prototype. A clutch was added to adjust the height of the weight during a test without perturbing the specimen. Also, the loading procedure was modified to obtain the desired loading rate. Finally, in addition to strain, temperature, and humidity, load is now integrated in the data acquisition system and can be measured simultaneously.

Creep Rupture Test Fixture Details

As stated in report 7A, to achieve the goal of developing a compact, inexpensive creep rupture fixture, several design specifications were targeted. These specifications are

- capability of testing materials such as aerospace-grade carbon fiber composites.
- maximum load application of 25132 N (5650 lb) on a test specimen [assuming an ultimate tensile strength of 620.5 MPa (90 ksi) for a specimen of 12.7×3.175 mm (0.5×0.125 in.] cross section]
- load multiplication of at least 180:1.
- geometric envelope of $500 \times 250 \times 500$ mm
- weight of less than 35 kg (77 lb)
- ability to test specimens in various environments (water, etc.)
- maintenance of $\geq 95\%$ of the initial load
- low cost compared with a conventional testing machine: fixture cost of less than approximately $3000 without the data acquisition system
- easy conversion to the spring-loaded in-situ creep fixture previously developed (patent pending, U.S. Patent 9,821,280)

A load multiplication of at least 180:1 reduces the required input load to a maximum of no more than 50 lb, for a maximum specimen load of 5650 lb.

The final prototype is composed of two main parts: the fixture and the load multiplier (Figure 1). One lever-arm, two pulleys, and two sprockets enable the fixture to achieve the desired ratio of 180:1. The lever-arm is connected to a small pulley located on the upper axle of the load multiplier. This axle is coupled to the lower axle using two sprockets and a chain. Little tension was applied on the chain to reduce friction within the system. A weight hangs from a large pulley next to the small sprocket on the lower axle. Because of the load multiplication of the fixture, the weight moves much farther than any of the other components in the system. For this reason, it is useful to be able to raise the weight without disturbing the other components in the system. To allow this, a one-way clutch was installed on the large pulley.

A load cell was then placed between the lever-arm and the cable to record any load variation during a test, as shown in Figure 1.

A Labview program was developed to record the load simultaneously with strain, temperature, and humidity during a test in order to assess any environmental influences on the overall fixture.

Finally, a first attempt was made to load the specimen at a constant predetermined loading rate. A threaded rod was placed horizontally through the load multiplier; upon loading, it contacts the lever-arm to stop it from deflecting. To load the specimen, the threaded rod would turn at a constant rate to slowly release the lever-arm, thereby placing the specimen in tension. However, high compression forces on the threaded rod made loading the specimen difficult. The rod could barely turn. Following this experiment, a second version of that concept was developed. A small steel ball was placed on the right end of the threaded rod in lieu of a urethane stopper, and an adjustable thrust bearing was installed on the lever arm. This arrangement resulted in much smoother and easier loading and unloading of the specimen.

Verification of Fixture Multiplication Ratio

This prototype was sized to achieve a load multiplication ratio of 216:1. However, possible friction and/or geometric variation of components within the system can reduce the actual ratio of the fixture. Load multiplication verification was performed to determine the actual ratio. A test was run using two separate load cells, one placed between the load multiplier and the creep fixture and one locked in the fixture grips. This arrangement resulted in an actual total load ratio of 187:1. Individually, the actual multiplication ratio of the lever arm component was approximately 5.94:1, while that of the load multiplier component was approximately 31.5:1.

Analysis of Cyclic Loading

The function of this test was to verify the repeatability of the fixture. To do so, it was preferable not to have creep during the test. Thus a steel test specimen was placed in the grips, and cyclic loading tests were performed to see if the output load was always the same for a given input load. These tests also revealed the significance of any variation of the output load (Figure 2).

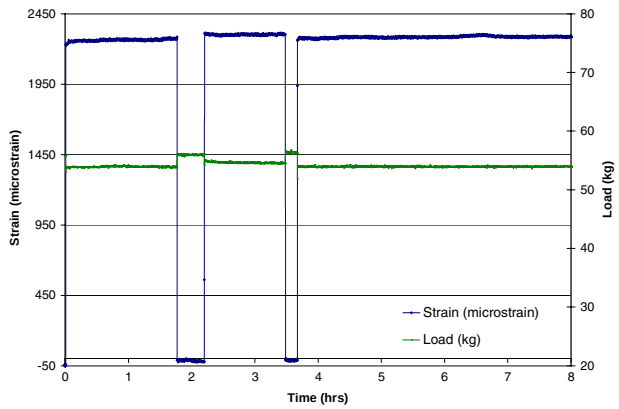

Figure 2. Cyclic loading test results.

The lower curve represents the load recorded between the lever arm and the load multiplier, while the upper curve represents the strain measured on the steel specimen. The cycle loading test shows that for an identical input load, the output load before the lever arm can vary by 1.25 %. Also, it was observed that while the load should remain constant when the test specimen is unloaded, a small increase is noticed instead. This increase demonstrates the presence of friction within the load multiplier. However, the load returns to the previous desired level once the specimen is reloaded. Because the test fixture is designed to characterize creep and creep rupture, the main interest is that the load remain constant over the entire test period.

Environmental Testing Results

A review of the data recorded during a typical experiment on the P4 material revealed that temperature and humidity varied significantly throughout the test. The load fluctuation was further analyzed to see if there were any correlations among temperature, humidity, and load.

To explore environmental effects on the test fixture or load, the fixture was placed in an environmental chamber where temperature and humidity could be controlled. However, the environmental conditions could not be kept completely constant over the test period.

Nonetheless, a designed experiment was developed to help with the analysis. Then a series of tests for each environmental condition were performed. For each test, temperature, humidity, and load were recorded simultaneously. Initial statistical analysis showed no significant influence on the load from the environment. However, graphical analysis seems to show there could be some effect from temperature variation on load (Figure 3).

It appears that as the temperature increases, the load decreases, and vice versa. Because of the fixture design and the material used, it seems more probable that only temperature affects the fixture system, not humidity. For example, if parts such as the pivot pin in the lever arm or the shafts in the load multiplier dilate, friction might increase.

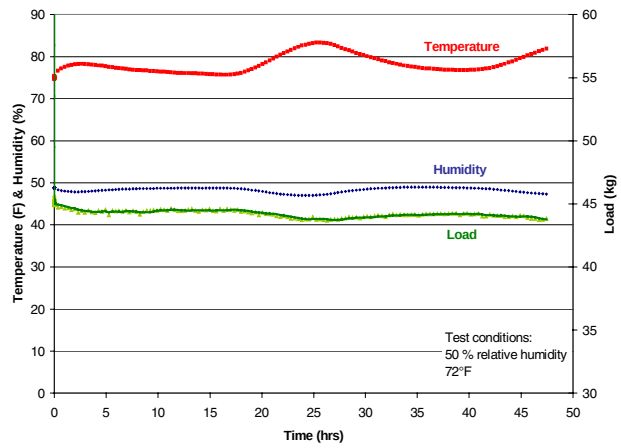

Figure 3. Test results for conditions set at 50% relative humidity and 72ºF.

Creep Compliance/Creep Rupture Test Results

Additional series of tests were performed on Bayer P4 composite specimens. These tests further verified the fixture's ability to creep and creep rupture, therefore proving the feasibility of the concept selected. Test data show encouraging results and compare well with Oak Ridge National Laboratory (ORNL) results generated on standard dead-weight machines (see report 7A).

Creep compliance was determined in order to compare ORNL and University of Tulsa (TU) test results. TU creep compliance data were compared with ORNL experimental data to see if there was any significant difference between the two test methods. Figure 4 shows creep compliance comparison between TU and ORNL data at 60 and 40 hours. Tests run on the TU fixture have a larger variation than those from ORNL; however, the TU data are not normalized.

Normalizing the data first requires dividing the individual modulus for each specimen by the average modulus for each plaque of material. This

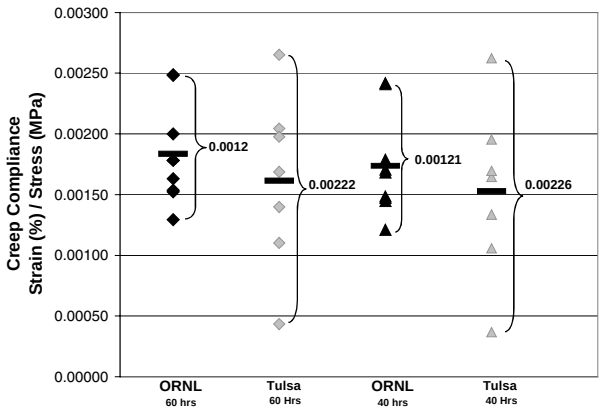

Figure 4. Comparison of TU and ORNL creep compliance data at 60 and 40 hours.

modulus ratio is then multiplied by the creep compliance to give the normalized creep compliance. ORNL uses normalized creep compliance to help minimize data scatter. The TU data may show greater scatter than the ORNL data because TU data are not normalized. Nonetheless, a student t-distribution statistical analysis showed the means of TU versus ORNL creep compliance to be statistically indistinguishable. We will attempt to normalize data acquired from the TU fixture in future tests to further test this hypothesis.

During testing of the P4 material, a number of specimens reached rupture. The TU rupture data were compared with data from ORNL. Figure 5 shows the results of this comparison.

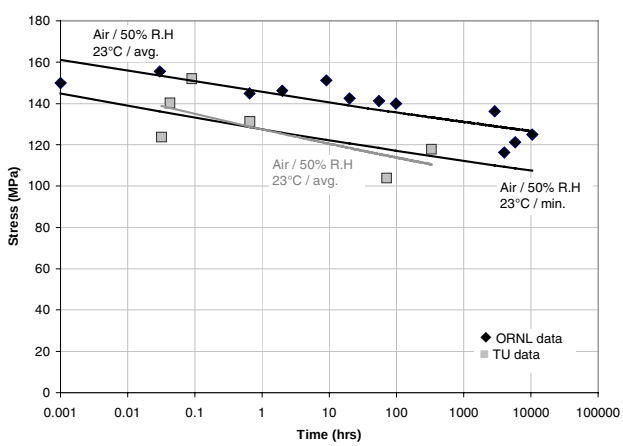

Figure 5. TU and ORNL creep rupture comparison.

It can be seen from Figure 5 that TU creep rupture values are lower than those of ORNL. However, the TU average is close to the minimum ORNL values. Again, this discrepancy may be heightened by the non-normalization of the TU data.

Polycarbonate Testing Results

Several tests were performed at 22.2°C (72°F) and 50% relative humidity on unreinforced polycarbonate. Test results were compared with a model developed from literature data. In order to compare the test results from the creep rupture fixture to the data from the literature, it was necessary to plot the literature data in a different manner. Therefore, data points for several tensile stress levels were taken and replotted as strain versus time. Then the data were curve-fitted with a power law for each stress level. Creep can be modeled by a power law of the form: $\varepsilon(t) = A\,\sigma\,t^n$. The values for A and n were determined for each curve fit obtained from the polycarbonate isochronous stress-strain data, representing various stress levels.

Figure 6 presents the results of both TU data and the literature models. The upper curve represents the model calculated at 4000 psi using the A and n values found at 34.5 MPa (5000 psi). The middle curve corresponds to the model calculated at 4000 psi using the A and n values found at 7.6 MPa (4000 psi). Finally, the lower curve represents the model calculated at 4000 psi using the A and n values found at 10.34 MPa (1500 psi). It can be observed from Figure 6 that the TU test results are within expected values and in fact match the literature data for polycarbonate quite well.

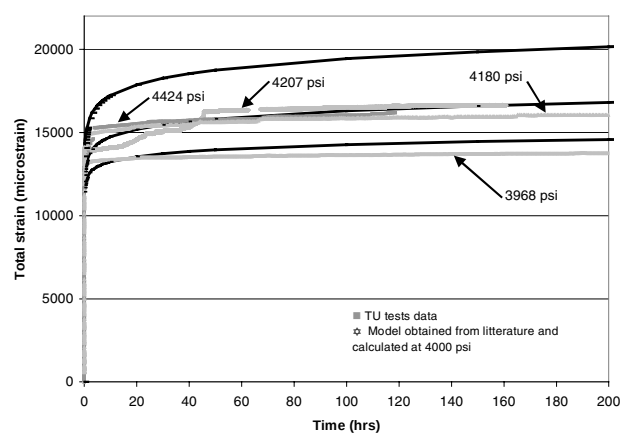

Figure 6. Comparison of TU to model for polycarbonate material.

DAQ/Laptop Modifications

Both the laptop and data acquisition system responsible for all TU creep/creep rupture data gathering were enhanced (Figure 7). The system was made network-ready by installing an Ethernet card in the laptop; and appropriate measures were taken to connect it to the TU server, including several software updates. This arrangement enables easier data transfer from the data acquisition laptop to other computers on the campus server. Larger data files can now be transferred at a greater speed and efficiency, as the system is no longer limited by the capacities of removable media.

Another modification involved writing a small batch file that copies test data directly from the data acquisition laptop to a shared network drive accessible to those with a password. The program runs every 30 minutes, allowing other computers across the campus network to monitor the test data as they are being generated.

Ongoing/Future Work

- Low-/high-range load testing (requires a lower-capacity load cell)
- Further testing of P4 material (with normalization of data)
- Water immersion testing
- Obtaining a small loading motor to replace the hand crank
- Continued environmental testing
- Development of creep rupture test fixture standard

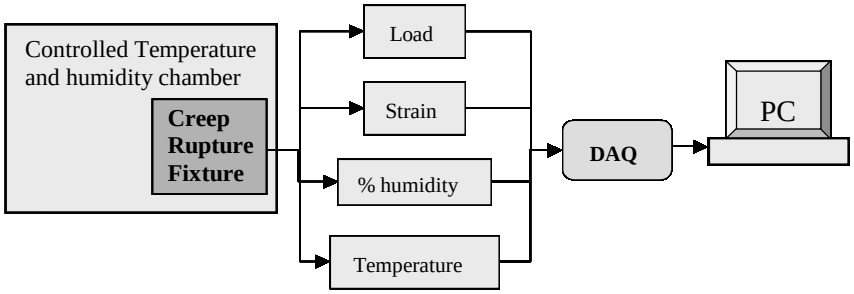

Figure 7. Schematic of the fixture and data acquisition system.

C. Modeling of Composite Materials for Energy Absorption

Edward Zywicz and Steve DeTeresa
Lawrence Livermore National Laboratory
Livermore, CA 94550
(925) 423-5632; fax: (925) 424-2135

Srdan Simunovic, J. Michael Starbuck, and Raymond G. Boeman
Oak Ridge National Laboratory
Oak Ridge, TN 37831-6359
(865) 241-3863; fax: (865) 574-7463

Field Project Manager: C. David Warren
Oak Ridge National Laboratory
P.O. Box 2009, Oak Ridge, TN 37831-8050
(865) 574-9693; fax: (865) 574-4963; e-mail: warrencd@ornl.gov

Technology Development Manager: Joseph A. Carpenter
(202) 586-1022; fax: (202) 586-1600; e-mail: joseph.carpenter@ee.doe.gov
Field Technical Manager: Philip S. Sklad
(865) 574-5069; fax: (865) 576-4963; e-mail: skladps@ornl.gov

---

Contractor: Oak Ridge National Laboratory, Lawrence Livermore National Laboratory
Contract No.: DE-AC05-OR22725, W-7405-ENG

Objective

- Develop analytical and numerical tools that efficiently predict the behavior of carbon-fiber- (CF-) based composites in vehicular crashworthiness simulations. These tools are intended to decrease the automotive design process time and cost by reducing component testing and to increase the simulation accuracy of CF-reinforced structures. The developed tools are used in conjunction with existing crash simulation software.

Accomplishments

- Extended in several ways the finite element approach used to numerically replicate cracks in the braided composite, the assumed enhanced strain (AES) formulation.
  - Incorporated "crack" mass to provide an energetically consistent formulation and to alleviate constitutive snap-through
  - Incorporated alternative methods for selecting enhancement fields
- Developed consistent damage initiation criteria to initiate the AES modes.
- Developed new methods for characterizing critical material parameters for modeling of crushing of discontinuous fiber composites.
- Developed programs for modeling of programmable powdered perform processing (P4) manufacturing and analysis.
- Extended the current material model to model crack nucleation.
- Initiated development of a new material model based on the analysis of P4 structure.

Future Direction

- Validate the braid and random fiber material model by simulating previously conducted strip and tube crush experiments.
- Develop new model for random fiber composite based on preform modeling.
- Document the current formulations.

Introduction

Automotive structures manufactured from CF composites offer the potential for significant advantages in weight, durability, design flexibility, and investment cost. While the aerospace community has substantial experience with graphite-fiber laminated composites, there is little knowledge of how CF composites respond in automotive applications during impact-induced "crash" loading conditions (i.e., "crush"). Furthermore, predictive analytical and numerical tools required to accurately evaluate and design CF automotive structures for crush do not currently exist. This project aims to understand and quantify the basic deformation and failure mechanisms active in CF materials during vehicular crush conditions. The project entails modeling, numerical, and experimental components and deals exclusively with automotive materials—braided, textile, and chopped random-fiber architectures.

Experimental Determination of Select Tow-Level Braided Carbon-Fiber Composite Properties

The present numerical model employs idealizations and material properties at two distinct length scales to predict overall braided composite response—the fiber and matrix level and the tow level. While the elasto-plastic tow-level response can be reliably predicted from micro-mechanical models and fiber and matrix properties, tow-level failure is much more difficult to accurately predict from its individual constituents. Consequently, the present formulation uses tow-level failure quantities as "primitive" values.

The transverse tensile, compressive, and shear strengths of unidirectional CF composite tows were measured. Since unidirectional tow material was not available from the Automotive Composites Consortium (ACC), Lawrence Livermore National Laboratory fabricated its own test CF composite rods using a low-volume squeeze-casting technique. The rods, manufactured using the same fiber and resin and cure cycle as the ACC composites, yielded material with nearly identical microstructure and characteristics. The transverse tensile and compressive strengths were obtained from diametrical compression tests, and the transverse shear strength was measured from torsion tests. The latter yielded a complete nonlinear stress-strain curve (see Figure 1) that is also useful in validating the tow model. These data, along with those previously summarized in DeTeresa et al.,[1] provide the necessary information to model the CF composite braids with the present numerical model.

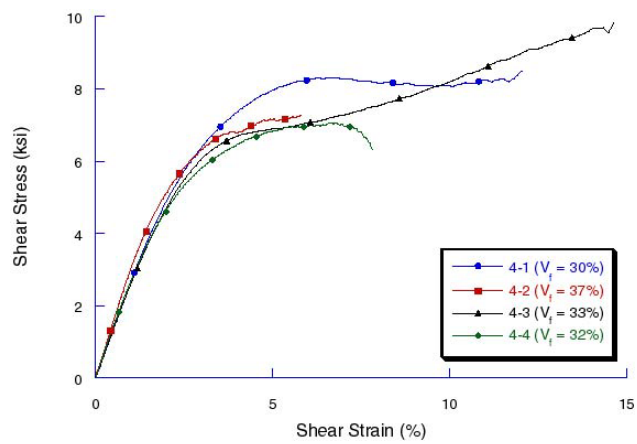

Figure 1. Stress-strain response from transverse torsion tests on uni-directional CF composite rods.

Damage Model for Braided Carbon-Fiber Composites

The framework to numerically simulate the behavior of large-tow triaxially-braided CF composites and the basic elasto-plastic tow-level constitutive relationship developed in FY 2000[2] remain the basis for the current work. Efforts in FY 2002 focused on incorporating and improving the compressive and tensile damage mechanisms within the tow-level constitutive model.

Unfortunately, numerical testing revealed several pathological deficiencies and necessitated substantial modifications to the damage portion of the tow model.

As previously summarized, the layered composite material is represented on a layer-by-layer basis and depicts the complex fiber geometry using a simplified unit cell approach. The material within the braid's unit cell is partitioned into three distinct layers, and then each layer is individually homogenized. The behavior within each layer is simulated using a tow-level constitutive model that represents the basic elastic, plastic, and damage behavior of the straight fibers, and an undulation model that replicates how the curved fiber regions respond.

The basic tow-level constitutive model depicts the nonlinear pre-damage and post-damage response. The elasto-plastic unidirectional tow response in straight fiber sections is assembled from the individual fiber and matrix constitutive behaviors using a simple homogenization approach. The tow model is coupled in series with a nonlinear undulation model. The latter replicates the complex and highly nonlinear behavior of the curved fiber sections.

Under both tensile and compressive loadings, substantial cracking occurs parallel and perpendicular to the fiber axis that reduces the ability of the composite to carry load, i.e., damage. The crack evolution is complex and inherently three-dimensional in nature. Four separate mechanisms (tensile and compressive cracking both perpendicular and parallel to the fiber) have been incorporated into the tow model to replicate the damage.

The tensile crack models are based upon an AES element formulation.[3] This approach decomposes the total displacement into a portion due to material deformation and cracking. The discrete cracks are conceptually amalgamated into a single effective macro crack within each element, and a rigid-strain softening traction-displacement relationship determines the tractions imposed upon the amalgamated crack face as a function of the local crack opening displacement. The AES formulation was transformed from a static to a dynamic idealization by explicitly including mass in its derivation. The addition of mass eliminates the problem of element snap-through by properly accounting for the associated kinetic energy generated by cracking. The additional local equations of motion describing the crack dynamics are integrated explicitly and have no impact on the overall finite element time-step size.

The resulting formulation is naturally mesh-independent and energetically consistent. Figure 2 shows the response of a single unidirectional ply subjected to uniaxial stressing in the transverse direction for two different element sizes, a 1-in.^{2} and a 10-in.^{2} element. The smaller element displays the conventional pre- and post-damage bilinear response. In the larger element, the compressive behavior arises from the crack dynamics; in a multi-element problem, it would create a compressive stress wave that propagates into the adjacent elements. While the unloading may appear instantaneous, the new "crack mass" ensures a finite unloading slope.

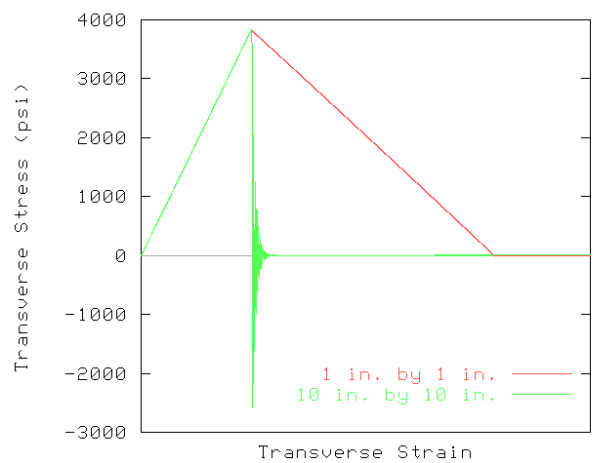

Figure 2. Stress-strain response from a constant strain-rate uniaxial stress test in the transverse direction on a unidirectional CF composite.

The two-dimensional compressive failure mechanism attempts to emulate the very complex three-dimensional behavior in an idealized manner. Non-local damage initiation surfaces are developed based, in part, upon those in Christensen.[4] The fiber-direction criterion depends upon both the local strain and the through-the-thickness curvature—a behavior unique to braided materials. At initiation, the fiber's axial response (fiber-direction damage only) and the matrix yield strength are idealized as elastic/perfectly-plastic with a degraded "flow" strength. Since "crushing" really constitutes extensive cracking and pulverization of the material, the corresponding tensile surface is activated, too. The

rapid unload at failure is consistent with the extremely brittle nature of CF composites.

Conclusions

The present plane-stress micromechanical-based finite-deformation constitutive model has been developed and implemented into the nonlinear, finite element code DYNA3D. In FY 2002, the post-peak damage response has been enhanced to more accurately replicate the underlying physics, as well as minimize numerical problems arising from mesh and reinforcement misalignment. Various numerical issues have been addressed, e.g., mesh dependence in tension and progressive softening in compression.

Modeling of Random Carbon Fiber Composites

From a macroscopic perspective, random fiber composites have a very simple structure that can be described with a few parameters. However, when it comes to deriving the material's mechanical properties from its constituents—especially the impact, strength and fracture properties—the usual assumptions of isotropy and homogeneity do not yield accurate results. Figures 3 and 4 illustrate two fiber networks with the same macroscopic density but with significantly different formation characteristics.

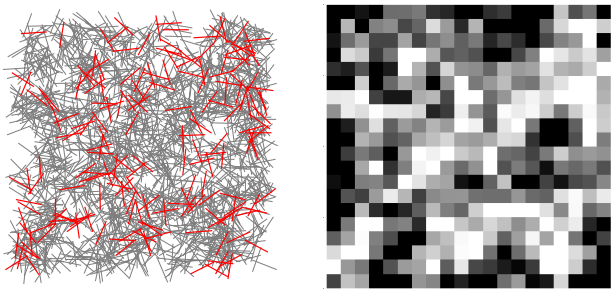

Figure 3. Flocculated fiber structure and its density map.

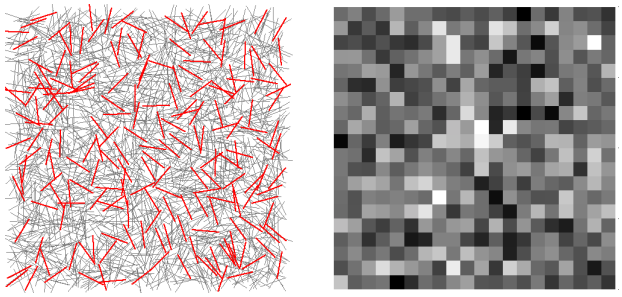

Figure 4. Dispersed fiber structure and its density map.

The two structures have very similar macroscopic elastic properties; however, the flocculated network in Figure 3 will have much lower and scattered strength.

In this research, it has been established that out of many possible fracture and energy-dissipation-related parameters, the sizes of the fiber segments that break and the number of broken bonds (fibers or their segments) are of the utmost importance since they determine the nature and the amount of energy that is dissipated in fracture. The fracture zone size is related to the effective breaking length of fibers and is the internal scale of the material, its cohesion length. The cohesion length forms a link between the conventional tensile strength and toughness, and it can be formally implemented in random fiber material models using the cohesion band approach.

The objectives of the research on the random fiber composites in this period were to

1. Investigate the fundamentals of damage and failure of disordered media and link them to the material model for random-fiber composites.
2. Analyze the constituents and model the formation of P4 composite.
3. Develop methods for derivation of P4's critical properties from its structure.
4. Further develop and validate the current P4 material model.

Fundamentals of Deformation for Disordered Brittle Solids

Failure of disordered brittle materials has been modeled using lattice models to illustrate the main characteristics of the damage process and to link them to the properties of random fiber composites. The damage evolution can be divided into three main phases. The first phase, percolation (Figure 5), consists of random failures of lattice links that are driven mainly by the distribution of disorder and weak links in the material. The dark links in the figure denote the broken links. The load has been applied in the vertical direction, and the boundary condition in the horizontal condition was cyclic.

In the second phase, crack growth, the weak sites have been mostly depleted; now the damage progresses through the growth of the existing damage clusters. The damage characteristic of this phase is illustrated in Figure 6.

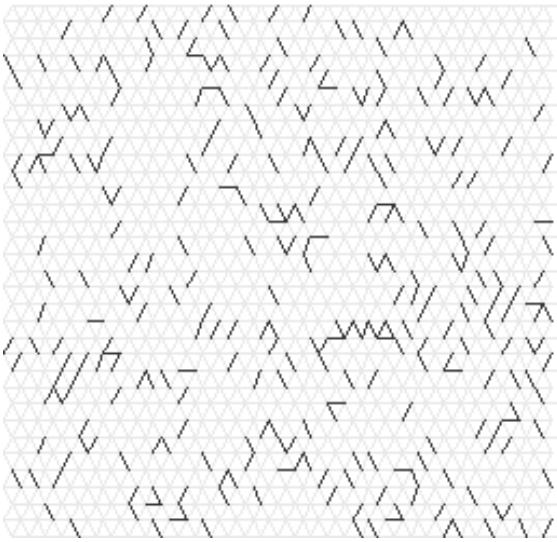

Figure 5. Percolation phase of damage evolution.

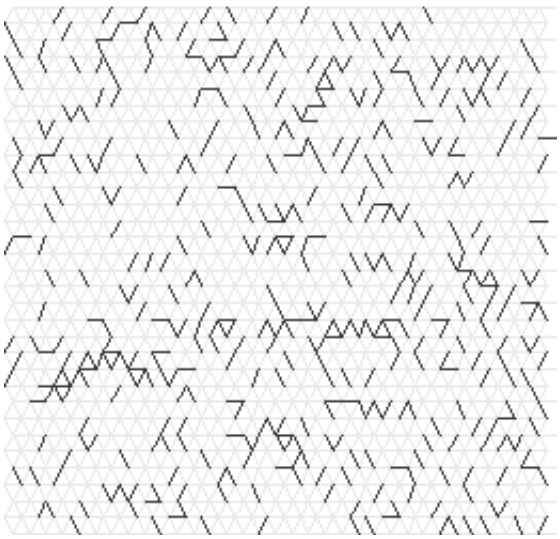

Figure 6. Crack growth phase of damage evolution.

Finally, in the third phase, localization and failure, the lattice becomes disconnected (Figure 7). Notice the cluster of broken links that spans the domain and cuts it in two distinct parts.

A characteristic force-displacement diagram is shown in Figure 8. It is important to note that the averaging procedure is feasible in the material hardening regime, but that it totally breaks down in the softening regime.

The number of specimens needed to get an averaged response for the softening regime is prohibitive for physical experiments; and even if

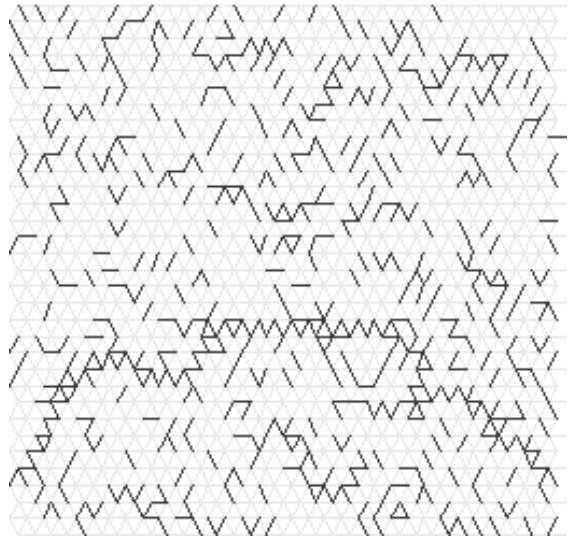

Figure 7. Localization and failure phase of damage evolution.

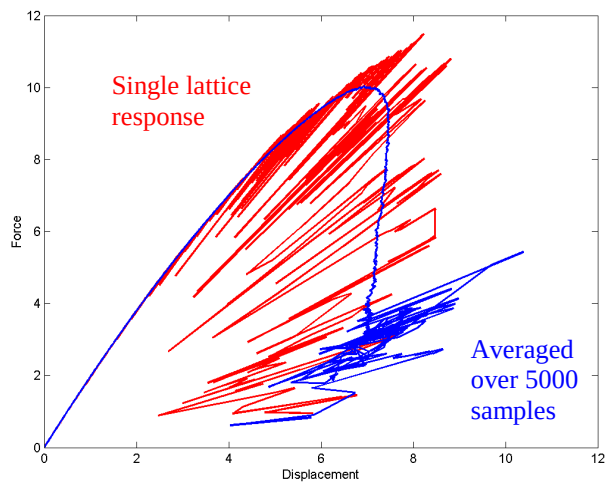

Figure 8. Force-time diagram for lattice failure.

a machine of an infinite stiffness were available, the scaling laws would have to be developed to render the results usable for engineering simulations.

The above fundamental problems are to some extent alleviated for materials made with short, random fibers. The damage has been shown to localize (localization and failure phase) in the one-dimensional uncorrelated zone of finite width, which makes it possible to use a cohesive model framework to model material failure. In the illustrated simulations, the total number of broken links has been shown to scale as $L^{1.7}$ where L denotes a characteristic domain size. This scaling

relation will be used in the following sections to link the material structure to its macroscopic properties.

The current material model for random-fiber composites is based on fracture mechanics, and it addresses the first two phases of damage evolution. The model uses several assumptions on the crack size and orientation distribution that yields reasonable results in crash simulations. However, the more rigorous model would need to be coupled with detailed experimental investigations of damage evolution under general loading conditions, which will most certainly result in a revision of the model assumptions. Such a program was outside the scope of this research.

Modeling of P4 Manufacturing

The objective of this task was to develop methods for modeling and characterization of the structure of random-fiber materials (such as those made by P4) and to determine the implications of the material structure for mechanical properties. The most important new control parameter identified as a result of this study is the fiber segment length over which fiber rupture occurs during the localization and failure of the composite (cohesive length). This parameter provides the framework for modeling strain softening and localization in random-fiber composites for tensile strength, because it gives the size of the cohesion (damage) zone in failure. This cohesion length is to a large extent determined by the preform manufacturing. In a case when the preform mat is not compressed and the fibers are not flexible, the fiber-matrix adhesion and fiber pullout should be related through the classical shear-lag theory. On the other hand, when the fiber mat is compressed and fibers are flexible—as is the case in P4 composites—fibers get anchored into the network by their undulations, and the force in a fiber can be entirely transferred to the crossing fiber.

ORNL's FN-Sim program for modeling of fiber deposition has been further developed to accommodate the fiber and preform characteristics of P4. The original program assumed much shorter and more-flexible fibers. Several assumptions were originally made to speed up the program and had to be revisited for the evolving material specifications during the project.

Figure 9 shows the control panel of the program. The input parameters define fiber characteristics,

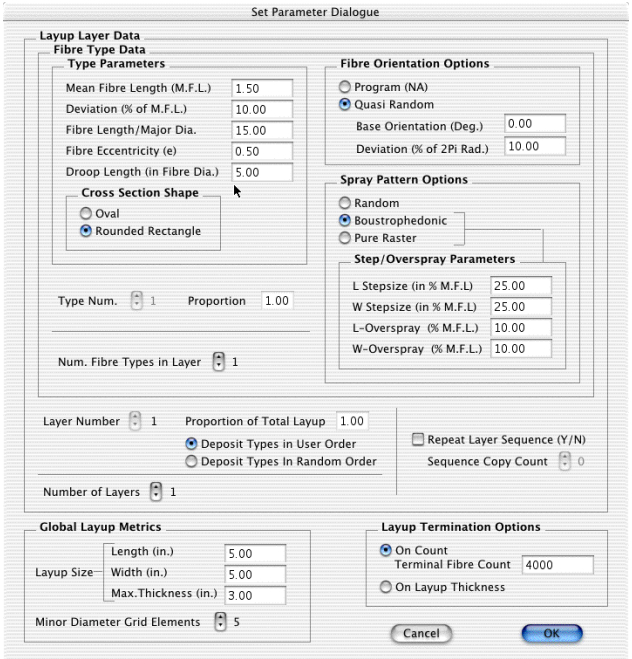

Figure 9. FNSim control panel.

layers, orientations, property variations, and pattern of fiber deposition.

The simulated P4 preform for relatively inflexible fibers is shown in Figure 10. This simulation used 400 fibers that are 2 in. long.

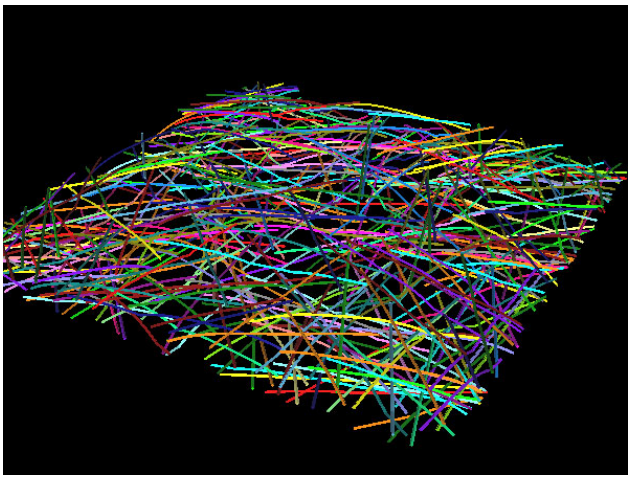

Figure 10. Simulated fiber network for rigid fibers.

Figure 11 illustrates the effect of fiber flexibility and mat compression. Fibers develop undulation when they come in contact with other fibers, and such undulations form anchor points in the network.

Another immediately apparent characteristic of random-fiber preforms is their layered structure. Tube and strip crush experiments have shown that

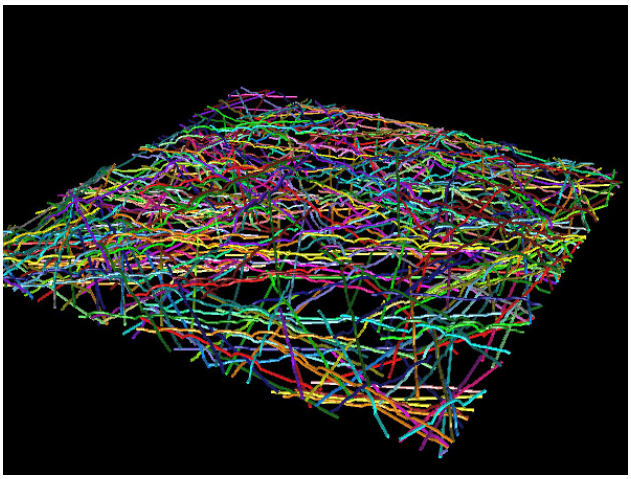

Figure 11. Fiber network for flexible fibers.

random-fiber composites delaminate, and the delamination process is an important factor in energy dissipation and the number of delaminations. A new theoretical formula has been developed for the number of delamination layers in random-fiber composites. The formula is in good agreement with the direct simulations and experimental observations. The number of delamination plies is a function of network coverage, fiber length and width, compression ratio, and fiber volume fraction.

Effect of Manufacturing and Mat Properties on Mechanical Behavior

Energy to break

Fiber total length is just one of the important length-scale parameters for random-fiber composites. Fiber failure segment length, defined in the previous subsection, is an intrinsic material property that is stable over length scales of interest for compressed-fiber networks. A new theoretical estimate for fiber segment length has been developed and has been validated by the fiber network simulations and experiments. The estimates of the work to fracture based on the developed cohesion parameters show very good agreement with the measured values from the variable-ligament double-edge notch tension (DENT) fracture test for P4. Energy-to-break in the P4 DENT test is estimated as follows. First, a model for energy-to-break of the fiber segment model is developed based on the fiber manufacturer data. Next, fiber deposition simulation is used to determine the number of segments that break during the test. The measured macroscopic energy-to-break is then determined as a sum of energy-to-break of all the segments involved in the fracture.

Fiber segment model

The stress-strain relation for a fiber tow segment has been derived from the material properties of the fiber manufacturer[5–7] and the results from the literature. A typical stress-strain diagram for a fiber tow is shown in Figure 12. Note that the shape of the diagram depends on the fiber length.

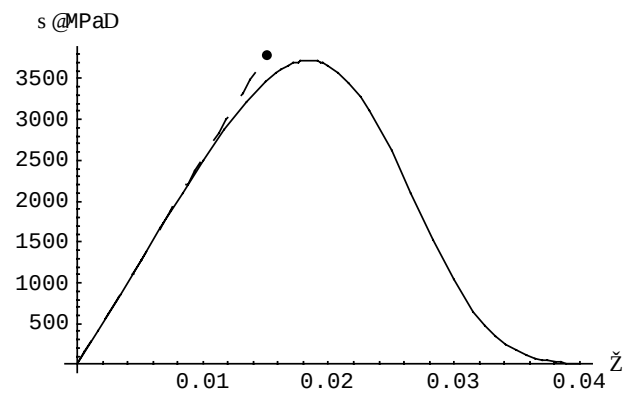

Figure 12. Stress-strain diagram for a fiber test specimen.

In the subsequent calculations, two estimates for energy density were used: one that equals the energy under the stress-strain curve until the peak stress and another that is an integral of the entire curve.

Number of fibers that break

Another critical parameter responsible for a good correlation in Figure 8 is the number of fibers that break or pull out. It was shown experimentally that random-fiber composites break along the line normal to the direction of principal stress. Therefore, the number of intersections of the fibers with straight lines in the network is used to estimate the number of fibers that are involved in the failure regime and the corresponding dissipated energy. Successive lines perpendicular to x direction were used to scan the fiber network and to determine the number of fibers crossing the potential failure lines. An illustration of the scanning process is shown in Figure 13.

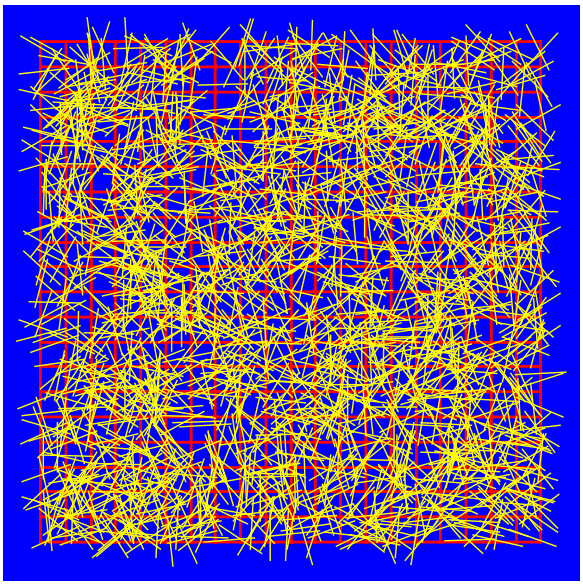

Figure 13. Scanning grid for random fiber distribution.

The number of fibers crossing successive cross-sections of the tested specimen is shown in Figure 14.

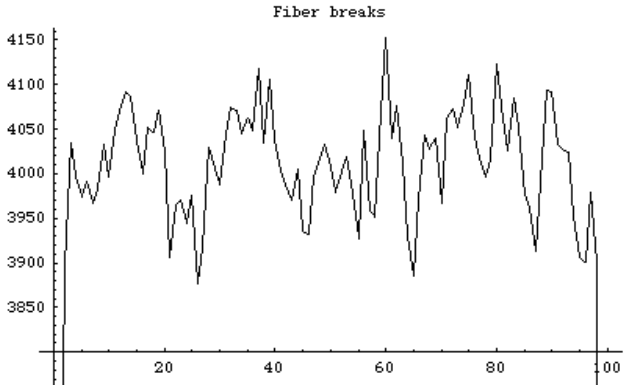

Figure 14. Distribution of number of fiber segments in cross-section.

The number of broken fibers is estimated by the number of fibers in an average cross-section and then multiplied by the strain energy density and the length of the characteristic fiber segment together with the strain energy from the matrix deformation. This product is an estimate of the energy-to-break in the DENT test. Figure 15 shows the results for two estimates based on two different strain energy densities for segment failures. Dots in the graph denote experiments (the dashed line is merely to guide the eye).

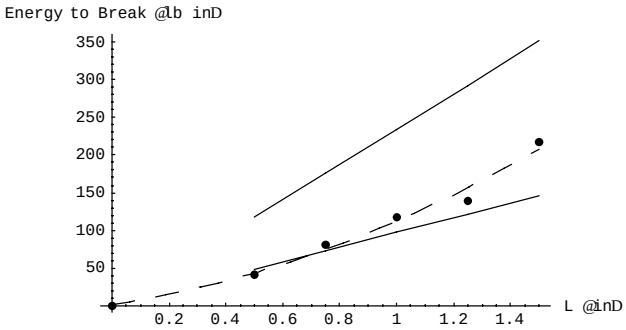

Figure 15. Comparison of theoretical and experimental values for energy-to-fracture in DENT experiments.

The correlation between the experiments (points) and the model based on the lower fiber segment strain energy estimate (lower line) is very good. The model based on the total segment energy-to-break provides a good upper bound. However, when the number of segments that break in a specimen of a given size is scaled by the exponent 1.7 developed earlier in the theoretical failure model, the correlation is remarkable, as can be seen in Figure 16.

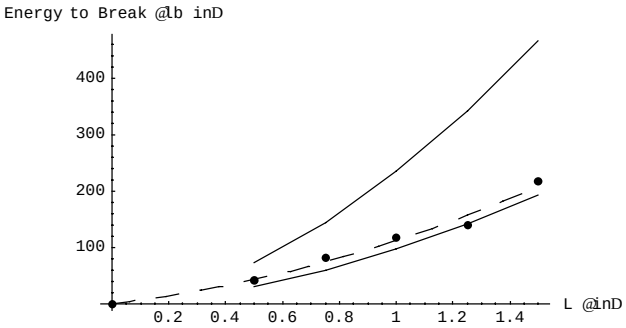

Figure 16. Comparison of scaled theoretical and experimental values for energy-to-fracture.

A good fit of the measured energy and the model indicates the validity of the developed cohesive length estimate, the findings about damage evolution in a disordered media, and applicability of the cohesive failure models for finite element modeling (FEM). The estimates are obviously dependent on the estimates of the fiber segment length, and the process simulation program can be used to further improve the accuracy of the model.

The results also provide a foundation for development of a new constitutive model, based on the fiber network architecture, that will be pursued in future studies.

Validation and Development of Current Fracture Damage Model for P4

The results from the DENT and compact tension (CT) fracture experiments were used to determine the parameters of the current fracture damage model.[8–9] The experiments provided estimates for fracture toughness, and the preform simulations provided parameters of damage topology. The material model requires an estimate for the initial damage in the material that is then evolved by the external loading. It is formalized as the representative density and size of microcracks. Figure 17 shows the material model in which the model parameters were determined from the fit to the tension test. The initial crack density was estimated as the density of fibers in the network, and the representative crack size used in the model is scaled to fit the experimental data.[10]

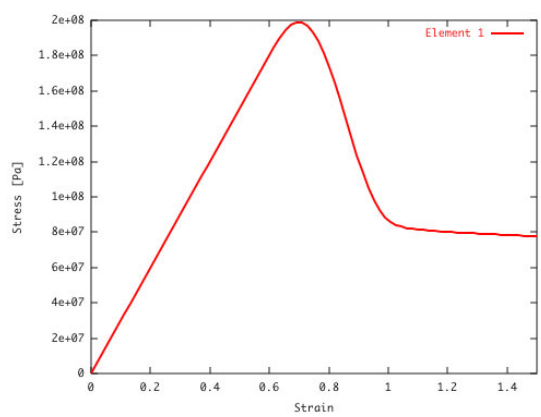

Figure 17. Stress-strain diagram for the developed model.

The shape of the softening regime is obviously size-dependent, and the trailing plateau was added for the numerical stability in the FEM programs. The localization aspects become immediately apparent when multiple elements are used. Figures 18 and 19 show the stress and damage localization in a three-element assembly used for simulation of a tensile test.

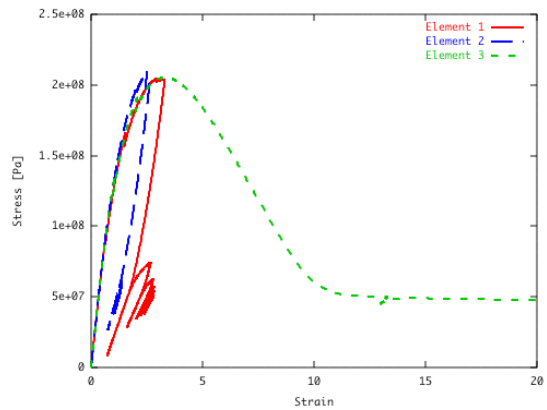

Figure 18. Stress-strain diagram for the assembly of three finite elements.

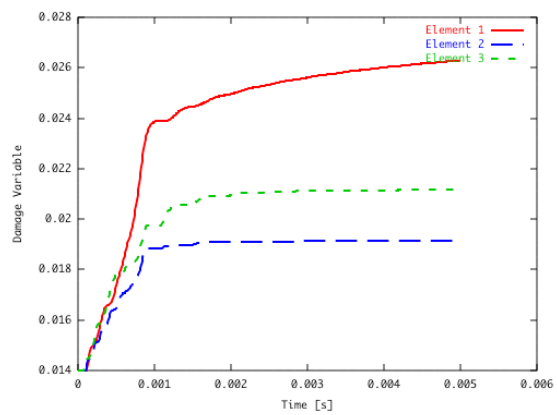

Figure 19. Damage evolution in three-element assembly.

The material model will lead to localization into the smallest element in the finite element mesh. Further modification of the model is necessary to eliminate this effect (introduction of internal length via cohesive-zone theory and/or rate effects). However, in the dynamic situations, the progressive crush mechanism controls the material response. As long as the finite element mesh discretization is of the order of the characteristic crush front width, the model remains physical. The description of the localization and crush front problem is beyond the scope of this document. A proper treatment of the problem requires a detailed experimental program to determine the cohesive-zone size and material rate characteristics relevant for the localization model. Experiments to determine the crush front features are under way that will provide information for further model modification.

Simulations of random-fiber tube crush were performed with the developed model. The deformed structure and the resulting impact force are shown in Figures 20 and 21, respectively.

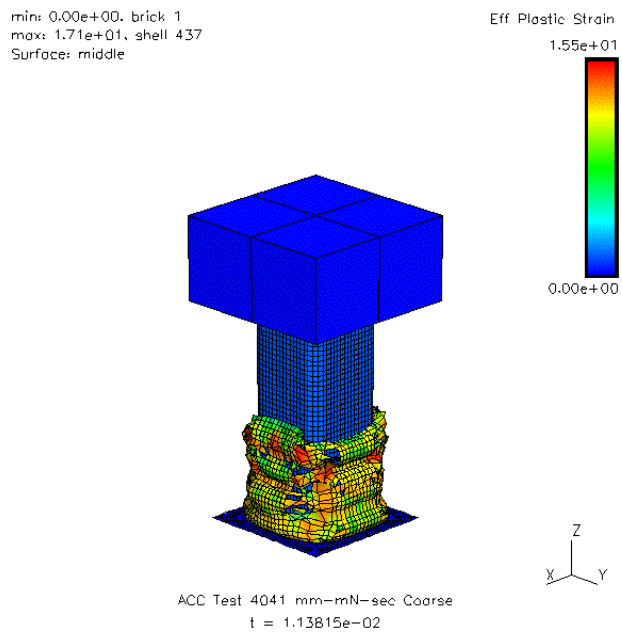

Figure 20. Tube crush simulation.

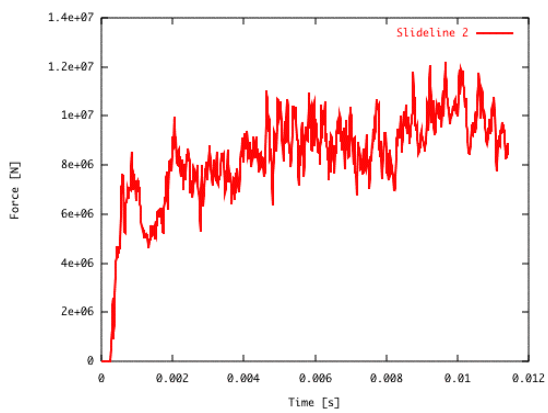

Figure 21. Impact force history.

Unfortunately, no crush experiments were available for comparison with the model prediction because of the lack of random-CF material. However, the deformation and the crush force levels appear reasonable.

Summary of the Current Material Model for Random Fiber Composites

Despite the overall good performance of the existing damage model, its apparent limitations are in the numerous assumptions made to simplify the damage evolution process. Recent findings based on explicit modeling of the fiber network structure (DENT test correlation) indicate that an improved model can be developed based on the fiber network theory. Such a model would provide a rigorous framework for damage description, link processing to performance, and eliminate many of the drawbacks and inconsistencies of the present model. The development of the model based on the new approach is planned for future research activities.

Experimental Characterization of Random-Carbon-Fiber Composite

In support of developing analytical material models for predicting the crashworthiness of chopped-CF composite structures, an experimental program has been defined and initiated. This effort expands upon the progressive crush strip testing that was accomplished in FY 2001. One objective of the previous work was to identify the key material parameters that had the greatest influence on energy absorption in chopped-CF composite material systems. A systematic review of the experimental data, based on the design of experiment techniques, showed that the fiber areal density had the greatest effect on specific energy absorption. The results showed that a lower fiber areal density gives higher energy absorption. These tests were all conducted at quasi-static loading rates and were more a structural test than a basic material test. Consequently, the experimental program planned for FY 2002 and currently in progress is based on running basic material property tests at quasi-static and dynamic loading rates. The tests consist of fracture toughness measurements using single-edge-notch bending (SENB) tests and uniaxial tension and compression tests at five different loading rates. The test plan defines the different loading rates as 0.001 in./sec (quasi-static), 0.1 in./sec, 5 in./sec, 50 in./sec, and 150 in./sec. Based on these experimental results, the strain rate dependencies of chopped-CF composites will be determined; and the necessary material parameters will be extracted to formulate the analytical model. Dynamic progressive crush tests are also planned, using the strip test specimen

geometry. The resulting data will be used as part of the analytical model validation.

The chopped-CF material system used in the strip tests was a compression-molding compound supplied by YLA that used T700 CF with an epoxy resin. The test plaques were fabricated by CCS Composites. This material system was selected in lieu of the P4 material as a direct result of P4's unavailability in FY 2001. In the current test program, chopped-CF molding compounds will continue to be evaluated, as well as the P4 material. The plaques molded by CCS have a 1-in. fiber length, 50% fiber volume fraction, and a fiber areal density of 100 gsm. As a quick comparison with the CCS material, HexMC, another chopped-CF material that is supplied by Hexcel, will be tested under quasi-static conditions only. For the P4 plaques, the fiber is a Zoltek 48-K tow that is split 7 times and chopped to a 2-in. length. The fiber volume fraction for the P4 plaques is 40%.

Preliminary quasi-static SENB tests were conducted using material that was left over from the strip tests conducted in FY 2001. This material is the same material supplied by CCS for the current test plan but with an areal density of 150 gsm. The tests followed ASTM D5045-99 and initially used specimen geometries having a width-to-thickness ratio (w/b) equal to 2.0. This geometry failed the validity check according to the ASTM standard, and the tests were repeated with w/b = 4. Valid fracture toughness values were calculated using this specimen geometry; therefore, w/b = 4 will be used for the remainder of the fracture toughness tests.

SENB fracture toughness tests loaded at a rate of 0.001 in./s have been completed on the 100-gsm and 150-gsm CCS material and on the HexMC material. The results for fracture toughness, K_{IC}, and strain energy release rate, G_{IC}, are summarized in Table 1. A typical crack-tip fracture surface is shown in Figure 22 using a scanning electron microscope at 40X magnification.

Table 1. Single-edge-notch bending quasi-static test results for fracture toughness.

Test result	K_{IC} (MPa – m^{½})			G_{IC} (kJ/m^2)		
	CCS 150	CCS 100	Hex MC	CCS 150	CCS 100	Hex MC
Mean	6.26	5.79	6.64	5.76	5.56	5.36
StDev	2.91	0.961	0.328	2.69	0.92	0.550
CV (%)	46.5	16.6	4.9	46.7	16.6	10.3

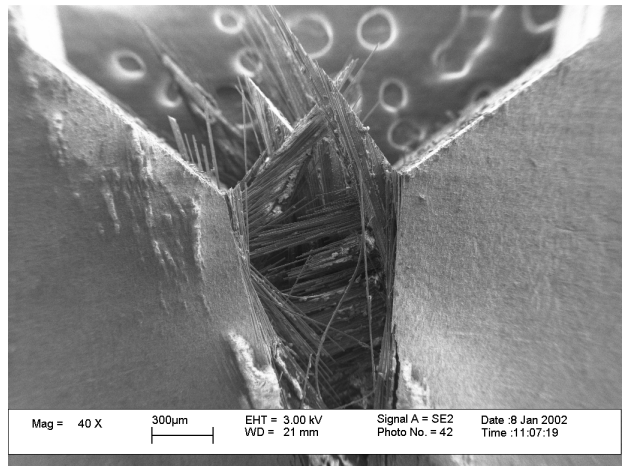

Figure 22. SEM photograph at 40X for failed single-edge-notch bending specimen.

Sufficient material has been ordered and received for both P4 and the 100-gsm CCS material to complete the planned tests. The test specimens have all been machined, and data acquisition software has been updated to trigger the collection of data during the dynamic tests. Current efforts are under way to develop in-situ real-time techniques for capturing the damage mechanisms that form during crack propagation in the SENB tests.

Future Work

The primary emphasis of future work will be upon validating and modifying the present models against experimental results, as well as preparing documentation on their theoretical formulations. The models will be used in validation simulations of the basic material tests, strip crush tests, and drop-tower tube crush tests of CF composite specimens. Using the same material properties, the models will then be used to predict drop-tower tube crush tests of $0^o/\pm45^o$, $0^o/\pm60^o$ braided and random CF composite architectures. New models for random CF composites will also be developed based on the analysis of P4 material obtained in this project period.

References

1. A. DeTeresa, Cunningham, Freeman, Saculla, Sanchez, and Winchester, *Experimental Results in Support of Simulating Progressive Crush in Carbon-Fiber Textile Composites*, UCRL-ID, 2001.

2. E. Zywicz, *A Tow-Level Progressive Damage Model for Simulating Carbon-Fiber Textile Composites: Interm Report*, UCRL-ID-139828, 2000.
3. E. Zywicz, "A Constitutive-Level Enhanced-Strain Element Formulation for Simulating Brittle Damage," presented at Multiscale Modeling of Materials: Strength and Failure Workshop, Bodega Bay, California, UCRL-145514, 2001.
4. Christensen, "Stress Based Yield/Failure Criteria for Fiber Composites," *Int. J. Solids Structures*, **34**(5), pp. 529–543 (1997).
5. *Processing Techniques and Recommendations to Optimize Composite Properties PANEX® 33 48 K*, http://www.zoltek.com/technical_resources/composite_design_manual.shtml, Zoltek, 2002.
6. *User's Guide for Short Fiber Composites*, http://www.zoltek.com/technical_resources/chopped_guide.shtml, Zoltek, 2000.
7. *HETRON® and AROPOL® Resin Selection Guide*, Ashland Chemicals, 2001.
8. H-K. Lee and S. Simunovic, "A Constitutive Model for the Effective Mechanical Properties of Damage-Tolerant Brittle Solids," submitted for publication.
9. H-K. Lee and S. Simunovic, "Modeling of Random Fiber Composites for Energy Absorption," Society for the Advancement of Material and Process Engineering Conference, 2002.
10. Automotive Composite Consortium test data for P4, 2002.

D. Intermediate-Rate Crush Response of Crash Energy Management Structures

Principal Investigator: Raymond G. Boeman
Oak Ridge National Laboratory
53-1/2 W. Huron St., Suite 213
Pontiac, MI 48342
(248) 452-0336; fax: (248) 452-8992; e-mail: boemanrg@ornl.gov

ISRM Facility Coordinator: J. Michael Starbuck
Oak Ridge National Laboratory
P.O. Box 2009, Oak Ridge, TN 37831-8048
(865) 576-3633; fax: (865) 574-8257; e-mail: starbuckjm@ornl.gov

ACC Coordinator: Ari Caliskan
Ford Motor Company
20000 Rotunda Dr., MD 2115 SRL, P.O. Box 2053
Dearborn, MI 48121-2053
(313) 248-8575; fax: (313) 702-2005; e-mail: acaliska@ford.com

Field Project Manager: C. David Warren
Oak Ridge National Laboratory
P.O. Box 2008, Oak Ridge, TN 37831-6065
(865) 574-9693; fax: (865) 576-4963; e-mail: warrencd@ornl.gov

Technology Development Manager: Joseph A. Carpenter
(202) 586-1022; fax: (202) 586-1600; e-mail: joseph.carpenter@ee.doe.gov
Field Technical Manager: Philip S. Sklad
(865) 574-5069; fax: (865) 576-4963; e-mail: skladps@ornl.gov

---

Contractor: Oak Ridge National Laboratory
Contract No.: DE-AC05-00OR22725

Objectives

- Develop a unique characterization facility for controlled progressive crush experiments, at intermediate rates, on automotive materials (polymer composites, high-strength steels, aluminum) and structures.
- Study the deformation and failure mechanisms of automotive materials subjected to crush forces as a function of impact velocity.
- Obtain specific energy absorption and strain data and correlate them with deformation and failure mechanisms to describe the unknown transitional effects from quasi-static to high-rate for polymer composites.
- Characterize the strain rate effects for metallic materials and components.

Approach

- Develop a unique high-force (270 kN), high-velocity (6 m/s) servo-hydraulic machine to conduct progressive crush experiments on structural components at intermediate rates.
- Use high-speed imaging to observe and document deformation and damage mechanisms during the crush event.

- Conduct strain measurements at discrete locations and explore full-field measurements of strains and curvatures.
- Coordinate polymer composites investigations with the Automotive Composites Consortium (ACC) Energy Management Group.
- Coordinate steel investigations with the Auto/Steel Partnership.

Accomplishments

- Completed design and fabrication of equipment.
- Completed acceptance tests, which indicate better-than-expected performance.
- Defined a new specification for the equipment to utilize the enhanced performance.
- Completed specification and procurement of high-speed data acquisition system and data management software.

Future Direction

- Install equipment at the National Transportation Research Center (NTRC) near Oak Ridge, Tennessee.
- Conduct final post-installation acceptance tests.
- Procure high-speed video.
- Explore techniques for full-field measurement of strains and curvatures.

Introduction

Progressive crush is an important mechanism by which the kinetic energy of a traveling automobile is dissipated in a collision to protect the safety of passengers. Unfortunately, the progressive crush response of some emerging lightweight materials is not well understood. Additionally, many of these materials are known to exhibit responses that are sensitive to strain rate.

The difference in load response is important for crashworthiness because accidents can occur at various velocities. As a result, it is important to understand the behavior of materials at various loading rates so that a given structure can be designed to absorb impact energy at both low and high speeds.

Typically, standard test machines are employed for experiments at quasi-static rates, whereas drop towers or impact sleds are the convention for dynamic rates. These two approaches bound a regime within which data for experiments at constant impact velocity are not currently available (see Figure 1). This regime is termed herein the "intermediate-rate" regime and is defined by impact velocities ranging from 1 to 5 m/s. Investigation of rate effects within this regime requires experimental equipment that can supply a large force with constant velocity within these rates. Using a drop tower or sled at intermediate rates, although technically possible, is problematic because of the

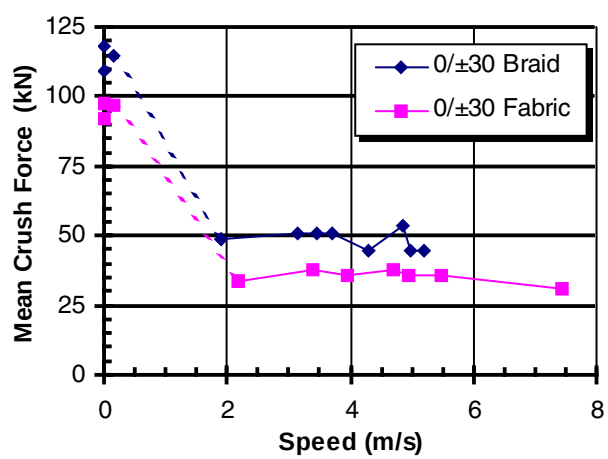

Figure 1. Mean crush force as a function of crush speed for (0/±30) fabric and braided tubes from a previous ACC study. Note that the response is essentially constant at quasi-static rates (near 0 m/s) and dynamic-rates (2–8 m/s) but changes in an unknown manner in between. *(Source: Ari Caliskan, ACC)*

prohibitively large mass required to maintain constant velocity during the crush.

Consequently, the Oak Ridge National Laboratory (ORNL) and the ACC are developing a unique experimental capability to conduct experiments on automotive materials within the intermediate rate regime. The unique capability will feature an integrated hardware and software solution for crush experiments. The new experimental facility will be used to understand the crush behavior between the static and dynamic (6 m/s) conditions.

Intermediate Strain Rate Machine

ORNL and the ACC have collaborated to define specifications for a unique experimental apparatus that mitigates the shortcomings of existing equipment. MTS Systems Corporation was selected to design and build the Intermediate Strain Rate Machine (ISRM) to meet the specifications (Figure 2).

Figure 2. Intermediate Strain Rate Machine custom-designed to ORNL and ACC specifications.

Requirements

The performance requirements for the machine were set as follows:

- *No-load operation:* Stroke ≥ 220 mm at velocities ≥6 m/s. Velocity constant to within ±10% for 115 mm.
- *133 kN mean crush force:* Stroke ≥ 240 mm at velocities ≥4 m/s. Velocity constant to within ±10% for 115 mm.
- *267 kN mean crush force:* Stroke ≥ 115 mm at velocities ≥4 m/s. Velocity constant to within ±10% for 115 mm.

The design was required to support axial crush experiments on long specimens by providing a minimum daylight of 900 mm that could be reduced with spacers and fixtures for shorter samples. No capability meeting these requirements is known to exist elsewhere in the world.

Hardware Features

The machine, as seen in Figure 2, is a closed-loop servo-hydraulic machine operating in open-loop mode for dynamic experiments.

The machine features a four-column, fixed-crosshead design, which provides exceptional stiffness. An actuator-mounted mass of 450 kg is provided to store additional energy to mitigate influences of peak forces and specimen variations. Dedicated data acquisition cards and the LabVIEW Virtual Instrument software will provide additional high-speed data acquisition.

Software Features

Software components of the system consist primarily of the following three interacting components (see Figure 3):

- *TestStar*: This software provides the real-time software interface to the electronics and hardware for machine control.
- *Advanced drive file generation (ADFG):* This component is required because the response time of the feedback signal is not sufficient for closed-loop operation. From input data on machine characteristics and anticipated specimen response, it generates a complex servo drive file to be used by TestStar to control the machine response. Prior to a physical experiment, it is used in conjunction with the

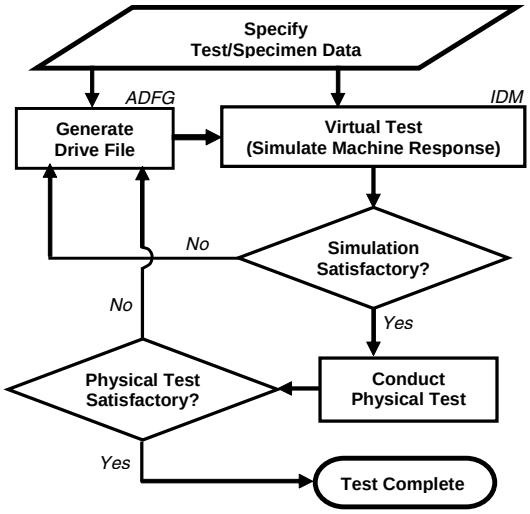

Figure 3. Experimental procedure and software interaction for the Intermediate Strain Rate Machine.

interactive dynamics model to iterate until convergence is obtained for the input parameters given.

- *Interactive dynamics model:* This component takes the drive file generated by ADFG and runs a simulation of the machine response. Prior to a physical experiment, it is used in conjunction with the ADFG to iterate until convergence is obtained for the input parameters given.

Status

In April 2002, acceptance tests were conducted at the facilities of the vendor, MTS Systems, to determine conformance to design specifications (see Figure 4). It was determined that some recent modifications to the actuator and manifold designs had significantly enhanced the hydraulic flow performance. This resulted in a considerable increase in the velocity potential of the machine. Increased force capacity at mid-range velocities is expected, as well as increased velocity at the no-load, 133-kN, and 267-kN force levels. The

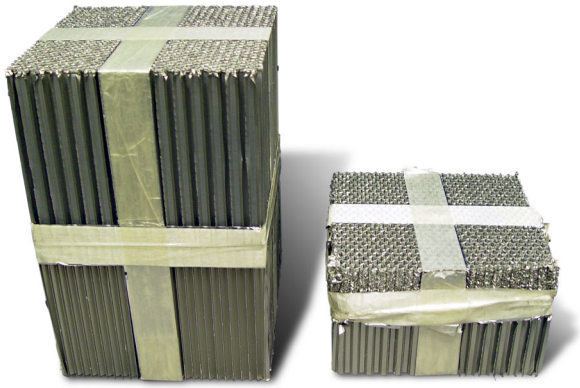

Figure 4. Aluminum honeycomb specimen before and after crush during acceptance test. Results demonstrate machine performance specifications (sustained crush force of 133 kN at a velocity of 6 m/s constant to within 10% over 115 mm of crush) were exceeded. Total crush distance was 230 mm.

increased performance, essentially a one-third increase in the operating velocity, was determined to have considerable value. Consequently, new performance specifications were established and design modifications were undertaken to ensure the safe operation of the equipment at the highest velocity levels.

On September 16, 2002, final pre-shipment acceptance tests were conducted at the vendor facility. The machine met or surpassed the new specifications, including these:

- No-load velocity of 8 m/s constant to within 10% over 115 mm.
- Sustained crush force of 133 kN at 6 m/s constant to within 10% over 115 mm.
- Sustained crush force of 267 kN at 4 m/s constant to within 10% over 115 mm.

The ISRM has been shipped to and installed in the NTRC and will be put into operation during the first quarter of FY 2003.

E. Composite Crash Energy Management

Principal Investigator: Richard Jeryan
Ford Research Laboratories
2101 Village Road
MD2115 SRL, Rm 2621D
Dearborn, MI 48124-2053
Tel: (313) 594-4903, Fax: (313) 845-4724, E-mail: rjeryan@ford.com

Field Project Manager: C. David Warren
Oak Ridge National Laboratory
P.O. Box 2009, Oak Ridge, TN 37831-8050
(865) 574-9693; fax: (865) 574-0740; e-mail: warrencd@ornl.gov

Technology Development Manager: Joseph Carpenter
(202) 586-1022; fax: (202) 586-1600; e-mail: Joseph.Carpenter@ee.doe.gov
Field Technical Manager: Philip S. Sklad
(865) 574-5069; fax: (865) 576-4963; e-mail: skladps@ornl.gov

---

Contractor: U.S. Automotive Materials Partnership (cooperative agreement)
Contract No.: DE- FC05-02OR22910

Objective

Crash impact performance is a requirement in virtually every potential application of automotive composites. It is the mission of the Energy Management Working Group of the Automotive Composites Consortium to develop and demonstrate the technology required to apply production feasible structural composites in crash and energy management applications. The data, know-how and methods developed by the Working Group have already been used by the ACC Partners on proprietary applications ranging from bumper beams to hoods to primary body structures. The future efforts of the Working Group will continue to apply to the broad range of materials, processes and applications required to meet the Partners' needs.

To accomplish its mission, the EMWG plans to:

- Experimentally determine the effects of material, design, environment and loading on macroscopic crash performance to guide design and the development of predictive tools.
- Determine the key mechanisms responsible for crash energy absorption and examine microstructural behavior during crash to direct the development of material models.
- Develop analytical methods for the prediction of energy absorption and crash behavior of components and structures.
- Conduct experiments to validate analytical tools and design practices.
- Develop and demonstrate crash design guidelines and practices.
- Develop and support design concepts for application in demonstration projects.

Approach

The EMWG uses an integrated portfolio of projects proposed to meet its objectives. A continuous process of technical review, revision and prioritization is conducted by the Group to manage the projects. The projects are conducted by the ACC partners, selected suppliers and universities and coordinated with National Laboratories. Each project has an ACC leader/monitor, objectives and milestones, a time line and budget estimate. Three technical

exchange and crash project coordination meetings were held at USCAR, Southfield, MI on January 16, May 22, and September 19, 2002.

The Working Group portfolio is composed of experimental projects, analysis development projects and design/application projects. The experimental projects are conducted to understand the global and macro influences of major variables on crash performance. These are used to create crash intuition, guidelines and rules-of-thumb and data for the validation of analysis developments. Microscopic experimental characterization is conducted to define the mechanisms that occur during and as a result of the crash process. This information is key to our understanding of the crash phenomenon and the definition of analytical mechanisms and material models used in the development of analyses.

FY 2002 Project Accomplishments

1. Carbon reinforced tube performance

Objective: Experimental determination of the effects of material, design, environment and loading on carbon fiber reinforced tubes to guide automotive design and analysis development. Conduct microscopic characterization of crush mechanisms for a range of material types and loading to identify the key mechanisms responsible for crash energy absorption and to direct the development of material models.

Accomplishments: To expand on the knowledge gained from the 25 mm square cross-section tubes which were tested in FY2001, alternate geometries of 25 x 50 mm and 50 mm square cross-section were dynamically tested at room temperature under axial and off-axis loading conditions. Dynamic axial tests were done at GM utilizing their drop tower and sled facilities. Off-axis crush tests were done on the sled at Ford. Specific energy absorption (SEA) and mean crush force were determined for each of the architectures and crush morphologies of the various architectures were compared. Shown in the figure is one of the thick tubes that was tested on the sled to obtain sufficient crush distance. This tube is 7.1 mm thick and is made of tri-axially braided Fortail and Grafil fibers oriented at 0/±30°. By testing this tube on the sled, providing greater impact energy than available from the drop tower, we were able to obtain a crush distance of 175 mm. Energy dissipation mechanisms include resin fracture and plastic deformation, fiber fracture and pullout, and inter-ply delamination.

2. Static vs dynamic performance

Objective: Experimentally determine the sensitivity of tube crush performance to impact velocity. Determine the mechanisms that control the

observed impact velocity effect to support the development of analytical models. Supported by an additional university research project and a planned intermediate-rate testing facility at ORNL.

Accomplishment: Construction of the intermediate strain rate machine has been completed. The intermediate rate machine will be delivered and installed at ORNL in Q1 FY2003. The work on examining the effects of strain rate on energy absorption has shown that for stitched unidirectional carbon samples, there is a reduction in the fracture toughness of the material during dynamic loading. Possible sources of this result can be attributed to poor wet-out of the fibers, voids within fiber bundles, or poor adhesion between the resin and fiber tows. Next phase of the work will examine fabric and braided architectures.

3. Effects of Pre-existing Damage on Crash Behavior

Objective: Provide an understanding of the effects of a range of material variability on the mode of failure and consequent energy absorption characteristics of generic and practical vehicle structure geometries. Specifically, the work will

focus on the effect on energy absorption associated with delamination, through thickness and local point loading on generic, circular and square, tube type components. At the conclusion of the project a generic guideline will be created that will help in designing more robust crash structures, which will be less sensitive to manufacturing and variability.

Accomplishments: Thus far the effects of damage circular and square tubes have been examined. Damage has been simulated by drilling holes of a certain size and location on the tube walls and corners. Delamination damage has also been simulated by placing an insert in between layers, and impact damage by dropping a tup on the walls of the tubes. Overall the results show that under dynamic crush the structures are less sensitive to damage than tubes crushed statically. In addition, square tubes are more sensitive to damage than circular tubes. The work will continue to examine tubes made of braid and fabric architectures and differing resin systems.

4. Friction Effects on Crash Performance

Objective: Experimentally determine the relative energy absorption due to each failure mode of a progressively crushed composite tube and isolate that portion of energy absorption due to friction. Evaluate differences in friction energy absorption between quasi-static and dynamic crush.

Accomplishments: Preliminary testing using (0/90/0/90/0) fiberglass reinforced vinyl ester resin composite 2-inch square tubes has been performed. Future testing will be performed using carbon composite. Normalization of 2001 test results show energy absorption due to corner splitting to be 92 J (98 J previously reported), delamination 323 J (377 J previously reported). The shallow angle trigger test results show average energy absorption of 1380 J (764 J previously reported), only 28.7% that of the normal trigger. Tubes crushed using the tapered trigger showed only corner splitting, friction, and elastic bending as the modes of energy absorption/storage. Use of the tapered trigger effectively removes delamination and matrix fracturing due to bending as energy absorption modes. Triggers coated with a diamond like carbon coating were fabricated and tested with mixed results. The coated standard trigger produced energy absorption that was 7.1% less than the uncoated trigger. There was no measurable difference in energy absorption between the coated and uncoated tapered triggers. Coefficient of friction for both static and dynamic cases were measured for coated, greased, and plain steel against composite.

5. Biaxial material studies

Objective: Experimentally determine strain fields around an advancing damage zone emanating from a notch in a braided carbon fiber composite under biaxial load. Determine the effects of load biaxiality and microstructure on damage accumulation. Assess the potential for developing continuum damage mechanics formulations based on biaxial test data for braided carbon composites.

Accomplishments: A detailed study of the 2D Triaxially Braided Carbon Composites (2DTBC) strips from the tubes revealed an understanding of the size effects. It also provided a simple benchmark for verifying detailed nonlinear analyses. Analysis of the detailed 3D model was carried out to comprehend the role played by material nonlinearity and natural geometric imperfections in the braided structure. Off axis tests to characterize homogenized inelastic stress-strain response of the composites were carried out. Biaxial tests on plaques with the same thickness as the tubes exposed a bending issue. Biaxial tests on thicker plates have been completed.

Continuum damage mechanics models have been developed for predictive capability. Some of the main important outcomes include: a) descending branch of 2DTBC stress-strain relation may not be a purely material property; b) proportional dependency of local compressive strains on the global bending strains; c) successful prediction of the dependency of post-peak softening on the local biaxiality using physical parameters; d) successful implementation of Digital Speckle Photography technique; and e) observed failure mechanisms depend on the amount of tension present in the damage zone. The project has been successfully completed.

6. Impact performance of bonded structures

Objective: Evaluate the performance of bonded structures under crash loads (see report 7F). Examine the influence of bond design concepts, impact velocity, environmental conditions and other material issues. Fabricate new molding tools to produce simulated automotive structures. This is a joint program with the ACC Joining Work Group and part of Focal Project 3 design studies.

Accomplishments: Visteon Corporation, a Tier I automotive supplier, is leading this effort jointly with Focal Project 3 and ACC Energy Management and Joining Work Groups. A comprehensive work plan has been established to develop experimental and analytical methodologies to analyze and design adhesively bonded automotive composite structures to sustain axial, off-axis and lateral crash/impact loads. The key tasks of the proposed work plan are:

- Selection of representative sub-component geometry, and substrate and adhesive material systems,
- Generation of coupon level material data for substrate and adhesive materials for static and dynamic loading at various strain rates,
- Fabrication and testing of the sub-component geometry under quasi-static and dynamic impact loads at various strain rates,
- Development of finite element based computational tools with adhesive material models and progressive damage/debonding algorithms,
- Development of standard tests and procedures to characterize Modes I, II and III, and Mixed mode dynamic fracture in adhesive bonded joints,
- Incorporation of the complete design methodology in commercial FEA code such as ABAQUS or LS-DYNA, and
- Validation of computational tools with test results.

The proposed work plan will address the issues related to the adhesively bonded joints including

- Joint strength under static, dynamic and crash/impact loads,
- Influence of joint design parameters like bond line thickness, overlap length, and fillet effects,
- Adhesive material behavior including nonlinearity and strain-rate effect.

Task 1: Select a representative sub-component geometry, substrate and adhesive material.

Hexcel's HexMC™ was selected as the substrate material for the project. HexMC is a random chopped prepreg with carbon fibers in epoxy matrix. It can be compression molded at about 1000 psi and 100 to 150°C and has a 4- to 15-minute cycle time. SIA 731SI, a two-part toughened epoxy, was chosen as the adhesive material. Standard surface preparation, such as sanding with Scotch Brite and subsequently using solvent wash, would be used to prepare both bonded joint specimens and sub-components.

Task 2: Generate coupon level material data for substrate, adhesive materials and single-lap joint configurations for static and dynamic loading.

ORNL has successfully developed tools and methods to cast flat panels and cylindrical rods of the selected adhesive system for characterizing the bulk properties. Two test configurations, single-lap and double-notch shear joints (see Figures 1 and 2), were chosen to investigate stiffness, strength, and fracture properties of the adhesive joint coupons. The detailed plans have been developed to test adhesive and substrate materials, joint specimens and sub-components under quasi-static and dynamic loads at various strain rates. The static and dynamic testing is expected to start in Q1 FY 2003 on the Intermediate Strain Rate Machine (ISRM) at ORNL.

Task 3: Build un-bonded and bonded sub-components, and test them subjected to quasi-static and dynamic loads.

Square section tubes with 2–3 mm wall thickness were chosen as the sub-component geometry. Both un-bonded and bonded square tubes (see Figure 3) will be fabricated using HexMC™. Tubes will be offset cut and bonded with overlaps. Two molded tubes will be necessary to make one bonded tube. Un-bonded and bonded tubes will be tested and compared for energy absorption. HexMC™ is also being used for the ORNL Adhesives Hat Section project. This will give the team experience in molding with HexMC™ before attempting to mold the more difficult tubes for this project. Modifications to add shear edges to the hat section tools were completed.

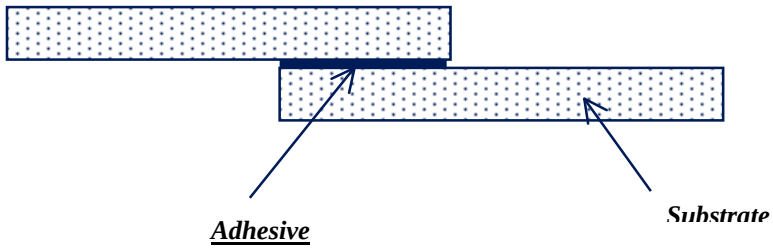

Figure 1. Single-lap bonded joint.

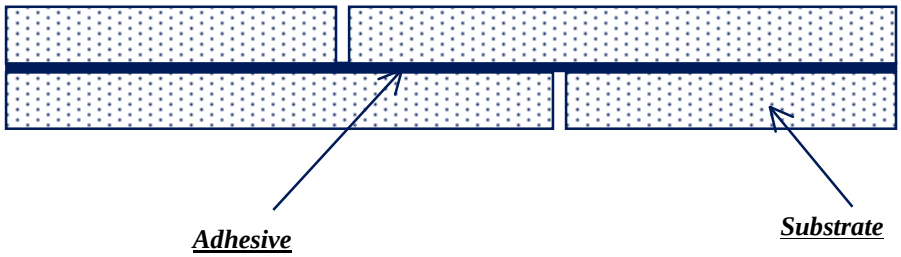

Figure 2. Double-notch shear bonded joint.

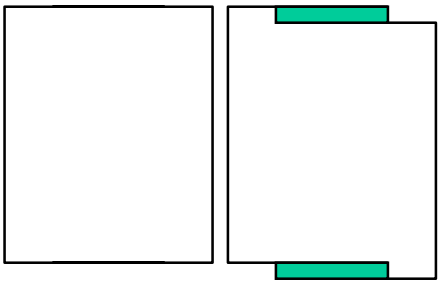

Figure 3. Unbonded and bonded tubes.

Task 4: Develop analytical tools incorporating adhesive elements, material models and progressive damage algorithms, and correlate them with coupon and sub-component test results.

Analytical modeling work was initiated at Visteon using commercial FEA tools such as ABAQUS and LS-DYNA. A typical single-lap bonded joint was analyzed using I-DEAS and ABAQUS. The contours of axial (*x*-component) and transverse (*z*-component) displacements in the joint region obtained from the analyses were compared with the results published in the open literature using test data from Moiré interferometery. The work on fracture mechanics based modeling of adhesive joints in single-lap shear configuration was also initiated to evaluate the progressive damage mechanisms. Furthermore, requests for proposals to various universities were sent out to aid the development of novel finite elements and progressive damage algorithms to perform crash analyses of adhesively bonded automotive structures. The proposals received were evaluated thoroughly. The proposal from Virginia Tech has been selected to perform the advanced experimental and analytical development work in FY2003-2005.

7. Viability and crashworthiness of novel sandwich composite concepts

Objective: To investigate the viability and crashworthiness of novel sandwich composite concepts for automotive applications

Accomplishments: A review of the literature on the subject was conducted. Topics such as wrinkling, face-sheet de-bonding, Poisson's effects and core-skin property mismatch, load rate effects, and impact damage modes and energy absorption, to mention a few, were highlighted as requiring further research and characterization. A sub-team was formed with participation from DaimlerChrysler, Ford, GM and ORNL. Based on the needs of the various other working groups within the ACC, vehicle roof and floor panels were identified as the primary locations for use of sandwich composites. Various materials, adhesives and test methods (representative of the loading methods) to evaluate those materials were identified. Further investigation on the materials, test methods and issues outlined above and development of models with predictive

capabilities was initiated. In this regard, proposals were solicited from three researchers from the University of Maryland, University of Michigan and University of Utah to continue further collaboration with the ACC. Discussions amongst the Energy Management resulted in selection of the proposal submitted by the University of Utah. The proposed work is split into three phase-specific objectives:

Phase I: To evaluate candidate materials, concepts, and manufacturing methods for automotive sandwich composites. This two-round experimental evaluation of energy absorption, damage mechanisms, and mechanical properties will be used to identify the best-suited sandwich composite concepts for further investigation in the second phase.

Phase II: To develop an understanding of the structural response of selected sandwich composite concepts identified in Phase I. This investigation will focus on damage modes and energy absorption mechanisms during impact loading as well as static loading.

Phase III: To develop and validate finite element based methodologies for predicting damage formation and energy absorption in candidate sandwich composite concepts identified in the first two phases of the program.

Some of the material systems that will be studied include:

- Polypropylene, Aluminum, Polymer, Balsa wood (Core)
- Carbon/epoxy, Aluminum (Skin)
- EAF-220, UAF-420, FM-300, SIA 731 SI (adhesive)

8. Energy Absorption of Triaxial Braided Composite Tubes

Objective: Carbon fiber braided composites exhibit complex energy absorbing mechanisms, which need to be understood precisely for adequate simulation of crashworthiness of tubular structures made from them. In an earlier two-year project, a smeared micromechanics model was developed for simulating the crush of braided carbon fiber tubes. The analysis was based on certain assumptions regarding the role of tow-scissoring, material degradation and the size of the unit cell with smeared properties relative to the size of the finite elements. Moreover, the earlier project dealt with only quasi-static loading.

In the current three-year project, the energy absorbing mechanisms introduced in the previous project are being thoroughly investigated to study their precise role in the micromechanics model and ensure an objective formulation. The material scale relative to the size of the finite elements is being studied for enhanced robustness of the analysis. Dynamic tests on tubes, and simulation of those tests using the revisited and enhanced smeared micromechanics models is planned as a final step.

Accomplishments: The smeared micromechanics unit cell model code has been rewritten to improve its computational efficiency. The smeared micromechanics model can currently be run in a fraction of the time that was necessary in the previous project. A thorough validation of the computer code is being carried out to verify that the results are the same as those obtained with the less computationally efficient version.

The effect of stress-concentration on damage evolution has been studied using X-rays and die penetration in tension specimens with holes and in square tubes. This will serve as a good basis to understand the role played by stress-concentration on damage evolution, and to some extent the effect of material scale on damage evolution. Based on this study, the effect of stress concentration will be built explicitly into the smeared micromechanics model for better prediction of damage evolution.

The earlier two-year project introduced the effect of tow scissoring to account for load pick up based on tow jamming. This heuristic model is being studied closely in order to provide it with a sound foundation. For this, circular tubes with low resin content are being studied. The results of the study on braided circular tubes with low resin volume will allow an objective development of a mathematical model for representing scissoring.

9. Lateral Impact Study

Objective: Absorption of energy based on axial crushing of tubes has been studied extensively by ACC. Energy absorbing mechanisms that play a dominant role in bending of composites have not been studied extensively. In order to understand the energy absorbing failure mechanisms in braided

carbon fiber composites subjected to lateral loads, a combined approach based on analytical simulation and experiment has been proposed.

The approach is based on a preliminary analysis with the smeared micromechanics model developed by Stanford. The analysis based on smeared micromechanics is expected to lead to the development of a realistic specimen, which will be used to represent a typical automotive component subjected to lateral loads. The crashworthiness of axially loaded thin-walled components, which absorb energy primarily by local bending, is also expected to be studied.

Accomplishments: The smeared micromechanics unit cell model developed by Stanford has been used to analyze quasi-static tube crush problems to become familiar with the use of the subroutine and its limitations. The smeared micromechanics unit cell model code has then been used to analyze the combined loading of braided carbon fiber flat strips with hinged end conditions. The strips have been subjected to axial loading applied eccentrically, resulting in combined axial and bending loading of the strip. These tests have been carried out by University of Michigan as a part of the biaxial loading project.

The braided carbon fiber composite strip has been modeled using solid elements. In order to capture inter-laminar failure, each layer has been modeled as a layer of solid finite elements. Preliminary runs with the smeared micromechanics model have been carried out. Interpretation of the experimental results by observing the experimental results is being carried out.

F. Energy Absorption in Adhesively-Bonded Composites

Co-Principal Investigator: J. Michael Starbuck
Oak Ridge National Laboratory
P.O. Box 2009, Oak Ridge, TN 37831-8048
(865) 576-3633; fax: (865)-574-8257; e-mail: starbuckjm@ornl.gov

Co-Principal Investigator: Raymond G. Boeman
Oak Ridge National Laboratory
53-1/2 W. Huron St., Suite 213
Pontiac, MI 48342
(248) 452-0336; fax: (248) 452-8992; e-mail: boemanrg@ornl.gov

ACC Collaboration Contact: Naveen Rastogi
Visteon Corporation
6100 Mercury Drive, SW61-025, Dearborn, MI 48126
(313) 755-6264; fax: (313) 755-4229; e-mail: nrastogi@visteon.com

Field Project Manager: C. David Warren
Oak Ridge National Laboratory
P.O. Box 2008, Oak Ridge, TN 37831-6065
(865) 574-9693; fax: (865) 576-4963; e-mail: warrencd@ornl.gov

Technology Development Manager: Joseph A. Carpenter
(202) 586-1022; fax: (202) 586-1600; e-mail: joseph.carpenter@ee.doe.gov
Field Technical Manager: Philip S. Sklad
(865) 574-5069; fax: (865) 576-4963; e-mail: skladps@ornl.gov

---

Contractor: Oak Ridge National Laboratory
Contract No.: DE-AC05-00OR22725

Objectives

- Develop a comprehensive experimental and analytical methodology to analyze and design adhesively bonded automotive composite structures to sustain axial, off-axis, and lateral crash/impact loads.
- Determine the rate sensitivity of bonded tubes to crush through experiments on the Oak Ridge National Laboratory (ORNL) intermediate strain rate machine (ISRM) (see report 7D).
- Determine the influence of critical joint design parameters—e.g., bond length, bond thickness, and fillet—on specific energy absorption.
- Experimentally determine the full-field deformations at joint discontinuities for validation of analytical/numerical results.

Approach

- Coordinate with the bonded joint experimental and analytical efforts undertaken in the Automotive Composites Consortium (ACC) project Composite Crash Energy Management (see report 7E).
- Select a substrate, adhesive, and representative subcomponent joint geometry for evaluation.
- Characterize substrate material, adhesive material, and coupon-level joints under static and dynamic loads.

- Build and test unbonded and bonded rail components under static and dynamic crush loads.
- Correlate experimental results with analytical results by developing finite-element–based tools with appropriate material models and progressive damage algorithms.
- Enhance the understanding of joint performance by conducting full-field deformation measurements using Moiré interferometry.

Accomplishments

- Completed materials selection and screening for the sub-component geometry, substrate, and adhesive material systems.
- Prepared a detailed test plan for characterizing the substrate material, adhesive material, coupon-level joints, and sub-component joints.
- Developed a manufacturing process for fabricating the bulk adhesive panels and cylindrical rods that are needed for machining test coupons.

Future Direction

- Design and fabricate required test fixtures for conducting dynamic tests on ISRM.
- Complete static and dynamic testing of substrate, bulk adhesive, and coupon-level joints.
- Install and set up Moiré interferometric test equipment for characterizing full-field deformation patterns in adhesive joints.

Introduction

The objective of this project is to develop a comprehensive experimental and analytical methodology for analyzing and designing adhesively bonded automotive composite structures to sustain axial, off-axis, and lateral crash loads. This directly-funded project will be closely aligned with the experimental and analytical efforts undertaken in the ACC for composite substrates (see report 7E). The focus of this work, however, will be restricted to issues related to the adhesive joints. The key to methodology development is understanding how critical joint design parameters, e.g., bond length, bond thickness, and fillet, affect energy absorption. Recent investigations at ORNL have provided valuable insight toward the understanding of composite joint performance and composite crashworthiness. The next logical step is determining the correlation between measurable adhesive joint parameters and their influence on the structure to aid in developing designs that dissipate energy and ultimately predict crashworthiness for a particular composite design.

Experimental tasks include materials testing under quasi-static and dynamic loads for substrates, adhesives, and joints; full-field deformation mapping of joints with Moiré interferometry for correlation with computational results; strain-rate sensitivity studies; fracture toughness testing; and test method development as required. These experimental results will provide the building blocks for model development—first at the coupon level, then progressing in complexity to the component level. Correlation with experimental results will provide the basis for analytical development, including constitutive laws, materials models, damage algorithms, and new finite elements. Structural tests will be conducted on the new ISRM at ORNL.

Project Deliverables

At the end of this multi-year program, joint parameters that have significant influence on energy dissipation will be identified, and their influence quantified, using appropriate analytical models and experimentation. In collaboration with the ACC's Composite Crash Energy Management project, a predictive capability for joint performance will be demonstrated and the validity of the prediction assessed through structural crash testing.

Planned Approach

The technical approach involves both experimental and analytical tasks. There are four major tasks: 1—Materials Selection and Screening, 2—Material Characterization, 3—Component Testing, and 4—Computational Tools Development.

The duration of Task 1 was 6 months; it was completed during FY 2002. The materials selection and screening process was a collaboration between ACC, Visteon, and ORNL and included the sub-component geometry, substrate, and adhesive material systems. The selected substrate is a chopped-carbon-fiber–reinforced epoxy system provided by Hexcel Corporation. The product, designated as HexMC, is basically a chopped prepreg system and is processed using conventional compression molding techniques. The selected adhesive system is a two-part toughened epoxy produced by SIA Adhesive with the designation PL731 A/B. Joints are commonly made with this system using a static mixing gun; this is the same system being used in the project on performance evaluation and durability prediction of dissimilar material hybrid joints (report 7I). The selected sub-component geometry was a 100 × 100 mm square tube with a 2-mm to 3-mm wall thickness.

Task 2 was initiated during FY 2002 and is scheduled to be completed during the third quarter of FY 2003. At the conclusion of Task 2, coupon-level data will have been generated for the substrate, the adhesive, and several different coupon-level joint configurations under both static and dynamic load conditions. A test plan has been drafted that lists the tests, their measured parameters, any applicable test standard, number of replicates, specimen geometry, and load rates.

The HexMC substrate will be characterized by conducting tension, compression, and in-plane shear tests. The degree of anisotropy in the material will be qualified by testing specimens that are machined from two different orthogonal directions in the panels. This work will be contracted out to an independent testing laboratory.

The bulk adhesive testing will consist of tension, compression, shear, and fracture toughness. In addition, differential scanning calorimetry tests will be conducted to verify the degree of cure. The key to this task is success in fabricating high-quality specimens (e.g., with a low void content) to accurately quantify the bulk adhesive mechanical properties. The compression and shear testing will be accomplished using a cylindrical rod specimen geometry. Previous efforts at ORNL have demonstrated that these types of specimens can be fabricated using centrifugation and using glass test tubes as molds. Trial fabrications using this technique with the SIA PL731 system have proved to be successful.

However, initial attempts to fabricate the flat panels needed for machining tensile specimens were unsuccessful; large pockets of air were trapped within the panels. The basic approach used was to pull a vacuum on a mold while filling the mold with adhesive. The viscosity of the adhesive is such that it must be heated to have any flow characteristics whatsoever. Once the mold was filled, the vacuum was removed, and the mold was placed in the oven to cure. During cure, a large degree of shrinkage took place, and air was sucked back into the mold cavity.

The solution to this problem was to provide an adequate supply of excess adhesive under pressure to back-fill the mold cavity. The mold filling process is depicted in Figure 1. Additional quality improvements in the panels were achieved by repackaging the bulk adhesive in the static mixer after degassing the system via centrifugation. The fracture toughness specimens will require using the same technique but filling a much thicker mold cavity.

Figure 1. Fabrication of bulk adhesive panel.

Coupon-level joint configurations will consist of double-notch shear and single-lap shear (SLS) test specimen geometries. Joint parameters that will be

investigated are adhesive thickness, overlap length, and fillet geometry. Moire interferometry will be used to study the full-field deformation pattern in the bond-line during static testing of the SLS joint specimens. The crack growth characteristics of an adhesive joint will be quantified by conducting mode 1, mode 2, and mixed-mode fracture tests using double cantilever beam, end-notch flexure, and mixed-mode bending specimen geometries, respectively.

Component testing in Task 3 will commence in the last half of FY 2003 and will consist of unbonded and adhesively bonded upper rail sections (see Figure 2). The testing will include static and dynamic crush loads and axial and lateral impact loads. The ISRM at ORNL and test sleds will be used for the dynamic testing. The unbonded tests are to establish a baseline; then the results from Task 2 will guide the joint design so that bonded sections will be built to either fail or not fail in the joint. Some of these tests will be repeated using scaled geometries to get an initial look at scale effects.

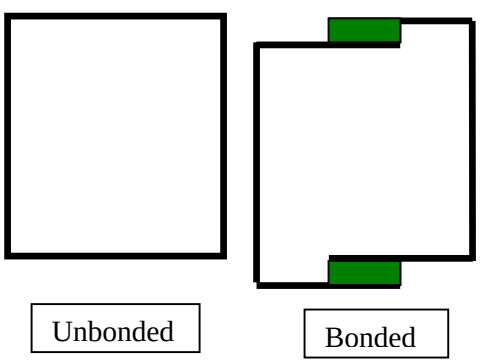

Figure 2. Sub-component upper rail test geometry.

In Task 4, the computational tools development will consist of analyzing the test geometries at both the coupon level and component level, developing new material models, and developing new test methods to support the model development. This task will be conducted in parallel with Tasks 2 and 3. The coupon and component level analyses will be completed using existing material models that are available in finite element analysis tools such as ABAQUS and LS-DYNA. The bond-line deformations predicted by the analyses will be compared with the Moire experimental results. Also, the effects of bond-line thickness and length, fillet, and loading rate on the stress distribution in the joint will be correlated with the experimental results. The model development effort will consider new constitutive laws, progressive damage algorithms, new finite elements for modeling the adhesive layer, and new computationally efficient techniques. In support of this effort, new test methods will be developed for characterizing strain-rate effects and dynamic fracture. Proposals from universities will be considered for the model and test development effort.

Summary

These are highlights of the progress during FY 2002.

1. Completed substrate and adhesive material selections and selected the sub-component test geometry.
2. Developed the required test plan for characterizing the static and dynamic behavior of the substrate, adhesive, coupon-level joints, and sub-components.
3. Developed a manufacturing process for fabricating high-quality, consistent bulk adhesive panels.
4. Completed preliminary analyses of the effect of overlap on the local bond-line stress state for souble-notch shear specimens.

G. Long-Life Electrodes for Resistance Spot Welding of Aluminum Sheet Alloys and Coated High-Strength Steel Sheet

Project Manager: Eric Pakalnins
DaimlerChrysler Corporation
Body Materials Engineering
800 Chrysler Dr.
CIMS 482-00-11
Auburn Hills, MI 48326-2757
(248) 576-7454; fax: (248) 576-7490; e-mail: ep18@daimlerchrysler.com

Project Administrator: Warren Peterson
Edison Welding Institute
1250 Arthur E. Adams Drive
Columbus, OH 43221-3585
(614) 688-5261; fax: (614) 688-5001; e-mail: warren_peterson@ewi.org

Technology Development Manager: Joseph Carpenter
(202) 586-1022; fax: (202) 586-1600; e-mail: Joseph.Carpenter@ee.doe.gov
Field Technical Manager: Philip S. Sklad
(865) 574-5069 ; fax: (865) 576-4963; e-mail: skladps@ornl.gov

---

Contractor: U.S. Automotive Materials Partnership
Contract No.: DE-FC05-02OR22910

Objectives

- Survey the currently available technology for achieving long electrode life.
- Comparatively test a broad selection of existing and developmental electrode technologies that have technical merit.
- Confirm the test results through electrode metallography and computer modeling.
- Evaluate the best practices through beta-site testing of automobile applications.

Approach

- Conduct benchmarking (Phase 1) to produce a state-of-the-art report on electrode wear. The open literature and available corporate literature will be reviewed and industry experts interviewed.
- Screen candidate electrode technologies, conduct in-depth wear testing of selected electrodes, and beta-test selected electrode technologies in an automotive production environment (Phase 2).
- Conduct computer modeling of the electrode metallurgical and mechanical changes that occur as a result of electrode wear (Phase 3). The models will be used to define the mechanism(s) of electrode wear during resistance spot welding of aluminum and high-strength coated steels.

Accomplishments

- Completed a benchmarking study (Phase I).
- Initiated initial electrode screening tests for 1.0-mm 70/70 350-MPa high-strength hot dip galvanized (HDG) steel and 1.0-mm aluminum (Al 5754).

Introduction

Automotive companies have been increasing the use of high-strength steel and aluminum to reduce the curb weight of automobiles for improved fuel efficiency. Resistance spot welding has been the primary method for joining automotive assemblies in mass production. It is estimated that at least 70 billion spot welds are made on vehicles produced in North America annually. While the resistance welding process is cost-efficient, substantial cost reductions can be obtained by improving electrode life. However, electrode wear during welding of coated high-strength steels and aluminum has been a continuing and significant problem.

The effects of electrode wear on raw electrode costs, improved productivity, and enhanced product quality can be significant. To substantially reduce the costs associated with electrode wear, electrode life must at least double the existing electrode replacement period for most applications. The cost savings for tip replacement alone associated with doubling electrode life is estimated at an annual $20 million.

Electrode wear not only adversely affects the cost and productivity of automotive assembly welding but also reduces weld quality reliability and robustness. This necessitates additional inspection and mandates more strict control of the welding parameters. Ultimately, worn electrodes can result in deteriorated weld performance.

The purpose of this study is to identify and evaluate existing or developmental electrode compositions and designs that will double the life of electrodes used with HDG high-strength steels and significantly improve the electrode life of welds made on aluminum (Al) in the automotive industry.

Presently, electrode re-dressing and current stepping procedures are commonly used to extend electrode life in production. To achieve significant improvements in electrode life, new electrode materials and geometries will probably be required. The U.S. Council for Automotive Research has begun a program aimed at extending electrode life on galvanized high-strength steels and aluminum alloy sheet.

Benchmarking Study (Phase I)

As a first step, a benchmarking report was completed. This report reviewed the open literature and the results from interviews with automotive welding experts and evaluated the costs associated with tip replacement.

Electrode Wear in Galvanized Steel

Electrode wear in HDG steels is usually characterized by a sudden reduction in weld button size. Weld nugget initiation and growth are sensitive to changes in the electrode face diameter. Electrode wear results in reduced current density as a consequence of gross extrusion of electrode material from the electrode face. This occurs from thermal degradation of the electrode material after repeated welding operations. The operating current level, weld time, hold time, electrode cooling, electrode material properties, electrode geometry, and other factors affect the degradation of strength of the electrode material.

The electrode wear mechanism was described for HDG steel. During the initial welds in a new electrode, the electrode face achieves a chemical and metallurgical equilibrium with the galvanized coating. Brass alloys are formed from the diffusion of zinc, iron, and aluminum into the electrode material at face temperatures near the melting point of the brass alloys. Geometric changes on the electrode face (e.g., pitting, cracking) are produced from a nonuniform distribution of current and localized heating of the electrode face. Conversely, the literature contains some references to a beneficial form of alloying on the electrode face, called a “protrusion” in the benchmarking report, that extends electrode life by serving up to four functions:

- Acts as a zinc diffusion barrier
- Forms a renewable parting layer for brassing
- Increases current density by narrowing the effective electrode face diameter
- Thermally isolates the electrode from the steel substrate.

The development of these protrusions has been correlated with long electrode life because they maintain current density and enhance nugget initiation in spite of gross extrusion of the electrode material from the face. When the protrusion is eliminated, the current density defaults to the current density produced by gross extrusion of the electrode material. This results in the sudden loss of nugget size characteristic of galvanized steel at the end of electrode life.

Electrode Wear with Aluminum

The life of electrodes used to weld aluminum alloys differs substantially from the phenomenon observed on galvanized steel. Surface preparation is critical to welding aluminum. Nugget initiation occurs within the first half-cycle of welding. The inherent material and surface properties influence weld nugget development and growth, porosity formation, weldability issues, and wear patterns uniquely associated with aluminum alloys.

An electrode wear mechanism for aluminum is reported. Electrode wear is characterized by pitting erosion that results from the deposition of copper onto the aluminum sheet with nearly every weld. Pitting increases the heat developed at the electrode-sheet interface. On repeated welding, this influences the weld nugget morphology and porosity distribution within the weld and contributes to

- Sudden increases in the frequency of interfacial fracture
- Increases in excessive expulsion or sticking
- Loss of conduction
- Reduction in weld button size

Porosity is a very common attribute of welds on aluminum. While porosity at the nugget center is innocuous, porosity located at the nugget edge promotes random interfacial failures. Increased face diameter reduces the pressure retaining the molten weld nugget, promoting expulsion. Expulsion increases the severity of porosity and increases the likelihood of edge porosity responsible for button failure.

Although test results vary, both radiused and flat electrode faces have been recommended for welding aluminum. Soft electrode materials that reduce the electrode-sheet interface resistance are recommended. Cold work of the electrode face was beneficial to reducing the rate of pitting.

Benchmarking Survey

Industry experts were interviewed to define the problem of electrode wear in production, the factors contributing to electrode wear, the effectiveness of common remedial measures, and future work. The wear mechanisms for galvanized steel and aluminum were consistent with the collective findings from these interviews. Acceptable electrode life was defined as a robust and repeatable welded application in which the tips produce welds that meet corporate specifications and that do not need maintenance for a preset number of welds or between maintenance periods. Tip changes are required when the electrodes produce sub-minimum-size welds, require attention, or result in erratic weld behavior. The frequency of tip replacement for galvanized steel depends on the type of galvanized product, gun application, and severity of electrode wear relative to production scheduling. These numbers typically range from 2500 to 9000 welds after stepping and dressing options have been exhausted. The number of welds before tip replacement in welding of aluminum is much more limited (i.e., less than 3000 welds), and frequent electrode dressing is required.

Collectively, the factors described in these interviews are consistent with the mechanisms of electrode wear presented from the open literature review. Additionally, production factors, such as gun maintenance, were correlated with electrode wear. Generally, the effect of production factors on electrode wear appears to be significant, but several of these have not been well documented in the open literature.

Recommendations from Benchmarking Study (Phase I)

The recommendations for improved electrode life in welding galvanized steel include these:

- Improved high-temperature material properties (e.g., conductivity, strength, ductility)
- Reduced brass alloy formation
- Promotion of protrusion development
- Reduced electrode sticking
- Reduced heat input while maintaining weld button size
- Maximized electrode cooling

The recommendations for improved electrode life in welding aluminum include these:

- Reduced electrode-sheet interface resistance
- Reduced alloying and sticking between copper and aluminum
- Increased melting temperature of the CuAl alloy formed on the electrode face
- Improved electrode conductivity
- Maximized electrode cooling

Electrodes exhibiting these attributes were considered in the selection of electrodes for the initial electrode life testing phase of the program.

Screening of Candidate Electrodes (Phase II)

The committee identified several electrode materials and designs with guidance from the benchmarking study. These electrodes were different for HDG steel and aluminum; they are listed along with the electrode life test procedures used:

1.1-mm 70/70 HDG 350-MPa steel

(Male, E-cap, 5/8-in.-diam body, 6-mm face electrodes)

- CuZr
- Al_2O_3 oxygen-dispersion–strengthened (ODS) copper
- Al_2O_3 in P-cap design
- TiC-coated CuCrZr
- Composite CuZr core with ODS body
- W-faced copper body
- Internally finned copper
- Developmental electrode compositions

These will be tested using both a single-level weld current test (AWS D8.9-97) and a stepper test procedure (GM WS-5A-part 3) common for use on HDG steel.

1.0-mm Al 5754 uncoated aluminum

(Male, E-cap, 5/8-in.-diam body, 6-mm face electrodes)

- CuZr
- C107 oxygen free copper
- Heavily cold-worked CuZr
- TiC coated copper
- Internally finned copper

These electrodes will be evaluated using a single-level electrode life test specification (Ford BA113-07) typical of testing aluminum.

The goal is to identify the best technology in the form of either alloy selection, geometry, and/or coatings that will likely produce the best results. The electrode wear phenomena and metallurgical changes of selected electrodes will be evaluated in greater depth as part of the next phase of the program. The wear will also be numerically modeled in an effort to further interpret the electrode life data.

Single-Current Electrode Life Test Results

Most of the HDG steel electrodes have been tested to date. Those that have not been tested are still being produced. Figure 1 shows the standard electrode life data, in the form of button size vs number of weld curves, for six electrodes tested using AWS D8.9-97. The performance of the P-cap

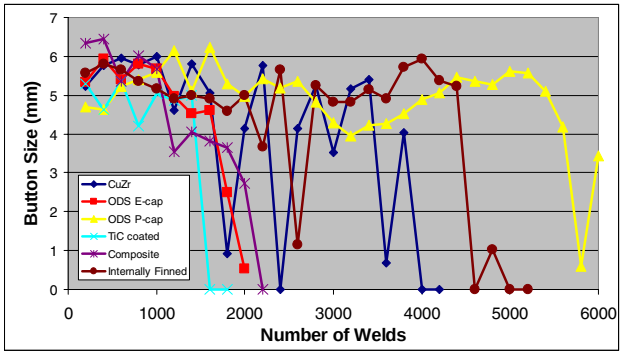

Figure 1. Summary of single-current electrode life (AWS D8.9-97) data for several electrodes on 1.1-mm 70/70 HDG 350-MPa high-strength steel.

and finned electrodes clearly demonstrates that electrode geometry plays an important role in electrode life. Material composition is also known to be very important, but the improved performance of these electrodes is probably due to geometry.

The P-cap electrode is composed of ODS copper. It was selected because of the anti-sticking properties of this material. Compared with the standard E-cap design for the same material, the P-cap design provides a columnar body of electrode material, which extrudes radially as wear progresses. Electrode life appears to be related to the length of the columnar protruded face.

The finned electrode is composed of copper that is high in conductivity compared with the other electrode material compositions. The cooling of the electrode face is maximized by the eight internal fins, reduced face thickness (distance from the face to the water cooling channel), and greater mass of the electrode body. The face thickness is half of the thickness of the standard male E-cap designs used for most of the electrodes. The success of this electrode design is currently attributed to an ability to better maintain a cool electrode-sheet interface. This limits the degradation of the underlying copper material and resists copper extrusion from the face.

The other electrode compositions were all E-cap designs. There was no significant difference in these results, based on Figure 1. However, other wear attributes may require inclusion of these electrodes in the next phase of the program.

Stepper Test Results

A comparison of the stepper test data is shown in Figure 2. The stepper data indicate the rate of weld current increase required as a function of electrode wear. More current is needed as the electrode faces increase in order to maintain at least a minimum-size weld button. These data indicate

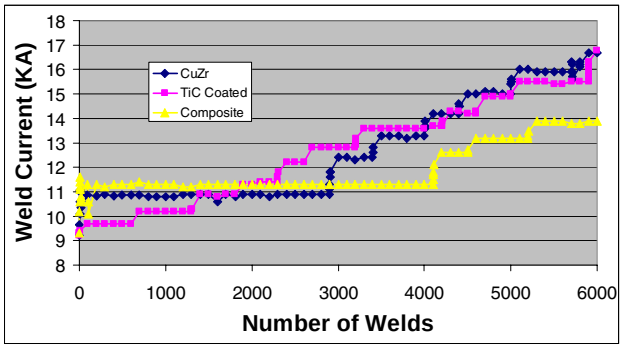

Figure 2. Summary of stepper current electrode life (GM WS-5A Part 3) data for several electrodes on 1.1-mm 70/70 HDG 350-MPa high-strength steel.

that the TiC-coated electrodes had a very predictable slope. Other electrodes had similar rates of current increase associated with enlargement of the face diameter. However, these electrodes did not begin current stepping until a large number of welds had been produced on the electrodes.

Computer Modeling

Oak Ridge National Laboratory (ORNL) is in the process of producing a computer model for HDG steel. Modeling of the aluminum will be started later. Simplifications were required to allow for economical evaluation of several electrode materials. Complete finite element analysis computer modeling of the whole electrode and of the changes that occur at the electrode face would be prohibitive over thousands of welds. Instead, ORNL's numerical model is focused directly on the face area in contact with the steel. Currently, the model is composed of only one layer. Additional layers will likely be added to show the effect of extrusion. Data from the initial screening and the next phase of the program will be used to tune the model.

H. Plasma Arc Welding of Lightweight Materials

Project Manager: William Marttila
DaimlerChrysler Corporation
Materials Engineering
800 Chrysler Dr.
CIMS 482-00-11
Auburn Hills, MI 48326
(248) 576-7446; fax: (248) 576-7490; e-mail: wam8@daimlerchrysler.com

Project Administrator: Frank G. LaManna
LaManna Enterprises
160 East Main Street
Northville, MI 48167
(248) 348-1761; fax: (248) 449-4095; e-mail: fglamanna@comcast.net

Technology Development Manager: Joseph Carpenter
(202) 586-1022; fax: (202) 586-1600; e-mail: joseph.carpenter@ee.doe.gov
Field Technical Manager: Philip S. Sklad
(865) 574-5069; fax: (865) 576-4963; e-mail: skladps@ornl.gov

---

Contractor: U.S. Automotive Materials Partnership
Contract No.: DE-FC05-02OR22910

Objective

- Develop and verify the welding technology required for the joining of lightweight materials (aluminum and magnesium) using plasma arc spot welding technology.
- Develop the necessary weld parameters and techniques required for a robust joining process.
- Develop guidelines for testing mechanical properties of the new technology that are appropriate for the various anticipated applications.

Approach

This project is divided into three phases: testing, analysis, and summary.

- Produce approximately 5000 material coupons to be used for tensile, shear, and metallurgical analysis and testing (Phase 1).
- Modify the material alloys based on Phase 1 results (Phase 2).
- Produce guidelines for welding parameters and quality control (Phase 3).

Accomplishments

- Finalized the test matrix (material selections and combinations).
- Formed the project team and conducted official meetings.
- Secured agreement from ALCAN and ALCOA to supply required material for the program.
- Obtained material from ALCAN and ALCOA to produce coupons for testing.

- Secured robots from ABB Robots [accomplished by General Motors (GM)].
- Designed and fabricated a fixture to ensure uniform coupon production.
- Installed all welding equipment and robot and made them operational.
- Produced and analyzed initial samples.
- Investigated a method to eliminate thinning of the top sheet and potential solutions.
- Tried a commercially acceptable cleaning method that eliminates thinning.
- Redesigned the plasma arc torch (reduced the tip size) to allow for reduction in flange size.

Future Direction

- Rerun Phase 2 using new material chemically etched by ALCOA.
- Based on satisfactory completion of the tensile testing and metallurgical analysis, intensify the program schedule to return to the original timetable.

Introduction

The current joining technology for aluminum relies heavily on resistance spot welding, which is at best a marginal process. High maintenance and tip wear continue to be major concerns (see report 7G). Rivets and/or mechanical clinching are costly (see report 7J) alternatives that require high capital investment. Plasma arc spot welding has entered the picture as a potential alternative through the efforts of Arc Kinetics, Ltd., the leading developer of the plasma arc welding process in both steel and lightweight materials. Arc Kinetics developed its original process for single-sided plasma arc spot welding for Jaguar Motor Cars to weld a sheet metal floor pan assembly that was not accessible with conventional resistance spot welding equipment. In a separate effort, the company developed a process called aluminum plasma arc welding (APAW). By combining single-sided spot welds and APAW, Arc Kinetics developed a process that demonstrates excellent potential for the joining of lightweight materials, aluminum, and magnesium. During the past year, several modifications and improvements to the APAW spot welding process have been implemented.

Team Development

A project team was formed with a representative from DaimlerChrysler as the leader. Representatives from GM, Ford, DaimlerChrysler, and Arc Kinetics met to discuss the program and selected a previous team member, F. G. LaManna (of LaManna Enterprises, LLC) to manage the program.

Additional team members were solicited from the automotive industry. Rite-on Industries, ABB Robots, ALCAN, and ALCOA are currently part of the program. Additional suppliers may also be invited to participate.

Work Matrix Approval

A work matrix (material) approved by GM, Ford, and DaimlerChrysler was presented to the team. The plan calls for initially two phases, which require producing material coupons for various testing, tensile, shear, and metallurgical analysis and testing.

Evaluation of these test results will determine the next phases of the program. Phase 2 will be a repeat of Phase 1 with modification to the material alloys based on Phase 1 results. Phase 3 will be the reporting phase of the program. Completion of the initiative is expected in the fourth quarter of 2002.

Phases 1 and 2: Base Testing Programs

Coupon testing will consist of tensile, shear, and metallurgical analysis. Coupons will be evaluated to ensure weld integrity and establish equipment parameters to be used in future applications.

Project Summary

The data from the testing in Phases 1 and 2 will be compiled and used to produce guidelines for welding parameters and quality. During the testing of Phase 1 coupons, thinning of the top sheet was detected. This condition can be described as similar to outgassing, which occurs in welding of zinc-coated materials (expanding of the zinc as it escapes through the molten pool). It was determined that the cause was hydration of the material (moisture trapped in the oxidation layer). This development was a major setback to the program. Without a method to eliminate this thinning, the process will not be commercially acceptable.

Developments/Actions Taken

Various approaches were taken to eliminate the thinning condition:

- acetone wash of coupons
- acetone wash and manual abrasion of the contact surfaces
- mineral spirit wash
- mineral spirit wash and manual abrasion of the contact surfaces
- caustic wash
- caustic wash and acid rinse
- caustic wash and manual abrasion of the contact surfaces

The thinning of the top sheet was eliminated in all cases when the coupons were manually abraded. The abrading breaks the oxide surface and eliminates the trapped moisture. However, this method is not commercially viable.

ALCOA suggested using a chemical cleaning method it uses at an ALCOA facility in Toledo, a phosphoric acid etch under controlled conditions. ALCOA has since prepared several thousand coupons for testing. Preliminary results show the thinning condition has been eliminated. However, test samples exhibit microscopic gas holes and minor cracking. These defects may be reduced or eliminated by varying the gas flow rates and/or the filler wire alloy. It should be noted that these samples were produced with 6022 material and 4043 filler wire.

Future Direction

Phase 2 will be rerun using the new material that was chemically etched by ALCOA. Based on satisfactory completion of the tensile testing and metallurgical analysis, the program schedule will be intensified to get the program timing back on track.

I. Performance Evaluation and Durability Prediction of Dissimilar Material Hybrid Joints

Principal Investigator: D. L. Erdman
Oak Ridge National Laboratory
P.O. Box 2009, Oak Ridge, TN 37831-8048
(865) 574-0743; fax: (865) 574-8257; e-mail: erdmandl@ornl.gov

Field Project Manager: C. David Warren
Oak Ridge National Laboratory
P.O. Box 2009, Oak Ridge, TN 37831-8050
(865) 574-9693; fax: (865) 574-4963; e-mail: warrencd@ornl.gov

Technology Development Manager: Joseph Carpenter
(202) 586-1022; fax: (202) 586-1600; e-mail: joseph.carpenter@ee.doe.gov
Field Technical Manager: Philip S. Sklad
(865) 574-5069; fax: (865) 576-4963; e-mail: skladps@ornl.gov

---

Contractor: Oak Ridge National Laboratory
Contract No.: DE-AC05-00OR22725

Objective

- Develop new experimental methods and analysis techniques to enable hybrid joining as a viable attachment technology in automotive structures. This will be accomplished by evaluating the mechanical behavior of composite/metal joints assembled using a variety of hybrid joining methods and quantifying the resultant damage mechanisms under environmental exposures, including temperature extremes and automotive fluids, for the ultimate development of practical modeling techniques that offer global predictions for joint durability.

Approach

- Characterize the structural hybrid joint to quasi-static load conditions.
- Characterize response to fatigue, creep, and environmental exposures.
- Conduct predictive analysis.

Accomplishments

- Completed the mechanical static testing of the existing supply of glass and carbon fiber hybrid joint specimens.
- Modified the mechanical test set-up for increased structural integrity to eliminate load train failures.
- Completed the planned exploratory creep and fatigue testing of the hybrid rail specimen.
- Developed fundamental finite element (FE) models to initiate the effort to predict structural durability.

Future Direction

- Continue static creep and fatigue testing with new carbon composite material (HexMC).
- Refine FE models to include damage accumulation and correlate with experimental result.
- Develop realistic, practical models to predict joint durability and/or failure under a variety of load conditions and environmental exposures.

Introduction

Weight can be reduced and fuel efficiency increased in automobiles, without compromising structural integrity or utility, by incorporating innovative designs that strategically utilize modern lightweight materials—such as polymeric composites—in conjunction with traditional structural materials such as aluminum, magnesium and steel. Despite the advantages associated with such dissimilar or hybrid material systems, there is reluctance to adopt them for primary structural applications. In part, this reluctance can be attributed to the limited knowledge of joining techniques with such disparate materials where traditional fastening methods such as welding, riveting, screw-type fasteners, and bolted joints may not be appropriate.

One solution to this problem is the use of hybrid joining techniques by which a combination of two or more fastening methods is employed to attach similar or dissimilar materials. One example is a mechanically fastened joint (i.e., bolted or riveted) that is also bonded with adhesive. These types of joints could provide a compromise between a familiar mechanical attachment that has proven reliability, and the reduction of problematic issues such as stress concentrations and crack nucleation sites introduced by using mechanical fasteners with polymeric composites.

The use of hybrid joining could also lead to other potential benefits such as increased joint rigidity, contributing to overall stiffness gains and a reduction of vehicle mass. Additionally, the use of adhesives in conjunction with mechanical fasteners could significantly reduce stress concentrations, which serve as locations for crack starters. Hybrid joining methods can also provide additional joint continuity to allow increased spacing between fasteners or welds.

Although numerous benefits are derived from using hybrid joining techniques, and the joining of dissimilar materials is becoming a reality, little or no practical information is available concerning the performance and durability of hybrid joints. Therefore this project has taken on the task of developing new technologies to quantify joint toughness and predict long-term durability. This will necessitate identifying and developing an understanding of key issues associated with hybrid joint performance, such as creep, fatigue, and effects of environmental exposure.

To initiate this study, it was necessary to choose a candidate hybrid joint representative of those typically encountered in automobiles. Because of their wide applicability in automotive structures, several combinations of hat-section geometries were considered. Hat-sections can be incorporated into a variety of generic automotive structural components, such as crush-tubes or frame rails, when they are bonded and mechanically fastened to other geometries. For the current study, the Joining Task Force selected a composite hat-section bonded and riveted to a steel base, as shown in Figure 1. This selection was made on the basis of general applicability to a variety of automobile structural components. Members of the Joining Task Force identified industry partners for sources for the steel, rivets, composite hat-section, and adhesive.

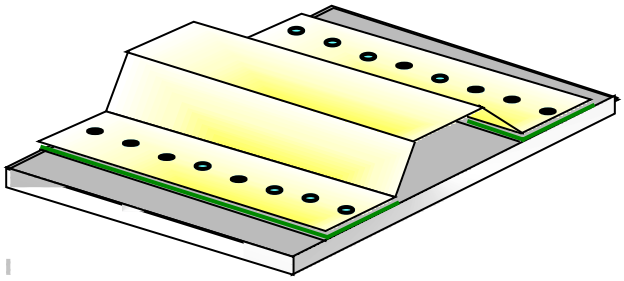

Figure 1. Hybrid joint schematic.

To determine the influences of the adhesive and the rivets on the structural performance of the rail, it

was also decided to investigate bonded specimens without rivets and riveted specimens without adhesive.

Load Train Refinements

Since a large effort was put forth to characterize the mechanical performance and damage processes unique to this type of structure, it was essential to devise suitable load-train fixtures to simulate the types of in-service loading typically included in automotive structures. Several iterations during exploratory static testing resulted in modifications to the roller design to achieve three-point bend conditions that would be suitable for the planned tensile, creep and fatigue tests. Therefore, the original fixture design for the rail tests was modified to eliminate yielding of the center support of the three-point bend fixture and increase the support radius of the center roller. These changes reduced stress concentrations that had resulted in roller penetration, which led to undesirable damage at the contact points between the specimen and the fixture. A 1-in.-diameter steel bar, which spanned the width of the specimen previously used for the center roller, was replaced with a fully supported 2-in. roller, as shown in Figure 2. This configuration was also found to work well for the creep and fatigue experiments. Figure 3 depicts the alternative configuration for this set-up with the hat-section of the specimen in compression.

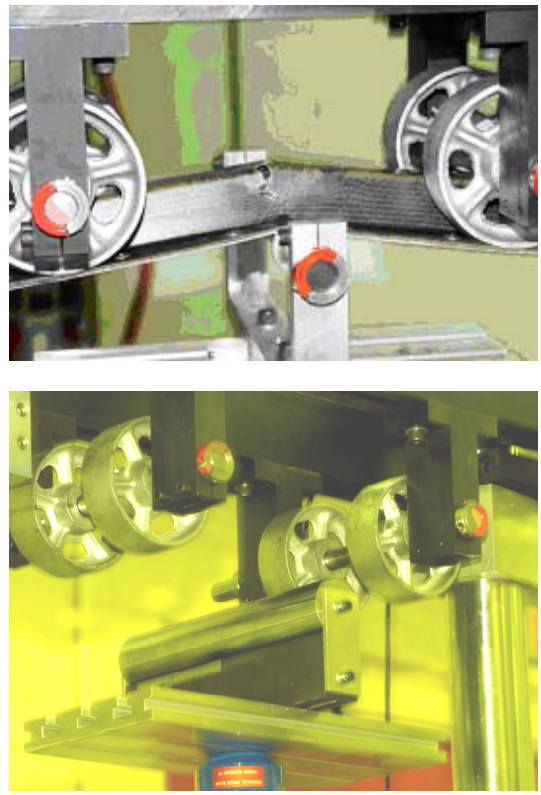

Figure 2. Original and modified three-point bend fixture with 2-in.-diameter center support.

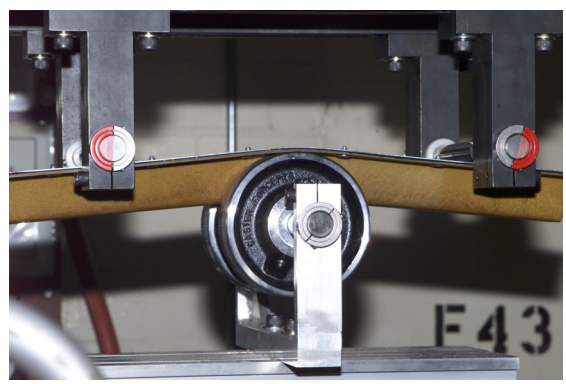

Figure 3. Typical rail test with the specimen in compression.

Hybrid Rail Tensile Tests

A comprehensive tensile test matrix was adopted to explore the occurring damage mechanisms and subsequent failure process as the specimen was quasi-statically loaded to failure. Tests were conducted on stitched carbon-fiber composites, as well as on swirled matt glass composite hat-sections. In either case, the hat-section was bonded and/or riveted to a 1-mm draw-grade steel substrate chosen for wide applicability in current automotive applications. A total of 14 glass rail specimens and 7 carbon fiber specimens were tested. Table 1 lists permutations for the various combinations of loading conditions and fastening methods.

Table 1. Specimen permutations for mechanical testing of the hybrid rails.

Compression	Tension
Rivets and adhesive	Rivets and adhesive
Rivets only	Rivets only
Adhesive only	Adhesive only

In addition to discovering observable damage to understand failure behavior, it was also necessary to measure the global load-displacement response of

the specimens, to correlate with modeling efforts. Agreement between measured displacements and strains at various stages in the loading history is essential to ensure the models are realistically capturing the mechanical response of the specimen. Figure 4 is a schematic of the strain gage locations that were chosen.

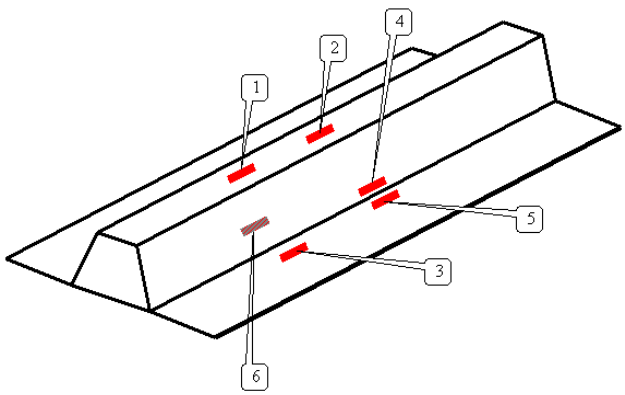

Figure 4. Strain gage placement on the hybrid-joint rail specimen.

Typical tensile test results from two tensile hybrid rail tests are shown in Figures 5 and 6 for a carbon fiber and a glass specimen, respectively. The top plot in each figure consists of the measured strains as a function of applied displacement, and the bottom plots are the resultant load-displacement curves. It is obvious from these two figures that there are distinct dissimilarities between the glass and carbon fiber specimens that indicate the need to account for the effect of the composite hat-section material selection. Also, the strain data indicate a complex strain field that rapidly changes as the failure process in the specimen occurs. This information will be crucial in the later stages of this program to accurately predict the sequential failure process in the modeling endeavor.

Although the static tensile testing revealed essential characteristics of the behavior of the hybrid rail structure, and indications concerning the build-up of stress and strain field during the various stages of loading, no discernable joint failure was consistently observed. On the other hand, it is very important to point out that the joining method (i.e., bonding and/or riveting) and composite hat-section material highly influenced the load-carrying capability of the specimen and the type of failure. Several examples of damage are shown in Figures 7

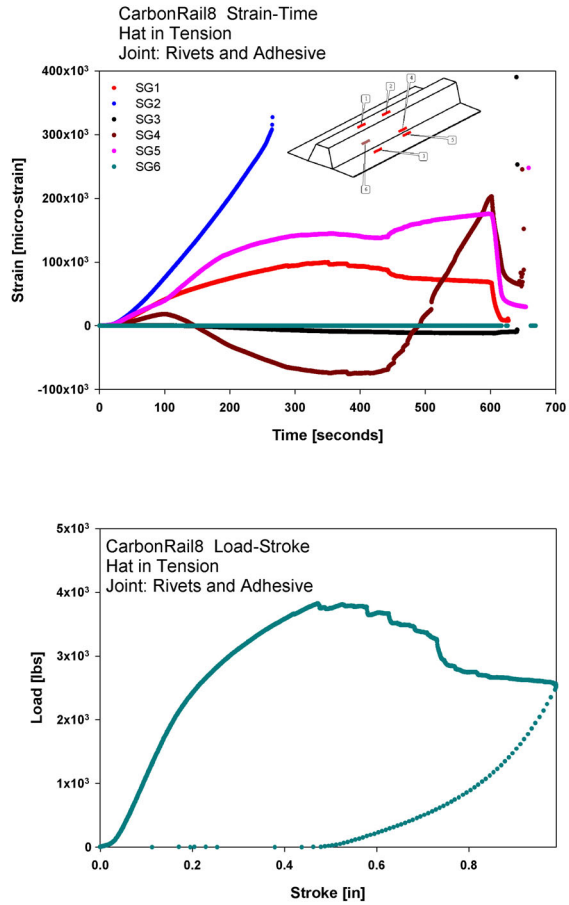

Figure 5. Carbon rail 8 test data.

and 8. In the first, there is evidence of large-scale yielding of the metal substrate, which continuously increases up to the point of failure. In the second photo, the extensive composite damage, which accompanies structural failure, is evident.

Hybrid Rail Fatigue Tests

Fatigue tests were carried out on various joint and material combinations. These tests were conducted in constant amplitude load control at 85% of the failure load measured during the tensile tests. Although this is a relatively high load range with respect to failure load, it was chosen with the intention to observe any well-defined failure process that would take place over a relatively short period of time. It turned out that the failure process was actually very systematic, consisting of crack formation at discontinuities such as rivet holes and the regions where the hat portion of the composite met the flange region of the rail. These crack initiation sites then extended into other regions of

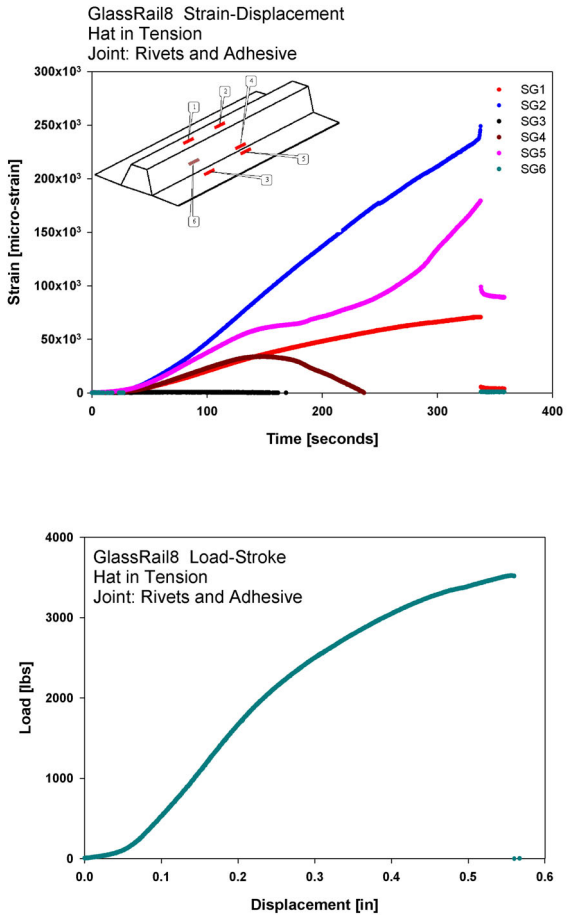

Figure 6. Glass rail 8 test data.

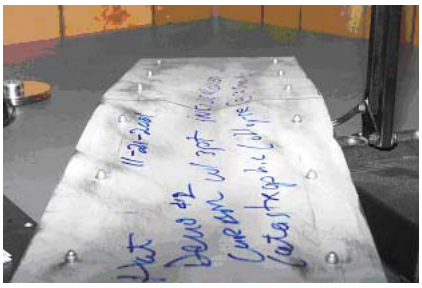

Figure 7. Static yielding of the metal substrate.

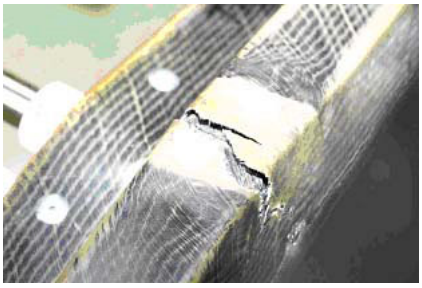

Figure 8. Static failure in graphite composite.

the structure; and as they coalesced, they formed increasingly larger damage sites, which interacted with the progressive yielding of the steel substrate. Additionally, although no joint failures were observed in the static tests, the fatigue failures were the result of significant damage in the joints. Specifically, de-bonding of the adhesive and rivet failures were observed. This observation is significant because of the cyclic nature of the service loads encountered in automotive applications. It needs to be addressed in the predictive modeling for the durability of these types of structures. Several examples of the extensive joint failure are shown in Figures 9 and 10. The contrast between the tensile failures, which exhibited damage only in the composite and the yielding of the steel, and the extensive joint failure for the fatigue tests indicates the huge dissimilarities between the two loading scenarios. It should also be pointed out that the actual number of cycles to

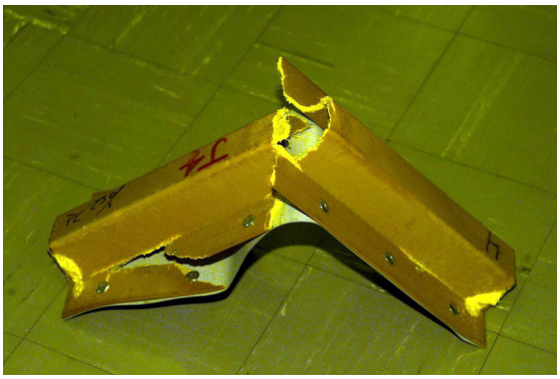

Figure 9. Catastrophic fatigue failure of a glass composite specimen.

Figure 10. Details of fatigue joint failure at rivet locations and in the flange/hat.

failure was consistently less than 5000, which should be a major concern for the durability of such structures.

Hybrid Rail Creep Tests

Five exploratory creep tests were carried out to determine if this type of loading (a constant load maintained over a period of time) would produce significant specimen response for further investigation. As with the fatigue testing, the applied loading was chosen to be 85% of the failure loads observed in the static testing. Although the composite materials used in the hat-section have been reported to exhibit increasing strain with constant applied load, the resulting behavior due to the interaction with the attached steel base, which exhibits little if any creep behavior, was unknown. The results from a typical test are shown in Figure 11. It is evident that there is continuously increasing displacement during the application of the load and significant non-recoverable deformation due to yielding of the metal substrate and possible damage in the composite.

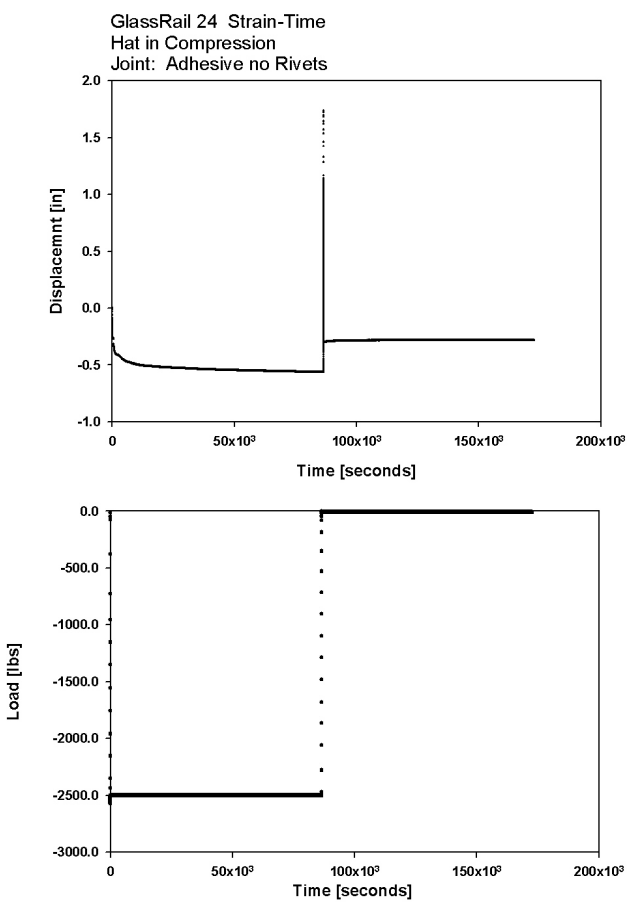

Figure 11. Creep test results.

Modeling Efforts

The primary long-term objective of the modeling effort for this project is to predict the durability of the hybrid joint structure under load, using realistic models that account for interaction between the dissimilar materials, adhesive bonds, and mechanical fasteners. Once a comprehensive model has been developed, a second major task will be to simplify the analysis, while retaining the salient features, to reduce computational overhead. This will yield a practical tool for the automotive industry. With this in mind, it was decided to explore modeling all details of the hybrid joint at the onset to determine which aspects were necessary to obtain accurate predictions. Specifically, the current models include the following features:

- 108,000 degrees of freedom
- Roller contact
- Orthotropic and isotropic composite material properties
- Detailed inclusion of the rivets
- Geometric and material non-linearity

Needless to say, a number of models were developed to include all permutations of the material properties, loading conditions (i.e., tension and compression), and fastening methods, in addition to the FE-specific features listed. All analyses were carried out using ABAQUS (developed by Hibbit, Karlsson, and Sorensen, Inc.) to take advantage of the enhanced capability and flexibility provided by this extremely powerful package.

For brevity, all the results from all the modeling efforts cannot be presented in this summary report; however, the results for one of the more comprehensive cases will be discussed. For this model, both isotropic material properties for the glass composite and orthotropic properties for the carbon composite are considered; the joining includes rivets and adhesive bonds. Non-linearity and roller contact were also considered. Because of the symmetry of the specimen, it is possible to employ quarter geometry with appropriate boundary conditions to reduce the computational overhead.

The mesh for this model is shown in Figure 12 and a schematic of the cross-section in Figure 13. Figure 14 depicts the calculated displacement field for the analysis, and the corresponding stress field is shown in Figure 15.

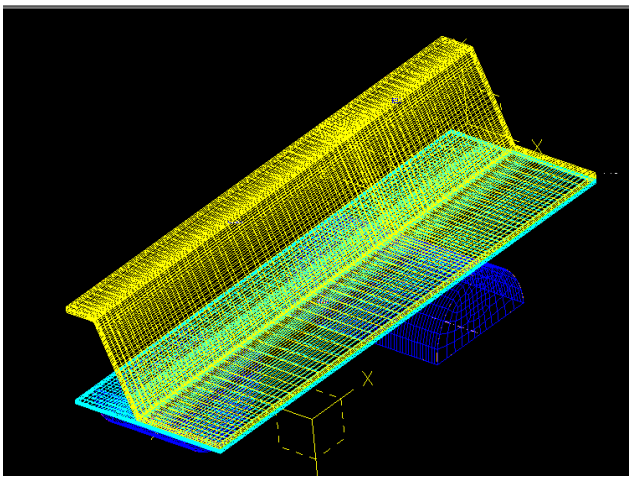

Figure 12. Typical mesh used to model the hybrid joint.

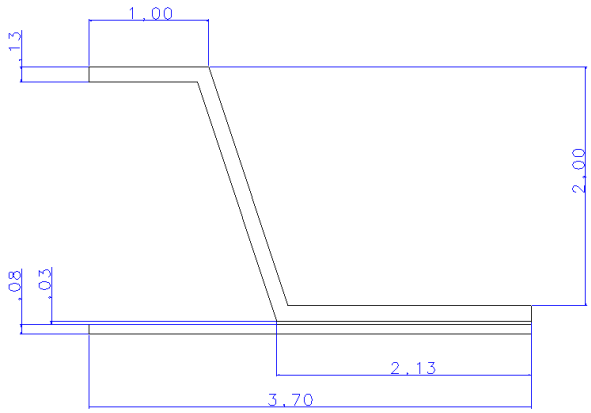

Figure 13. Idealized cross-section of the specimen.

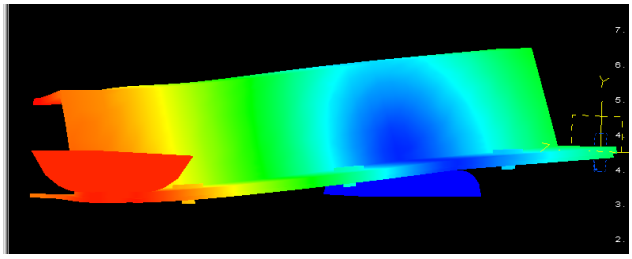

Figure 14. Displacement field for a model with rivets.

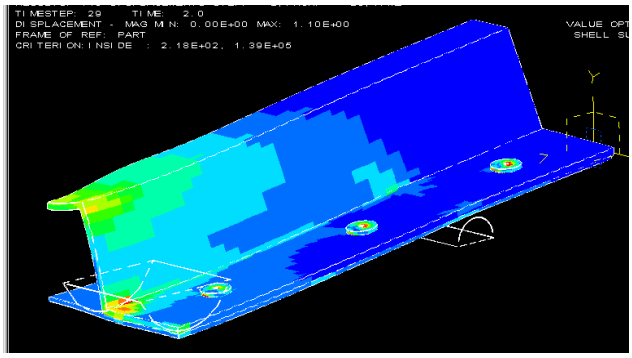

Figure 15. Von Mises stress for a model with rivets.

A saddle-like plastic deformation in the mid-section of the specimen can be observed, as well as lifting of the flange from the roller. Both of these results were in agreement with the displacements observed during the mechanical testing, which gives confidence to the accuracy of the approach.

In addition to the full-field displacement information, another indication that the model is representative of the structure is the ability to predict the global load-displacement response of the specimen and obtain results that agree with the experimental data shown in Figure 16. It can be seen from the plots that the experimental data and FE model prediction are in good agreement at the earlier stages of the loading history, up the point where damage initiates in the specimen and curves start to diverge. This obviates the need to include a sequential damage progression algorithm, which is currently being developed.

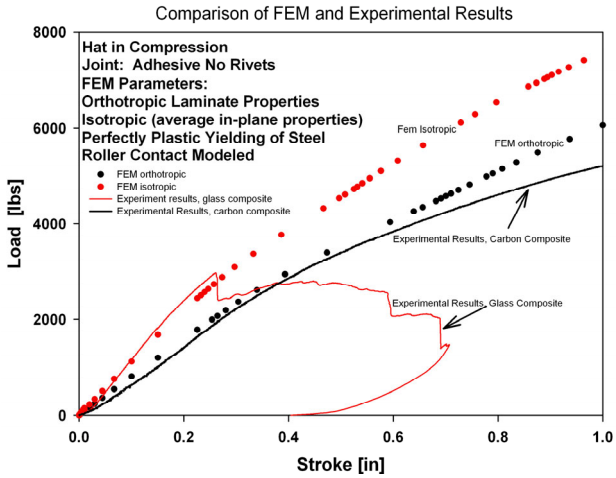

Figure 16. Comparison plots for experimental glass and carbon rail specimens and finite element model results.

Conclusions

Excellent progress has been made on both the experimental and analytical tasks during FY 2002. All mechanical testing has been completed on or ahead of schedule. The modeling effort is progressing ahead of schedule, which will facilitate the difficult task of developing a solid damage algorithm to predict the overall response of the hybrid joint structure. The successes over the past year give a good indication that it will be possible to efficiently incorporate new composite materials into automotive structures, since the use of proper design methods has been shown to produce failures that were in neither the composite nor the joints. Completion of joining research will be critical for incorporating low-mass composites into automotive structures. Regardless of the material chosen, it must be attached to both metallic and non-metallic materials. Further development of the technologies being pursued in this project will make the joining of composites to many potential classes of material a technically and economically attractive alternative. This is critical for increasing fuel efficiency by means of vehicle curb weight reduction.

J. Joining of Dissimilar Metals for Automotive Applications: From Process to Performance

Principal Investigator: Moe Khaleel
Pacific Northwest National Laboratory
(509) 375-2438; fax: (509) 375-6605; e-mail: moe.khaleel@pnl.gov

USCAR Joining Team Contact: Jim Quinn
(248) 680-4732; fax: (248) 680-2874; e-mail: james.f.quinn@gm.com

Technology Development Manager: Joseph A. Carpenter
(202) 586-1022; fax: (202) 586-1600; e-mail: joseph.carpenter@ee.doe.gov
Field Technical Manager: Philip S. Sklad
(865) 574-5069; fax: (865) 576-4963; e-mail: skladps@ornl.gov

---

Contractor: Pacific Northwest National Laboratory
Contract No.: DE-AC06-76RL01830

Objective

- Develop and evaluate different technologies for joining dissimilar aluminum alloys and aluminum to steel.
- Characterize the performance of these joints.
- Develop a unified modeling procedure to represent these joints in vehicle structural simulation. The steel materials include mild, high-strength, low-alloy, and dual-phase steels.

Approach

- Further develop and/or enhance self-piercing rivets and resistance spot welding, with and without adhesives, for joining dissimilar metals.
- Develop a database for the static, dynamic, fatigue, and corrosion behavior of dissimilar material joints consisting of different material selections and different joining techniques.
- Incorporate and represent the joint performance data into current computer-aided engineering (CAE) codes for evaluation of impact and fatigue performances of joint components.
- Develop design guidelines in the forms of tables and charts for use in joint structural and crash design

Accomplishments

- Using both experiments and numerical techniques, developed lap shear, cross-tension, and coach peel specimen designs.
- Experimentally investigated the static, fatigue, and dynamic behavior of several combinations of joined dissimilar materials:

  Joint ID 7: SPR 5182-O (2 mm) and 5182-O (2 mm)

  Joint ID 8: SPR 5182-O (1 mm) and 5182-O (2 mm)

  Joint ID 9: SPR 1008 (1.6 mm) and 5182-O (2 mm)

  Joint ID 10: SPR 5182-O (2 mm) and HSLA 350 (1 mm)

  Joint ID 12: SPR 5182-O (2 mm) and DP 600 (1.6 mm)

Joint ID 14: RSW 5182-O (2 mm) and 5182-O (2 mm)

Joint ID 15: RSW 5182-O (2 mm) and 6111-T4 (2 mm)

- Examined failure modes in aluminum spot weld samples using experimental, statistical, and analytical tools and concluded that peak load and energy absorption levels are independent of failure mode.
- Developed an analytical method for estimating rivet strength for similar and dissimilar materials.
- Formulated a joint beam element to incorporate the impact test data into a stress-based failure criterion and tested it on single joint coupons.
- Performed crash simulation on a component-level hat-section to illustrate the concept of the proposed impact failure criterion for frontal and side impact simulations.
- Developed a fatigue analysis procedure for rivets.
- Applied the fatigue analysis procedure to joint ID 7 testing data for validation, analyzed single-joint coupons, predicted fatigue life to compare with experimental data for joint ID 7, and applied the fatigue analysis procedure to component-level hat-section for prediction of fatigue life.

Future Direction

- Join high-strength steel (HSLA 350 and DP 600) and 5000-series aluminum alloy specimens using self-piercing rivets with adhesive (DOW Betamate 4601).
- Conduct static, dynamic, and fatigue testing.
- Initiate corrosion work on the specimens.
- Conduct durability testing of DP600 and 5000-series aluminum alloy specimens in which a group is exposed to 500 h of salt spray/fog and then tested (static, dynamic, and fatigue).
- Develop interlayer material for use in spot welding of dissimilar metals.
- Conduct mechanical and microstructural evaluation of dissimilar metal joints subjected to static, dynamic, and fatigue loads and investigate the effect of structural adhesives, temperature, and loading rates.
- Develop joint failure criteria for CAE safety and fatigue simulations based on the performance database established in the experiments.
- Develop design guidelines in the form of a design space that contains strength, energy absorption, normalized dimensional parameters, material combinations, etc.

Introduction

This project is a collaborative effort between DOE, Pacific Northwest National Laboratory, and the Metals Joining Team of the U.S. Council for Automotive Research (USCAR). The work started in April 2001.

The automotive industry envisions that an optimized vehicle, in terms of performance and cost, can be achieved only by using different materials at different vehicle locations to utilize the materials' functionalities to the fullest extent. Currently, aluminum and steel are the most important construction materials for the mass production of automotive structures. High-volume, non-steel joining is a significant new problem to the industry. For joining dissimilar aluminum alloys, the leading candidate joining methods are spot welding and self-piercing rivets with or without adhesives. The major concerns with aluminum spot welding are its high energy consumption, low electrode life (see report 7G), and structural performance concerns related to weld porosity. For joining aluminum to steel, the industry is currently comfortable with self-piercing rivets (with and without adhesives). However, there are a number of barriers to the widespread exploitation and high-volume production of the riveting technology. One of these barriers is the limited performance data relative to automotive applications.

On the other hand, in order to shorten the vehicle development cycle, more and more CAE analyses are performed before the actual prototype is built. The question the CAE engineers ask most often is how to represent the structural joints in crash simulation and fatigue simulation. Currently, there is no unified approach to representing the structural joints that works for different material combinations under multi-axial loading. This is particularly true for dissimilar material joints, where even the basic performance information on the joint coupon level does not exist.

Joint Population

We experimentally investigated the static, fatigue and dynamic behavior of several dissimilar material joint populations:

Joint ID 7: SPR 5182-O (2 mm) and 5182-O (2 mm)
Joint ID 8: SPR 5182-O (1 mm) and 5182-O (2 mm)
Joint ID 9: SPR 1008 (1.6 mm) and 5182-O (2 mm)
Joint ID 10: SPR 5182-O (2 mm) and HSLA 350 (1 mm)
Joint ID 12: SPR 5182-O (2 mm) and DP 600 (1.6 mm)
Joint ID 14: RSW 5182-O (2 mm) and 5182-O (2 mm)
Joint ID 15: RSW 5182-O (2 mm) and 6111-T4 (2 mm)

Static Joint Strength Evaluation

Static tests were performed for three loading configurations for each sample population in order to derive the overload failure envelope for that population. These three loading configurations are lap shear, coach peel, and cross-tension (see Figures 1 through 3). The results of the static tests were then post-processed to obtain the peak load, failure displacement, and energy absorption upon failure to validate the proposed energy-based failure criterion. Results from static testing of self-piercing rivets of aluminum 5182-O and high-strength steels (HSLA 350 or DP 600) are shown in Figures 4 and 5. Shorter length and harder rivets contribute to the performance of Joint ID 10 (5182-O/HSLA) and Joint ID 12 (5182-O/DP 600) in comparison to Joint ID 7 (5182-O/5182-O), which has a longer and softer rivet. The rivets used in ID 10 and ID 12 do not clinch as much material, which contributes to the behavior. We are currently performing experiments to investigate the effect of rivet length on the static performance of joints.

The failure modes of these tests were documented in a topical report. The static strength of the joints was studied using Weibull probability plots and will also be documented in a topical report. These failure modes and static strength data can help the designer of a light-weighted vehicle choose the correct material combinations for desired static vehicle performance.

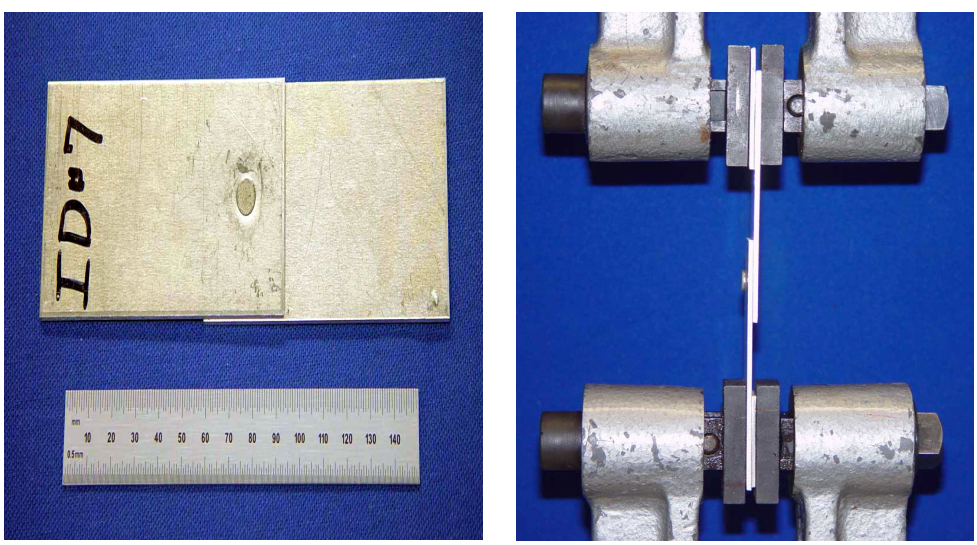

Figure 1. Lap-shear coupon design (left) and test fixture.

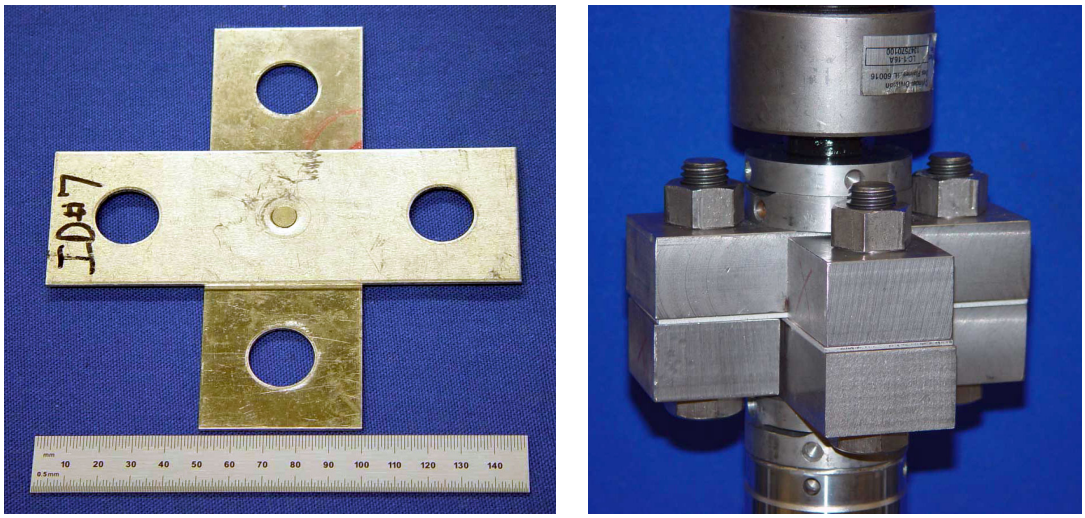

Figure 2. Cross-tension coupon design (left) and test fixture.

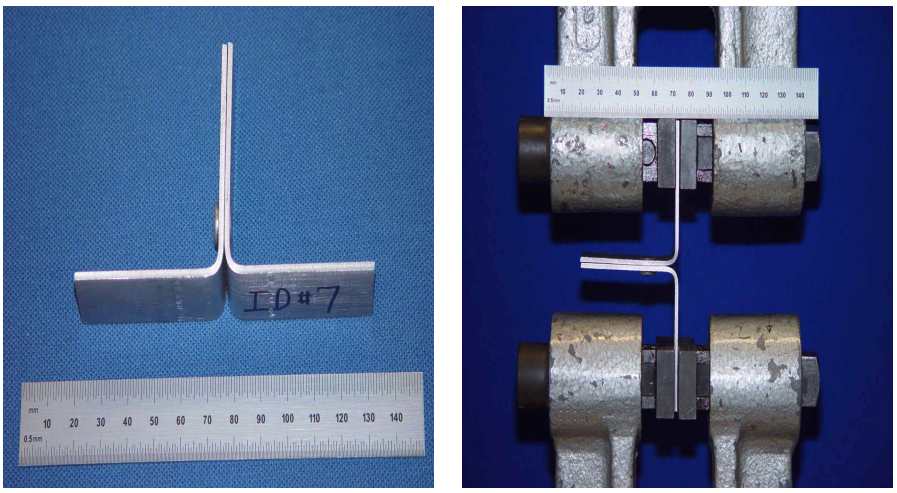

Figure 3. Coach peel coupon design (left) and test fixture.

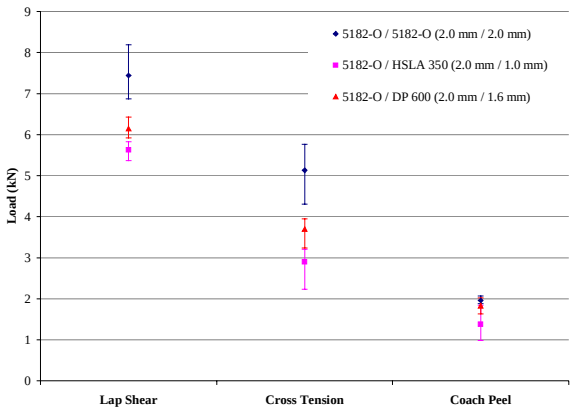

Figure 4. Static strength testing peak load—5182-O/5182-O, 5182-O/HSLA 350, and 5182-O/DP-600 SPR.

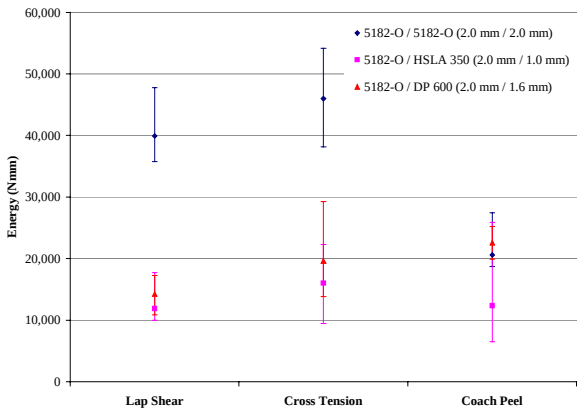

Figure 5. Static strength testing energy—5182-O/5182-O, 5182-O/HSLA 350, and 5182-O/DP-600 SPR.

Dynamic Joint Strength Evaluation

Dynamic impact tests of 10 mph and 20 mph were performed for the three sample populations under three loading configurations. Example results of lap shear for ID 14 are shown in Figure 6. To determine the dynamic strength accurately, two sets of unique light-weighted fixtures were designed for the coupon configurations. These fixtures are rigid, and they connect themselves directly to the piezoelectric load cell, thereby eliminating the possibility of a fictitious load signal resulting from inertia effects. The rigidity, or compliance, of the testing frame was also adjusted prior to the dynamic tests to ensure that the test frame is rigid enough that its natural frequency is much higher than the response frequency of the tested sample. Ringing effect was thus minimized to the greatest extent possible. The dynamic test results were then post-processed to obtain the peak load, failure displacement, and energy absorption upon failure to populate the failure envelope and to validate the proposed energy-based failure criterion.

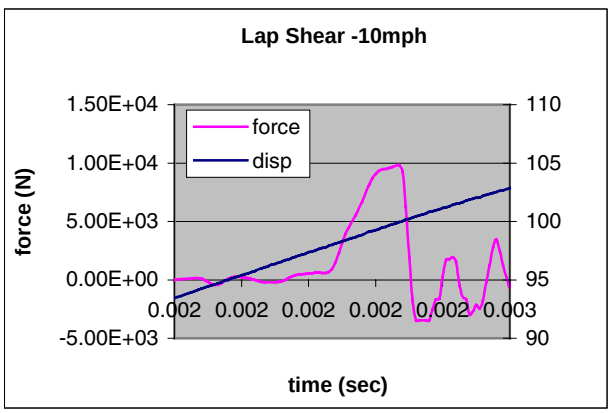

Figure 6. Dynamic test results for ID 14 [RSW 5182-O (2 mm) and 5182-O (2 mm)].

The failure modes of these dynamic tests were also documented in the failure mode report. The strain-rate sensitivity of the test samples was addressed. The failure mode and dynamic strength data can help the designer in selecting material for desired dynamic performance.

Joint Fatigue Strength Evaluation

Cyclic fatigue tests were performed on all sample populations under a tension-tension ratio of R = 0.1. Fatigue tests were conducted on all specimen designs (lap shear, cross-tension, and coach peel). It was found that the coach peel coupons exhibit the lowest fatigue life for the three coupon configurations because of the high stress concentrations for this loading condition. Among the three loading conditions, lap shear had the highest fatigue life. Figure 7 shows that the stress intensity factor can be used to quantitatively evaluate the fatigue strength of different joint types and different coupon configurations.

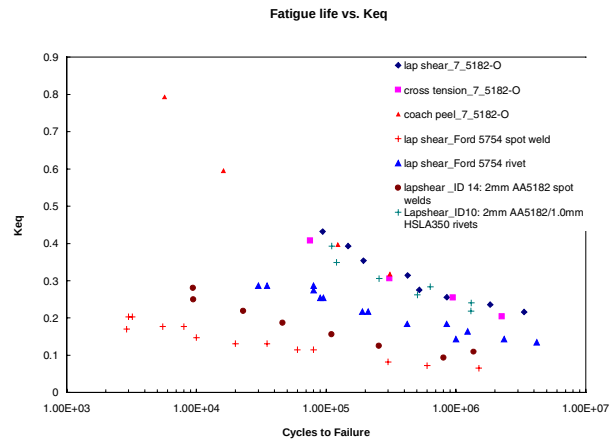

Figure 7. Stress intensity factor versus the number of cycles to failure.

Joint Computer-Aided Engineering

Analyzing and predicting weld structural failure is a challenging problem in solid mechanics. This is so because the representation of a small structural joint in the entire vehicle simulation or component-level simulation is grossly simplified for computational efficiency in modeling the entire vehicle. The additional issues are related to the failure mode and failure location of these joints. Neither the failure mode nor location is known in advance, since both are determined by the interaction between type of loading, joint geometry, and material combination. Yet the failure loads of such structure joints are very much failure-mode dependent.

During this reporting period, a joint beam element was formulated to incorporate the static and dynamic test results into the failure envelope of the beam. Since the joint strength tests were all performed under simple and uniaxial loading conditions, and the joint loading in an actual vehicle is complicated and multiaxial, a failure envelope in a

three-dimensional space of tension, shear, and bending moment was formulated.

Frontal and side crash simulations were performed for a component-level riveted hat-section. A relatively fine mesh was used to observe the local stress patterns around the joints as shown in Figure 8. The rivet force components during impact were monitored and compared with the corresponding failure envelope. Failure was then predicted according to the position of the rivet forces on the preliminary failure envelopes.

Further study is needed in this area to incorporate the failure envelope into the dynamic simulation package so that the joint element can be eliminated automatically when the joint forces are outside the corresponding failure envelope. Also, more work needs to be done to incorporate the energy-based failure criterion in the simulation package.

During the past quarter, a procedure to analyze fatigue failure based on a stress intensity factor was formulated to incorporate the fatigue test results into the CAE fatigue prediction. Fatigue test data for different coupon configurations collapse well onto a single curve on the plot charting the stress intensity factor versus fatigue life. The next step would be to obtain the stress intensity factors for each individual joint from component-level simulations to predict the corresponding fatigue life. The predictions will then be compared with actual component fatigue tests to validate the proposed approach.

Meetings

Project review meetings were held on March 1 and June 27, 2002, at the U.S. Council for Automotive Research. Members of the joining team participated.

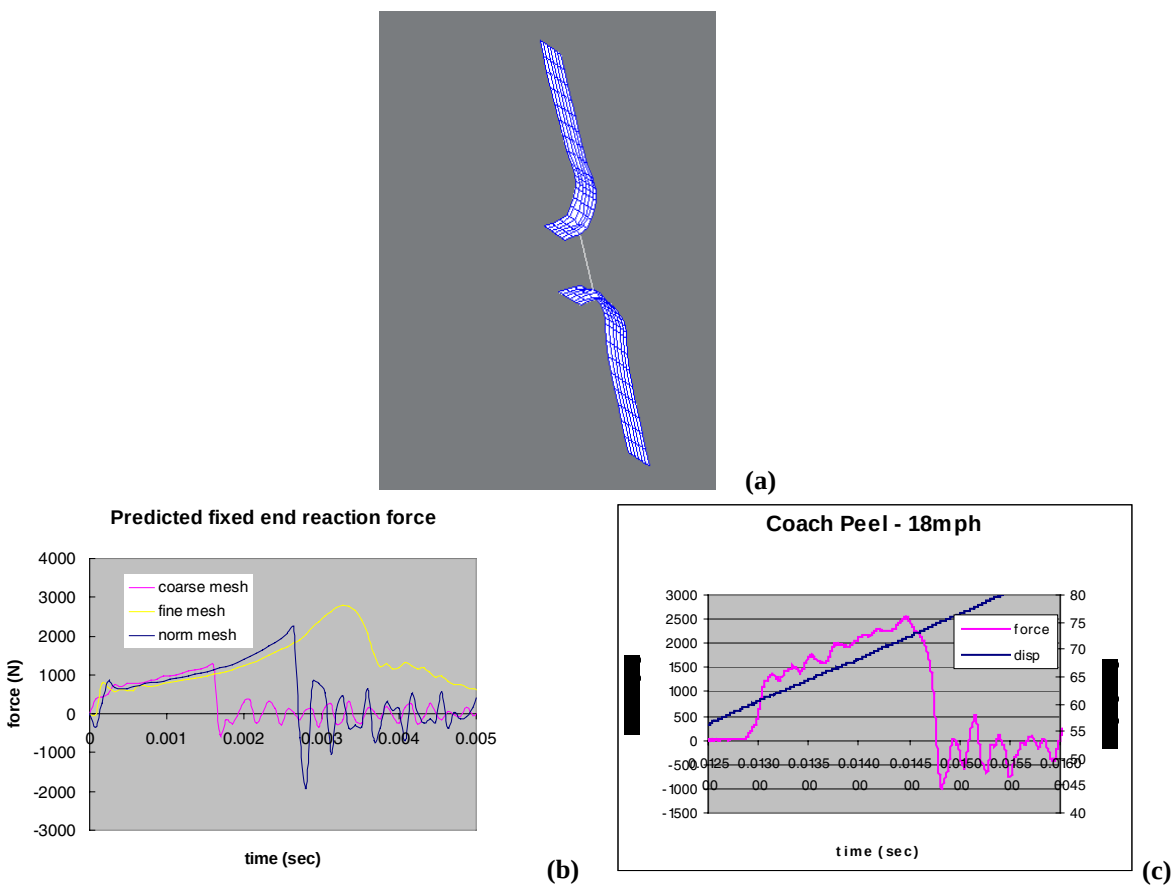

Figure 8. Results for dynamic testing at about 20 mph (a) joint; (b) simulation prediction for 3 mesh types; and (c) experimental results.

K. Nondestructive Evaluation Tools for Evaluation of Laser-Welded Metals

Project Leader: William Charron
Ford Motor Company
24500 Glendale Avenue
Redford, MI 48239
(313) 592-2296; fax: (313) 592-2111; e-mail: wcharron@ford.com

Project Administrator: Constance J. S. Philips
National Center for Manufacturing Sciences
3025 Boardwalk
Ann Arbor, MI 48108-3266
(734) 995-7051; fax: (734) 995-1150; e-mail: conniep@ncms.org

Technology Development Manager: Joseph Carpenter
(202) 586-1022; fax: (202) 586-1600; e-mail: joseph.carpenter@ee.doe.gov
Field Technical Manager: Philip S. Sklad
(865) 574-5069; fax: (865) 576-4963; e-mail: skladps@ornl.gov

---

Contractor: U.S. Automotive Materials Partnership
Contract No.: DE-FC05-02OR22910

Objectives

- Develop fast, accurate, robust, non-contact non-destructive evaluation (NDE) tools and methodologies to replace current manual destructive testing of laser-welded sheet and structures in (zinc-coated) steel and aluminum.
- Demonstrate the accuracy and repeatability of the technologies developed or applied.
- Eliminate the need for a highly trained /experienced NDE evaluator.

Approach

- Phase 1: assess state-of-the-art technologies, down-select, conduct validation testing using fabricated welded coupons in steel, correlate NDE test results with destructive test results, and select technologies.
- Phase 2: develop and build bench prototype(s) of the selected NDE methodology(ies), conduct further validation testing using laser-welded production parts in steel, and correlate NDE test results with destructive test results.
- Concurrent with Phase 2, undertake the study of aluminum using an approach similar to that used in the previous phases.

Accomplishments

- Completed preliminary weld flaw characterization of metals from original equipment manufacturers (OEMs).
- Completed selection of target laser welding application.
- Completed preliminary NDE system functional specifications.
- Completed initial assessment of NDE state-of-the-art technologies.
- Completed controlled testing of four selected NDE technologies using fabricated roof ditch laser weld coupons.

- Completed analysis of test results.
- Selected strategic course of action for Phase 2; implementation is under way.
- Initiated actions to undertake a study of aluminum.

Introduction

Laser welding has been widely accepted by the automotive industry as an industrial process. Its uses range from welding tailor-welded blanks to transmission components to airbag inflation modules. The use of lasers continues to increase, and some manufacturers are considering the use of lasers for welding of the "body in white."

Although laser welding has been accepted by the industry, cost factors are always an issue, particularly in the case of weld defects. Because of the high speed and high volume of laser welding, coupled with the relatively small critical flaw size, finding these defects can be time-consuming, difficult, and hence expensive. If not detected before subsequent processing and/or use, they could cause failures during processing down the line or while in use. For example, pinhole porosity in a laser-welded tailor blank can cause failure during the stamping operation, which can damage the dies and require downtime for the press. To prevent this, laser welding needs to be accomplished with no detrimental flaws and be monitored with a high degree of reliability.

A number of systems have been developed to monitor laser welding systems in real time. Generally, these systems examine the byproducts of the laser-to-metal interaction to determine the quality of the weld. The detection methods may include examining the frequency and intensity of the light that is given off and comparing it with a known "acceptable" weld. Most of the monitoring systems use this "training" method as a basis for determining acceptable welds versus welds to be rejected. Generally, these systems interpolate between known parameter variations. Some systems use software based on neural networks rather than on function. As of this writing, these systems have had limited success in the production environment.

The United States Automotive Materials Partnership (USAMP) is exploring NDE tools for use upon completion of the weld. Of specific interest is the identification of progressive and emerging technologies in NDE. As part of this effort, the Automotive Metals Division (AMD) 303 project performed a technology assessment of NDE. From this assessment, specific technology recommendations are being reviewed with a goal of having an NDE prototype system ready for installation in a factory setting by the end of calendar year 2003.

This project has two primary investigative missions: (1) evaluate and develop new NDE tools for laser-welded steel (zinc or organically coated) and (2) evaluate and develop new NDE tools for laser-welded aluminum. The investigative strategy is to

- Conduct a comprehensive assessment of existing and emerging NDE tools for steel and aluminum
- Down-select technologies to the most promising methodology(ies)
- Conduct validation testing of the selected methodology(ies) against the destructive test methods currently in use, first for fabricated welded coupons and then for production laser-welded parts
- Demonstrate the selected methodology(ies) through a bench prototype system

With the approval of USAMP/AMD, the project has been extended for an additional 12 months with additional funding to allow sufficient time and resources to promote the development of NDE system(s) for the target application.

Details of Phase 1

Phase 1 is the assessment of state-of-the-art technologies, down-selection, validation testing using fabricated welded coupons, correlation of NDE test results with destructive test results, and technology selection.

The NDE system sought was conceptually defined in terms of its functionality and the laser weld flaws or defects that it must be able to detect were characterized.

An initial assessment of NDE technologies, from which four technologies were selected for further evaluation, was completed in July 2001. Commercial off-the-shelf systems were identified in addition to emerging NDE technologies. The techniques identified by our initial assessment can be applied to steel and aluminum structures. However, one needs to bear in mind that procedures or equipment developed for one material might require redesign for the other material. For example, ultrasonic transducers developed for steel would need to be redesigned for aluminum because of their different sound characteristics.

Preliminary findings arising out of this initial assessment provided insight into the functionalities desired from an NDE prototype system built for this project. The system should be

- Capable of autonomously evaluating and assessing welds in the production system with minimal operator intervention and a high degree of reliability.
- Adaptable to a variety of weld joint geometries and materials.
- Capable of being mounted on a robot arm or other automation.
- Capable of detecting and evaluating discontinuities in accordance with a uniform standard.

Vendors and their respective technologies were evaluated in a statistically controlled study. The goal of the study was to evaluate vendors' technology capability claims versus reality using fabricated weld samples that simulate laser-welded roof ditch welds. It was not expected that any of the vendor technologies would prove to be 100% effective in the demanding high-volume production environment common to the automotive industry. Rather, the goal was to determine which technology offered the best detection capabilities and potential for development of a prototype system suitable for eventual testing in an automotive laser welding production environment.

Edison Welding Institute (EWI) was selected as the contractor to fabricate the weld samples (see Figures 1 and 2) and to design and conduct the study of all four vendors' technologies. This study was completed in May 2002. Validation was conducted using micro-focus and conventional radiography

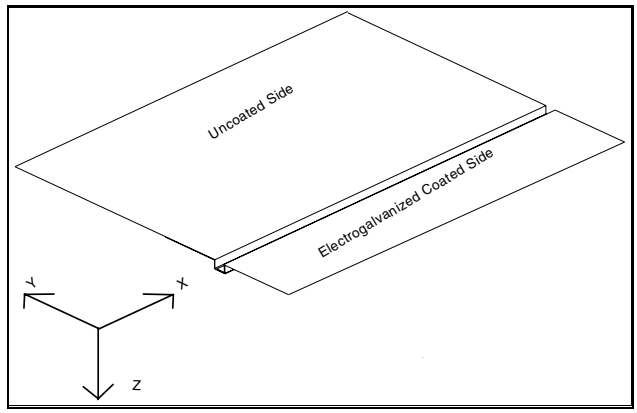

Figure 1. Overall dimensions of roof ditch weld sample: X = 400 mm; Y1 = 202 mm; Y2 = 89 mm; overall Y after bending = 287 mm; Z = 12 mm.

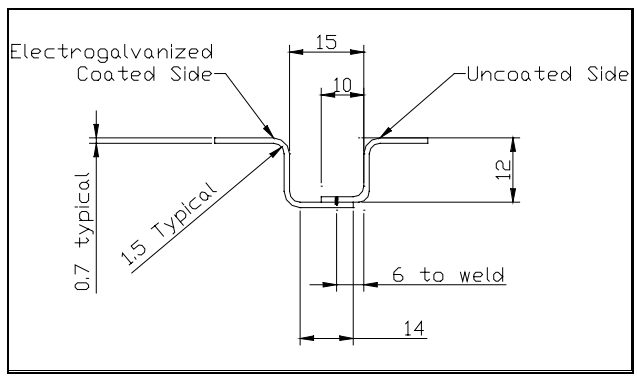

Figure 2. Weld joint details in millimeters.

and, where appropriate, metallurgical evaluation, rather than using destructive tear-down of the samples. The samples were viewed as too valuable to destroy and thereby lose the ability to conduct future testing. Following completion of the study, the AMD 303 Committee undertook an extensive analysis of the data, with the assistance of EWI and a Ford statistician, to arrive at an understanding of and consensus on a meaningful comparison of the vendor results. This period of analysis ended in September 2002 and resulted in the down-selection to the most promising technologies for further development.

Although this period introduced a delay in the originally proposed schedule for launching Phase 2, it produced a potentially more beneficial outcome: the generation of more than one commercial NDE system suitable for U.S. automotive operations.

The rationale for the selection of more than one technology and vendor is complex. First, these technologies were found to differ in their capability

to detect certain weld discontinuities that are judged critical by the OEMs and by a first-tier laser welding system integrator. These vendor systems performed comparably well (albeit on some differing discontinuities); our findings indicate they require additional development to perform acceptably well in the OEM production environment. The systems are viewed as being likely to produce a favorable development outcome, and the companies are viewed as having the requisite motivation to work toward automotive market objectives and as having the capability to bring the potential developments to market quickly.

EWI has been selected to continue as contractor to the committee. It will work with the committee to design and conduct a thorough system development and testing program in steel with the vendors, starting in the first quarter of FY 2003, and to initiate a study of aluminum. The variants in development needed to achieve acceptable detection capabilities in aluminum will be identified. The schedule for completion of Phase 2 is the fourth quarter of FY 2003.

L. Nondestructive Evaluation Techniques for On-Line Inspection of Automotive Structures

Principal Investigator: Deborah Hopkins, Ph.D.
Lawrence Berkeley National Laboratory
1 Cyclotron Road, MS 46A-1123, Berkeley, CA 94720
(510) 486-4922; fax: (510) 486-4711; e-mail: dlhopkins@lbl.gov

Field Project Manager, Composites: C. David Warren
Oak Ridge National Laboratory
P.O. Box 2009, Oak Ridge, TN 37831-8050
(865) 574-9693; fax: (865) 574-0740; e-mail: warrencd@ornl.gov

Technology Development Manager: Joseph A. Carpenter
(202) 586-1022; fax: (202) 586-1600; e-mail: joseph.carpenter@ee.doe.gov
Field Technical Manager: Philip S. Sklad
(865) 574-5069; fax: (865) 576-4963; e-mail: skladps@ornl.gov

Participants
NDE Steering Committee composed of representatives from DaimlerChrysler, Ford Motor Co., and General Motors
Frédéric Reverdy, Ph.D., Lawrence Berkeley National Laboratory
Daniel Türler, M.S., Lawrence Berkeley National Laboratory

Contractor: Lawrence Berkeley National Laboratory
Contract No.: DE-AC03-765F0095

Objective

- To evaluate and develop nondestructive evaluation (NDE) and testing techniques that are sufficiently fast, robust in manufacturing environments, accurate, and cost-effective to be suitable for inspection of automotive structures.

Approach

- Undertake a complete survey of the state of the art in spot-weld inspection to evaluate existing commercial systems and to help determine the requirements for the next generation of inspection systems.
- Perform laboratory experiments and develop numerical models to help interpret the results obtained with existing ultrasonic techniques and to evaluate the potential of alternative NDE methods.

Accomplishments

- Conducted acoustic, thermographic, and X-ray measurements on spot-welded test specimens.
- Evaluated commercially available spot-weld inspection systems.
- Adapted a finite-difference code to model acoustic waves generated by a phased-array probe.
- Developed pulsed-infrared-thermography data-post-processing algorithms to evaluate weld quality.

Future Direction

- Obtain a phased-array system from Ford Motor Company and learn the operating principle and technical approach.
- Determine system performance and limitations including sensitivity to sheet thickness, influence of surface roughness and weld indentation, and sensitivity to different types of welds.
- Develop algorithms to automate signal acquisition and data processing.
- Complete the evaluation of existing ultrasonic inspection systems.

Introduction

Decades of work in industry and research institutions aimed at development of nondestructive spot-weld inspection systems have not resulted in their widespread adoption in the United States, even though such systems are used successfully in foreign plants. These systems fall short of domestic industry requirements for a myriad of reasons: extensive training is required; parts to be tested are made from a wide range of materials, with varying thickness, requiring multiple probes; and resulting data are not evaluated or summarized sufficiently to provide useful input to plant managers. Work under way addresses each of these issues.

The industry steering committee for the project is composed of representatives from DaimlerChrysler, Ford, and General Motors with expertise in manufacturing, materials, and NDE. The committee asked Lawrence Berkeley National Laboratory (LBNL) to evaluate current vendor technology that is applicable to the inspection of spot welds. LBNL and the industry steering committee undertook a round-robin testing exercise to evaluate existing systems.

Work to date using a variety of NDE methods has indicated that surface indentation and roughness can have a strong effect on most measurements of spot-welded samples. During spot welding, the pressure of the electrodes and heating results in indentations in the upper and lower surfaces of the joint. Authors of a recent publication conclude that conventional ultrasonic systems that rely on analysis of acoustic attenuation in the weld are in actuality more sensitive to these surface indentations than to changes in steel grain structure that can be related to weld quality. To better understand the effect of surface indentation and roughness on acoustic measurements, surface topography measurements were compared with results of high-resolution acoustic microscopy.

The viability of using pulse-phase thermography (PPT) to assess spot-weld quality in galvanized steel is being investigated. The method is currently being refined to allow discrimination of satisfactory and undersized welds on calibration and reference samples.

Project Deliverables

- Paper submitted to Society of Automotive Engineers.
- Report summarizing laboratory experiments and modeling studies.
- Development of data post-processing techniques for the analysis of thermographic images of spot welds.

Planned Approach

Efforts under way build on work completed to date, including laboratory testing of NDE methods; evaluations of commercially available systems; a review of technologies under development; visits to manufacturing plants; meetings with suppliers; and discussions with industry welding engineers, inspectors, and plant managers. Based on this work, there is consensus among participants on system requirements that can be used to design, build, and test a prototype platform suitable for evaluation in a production environment. The platform will be utilized to build a system for inspection of spot welds in steel that will be deployed in a plant for testing and evaluation.

To evaluate existing ultrasonic systems, Ford used well-established welding protocols to create two sample sets. Test specimens contained satisfactory, undersized, and defective welds. Each

set consisted of 30 test coupons with five spot welds each, randomized with respect to weld quality. Each company also received 12 reference coupons for which the welding parameters were known. The reference samples were included to help calibrate the systems.

Conventional systems are based on a high-frequency ultrasonic probe working in pulse-echo mode. Weld quality is determined by analyzing acoustic signals, which are sensitive to structural changes in the weld nugget induced by the welding process. LBNL has studied these systems in depth, met with suppliers, and observed the systems being used in industrial settings to understand their positive features and drawbacks.

On the plus side, the systems are relatively inexpensive and are well tested. On the negative side, they require well-trained operators to achieve satisfactory results. Operators must manipulate the probe to obtain an acceptable signal, program the system to set threshold values and "gates" that are the basis for characterizing welds, and dump acquired data into a database to visualize the data and generate reports. The operator must also change probes depending on the size of the weld; welds on a single part can require several probe sizes. In positioning the sensor, both perpendicularity and lateral placement are critical to record a signal representative of the spot-weld structure. System programming is required for manipulating the data and reporting the quality of the welds. Plant managers complain about the lack of clarity in the results and the strong dependence on how system parameters are set.

The results of these inspections are being compared with assessments of the quality of the welds based on the known welding parameters. Reporting on the frequency and types of errors made by the commercial systems must wait until the test specimens are peeled to reveal the true size of the weld nuggets. However, initial results suggest that with well-trained operators and extensive calibration with intact and peeled samples, the systems can produce acceptable results.

In order to see the influence of surface roughness on acoustic microscopy results, coordinate-measuring machine (CMM) measurements were made on the same spot-welded galvanized samples evaluated by Professor Shinobu Satonaka at Kumamoto University using acoustic microscopy. Figure 1 shows the CMM measurements of the front surface (light gray lines) superimposed on the acoustic microscopy results (black lines and shading), for a satisfactory and an undersized weld. Pictures of the weld nuggets after the samples were peeled open are also shown. Acoustic microscopy measurements are usually based on the analysis of an ultrasonic wave focused at a specific depth. For the method developed at Kumamoto University, the focal point is below the sample, so that the acoustic signature contains multiple reflections of the acoustic wave in the specimen. Because the acoustic beam is completely defocused when it first encounters the front surface of the sample, the technique minimizes the influence of surface roughness. Despite this advantage, surface roughness appears to have a strong effect on the acoustic results. Each of the C-scans recorded using acoustic microscopy exhibits a dark ring that corresponds to the outer edge of the surface indentation created by the electrodes during welding. The dark areas in these C-scans result from a decrease in amplitude of the reflected acoustic waves caused by diffraction that occurs at the edge of the surface indentation. These dark rings are consistent with surface features visible in the CMM measurements.

Following the acoustic microscopy and CMM measurements, the samples were peeled to allow the exact diameter of the weld nugget to be measured. The C-scans display an interesting feature in the center of the welds, indicated by the circles. The size of the identifiable feature is very close to the nugget diameter measured on the peeled samples. If this relationship can be confirmed, then acoustic microscopy will be able to provide a nondestructive way to calibrate acoustic experiments and confirm the quality of test specimens by providing an accurate measurement of the weld-nugget diameter.

Several post-processing techniques have been applied to thermographic images of spot welds to help determine the feasibility of using thermography to nondestructively evaluate the size of weld nuggets on calibration and test specimens (Figure 2). The maximum-contrast image is of interest because it displays data obtained after the heat pulse has traveled through the specimen, at the point where the temperature difference between the spot weld and the surrounding sheet metal is at its maximum. As soon as a temperature difference develops, lateral heat flow begins to blur the spot weld in the image. Shortly before the maximum temperature contrast

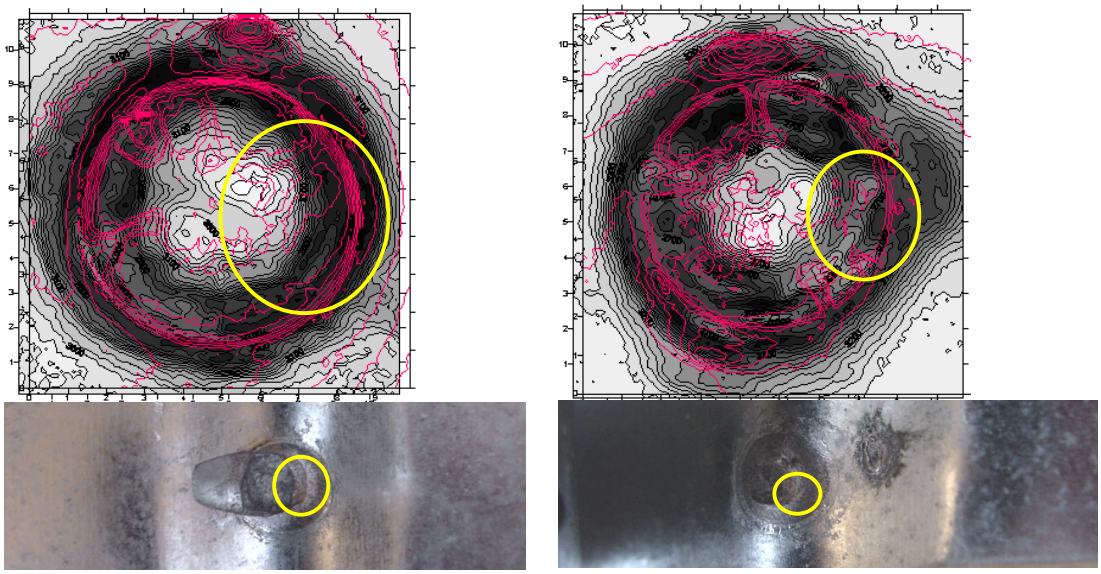

Figure 1. C-Scan images obtained using acoustic microscopy for a good weld (left) and an undersized weld (right). Pictures of the weld nuggets obtained after peeling the samples are shown in the lower images.

occurs, the spot weld appears with the sharpest boundary definition observable. This frame can be found by looking at the temperature-gradient images. The surface-temperature frame where the maximum gradient occurs is shown in the first row of Figure 2.

The processing that yields the smoothed, 3-dimensional (3D) maximum-contrast images is very sensitive to noise. Noise in the temperature data arises from many different mechanisms. The most significant sources include random photon emission and detection, spontaneous electron emission of the detector (dark current), amplification noise, and analog-to-digital conversion. An Epanechnikov smoothing function is applied to each frame. For each pixel of the frame, this function calculates a weighted temperature average of the surrounding pixels. The number of pixels included in the smoothing process is user-defined. A compromise between sufficiently smooth data and adequate representation of the features of interest is needed. Too much smoothing will blur contrast; too little smoothing will cause grainy images or possibly result in useless post-processed data. The pictures in row 2 of Figure 2 are 3D representations of smoothed data from the previous row.

The temperature-gradient image is calculated from the smoothed data and represents the first temperature derivative in two dimensions (for each frame). Numerically, the derivative is calculated as the difference between the original frame and a frame where the data were shifted right and down by one pixel. The final result is the square root of the sum of the squared differences. Because this method is based on a spatial pixel-to-pixel difference, one row and one column of data are lost.

Pulse-phase thermography (PPT) combines modulated thermography and pulsed thermography. The thermal pulse applied to the part is rectangular in time, with a uniform intensity for the entire duration of the pulse. This pulse is composed of a suite of frequencies and amplitudes that are propagated into the part. A discrete Fourier transformation of the smoothed temperature data is calculated for each pixel in the time series.

The Fourier transformation returns two values for each pixel of the frame, a real and an imaginary number. Successful implementation of this technique requires attention to the frame rate and the number of frames acquired. Frequency resolution depends on the length of the acquisition time. Acquisition times that are too short may result in the loss of valuable information, particularly low frequencies. The infrared (IR) camera physically limits the maximum frame rate and therefore the sampling rate. Aliasing errors are introduced if the signal bandwidth exceeds the sampling bandwidth.

The maximum-phase image is based on the maximum phase value calculated for each individual pixel in space. In general, maximum-phase images

	Good spot weld	Undersized spot weld	Stick weld
1. Maximum contrast of time series data based on temperature gradient	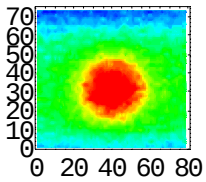	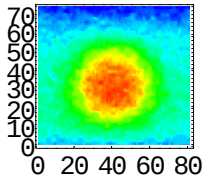	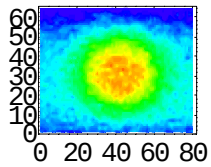
2. Smoothed, 3D maximum-contrast image	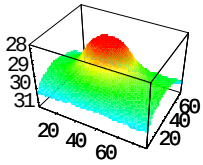	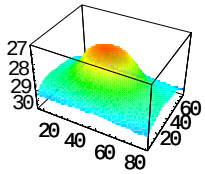	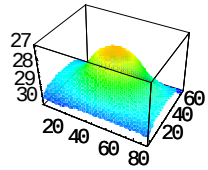
3. Temperature gradient image of maximum-contrast data	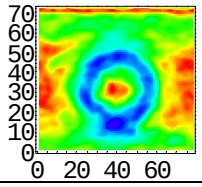	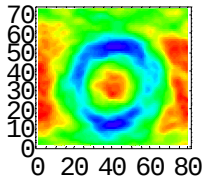	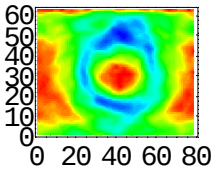
4. Maximum phase image	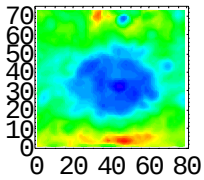	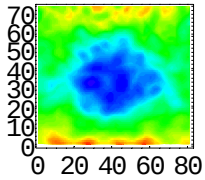	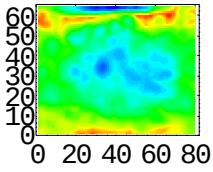
5. Maximum amplitude image	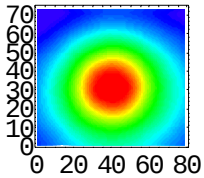	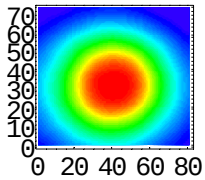	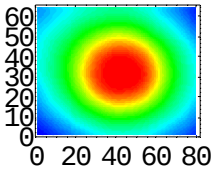
6. Evolution of temperature difference between spot weld and sheet		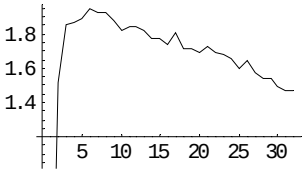	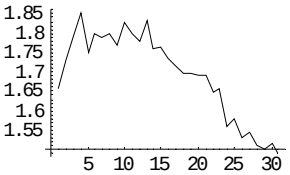
7. Maximum gradient	0.13488	0.134398	0.153436

Figure 2. Data post-processing techniques applied to thermographic images of resistance spot welds. Columns correspond to satisfactory, undersized, and stick welds.

can more accurately visualize defects at depth with clearer defect contours than can maximum-contrast images. In the case of spot welds, the maximum-phase image appears to be a good indicator of how well the two sheets are connected. Cold welds exhibit a different phase behavior because part of the thermal energy is reflected at the sheet interface instead of propagating into the second sheet through the nugget. This behavior can also be seen in the maximum-contrast images, where the maximum contrast occurs earlier in a cold weld than it does in a good weld.

Analogous to the calculation of maximum phase, the maximum amplitude is calculated for each pixel. This technique does not appear to return any valuable information about weld quality.

Initial results indicate that maximum-contrast images can be a good indicator of weld-nugget diameter but are not reliable in distinguishing cold welds from good welds in galvanized steel. Zinc solder zones that occur in welding galvanized steel show up in these images and, in the case of cold welds, contribute to the overall apparent size of the weld. The zinc solder zone also causes strong temperature gradients, making it impossible to use

gradient magnitude as an indicator of weld size in galvanized steel. It appears that good welds actually have smaller outlines in the gradient image than undersized and cold welds, perhaps because of higher temperatures present during welding that burn away the zinc in close proximity to the nugget.

The maximum-phase images appear to be a reliable indicator of cold welds. In this case, part of the thermal energy is reflected at the sheet boundary, leading to a difference in the phase response compared with satisfactory welds.

Conclusions

Initial results of round-robin testing performed to evaluate commercially available ultrasonic systems suggest that with well-trained operators and extensive calibration with intact and peeled samples, the systems can produce acceptable results.

Acoustic microscopy images exhibit a persistent feature that appears to correspond to the weld-nugget diameter measured on peeled samples. If this relationship can be confirmed, then acoustic microscopy will be able to provide a nondestructive way to calibrate acoustic experiments and confirm the quality of test specimens.

Several post-processing techniques were applied to thermographic images. Results show that it is possible to evaluate spot-weld quality based on the images. As is true with ultrasonic techniques, it is easier to evaluate welds in uncoated steel than in galvanized steel. Successful use of the techniques requires calibration using welds of known quality to set processing parameters.

Publications

Deborah Hopkins, Daniel Türler, Seiji Nakagawa, Kurt Nihei, and Guillaume Neau, "On-Line Nondestructive Inspection Techniques for Lightweight Automotive Structures," Society of Automotive Engineers, Paper no. 00FCC-124, 2000.

Daniel Türler, Frédéric Reverdy and Deborah Hopkins, "Nondestructive Evaluation of Spot-Welded and Weld-Bonded Joints," submitted to the Society of Automotive Engineers, 2002.

Guillaume Neau, Deborah Hopkins, Seiji Nakagawa, and Kurt Nihei, "Complications of Using Resonance-Frequency Shifts to Detect Defective Joints," to appear in Vol. 19 of *Review of Progress in Quantitative Nondestructive Evaluation*, D. O. Thompson and D. E. Chimenti, eds.

Daniel Türler, "Predicting the Geometry and Location of Defects in Adhesive and Spot-Welded Lap Joints Using Steady-State Thermographic Techniques," in *Proc. SPIE the International Society for Optical Engineering*, Vol. 3700, Dennis H. LeMieux and John R. Snell, Jr., eds., 1999.

Daniel Türler, Deborah Hopkins, Seiji Nakagawa, António Valente, and Kurt Nihei, "Thermographic and Acoustic Imaging of Spot-Welded and Weld-Bonded Joints," *Review of Progress in Quantitative Nondestructive Evaluation*, **18**, D. O. Thompson and D. E. Chimenti, eds., 1999.

Kurt Nihei, Seiji Nakagawa, and Deborah Hopkins, "Defect Detection Using the Reverberant Wavefield," *Review of Progress in Quantitative Nondestructive Evaluation*, **18**, D. O. Thompson and D. E. Chimenti, eds., 1999.

Deborah Hopkins, Seiji Nakagawa, Kurt Nihei, and Daniel Türler, "Imaging Flaws in Adhesive Joints Using Acoustic Techniques and Infrared Thermography," in *Review of Progress in Quantitative Nondestructive Evaluation*, **17**, D. O. Thompson and D. E. Chimenti, eds., 1998.

M. Technical Cost Modeling

Principal Investigator: Sujit Das
Oak Ridge National Laboratory
Oak Ridge, TN, 37831-6073
(865) 574-5182; fax: (865) 574-3851; e-mail: dass@ornl.gov

Technology Development Manager: Joseph A. Carpenter
(202) 586-1022; fax: (202) 586-1600; e-mail: joseph.carpenter@ee.doe.gov
Field Technical Manager: Philip S. Sklad
(865) 574-5069; fax: (865) 576-4963; e-mail: skladps@ornl.gov

Contractor: Oak Ridge National Laboratory
Contract No.: DE-AC05-00OR22725

Objectives

- Address the economic viability of new and existing lightweight materials technologies.
- Develop technical cost models to estimate the cost of lightweight materials technologies.

Approach

- Address the economic viability of lightweight materials technologies supported by Automotive Lightweighting Materials (ALM).
- Use cost modeling to estimate specific technology improvements and major cost drivers that are detrimental to the economic viability of these new technologies.
- Derive cost estimates based on a fair representation of the technical and economic parameters of each process step.
- Provide technical cost models and/or evaluations of the "realism" of cost projections of lightweight materials projects under consideration for ALM Program funding.
- Examine technical cost models of lightweight materials technologies that include (but are not limited to) aluminum sheet; carbon fiber precursor and precursor processing methods; fiber-reinforced polymer composites; and methods of producing primary aluminum, magnesium, and titanium and magnesium alloys with adequate high-temperature properties for powertrain applications.

Accomplishments

- Assessed the benefits attributable to three recently completed R&D projects funded by the ALM program
- Examined the cost of a carbon-reinforced composite automotive part

Future Direction

- Update the cost assessment of primary magnesium production technologies.
- Explore the economic viability of a carbon-fiber-composite–intensive body-in-white (BIW) part using alternative competing manufacturing technologies.
- Continue individual project-level cost modeling to identify specific technology improvements and major cost drivers that are detrimental to the economic viability of these technologies.

Major Accomplishments

The major accomplishments included the cost and benefit assessment of research and development (R&D) projects supported by ALM. The cost assessment focused on a carbon-reinforced-composite automotive part. Three recently completed ALM R&D projects were selected for the benefit assessment.

Benefits Estimates

Three methods developed during a prior similar study during FY 2001 were used to estimate benefits attributable to ALM R&D projects. The three methods were qualitative assessment, National Research Council indicators, and benefit-cost analysis, a combination of which addresses all-important aspects of the benefits of R&D projects. The qualitative assessment addresses short-term project outcomes at the project level. The indicators address standard measures associated with the quality of research projects. The benefit-cost analysis addresses both short-term and long-term benefits associated with commercializing new technologies. Since ALM projects encompass both the creation of new knowledge and the commercialization of new technologies, both the indicator and benefit-cost approaches were found to be appropriate for a comprehensive benefits assessment.

Three ALM R&D projects were evaluated using these benefit assessment methods: design and product optimization for cast light metals, durability of lightweight composite structures (report 7A), and rapid tooling for functional prototyping of metal mold processes. The three projects assessed all appear to have yielded high levels of benefits. In the qualitative assessment, all met their technical goals, increased knowledge, and led to increased collaboration. In one case, the private-sector participants indicated that they would not have participated in the R&D effort without federal funding; in the other two cases, some participants would have proceeded with R&D but with considerably less funding. With respect to the National Research Council indicators, the number of publications varied considerably, based primarily on the number of private-sector partners involved in the R&D effort. Some 32 organizations collaborated in the cast light metals project, while only one national laboratory and the Big 3 automakers joined in the project on durability of composite structures. The total number of publications ranged from 8 to 44 for these three projects. The study participants perceived that each R&D project improved U.S. international competitiveness; however, there were mixed views about whether the United States is leading in R&D for these areas.

The benefit-cost analysis yielded impressive benefit-to-cost ratios, which calculated the monetary benefits in energy efficiency, environmental protection, and energy security based on the estimated market penetration of the technologies as a result of the projects. Figure 1 shows the market forecasts for die castings resulting from rapid tooling for functional prototyping of metal mold processes, which were used to estimate benefits and costs. These benefit-cost ratios were calculated for three scenarios, reflecting a range of monetary values assigned to energy and emissions in the literature. In the moderate-case scenario, the benefit-cost ratios ranged from 63 to 211; the rapid tooling and the effort to improve the durability of lightweight composite structures represent the lower and upper limits, respectively. To improve the assessment of long-term benefits, publications and market penetration rates should be periodically revisited, and case studies should be undertaken to identify any valuable spin-off technologies.

Cost Estimate

The cost estimation is a part of an ongoing effort to develop a composite-intensive BIW structure by the Automotive Composites Consortium (ACC), a pre-competitive R&D partnership in collaboration with ALM. The ACC project objective is to design, analyze, and build a composite-intensive BIW offering a minimum of 60% weight savings over steel at a cost close to that of steel, while meeting manufacturing, assembly, crashworthiness, and performance objectives (see report 4B). A body side inner weighing 16.6 lb was the part under consideration, using the programmable powder preform process (P4) and structural reaction injection molding as preforming and molding technologies, respectively (report 4A). The part cost-assessment focus was on the production cost and on providing the bases for cost sensitivity analysis and

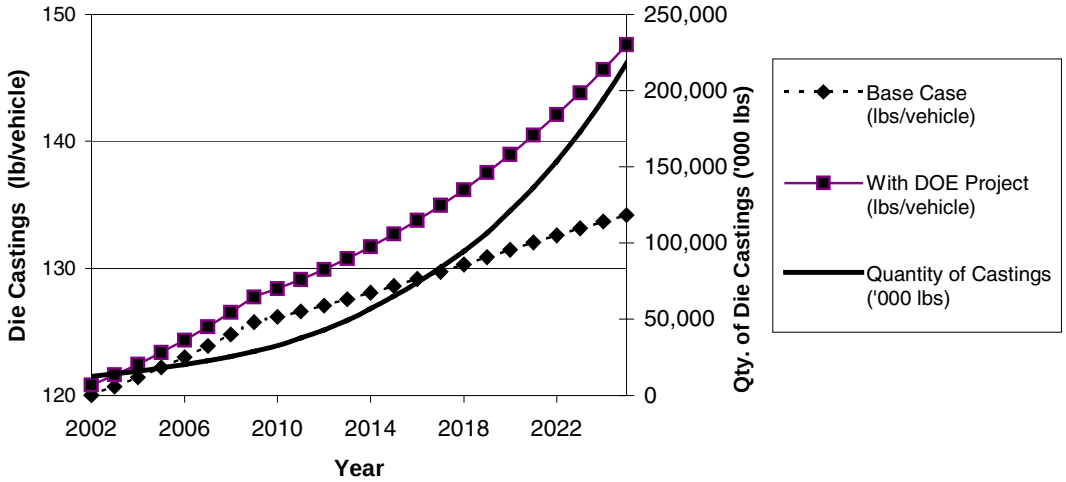

Figure 1. Market forecasts for die castings resulting from rapid tooling for functional prototyping of metal mold processes.

comparison with other processes, instead of an accurate assessment of absolute part cost. A cost modeling framework was also developed for examining the economic viability of various manufacturing options for producing composite BIW parts, including the cost estimation of a complete BIW.

The baseline production cost of a body side inner is estimated to be $88.53/part or $5.33/lb, and the contribution of material was the highest, i.e., 60% of total cost. A significant reduction in carbon fiber cost, from $8/lb to $2/lb, is expected to lower the part cost from $113.86 to $63.21. Besides material cost, other factors—i.e., production volume and cycle time—previously found to be detrimental to the economic viability of composites were found to be applicable in this case also, as shown in Figure 2. A minimum production cost was achieved around an annual production volume of 75 K, and a cycle time of 2 min instead of 3.5 min would lower the part cost from $88.53 to $75.33. A part cost range of from $59.58 to $140.87 was estimated when the five key input variables were maintained at their low and high values.

Even with a significant reduction in carbon fiber cost, the per-pound production cost of a body side inner made from carbon-reinforced polymer composite may not be cost-effective compared with the similar conventional steel part. But an examination of the economic viability of a single BIW part using a specific manufacturing technology does not provide a complete assessment of the economic viability of using carbon-fiber-reinforced polymer composites for the BIW. A part-by-part substitution is not a fair comparison in this case because it fails to capture the part consolidation and the net-shape processing characteristics of composites. It is appropriate to consider the complete BIW, even when considering only a single manufacturing process for all BIW parts, because doing so allows the analysis to take into account the optimization of capital and tooling requirements that may result when similar BIW parts are properly grouped and are manufactured in the same production facility. In addition, on a specific-part basis, other manufacturing technologies that satisfy both the cost reduction potential and technical requirements need further consideration to explore the potential economic viability of a complete carbon-reinforced-composite BIW.

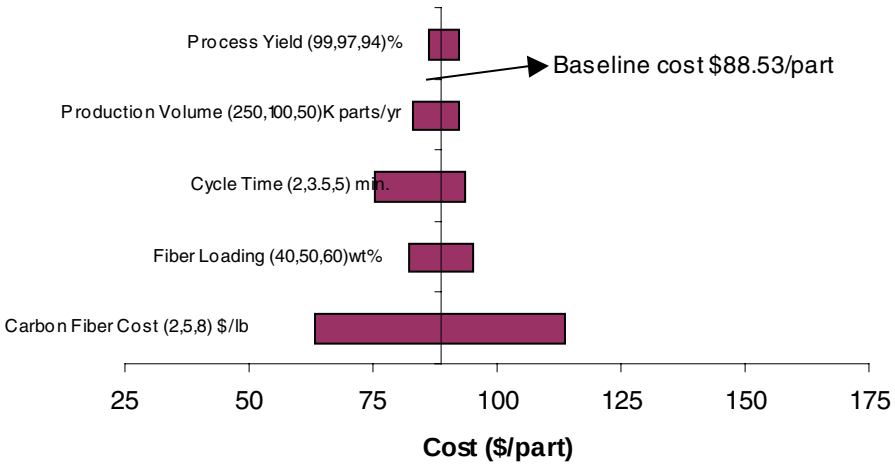

Figure 2. Body side inner cost sensitivity to key input variables.

8. HIGH-STRENGTH STEELS

A. Modeling of High-Strain-Rate Deformation of Steel Structures

Principal Investigator: Srdan Simunovic
Oak Ridge National Laboratory
Oak Ridge TN 37831-6359
(865) 241-3863; fax: (865) 574-7463

Technology Development Manager: Joseph Carpenter
(202) 586-1022; fax: (202) 586-1600; e-mail: joseph.carpenter@ee.doe.gov
Field Technical Manager: Philip S. Sklad
(865) 574-5069; fax: (865) 576-4963; e-mail: skladps@ornl.gov

---

Contractor: Oak Ridge National Laboratory
Contract No.: DE-AC05-00OR2275

Objective

- Develop numerical modeling guidelines to realistically assess the influence exerted by the properties of strain-rate-dependent materials in crashworthiness computations.

Approach

- Model dynamic loading problems using diverse combinations of modeling approaches (sub-models) that are essential in describing strain rate sensitivity in computational simulations. Sub-models to be examined include finite element method (FEM) formulations, constitutive materials models, material properties under different strain rates and loading conditions, and contact conditions, as well as material property changes caused by component processing.

Accomplishments

- Designed and conducted the high-strength steel (HSS) tube crush experiments at the GM Proving Grounds.
- Developed a strain-rate-dependent constitutive model (LSDYNA Model 24 tabulated strain rate curve data) for high-strength low-alloy (HSLA) 350 and dual-phase (DP) 600 steels
- Investigated and documented the effects of initial imperfections in the tubes and crush test setup on the mode of deformation of HSS tubes
- Developed programs for evaluation and visualization of tube collapse modes.
- Developed an experimental setup for tube crush tests in the intermediate strain rate machine based on the dominant imperfection in tube geometry.
- Developed an experimental setup for a new crashworthiness characterization test based on parallel plates buckling (test under way at the University of Dayton Research Institute).
- Determined peak force in tube crush and material information needed for accurate modeling of progressive collapse.
- Determined modeling approaches for accurate modeling of circular steel tubes.

Future Direction

- Conduct and analyze crush experiments (parallel plates and tube crush).
- Develop experimental guidelines based on those two tests.
- Determine optimal FEM formulations for modeling of crushing of rectangular tubes.
- Develop an experimental program for crushing of rectangular tubes.
- Develop modeling guidelines for rectangular tubes.
- Model damage in HSS.

Abstract

This project deals with the effects of various approaches for modeling of strain rate effects for mild steels and HSS on impact simulations. The material modeling is discussed in the context of the FEM modeling of progressive crush of energy-absorbing automotive components. The characteristics of piecewise linear plasticity strain-rate-dependent material models are analyzed, and various submodels for modeling of impact response of steel structures are investigated. The ranges of strains and strain rates that are calculated in typical FEM models for tube crush and their dependence on the material modeling approaches employed are reported. The models are compared with the experimental results from drop tower tests.

Introduction

Strain rate dependency of steels,[1] although long recognized and documented as an important effect,[2,3] has been more widely used in crash models only in the past few years.[4–6] Until recently, computational resource limitations dictated a size of the finite elements that could not conform to the detailed features of the vehicle crush. Large finite element sizes made the structures relatively stiff, so that the strain rate dependency was just one of the effects that was obfuscated by the heuristic modeling rules that were shown to give a good correlation with experiments.[3] With the increase in computational power, accompanied by the increasing FEM mesh density, it became possible for vehicle model components to conform to the actual physical deformation. However, without accounting for the strain rate sensitivity, finely discretized FEM models tend to soften as the element density increases. To counter this softening trend and, moreover, to model the physics of the process more accurately, the strain rate effects must be taken into account. In addition to better representation of the material response, strain rate sensitivity has an added benefit in promoting computational stability of simulations.[7] Pathological FEM mesh sensitivity, so characteristic of modeling of localized deformations, is reduced when strain-rate-sensitive materials are used. Material rate dependence introduces a length scale that is proportional to the length of propagation of elastic waves. This length scale has a physical character[7,8] as opposed to the length scale imposed by the element mesh spacing that governs the localization response when a rate-independent material model is used. For added accuracy and numerical stability, the constitutive model may also need to be modified to include viscosity, initial, and deformation-induced anisotropy, and other effects. Such model modifications are outside the scope of this paper. In our study, standard assumptions of isotropy, isotropic hardening, constant volume plastic deformation, and radial return plasticity are used; and only the strain rate dependency has been investigated for its influence on the crash simulations. It is assumed that accurate strain fields are readily available for the evaluation of constitutive material models. Nevertheless, numerical simulations will illustrate some of the issues of modeling of localized deformation and their interaction with the material model.

Determining the strain-rate-dependent properties of steel has not been a simple proposition. The range of strain rates in automotive impact spans several orders of magnitude (i.e., 10^{-3}/s to 10^{+3}/s).[9] One of the principal difficulties is interpretation and reconciliation of the data obtained from different experimental apparatus. In addition, the material properties in the strain rate orders of magnitude between 10^{+1}/s and 10^{+2}/s have been very difficult to obtain.[9–12] Interestingly enough, this is the range

where important vehicle crash events take place.[12] New experimental equipment for this range has recently been developed.[11] It revealed the importance of material effects that were not considered in crash modeling before. In addition, new structural tests,[13,14] accompanied by FEM models, have shown how structural experiments can be used for material characterization for the deformation modes of interest. Direct, coupon-level, experimental investigation of the strain rate dependency under generalized states of stress is still not practically possible, and structural tests combined with the FEM modeling are likely to provide sufficient information for the current modeling practices.

The paper is organized as follows. In the next section, general discussion on progressive crushing of tubular components is presented. Then, the current state of affairs in material modeling of strain rate effects in automotive crash is reviewed. The focus of the paper is on modeling strain rate effects using the material model based on piecewise linear plasticity. This model is used because of its prevailing use in automotive practice and its flexibility in representing complex material behavior as a function of strain and strain rate. The following section deals with effects of strain rate sensitivity and material modeling approaches on simulated plastic strains and strain rates in the axi-symmetric tube crush. Next, non-symmetric crushing of circular tubes in drop tower experiments for HSLA and DP circular tubes is modeled and compared with the experimental results. The range of strains and strain rates from crush simulations is summarized in the conclusions.

Modeling of Deformation in Tube Crushing

The response of metals under multiaxial states of stress and varying strain rates is still far from being described by a unified theory. During multi-axial, large plastic deformation, material undergoes significant changes of microstructure and texture[1,15] that lead to changes in material properties on the macroscopic level. From a practical standpoint, the goal is that the selected material model is applicable to the range of loading and deformation for the problem at hand. In tubular crush devices that are used as energy absorbers in vehicles, metallic sheets are subjected to large, localized deformations that organize into global collapse mechanisms.[16] For a long time, analytical and semi-analytical methods (see ref. 16 for review) were the only feasible routes for analyzing progressive structural collapse. The methods start from simplifying kinematics assumptions and idealization of material response, and derive the expressions for the structural response based on energy minimization principles. The advances in FEM and computational power have provided a framework where constraints of analytical approaches can be largely eliminated, and far more complex deformation and material responses can be modeled.

The standard practice for extracting strain-rate-relevant material parameters is to perform experiments with uniaxial loading configurations.[17,18] The ductility of uniaxial tensile loaded specimens is limited by the geometric instability. For automotive steel sheets, the magnitude of uniform plastic strains is limited to about 20%. However, the strains that are measured[13,14] and modeled[19] during tube crushing far exceed this limit. The physical reality of large deformations is not in question.[19] The biaxial loading and bending provides additional stability that allows the utilization of a material's strain hardening, ductility, and correspondingly large energy dissipation. The magnitude and distribution of plastic strains, large curvatures, and shifting of the neutral axis during fold formation clearly places the problem into the realm of large deformations.

Modeling of tube folds is the area where material models and finite element formulations are intrinsically linked. When shell elements are used to model tube crush, the issue of finite element resolution comes down to the number and type of bi-linear shell elements[20] that are used for modeling of a plastic fold. The experimentally measured curvature of full plastic folds is of the order of the material thickness. For the fold representation to be accurate, the element length should approach the shell thickness. It is at this point that the assumptions of the standard shell theory are stretched beyond their limits[19] and material models extrapolate far outside the experimentally verified range. On the other end of the spectrum, when the finite element resolution is fairly coarse (of the order of kinematic elements in analytical models), the material model extrapolation into large strains is not a concern because the strains get smeared over larger volumes and are within the range of uniaxial

experimental data. However, the kinematics of the deformation are compromised.

In both of the above FEM meshing scenarios, in order to match the experimental results with models, material model parameters are commonly modified in engineering simulations. While the practice may be appalling to material scientists, the justification for modification in one case is to compensate for the inability to represent local deformations, and in the other, to account for the significance of the large strain region for which experimental data are not available. The flexibility of computer programs now even provides methods for definition of optimization problems where the material parameters are determined so that they result in the optimal match between simulations and experiments[21] for crush measures such as impact force history and deceleration. These approaches are linked to specific structural problems, FEM mesh configurations, and loading situations. A more rigorous approach would be to make sure that the FEM element resolution and element formulations are sufficient for accurate kinematic representation of the problem, and then focus on compatible material modeling approaches.

Material Models for Strain Rate Sensitivity

Currently, the most commonly used approach to modeling strain-rate sensitivity in progressive crushing is to use isotropic plasticity models with a rate sensitivity component that has moderate requirements on the experimental program. The models that are frequently used for tube crush simulations are the Johnson-Cook model,[22] the Zerilli-Armstrong model,[23] and the piecewise linear strain-rate-sensitive material model.[24] The models are appealing because they have been implemented in commercial codes used for crash simulations and have a limited number of material parameters (≤6) that must be determined by experiments.

The strain rate sensitivity of body-centered cubic (BCC) materials is attributed to the rate-controlling mechanism of the thermal component of the flow stress.[1] Since the activation volume for BCC metals is considered to be constant, the increase in strain rates should theoretically be described by an upward translation of the quasi-static strain-stress curve. Experimental results for mild steels and HSS show that the strain hardening rate decreases with an increase in strain rate, and the case of constant hardening rate can be viewed as a limiting case. The Johnson-Cook material model is expressed in multiplicative form of strain, strain rate, and temperature terms:

$$\sigma = (A + B\varepsilon^n)\,(1 + C \ln \varepsilon\grave{Y})\,(1 - T^{*m}) \qquad (1)$$

where A, B, C, n, and m denote material constants, and T^* is homologous temperature. The consequence of the multiplicative form is that the strain hardening rate at a certain strain will increase when the strain rate increases. The strain-stress curves for increasing strain rates will tend to "fan out,"[25] which is in contrast to the experimental results for steel sheets. The material parameters can be selected so that strain hardening variations are insignificant. However, the model still cannot accommodate the global trend of reduction of strain hardening rate with increasing strain rate. Mehadevan et al.[4] reported that the Johnson-Cook model gave better results than the Zerilli-Armstrong in the crush analysis, although the assertion was linked to the element resolution and fit of the material model to the specific regions of experimental data. Their results illustrate a complex interplay between mesh resolution, deformation, and dominant ranges of strain and strain rates.

The Zerilli-Armstrong model for BCC metals is written in additive form akin to standard materials science expressions for flow stress as an aggregate of various strengthening mechanisms:

$$\sigma = C_0 + C_1 \exp\,(-C_3 T + C_4 T \ln \varepsilon\grave{Y}) + C_5\varepsilon^n \qquad (2)$$

where C_i and n denote material parameters, and T is the absolute temperature. The strain hardening in the Zerilli-Armstrong model is constant across the strain rates; therefore, the corresponding strain-stress curves are parallel. The correlation of yield stresses[4,25] with the Zerilli-Armstrong model has proved to be very good. However, the inherent inability to model the dependence of strain hardening on strain rate will unavoidably lead to adjustment of the element discretization and selection of specific strain intervals for material parameter derivation, as it does for the Johnson-Cook model. The focus on strain hardening is due to its crucial role in development of collapse pattern and bifurcation between crush modes.[26] Material models such as Bodner-Partom[27] and Khan-Huang[28] can offer added flexibility for modeling of strain

hardening, but they have not yet been widely implemented in commercial crash codes.

The most commonly used strain-rate-dependent material model in automotive engineering practice is the piecewise linear plasticity model. The model was used in this study because of its relevance to automotive crash modeling and flexibility for representation of strain rate sensitivity. In this approach, effective strain-stress curves are directly fed into the material models and require the least amount of effort for material model development. In simulations, for a given rate of strain (total or plastic), the resulting stress in the plastic region is linearly interpolated between the stress-strain values that were experimentally determined in strain rate tests. The blessing and the curse of this approach is that the model fits experimental data exactly, and whatever testing artifacts or errors are contained in the experimental data will be carried over to the simulations. The highest strain rate in the experimental data acts as a saturation plateau for strain rate effects. Typical experimental true plastic strain-stress data for various strain rates for drawing quality special-killed steel were developed by the Auto/Steel Partnership[29] and are shown in Figure 1.

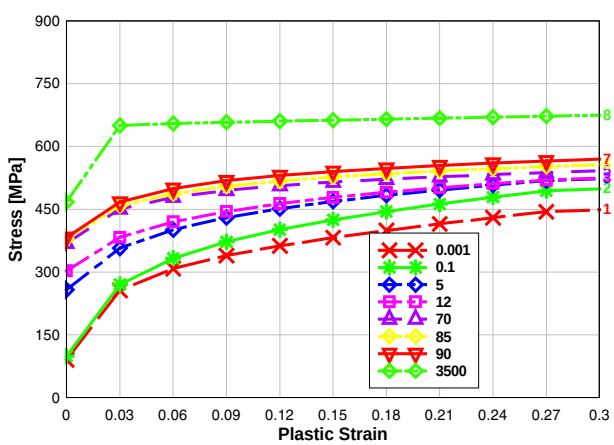

Figure 1. Drawing quality special-killed material data.

Important aspects of implementation of the piecewise linear plasticity model are the maximum strain rate for which the stress-strain data should be tested, and the number and arrangement of curves across the strain rate range. The data in Figure 1 contains all the available curves. The material model uses linear interpolation between the curves whereas it has been shown that the stress increment relation is logarithmic.[30] In the case when sufficient experimental data are available, the effects of linear interpolation should not be significant. Later in the article, it will be shown that adding logarithmically interpolated curves improves the model accuracy when experimental data is not available for the intermediate strain rates of 10^{+2}/s magnitudes. As also shown later, maximum calculated strain rates for crashworthiness simulations are of the order of 10^3/s so that an experimental strain rate of that order would suffice as an upper rate limit for the model.

Modeling of Strains and Strain Rates in Axisymmetric Crushing of Steel Tubes

The objective of our study on axisymmetric crushing was to investigate the trends and magnitudes in plastic strains and strain rates as calculated by the finite element program. As stated above, this information is important in deciding the extent of the experimental program for derivation of material models.

A simulation of a typical axi-symmetric tube crush experiment is shown in Figure 2. A tube is clamped on the bottom and is impacted on the top with a moving mass. The experimental configuration from ref. 31 was used. The tube is made of mild steel that is modeled using a piecewise linear plasticity model with strain-rate-tabulated curves as shown in Figure 1. Tube thickness is 1.2 mm, radius 28 mm, and tube length 180 mm.

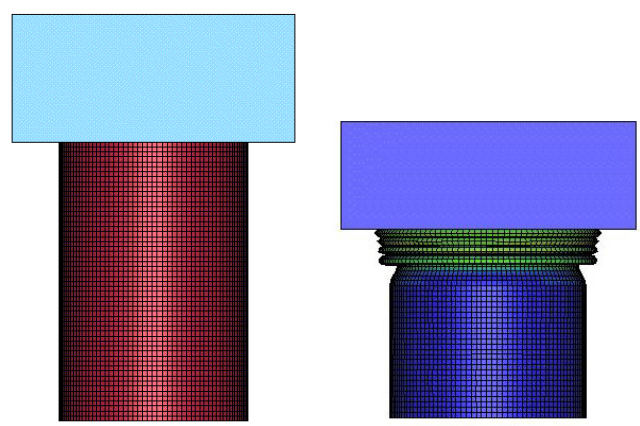

Figure 2. Tube crush test.

Because of the axial symmetry, the problem can be simplified by modeling a radial segment of the tube. The tube is modeled by a 2° wide cylinder segment with symmetry boundary conditions imposed on the radial sides. This results in a

characteristic shell element length in the circumferential direction of 0.98 mm, less than the tube thickness, so that the computational time increment will remain the same across different tube discretizations. Figure 3 shows the deformed tube segment for simulations using material with and without strain rate sensitivity. It is clear that the material strain rate sensitivity has a significant effect on the overall shortening of the tube.

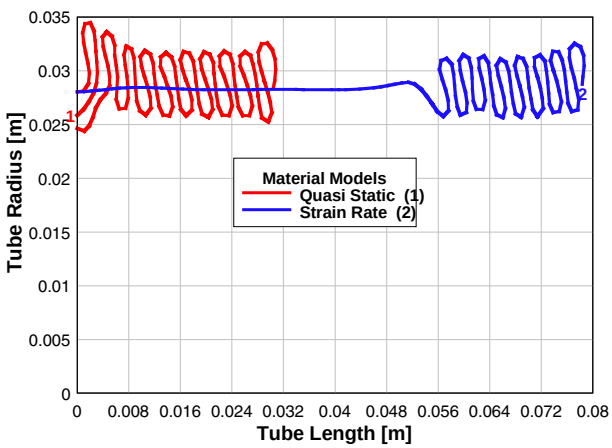

Figure 3. Deformed tube segment.

Element Discretization

In order to investigate the effect of the FEM element discretization on the deformation and strain distribution, we performed simulations with 23, 46, 92, and 160 elements. The length of an element in the 23-element configuration corresponds to the half-length of the fold in analytical models.[16] Figure 4 shows the final deformation of the tube for different element discretizations. For the case when 23 elements are used across the tube length, the FE mesh is apparently too coarse to describe the resulting crush mode. As a consequence, when the entire circumference of the tube is modeled, the crush mode will not be axisymmetric or regular. For the case when 46 elements are used along the tube length, the general features of the crush are acceptable, but the folds do not have smooth geometry. For 92 and 160 elements the deformation is smooth and in agreement with the fold features from the experiments.

The effect of element discretization is better illustrated when the shell directors are analyzed. Figure 5 shows the deformed configurations for increasing mesh density, together with the respective

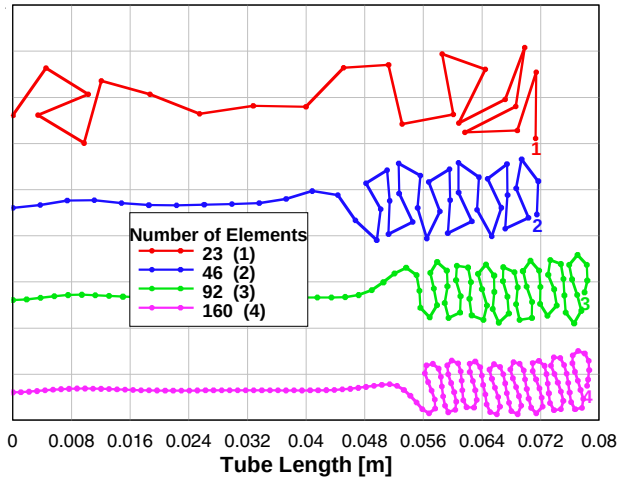

Figure 4. Deformed configurations for different FEM element discretizations.

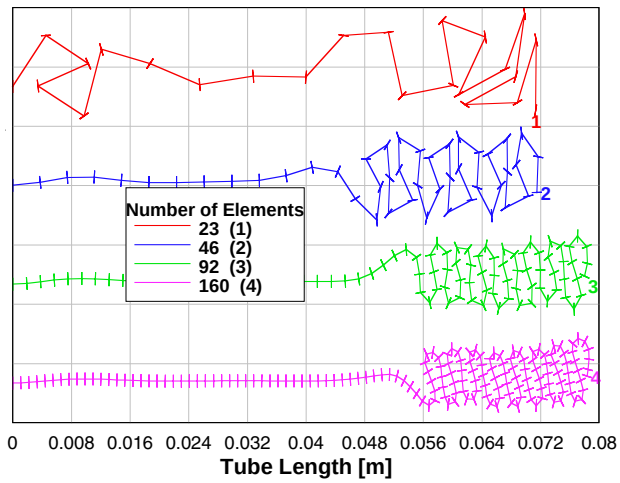

Figure 5. Shell directors for different element discretizations.

shell directors. The two coarsest meshes have large rotations of the directors that lead to poor description of strain fields.

In the case when 160 elements along the length are used, the element length is of the order of element thickness. The experimentally measured curvature of the tube fold is also of the same order. The curvature distributions along the undeformed length of the tube for different element discretizations are shown in Figure 6.

Strain Rates

Crashworthiness simulations are done almost exclusively using FEM programs with explicit time

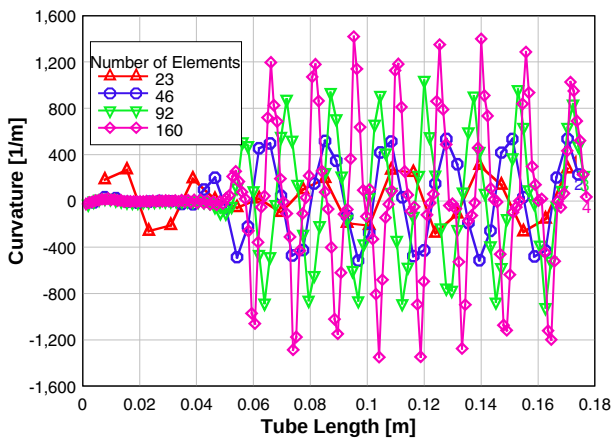

Figure 6. Curvature of the tube for different element discretizations.

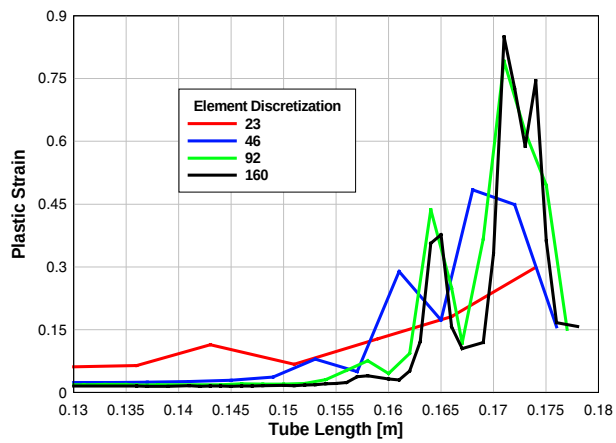

Figure 7. Maximum plastic strain distribution mapped on the original tube length.

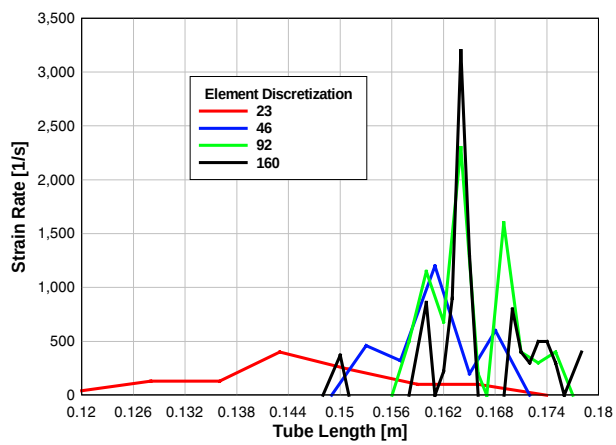

Figure 8. Maximum plastic strain rate distribution mapped on the original tube length.

integration.[24] The explicit time integration algorithms are only conditionally stable, which means that the integration time step must be smaller than the time for a disturbance to travel across the smallest finite element in the model. For example, for steel and a finite element characteristic length of 5 mm, this condition requires that the time step be smaller than 1 microsecond. The material constitutive relations and strain rates are calculated at this smallest time scale where wave propagation effects are important. The experimental data are determined on the higher time scales where the wave effects are not measured except for the experiments with highest rates. Therefore, it is important to determine the values of the strain rates in the explicit time integration calculations in order to define the extent of the required material experimental characterization program. FEM formulations and element discretization affect the magnitude and distribution of plastic strains and strain rates in the areas of large plastic deformations that determine the crush mode. It is also important to investigate these effects, since they can then be correlated to the tube crush experiments.[14]

The simulations show the clear dependence of the strain rate calculations on the element discretization. Characteristic plastic strains and plastic strain rates for different element discretizations at the time of formation of the second fold are shown in Figures 7 and 8.

Contrary to the plastic strains that tend to monotonically increase, strain rates exhibit intermittent bursts of activity in the area of evolving plastic folds. The strain and strain rate distributions for the 92- and 160-element discretization seem to stabilize in magnitude and distribution. The maximum strains are slowly changing in time, while strain rate curves violently oscillate as a result of passing disturbance waves in the structure[8] and the material model that is based on total strain rate.

When the material model uses plastic strain rate as the basis for stress calculation (VP = 1 in the LS-DYNA3D parlance),[32] the dynamics of strain rate distribution drastically change. The strain rates in the model oscillate much less compared with the situation where total strain rate is used. This is illustrated in Figures 9 and 10, respectively. The figures show the sequences of strain rate distributions for a 92-element mesh for ten time instances around a 3 ms simulation time that are about five computational time increments apart. The

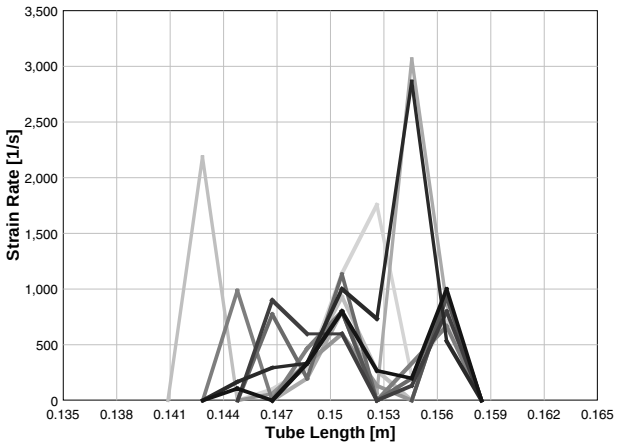

Figure 9. Strain rate history for material model based on total strain rate.

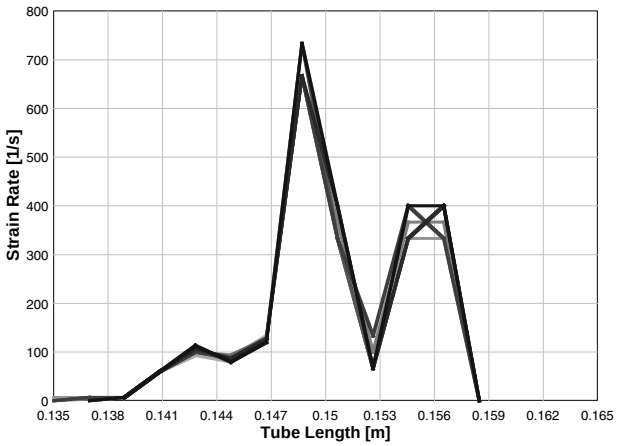

Figure 10. Strain rate history for material model based on plastic strain rate.

shade of gray for the curves denotes the time sequence in the increasing order. For a material model based on total strain rate in Figure 9, strain rate distributions vary significantly; in Figure 10, the variation in strain rate history is much more gradual.

The strain rate history from the model based on plastic strain rate in Figure 10 appears to be more physically realistic than the one for the model based on total strain rate. In the case of the model based on plastic strain, the strain rates change more gradually throughout the simulation and have strain rate magnitudes that rarely exceed the experimentally available values.

HSS Circular Tube Crush Experiments

Although notorious for its imperfection sensitivity[33,34] and abundance of crush modes of seemingly identical energy,[35] circular tube crushing can be used not only to verify the modeling methods but also to investigate the important material properties. The in-depth review of the experimental procedures for buckling of thin tubular structures can be found in recent monographs on the subject.[33,34]

In this project, HSS materials HSLA350 and DP600 were selected for drop tower experiments in order to investigate the accuracy of the constitutive models based on the piecewise linear plasticity model and various modeling approaches. The tests were modeled before the actual physical experiments to determine the test parameters. A test configuration for the HSLA350 steel tube and the final deformed shape are shown in Figures 11 and 12. The tube with a radius of 50 mm, thickness of 1.6 mm, and length of 160 mm was welded to the base plate, which was bolted to the test fixture. The drop weight of 315 kg impacts the tube at 6.39 m/s.

Figure 11. Test configuration.

Figure 12. HSLA350 tube at the end of experiment.

Force, acceleration, and high-speed photographs were recorded during the experiments.

Characteristic force-time traces from the HSLA350 tube crush experiment for two tests are shown in Figure 13.

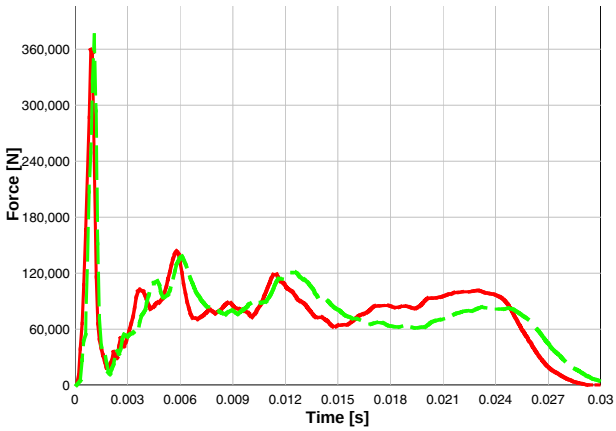

Figure 13. Force history for HSLA350 tubes.

The force-time diagram shows the characteristic peak followed by the force plateau associated with progressive tube folding. The HSLA350 tubes deformed in an anti-symmetric, triangular pattern. The anti-symmetric modes are principal mechanisms of deformation for the tube dimensions and the ranges of imperfections considered.

The deformed shape of the DP600 tube is shown in Figure 14. The tube radius was 40 mm, the tube thickness 1.24 mm, and length 120 mm. The weight of 315 kg and impact velocity of 5.6 m/s were selected to completely crush the tube without contacting the honeycomb stoppers. The corresponding force-time diagram for three samples is shown in Figure 15.

Similarly to the HSL350 tubes, the initial force peak is followed by the oscillations characteristic of the progressive crushing.

Piecewise Linear Plasticity Model for HSLA and DP Steels

Data from several testing methods have been used to develop the model parameters. The strain-stress curves for different rates are shown in Figures 16 and 17 for HSLA350 and DP600 materials, respectively.

The DP600 material has lower strain rate sensitivity than HSLA350. Also, the information was not always consistent for all strain rate levels of

Figure 14. DP600 tube at the end of experiment.

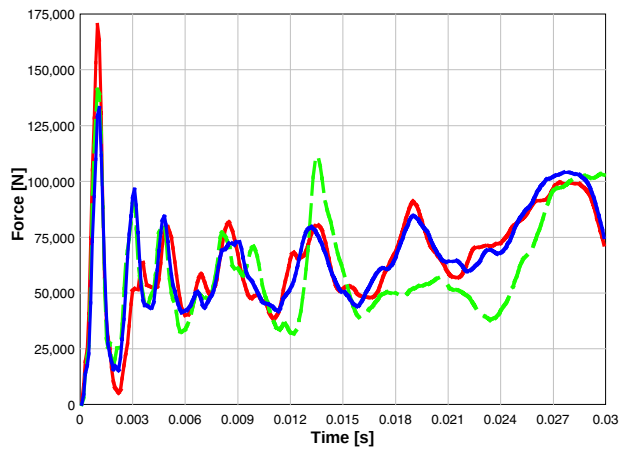

Figure 15. Force history for DP600 tubes.

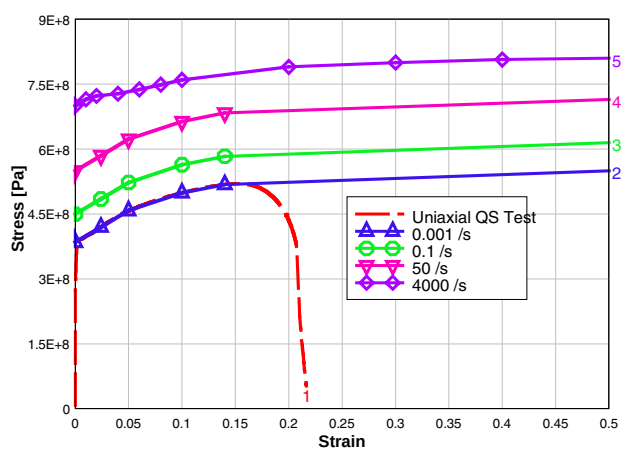

Figure 16. Material parameters for HSLA350.

magnitude between the minimum and maximum levels for HSLA350. Only the non-conflicting information has been used in the model. That resulted in having only stress-strain curves for

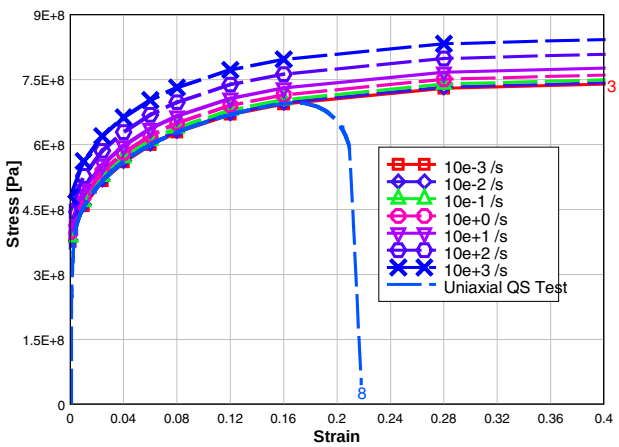

Figure 17. Material parameters for DP600.

strain rates of 50/s and 4000/s. However, it was shown in this study (see Figures 9 and 10) that the strain rate magnitudes of 10^{+2}/s are prevalent in the impact situations and mesh resolutions of interest. It was also shown that adding more stress-strain curves using logarithmic interpolation of strain rate magnitudes of 10^{+2}/s and 10^{+3}/s yields more accurate results and a smoother strain rate distribution history. In Figures 16 and 17, dashed curves show the results from the quasi-static uniaxial tensile experiments on material cut from the actual tubes.

Impact Simulations

Because of the imperfection sensitivity of circular tubes, it was necessary to incorporate imperfections into the models. The various modes and magnitudes of imperfections were considered to determine the controlling factors for tube fold formation. The main purpose was to investigate the relative influence on crush behavior of the various types of imperfections that were present in the tubes. It was determined that the tube height (or equivalently the loading plate angle) have dominant influence on tube crush for the imperfection ranges in the tubes. This finding is in agreement with experiments reported in the literature.[36] For a perfect tube and perfect loading conditions, the model predicts that the tube deforms by several axi-symmetric folds before it bifurcates into an anti-symmetric pattern. However, in the real world, imperfections are always present and tubes quickly bifurcate into anti-symmetric modes. The tubes were modeled using fully integrated shell elements (shell type 13 in LS-DYNA3D) with an element size equal to 1.9 element thicknesses. The comparison of the HSLA350 drop tower model with characteristic imperfections and the experiment is shown in Figure 18.

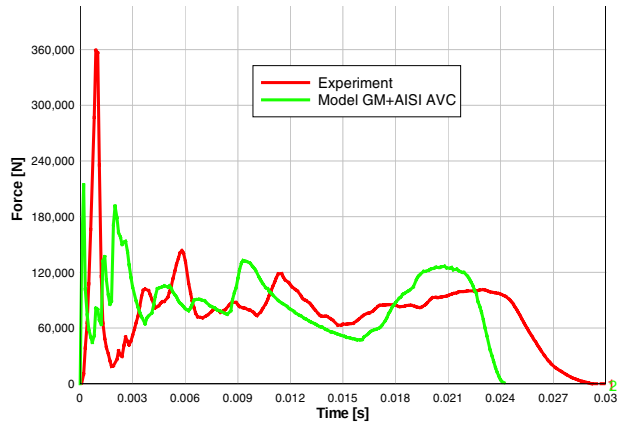

Figure 18. HSLA350 drop tower simulation.

The model for the HSLA350 tube underestimates the initial peak of the impact force. The remaining process of tube crushing shows relatively good agreement with the test. The initial increased flexibility of the system in the experimental data is a result of the details of the experimental setup (trigger strip, plywood and steel plate sandwich on drop mass) that were not included in the model. Figure 19 shows the force time diagram comparison for the DP600 tube. In this case, the model gives a good estimate of the initial force peak.

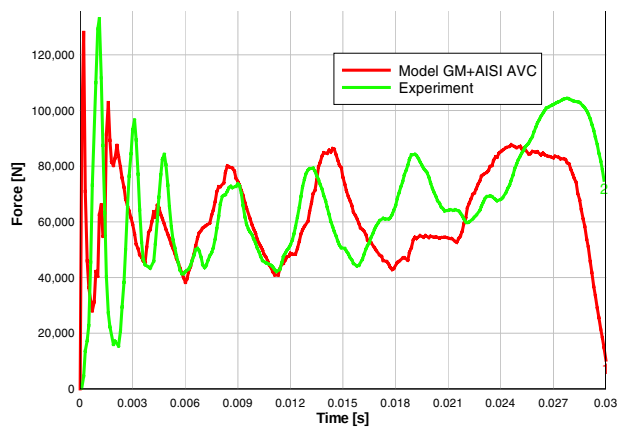

Figure 19. DP600 drop tower simulation.

The possible reasons for the discrepancy in the ability to model the force peak in the two different materials can be a result of different strain hardening

in the materials and the lack of modeling upper and lower yield point[37] in the HSLA350 tubes. The predicted tube collapse shape for HSLA350 tubes is shown in Figure 20. The folding pattern is square, whereas the tests exhibited the triangular pattern.

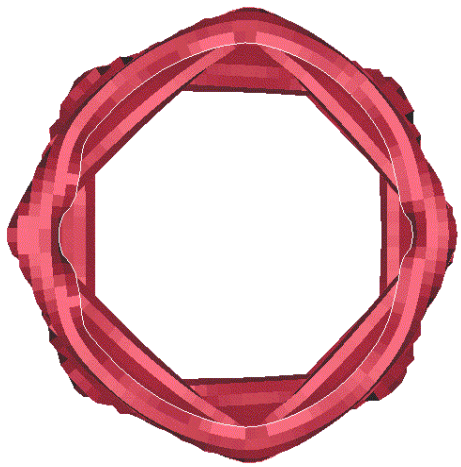

Figure 20. Folding pattern for original material model.

When the HSLA350 material model was modified by using a viscoplasticity option and adding logarithmically interpolated strain-stress curves for the 10^{+2}/s range, a triangular folding shape was obtained (Figure 21).

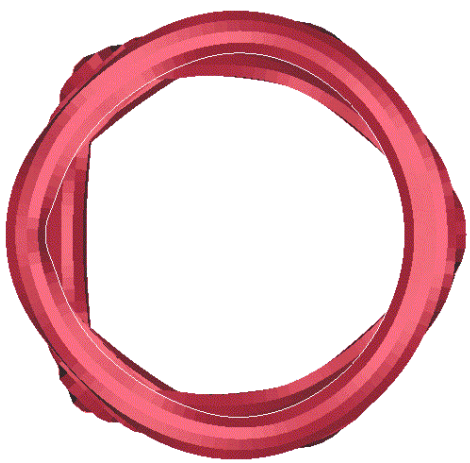

Figure 21. Folding pattern for material model with logarithmically interpolated material data.

The fact that the crushing modes have been changed illustrates the effect of details on modeling of structural collapse. The crush modes in circular tubes are very close, and different modes in simulations can also be influenced by other modeling factors (even more than by the material model), such as shell element formulation, FE mesh resolution, viscoplasticity option, etc. However, the simulations indicate that the peak force is directly related to the material model and the magnitude of imperfection. In the HSLA350 tube crush simulation, the simulated peak force was still lower than the experiment. Current research is looking at the effect of adding upper and lower yield behavior in the material models. Recent tests performed in the mid and high strain rates show pronounced upper and lower yield points for some steels.[11,18,29] The existence of this effect in HSLA steels has not been clearly established, but the discrepancy noted seems to be supporting such a premise. These results also support the premise that material properties at strain rates in the 10^{+2}/s range are very important for modeling of progressive tube crushing in automotive applications.

Conclusions

An improvement in predictive capability of the crashworthiness models is linked to development of realistic material models and finite elements with better representation of complex strain and stress states in progressive crushing. Strain rate sensitivity is an important component of the material models and needs to be incorporated in the crashworthiness models. The paper reports on the range of strains and strain rates calculated in the explicit FEM programs that are used for evaluation of constitutive models. Strain rate magnitudes of the order of 10^{+3}/s provide a reasonable upper limit for the model. Strain rate magnitudes of the order of 10^{+2}/s are prevalent for shell element sizes that are of the order of 1–2 tube shell thicknesses. The viscoplastic option for material modeling provides more realistically feasible strain rate histories. For modeling details of tube crushing, the FEM mesh discretization should be fine enough, as measured by the strain distribution, angle of shell directors, and resulting curvature, to model the crush fold formation. Once the kinematics are accurately approximated, the material model can be investigated for possible indications of material properties in the range where the experimental coupon tests are difficult to conduct. Current results

indicate a close link between the strain rate calculations and element type and discretization, and will be analyzed in more detail in the following publications.

References

1. F. B. Pickering, ed., *Constitution and Properties of Steels*, Vol. 7 of *Materials Science and Technology*, VCH, New York, 1992.
2. M. J. Manjoine, "Influence of rate of strain and temperature on yield stresses of mild steel," *J. Appl. Mech*. **11**, 211–218, 1944.
3. J. D. Campbell, *Dynamic Plasticity of Metals*, Springer, New York, 1972.
4. K. Mahadevan, J. R. Fekete, B. Schell, R. McCoy, and O. Faruque, "Strain-rate characterization of automotive steel and the effect of strain-rate in component crush analysis," SAE paper 982392, Society of Automotive Engineers, 1998.
5. K. Mahadevan, J. R. Fekete, and P. Liang, "Effect of strain-rate in full vehicle frontal crash analysis," SAE paper 2000-01-0625, Society of Automotive Engineers, 2000.
6. S. Simunovic, J. Shaw, and G. Aramayo, "Material modeling effects on impact deformation of ultralight steel auto body," SAE Paper 2000-01-2715, Society of Automotive Engineers, 2000.
7. A. Needleman, "Material rate dependence and mesh sensitivity in localization problems," *Computer Methods in Applied Mechanics and Engineering*, **67**(1), 69–85 (March 1988).
8. R. J. Clifton, "Plastic waves: Theory and experiment," p. 102–167 in S. Nemat-Nassser, ed., *Mechanics Today* 1, 1974.
9. W. Bleck and I Schael, "Determination of crash-relevant material parameters by dynamic tensile tests," *Steel Research*, **71**(5), 173–178, 2000.
10. T. Valentin, P. Magain, M. Quik, K. Labibes, and C Albertini, "Validation of constitutive equations for steel," *Journal de Physique IV (Colloque)*, **7**(C3), 611–616, 1997.
11. I. H. Hove, B. Andersson, T. E. Johnsen, "High speed tensile testing," *Journal de Physique IV (Colloque)*, **7**(C3), 229–234, 1997.
12. T. Hira, J. Hiramoto, and K Sakata, "Utilization of finite element method for expanding application of high strength steels for automotive body," *Kawasaki Steel Technical Report*, **46**, pp. 12–18, 2002.
13. L. L. Tam and C. R. Calladine, "Inertia and strain-rate effects in a simple plate-structure under impact loading," *International Journal of Impact Engineering*, **11**(3), 349–377, 1991.
14. M. Avalle and G. Belingardi, "Experimental evaluation of the strain field history during plastic progressive folding of aluminum circular tubes," *International Journal of Mechanical Sciences*, **39**(5), 575–583, 1997.
15. N. Hansen, X. Huang, and D. A. Hughes, "Microstructural evolution and hardening parameters," *Materials Science & Engineering A (Structural Materials: Properties, Microstructure and Processing)*, **A317**(1–2), 3–11, 2001.
16. N. Jones, *Structural Impact*, Cambridge University Press, 1989.
17. J. E. Field, S. M. Walley, N. K. Bourne, and J. M. Huntley, "Experimental methods at high rates of strain," *Journal de Physique IV (Colloque)*, **4**(C8), 3–22, 1994.
18. M. Quik, K. Labibes, C. Albertini, T. Valentin, and P. Magain, "Dynamic mechanical properties of automotive thin sheet steel in tension, compression and shear," *Journal de Physique IV (Colloque)*, **7**(C3), 379–384, 1997.
19. N. Triantafyllidis, A. Needleman, and V. Tvergaard, "On the development of shear bands in pure bending," *International Journal of Solids and Structures*, **18**(2), 121–138, 1982.
20. P. C. Galbraith and J. O. Hallquist, "Shell-element formulations in LS-DYNA3D: Their use in the modeling of sheet-metal forming," *Journal of Materials Processing Technology*, 50(1–4), 158–167, 1995.
21. E. Markiewicz, P. Ducrocq, and P. Drazetic, "Inverse approach to determine the constitutive model parameters from axial crushing of thin-walled square tubes," *International Journal of Impact Engineering*, **21**(6), 1998.
22. G. R. Johnson and W. H. Cook, "A constitutive model and data for metals subjected to large strains, high strain-rates and

high temperatures," p. 541–547 in *Proceedings of the Seventh International Symposium on Ballistic*, Hague, The Netherlands, 1983.

23. F. J. Zerilli and R. W. Armstrong, "Dislocation-mechanics-based constitutive relations for material dynamics calculations," *Journal of Applied Physics*, **61**(5), 1816–1825, 1987.
24. J. O. Hallquist, *LS-DYNA3D, An Explicit Finite Element Nonlinear Analysis Code for Structures in Three Dimensions*, LSTC Manual, 1995.
25. R. Liang and A. S. Khan, "Critical review of experimental results and constitutive models for BCC and FCC metals over a wide range of strain rates and temperatures," *International Journal of Plasticity*, 15(9), 963–980, 1999.
26. V. Tvergaard, "On the transition from a diamond mode to an axisymmetric mode of collapse in cylindrical shells," *International Journal of Solids and Structures*, **19**(10), 845–856, 1983.
27. S. R. Bodner and Y. Partom, "Constitutive equations for elastic-viscoplastic strain-hardening materials," *Journal of Applied Mechanics*, 385–389, 1975.
28. A. S. Khan and S. Huang, "Experimental and theoretical study of mechanical behavior of 1100 aluminum in the strain rate range 10-5–104 s-1," *International Journal of Plasticity*, **8**, 397–424, 1992.
29. http://www.a-sp.org, Auto Steel Partnership.
30. R. G. Davies and C. L. Magee, "The effect of strain-rate upon the tensile deformation of materials," *Journal of Engineering Materials and Technology*, **97**(2), 151–155, 1975.
31. W. Abramowicz and N. Jones, "Dynamic axial crushing of circular tubes," *Int. J. of Impact Eng.*, **2**(3), 263–281, 1984.
32. T. Berstad, O. Hopperstad, and M. Langseth, "Elasto-viscoplastic constitutive models in the explicit finite element code LS-DYNA3D," in *Proceedings of the Second LS-DYNA Conference*, 1994.
33. J. Singer, T. Weller, and J. Arbocz, *Basic Concepts, Columns, Beams and Plates*, Vol. 1 *of Buckling Experiments: Experimental Methods in Buckling of Thin-Walled Structures*, John Wiley & Son, 1998.
34. J. Singer, T. Weller, and J. Arbocz, *Buckling Experiments: Experimental Methods in Buckling of Thin-Walled Structures: Shells, Built-Up Structures and Additional Topics*, John Wiley & Son, 2002.
35. C. Calladine, *Theory of Shell Structures*, Cambridge Univ. Press, 1983.
36. A. Copa, "Effect of end conditions on buckling of cylindrical shells under axial compression impact," p.115–136 in *Test Methods for Compression Members*, ASTM Tech. Pub No. 419, American Society of Testing and Materials, 1966.
37. E. El-Magd, H. Scholles, and H. Weisshaupt, "Influence of strain rate on the stress-strain curve in the range of Luders strain," *Steel Research*, **67**(11), 495–500, 1996.

B. Enhanced Forming Limit Diagrams

Project Manager: Pat V. Villano
Auto/Steel Partnership
2000 Town Center Drive, Suite #320
Southfield, Michigan 48075-1123
(248) 945-4780; fax: (248) 356-8511; e-mail: pvillano@a-sp.org

Project Co-Chairman: John Siekirk
DaimlerChrysler Corporation
CIMS 484-34-01, 800 Chrysler Drive
Auburn Hills, Michigan 48326-2757
(248) 576-2567; fax: (248) 576-2155; e-mail: jfs@daimlercrysler.com

Technology Development Manager: Joseph Carpenter
(202) 586-1022; fax: (202) 586-1600; e-mail: joseph.carpenter@ee.doe.gov
Field Technical Manager: Philip S. Sklad
(865) 574-5069; fax: (865) 576-4963; e-mail: skladps@ornl.gov

---

Contractor: U.S. Automotive Materials Partnership
Contract No.: DE-FC05-02OR22910

Objective

- Provide information previously unavailable about relationships between die variables and increased forming limits that will be necessary to facilitate the manufacture of lightweight steel vehicles. This objective will be accomplished by using unique capabilities developed for this project.

Approach

- Analyze and document laboratory studies on the enhanced forming limits diagram (EFLD) concept to provide the necessary information for applying this technology in press shops.
- Develop a final research report describing and justifying the application methodology that provides guidelines for applying the EFLD technology.
- Conduct case studies for use in teaching the application of the EFLD technology.
- Prepare a teaching manual to be used for training sessions on applying EFLD technology.
- Conduct four one-day training seminars on applying the EFLD technology.

Accomplishments

- Completed the analysis and documentation of laboratory studies.
- Obtained from a partnership member 15 tensile tests for base material of stamped parts that will be used in the case studies.
- Completed both the *Analysis Strategy Based on Test Results* and the *Analysis of the Application of Current Predictive Equations for Aluminum-Killed Draw Quality (AKDQ) Steel Material.*
- Completed *Analysis and Documentation of the Laboratory Studies Research: Final Report*.

Final Direction

- Complete the applications technology final report.
- Complete the teaching manual to be used at training seminars.
- Conduct four training seminars.
- Link the research report files with the supporting database to allow users to access data online in real time via the website and an Internet connection.

Introduction

The EFLD concept is used to describe the effect of bending and straightening on conventional FLDs. Over the 4-year period ending December 31, 2001, experimental work was completed at the Industrial Research Development Institute (IRDI) in Midland, Ontario, that provided data to establish predictive relationships for determining the effects of bending and straightening on FLDs. Although some predictive relationships had been developed for aluminum-killed draw quality (AKDQ) steels, it became apparent that there was a need to determine similar relationships for high-strength steels and advanced high-strength steels. The project just completed focused on providing the necessary engineering relationships for developing an application methodology for using EFLD technology in press shops. Thus both knowledge of the research work and understanding of application issues are needed for successful completion of the project.

The work completed included descriptions of experimental and analysis procedures, empirical predictive equations, the range of applicability for the predictive equations, and identification of issues in applying the predictive equations in press shops. The predictive equations were set in terms of both net thickness strain and back tension and bending strain factor. Mechanistic understanding, sensitivity analysis, and statistical verification also support them. The statistical verification includes standard measures of fitness of fit for regression equations, comparison of predicted versus actual results, and estimates of experimental error and its effect on the variability between predicted and actual values.

The IRDI experimental work also provided substantial data not needed for the primary focus of the project; these “by-products” are packaged so that they are available in a convenient form to researchers who may want to use the information. These by-products fall into three major categories: curvature predictions, information on draw beads, and springback of channel draw pieces.

The final research report has been completed and is available on CD-ROM, as is the supporting raw data. Additional work is under way to link the report and the data online in real time via the website and an Internet connection.

Because production stampings are usually produced in non–steady-state, non–proportional-loading, and non–plane-strain conditions, the application methodology and teaching materials to use EFLD technology in press shops must be developed.

On a practical basis, the most important aspect of the EFLD technology will apply to steel that has been deformed over the die entry radius or that has passed through a draw bead and has deformed over the die entry radius. Because back tension and deformation rates vary throughout a press stroke, the enhancement in the FLD will vary through a press stroke. A further complication results from the fact that net deformation for material in a die cavity can be the sum of deformation prior to a draw bead, deformation from bending and straightening, and subsequent deformation in a die cavity. Given the complications of production stamping processes, application methodology will use a lower boundary approach. It is important, however, that these lower boundaries not be too conservative. The contractor selected has press shop experience including circle-grid, ultrasonic, forming limit curve, and other measurement analyses on production stampings required for this project.

The development of the application methodology will be a two-step process: the use of existing finite element analysis solutions followed by work in press shops. Parts to be studied include

hoods, deck lids, fenders, wheelhouses, body side outers, and floor pans.

Once the required technology is available, case studies will be prepared and teaching materials developed. Finally, a series of one-day seminars will be scheduled for the automotive partnership members and their suppliers to effectively transfer the knowledge. The contractor selected has the necessary background in developing and teaching practical sheet metal forming for both the press shop floor and the university environment.

The technology report will be made available on CD-ROM; and a hard copy of the technology report, along with the teaching manual, will be made available for all training seminar participants.

C. High-Strength Steel Stamping Project

Project Manager: Jack Noel
Auto/Steel Partnership
2000 Town Center, Suite 320, Southfield, MI 48075-1123
(248) 945-4778; fax: (248) 356-8511; e-mail: jnoel@a-sp.org

Co-Chairman: James Fekete
General Motors Corporation—Metal Fabricating Division
100 Kirts Blvd., Troy, MI 48007-5001
(248) 696-1176; fax: (248) 696-1101; e-mail: jim.fekete@gm.com

Co-Chairman: Changqing Du
DaimlerChrysler Corporation
800 Chrysler Drive, Auburn Hills, MI 48326
(248) 576-5168; fax: (248) 576-7910; e-mail: cd4@dcx.com

Technology Development Manager: Joseph Carpenter
(202) 586-1022; fax: (202) 586-1600; e-mail: joseph.carpenter@ee.doe.gov
Field Technical Manager: Philip S. Sklad
(865) 574-5069; fax: (865) 576-4963; e-mail: skladps@ornl.gov

---

Contractor: U.S. Automotive Materials Partnership
Contract No.: DE-FC05-02OR22910

Objectives

- Determine how to accurately predict the degree of springback in a variety of flanging conditions on parts made from high-strength steel (HSS) sheet prior to the construction of the production tooling.
- Identify designs and manufacturing processes that will reduce springback and other part distortions and recommend them to design and manufacturing engineers.

Approach

- Enhance HSS stamping springback predictability through finite element analysis (FEA).
- Improve HSS stamping springback control by developing a better understanding of part design geometries that affect flange springback and die processes that control springback.
- Design a part with 15 typical automotive flange conditions and construct a die to stamp the part.
- Stamp several grades and gauges of HSS and measure and record the springback for a die process and FEA simulation reference.

Accomplishments

- Studied FEAs of part designs and computer simulations of manufacturing processes to determine factors causing springback of HSS sheet metal stampings.
- Established optimum stamping die processes and weld flange designs by comparing simulation output with actual stamping die results. The simulation group is working to improve the FEA predictive accuracy for part designs that produce the least amount of springback and variation.

- Conducted springback control experiments using tooling designed to replicate actual production stamping die processes and typical automotive weld flange configurations. These experiments confirmed the importance of optimizing part geometry and the stamping process in order to reduce residual stress, flange springback, and part-to-part variation.
- Measured parts and recorded and analyzed data. Results will be published on the Auto/Steel Partnership web site (www.a-sp.org).

Introduction

The use of HSS in automotive applications has been increasing over the last 10 years. Owing to the mechanical properties of HSS, the springback after forming and the geometric dimensional control of the stamped parts have been critical issues in stamping tool construction and in the stamping industry. Because the actual dimensions of the HSS stamping off the tool are unpredictable with current FEA tools and technology, the average die face re-machining may take four to six times as long as is required for mild steel applications and result in 2 to 3 months of lost die tryout time.

Computer simulation has been widely applied in the stamping industry and has been recognized as a common virtual stamping tool to identify formability issues and evaluate solutions before the actual stamping dies are made. This technology has proved effective for predicting splits and buckles in drawn panels. However, experience has demonstrated that computer simulation data have not been reliable in predicting the degree and modes of springback for most stampings from form and flange dies, even with small form radii of two to three times the metal thickness.

Details

This project was initiated because of a necessity to improve predictive capabilities and shorten lead-time by providing additional data on HSS springback tendencies. These data are expected to enable more accurate springback correlation and compensation amounts for various flange types when using HSS. The data could also be used to improve the correlation between actual die performance and analytical tools. The approach used was to develop a test tool to form various flange types with different levels of material thickness and strength (Figures 1 and 2). The material yield strength levels considered ranged from 280 to 420 MPa, and thicknesses ranged from 1.0 to 2.0 mm. High-strength/low-alloy (HSLA) and dual-phase steels were tested.

(a)

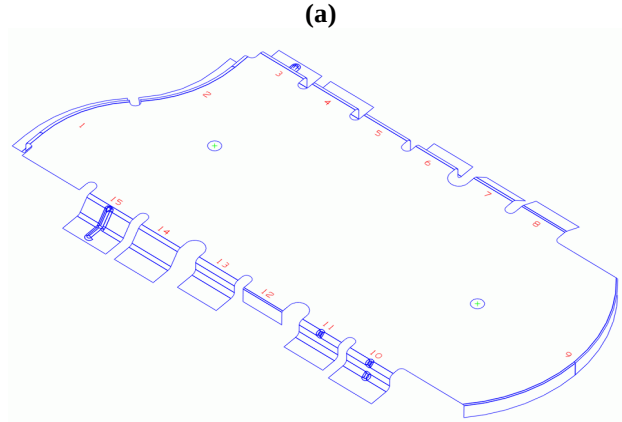

(b)

Figure 1. Experimental part design (a) with 15 different weld flange conditions (b).

Effect of Material Strength and Thickness

The results reported for the influence of material strength and thickness generally conformed to the expectations of the group. The comments are confined to observations from flat flanges, in the absence of embossments such as beads and darts. Features such as beads, darts, and tension/compression flanges mask the material effects. For flat, non-embossed flanges, springback angles were expected to be larger as the material reached higher

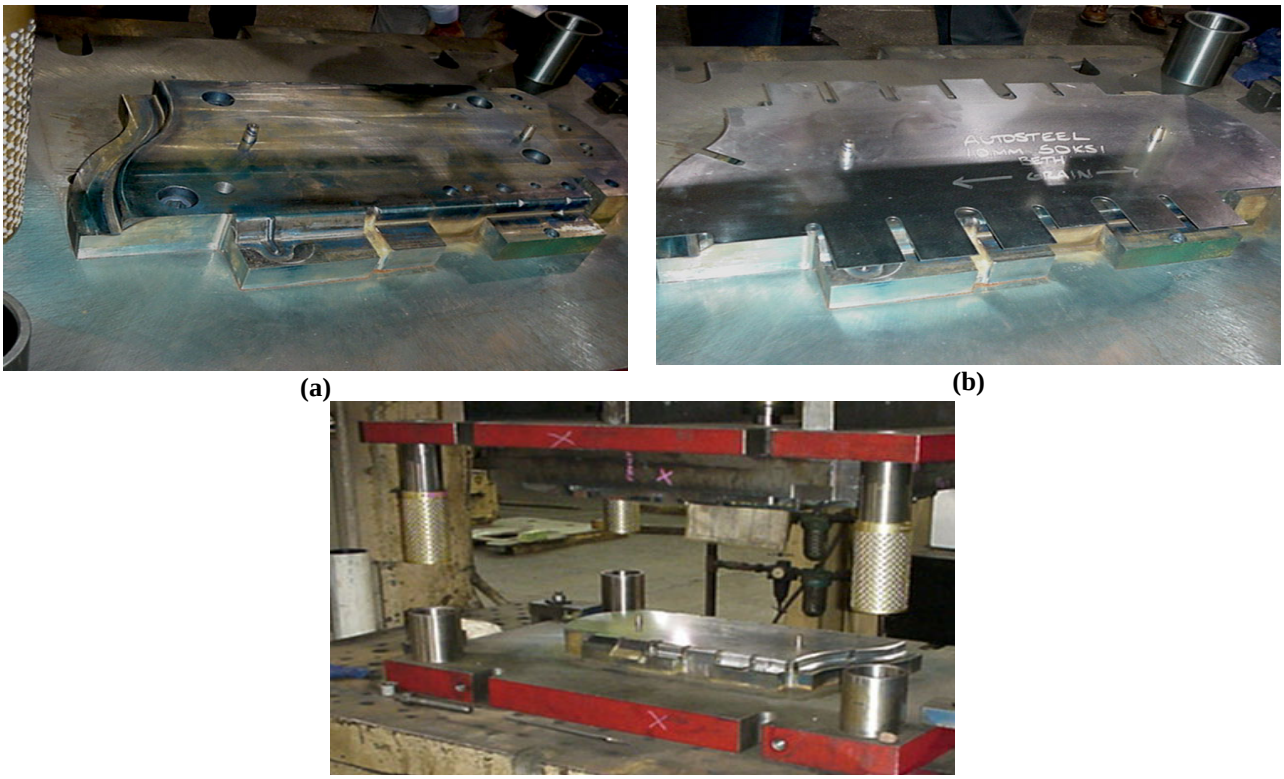

(a) **(b)** **(c)**

Figure 2. The die used to produce the panel shown in Figure 1. The wrought steel die contained inserts at the flange radii to adjust die clearance. A developed blank was used. (a) Lower die including two locating pins; (b) developed blank on the lower die; (c) complete die in the press after a hit.

strength and lower thickness. This expectation turned out to be true for most measurements.

For the HSLA materials, the effect of reducing thickness from 2.0 to 1.0 mm had a significantly greater effect than increasing the strength from 280 to 420 MPa. The thickness reduction at a given strength level had the effect of increasing the springback angle by ~1.0° to 1.5°. In one case (Flange 6), the reduction in thickness caused a 3° increase in springback angle for the 280-MPa material. The strength increase generally caused the springback angle to increase by ~ 0.2° to 1.0°. This indicates that guidelines for springback compensation in HSLA steel need to comprehend the effect of thickness.

This information is intended to supplement current design for manufacturing guidelines for cases where the parts use HSS. The resulting parts can then be designed with a clear understanding of the projected springback amount and its impact on the assembly or manufacturing process.

D. Hydroforming Materials and Lubricants Project

Project Manager: Jack Noel
Auto/Steel Partnership
2000 Town Center, Suite 320
Southfield, MI 48075-1123
(248) 945-4778; fax: (248) 356-8511; e-mail: jnoel@a-sp.org

Chairman: Robert Moses
Dofasco Inc., P.O. Box 2460
Hamilton, Ontario, Canada L8N 3J5
(905) 548-7200, ext. 6636; fax: (905) 548-4250; e-mail: robert_moses@dofasco.ca

Technology Development Manager: Joseph Carpenter
(202) 586-1022; fax: (202) 586-1600; e-mail: joseph.carpenter@ee.doe.gov
Field Technical Manager: Philip S. Sklad
(865) 574-5069; fax: (865) 576-4963; e-mail: skladps@ornl.gov

---

Contractor: U.S. Automotive Materials Partnership
Contract No.: DE-FC05-02OR22910

Objectives

- Develop mechanical test procedures for tubes.
- Improve the accuracy of and confidence in finite element modeling of tubular hydroforming.
- Develop an understanding of steel and lubricant requirements for hydroforming, using a combination of experiments and finite element modeling.

Approach

- Conduct a series of experiments to determine the free expansion and corner fill capabilities of various mild and high-strength steel tubes using internal pressurization.
- Conduct other experiments for tube expansion to determine the effects of axial compression in combination with internal pressurization and the effects of pre-bending and pre-forming on subsequent formability.
- Use the collected data to develop forming limit diagrams for tubular hydroforming. These are required for any computer simulation of hydroforming.

Accomplishments

- Modified the hydroform tooling to allow internal pressurization with axial compression of straight tubes.
- Procured tooling and prepared tubes for the internal pressurization and axial compression of bent tubing shapes.
- Cleaned, circle-gridded, lubricated, and labeled 125 tubes.
- Measured 75 of the 125 tubes for axial and hoop strains. Necking locations were recorded, and strains were measured in the vicinity of the neck. Corner strains and thickness were also measured and recorded.

- Began work on a final report on the project to be available in December 2002 in CD-ROM format and on the Auto/Steel Partnership web site, a-sp.org.

Background

The formability limits for steel in tubular hydroforming are poorly understood. Practitioners are using the sheet steel forming limits developed for conventional stamping processes to assess the formability of hydroformed components. For example, the effect of axial compression on the forming limits of steel is unknown. Likewise, the effect of prior strain induced in the tube-conversion and tube-bending processes that precede the hydroforming operation have been ignored. The accuracy of information about forming limits needs to be assessed and improved to allow the optimum application of tubular hydroforming in the lightweighting of vehicles.

In addition, the tests that tube producers use to evaluate tube quality do not properly address metal forming issues relevant to tubular hydroforming. The tests currently used focus on weld quality and the dimensional accuracy of the tubes, but they do not adequately describe the amount of ductility left in the tube for post-forming operations such as hydroforming. There is a need to develop and evaluate tube-testing methods that are suitable for evaluation and comparison of material formability and for input into finite element models.

Additional information is needed about the fundamental material attributes that control the hydroformability limits of steel. Such knowledge would allow steel makers to develop appropriate new steel grades or apply existing steel grades appropriately to hydroforming applications. Experiments will be conducted using the facilities of the Industrial Research and Development Institute of Midland, Ontario.

Figure 1 shows a section of the die and part for the free expansion and corner fill portions of the experiment for straight tubes. Figures 2 and 3 show a section of the hydroform die and bent tube for the inside and outside radius expansion tests, respectively.

Figure 1. Section of hydroform die and part for straight tube corner fill experiments.

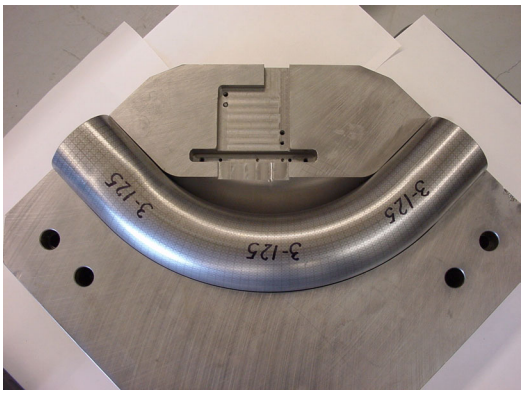

Figure 2. Section of hydroform die and bent tube for inside radius expansion tests.

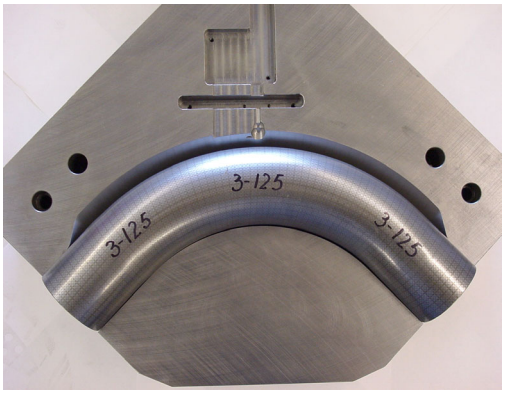

Figure 3. Section of hydroform die and bent tube for outside radius expansion tests.

E. High-Strength Steel Joining Technologies Project

Project Manager: Thomas D. Mackie
Auto/Steel Partnership
2000 Town Center, Suite 320, Southfield, MI 48075-1123
(248) 945-4781); fax: (248) 352-1740); e-mail: tmackie@a-sp.org

Co-Chairman: James Dolfi
Ford Motor Company
17000 Oakwood Blvd. P.O. Box 1586, mail code #E1425
Dearborn, MI 48121

Co-Chairman: Philip Coduti
Ispat Inland Inc.
3001 East Columbus Drive, mail code MC9-000
East Chicago, IN 46312

Technology Development Manager: Joseph Carpenter
(202) 586-1022; fax: (202) 586-1600; e-mail: joseph.carpenter@ee.doe.gov
Field Technical Manager: Philip S. Sklad
(865) 574-5069; fax: (865) 576-4963; e-mail: skladps@ornl.gov

---

Contractor: U.S. Automotive Materials Partnership
Contract No.: DE-FC05-02OR22910

Objective

- Facilitate the increased use of advanced high-strength steels (AHSS) in Auto/Steel Partnership lightweighting projects through the development of weld parameters and schedules that will produce quality welds in 12 grades of these advanced steels.

Approach

- Establish a weld window for 12 different AHSS materials using two resistance spot-welding systems, scissor gun, and “C” gun.
- Evaluate the welds using peel test, tensile shear, microhardness, and metallographic examination.
- Develop a fatigue test coupon and evaluate weld fatigue properties for the various AHSS materials.
- Develop an impact test model and evaluate impact characteristics for the various AHSS materials.
- Characterize the effects of electrode design, metallurgy, and coatings on the weldability of specific steels.
- Characterize the scissor gun and C gun machines as to rigidity and weldability.
- Determine the effect of weld bonding on tensile shear, impact, and fatigue on straight welded coupons.
- Evaluate the strain-controlled fatigue on ten AHSS materials, including the effect of chemistry, coatings, and weld bonding.
- Evaluate impact properties on the 12 AHSS materials.

- Develop a standard of acceptance for welds with inner-facial fractures that meet the strength requirements of welds that pull the traditional nugget.

Accomplishments

- Completed the weld lobe study.
- Made photographs and performed microhardness tests.
- Designed the fatigue test coupon and began machining test coupons for the first two materials.
- Performed preliminary impact tests.
- Completed preliminary weld-bonded tests.

Background

The use of AHSS is critical to the steel industry's efforts to make automotive components more lightweight without sacrificing strength or incurring escalating cost, an issue with the use of other lightweight materials. The development of welding parameters and physical testing parameters for the new steels qualifies them for various automotive components. Extensive work has been performed on the spot welding of mild steels during the Intelligent Resistant Welding Project of the Auto Body Consortium and various Auto/Steel Partnership welding and bonding projects.

The project is being approached from several perspectives, including weld lobe evaluation under peel test conditions to determine the optimum weld time and current, hardness, metallography, impact, and fatigue. Weld bonded joints are being evaluated, as are welded joints. Fracture characteristics of these welds will be documented and compared with the weld strengths in the development of a standard for partial thickness fractures.

F. Sheet Steel Fatigue Characterization

Project Manager: Gene Cowie
Auto/Steel Partnership
2000 Town Center, Suite 320, Southfield, MI 48075-1123
(248) 945-47798; fax: (248) 356-8511; e-mail: gcowie@a-sp.org

Ph.D. Chairman: Benda Yan
Staff Research Engineer, Product Applications
Ispat Inland Inc.
3001 E. Columbus Drive, East Chicago, IN 4312
(219) 399-6922; fax: (219) 399-6562; e-mail: bxyan@ispat.com

Technology Development Manager: Joseph Carpenter
(202) 586-1022; fax: (202) 586-1600; e-mail: joseph.carpenter@ee.doe.gov
Field Technical Manager: Philip S. Sklad
(865) 574-5069; fax: (865) 576-4963; e-mail: skladps@ornl.gov

---

Contractor: U.S. Automotive Materials Partnership
Contract No.: DE-FC05-02OR22910

Objectives

- Investigate advanced high-strength steels (AHSS) for weight reduction and crash energy management and investigate the performance of steels currently being used under variable-amplitude conditions. Specifically, these activities will
  - Investigate the work hardening effects of stamping and the strengthening effects of paint baking on the grades that exhibit such effects on constant amplitude strain-controlled fatigue properties, and compare them with similarly strained and baked conventional HSS.
  - Investigate the variable-amplitude performance of low-carbon steel to interstitial-free (IF) steel.
  - Investigate other new AHSS with various joining methods.

Approach

- Characterize the fatigue properties of selected grades of steel by identifying three fatigue coefficients and three fatigue exponents.
- Characterize the fatigue properties of welded and weld bonded joints of HSS and AHSS.
- Compile the results into a database that can be used by designers and design engineers to retrieve and compare the fatigue lives of sheet steel structural components in the design phase.

Accomplishments

- Completed Phase 4 testing.
- Developed and accepted procedures for testing spot welded and weld bonded joints in HSS and AHSS that will provide data useful to the participating auto manufacturers.

Introduction

In the era when vehicle mass was not a drawback, and in fact was sometimes considered an advantage, the primary concern in body design was rigidity. More recently, the need to reduce body mass to comply with mandated Corporate Average Fuel Economy standards caused design engineers to reexamine design procedures and materials. HSS, judiciously selected and applied, emerged as potential low-cost, reliable materials for mass reduction. As structural components are optimized and thinner-gauge, higher-strength materials are assessed, component fatigue life becomes a consideration. In order to assess the performance of a material in the design phase, its fatigue characteristics must be known. This project is currently addressing steel grades identified by the Lightweight Front End Structures initiative of the Auto/ Steel Partnership.

The long-term strategy for the sheet steel fatigue characteristics project originally consisted of four phases of work.

Details

Phase 4 was initiated, after discussion at several preceding meetings, upon agreement of the team members at the May 30, 2001 meeting. This phase of work comprises two projects:

Project 1 was an analysis of the strain + bake properties of dual-phase (DP) 600 vs transformation-induced plasticity 600 vs high-strength low-alloy (HSLA) 340 (50 ksi). Two prestrain conditions were specified with the understanding that, if they were not readily attainable, the closest possible attainable level would be employed subject to approval of the team. The two levels achieved and tested were

- Balanced biaxial stretch with an equivalent strain of 1.5% for the DP 600+ and HSLA 340 steels
- Balanced biaxial stretch with an equivalent strain of 5% for all three materials

This work was reported complete at the June 27, 2002, team meeting. The results are undergoing analysis. In general, pre-strain did have a noticeable effect on fatigue life. The variation depended on the amount of pre-strain, the load level, and the type of steel.

Project 2 was a comparison of low-carbon drawing steel with the interstitial-free steel tested in Phase 3 under constant amplitude and variable loading conditions. This work was completed on schedule on October 31, 2001. The results have been compiled into a report and distributed to team members for evaluation. Preliminary analysis indicates that there is essentially no difference between these two grades for the two test conditions.

Project Information from Phase 4 testing will be made public in a paper to be presented at the Society of Automotive Engineers in 2003. The title will be "A Comprehensive Strain-Life Database For Automotive Sheet Steels."

Welded and Weld Bonded Joints

It was determined that although the participating auto companies have been investigating the fatigue characteristics of spot welds, there remains a need for a joint effort to evaluate the fatigue characteristics of spot welded and weld bonded joints. The effort began with presentations by key researchers on the current state of the work at DaimlerChrysler, Ford Motor Company, and General Motors. Based on these presentations, the Sheet Steel Fatigue Team was able to develop parameters for a test program that would produce results beneficial to all three companies. Early in the planning, the Auto/Steel Partnership Joining Technologies Team was brought into the program, and it was agreed that that team would prepare the samples to be tested. This interaction ensured that the samples would be joined using procedures that were properly controlled and in adherence to the best current practices in sheet metal joining.

The following test parameters were developed and agreed upon.

- There will be two modes of testing: tension shear and coach peel.
- Weld fatigue performance is independent of metal thickness for mild steels and high-strength low-alloy grades. Therefore, tests on these grades will use only one metal thickness (1.6 mm).

- Since no such data are yet available for AHSS, several grades in this class will be tested at two thicknesses (1.6 mm and 0.7 mm).
- Testing will be done at two R ratios: 0.1 and 0.3. (R, the stress ratio, is defined as s_{min}/s_{max}.)
- Eight steel grades will be tested.
- Testing will include both spot welded and weld bonded joints.

Eight testing laboratories known to have capabilities in this type of testing were invited to submit proposals. Two have been selected and a portion of the work delegated to each.

G. Strain Rate Characterization

Project Manager: Pat V. Villano
Auto/Steel Partnership
2000 Town Center Drive, Suite 320, Southfield, MI 48075-1123
(248) 945-4780; fax: (248) 356-8511; e-mail: pvillano@a-sp.org

Chairman: James Fekete
General Motors Corporation—Metal Fabricating Division
100 Kirts Blvd., Troy, MI. 48007-5001
(248) 696-1176: fax: (248) 696-1101; e-mail: jim.feteke@gm.com

Technology Development Manager: Joseph Carpenter
(202) 586-1022; fax: (202) 586-1600; e-mail: joseph.carpenter@ee.doe.gov
Field Technical Manager: Philip S. Sklad
(865) 574-5069; fax: (865) 576-4963; e-mail: skladps@ornl.gov

Contractor: U.S. Automotive Materials Partnership
Contract No.: DE-FC05-02OR22910

Objective

- Provide excellent representation of the mechanical properties of sheet steel in dynamic computer models of vehicle structures and assess their impact.

Approach

- Conduct drop tower tube-crush tests of dual-phase (DP) and high-strength low-alloy (HSLA) steel tubes.
- Support Oak Ridge National Laboratory's strain rate modeling project (see report 8A).
- Support the American Iron and Steel Institute's project to characterize the fatigue and high strain rate deformation performance of new-generation high-strength steels.
- Conduct double hinge plate experiments and analyses to confirm the quality of the validation experiment.
- Conduct circular tube crush experiments and analyses of three steel grades to confirm the quality of the validation experiments.

Accomplishments

- Purchased HSLA and DP 600 steel tubes for drop tower test.
- Re-issued the purchase order for the double hinge plate experiment to University of Dayton Research Institute.

Introduction

Over the past several years, evaluating crashworthiness in new vehicle designs has become more and more dependent upon math-based engineering tools, including finite element analysis. The use of these tools enables rapid optimization of product designs, which reduces development time and cost while minimizing product mass. The growing dependence on these techniques and the desire to accelerate the replacement of physical testing with analytical validation of design solutions

is driving the need to improve the predictive capability of the math-based tools.

The accurate representation of the mechanical properties of the sheet metals used in current and future vehicles is a key element in the development of accurate math-based tools. One key aspect of these properties is the strain rate dependence of the stress/strain behavior. Previous Auto/Steel Partnership research has experimentally demonstrated the positive influence of strain rate sensitivity on the dynamic performance of sheet steel structures. However, efforts to accurately simulate this behavior using math-based tools have not been completely successful.

H. High-Strength Steel Tailor-Welded Blanks

Project Manager: Jack Noel
Auto/Steel Partnership
2000 Town Center, Suite 320, Southfield, MI 48075-1123
(248) 945-4778; fax: (248) 356-8511; e-mail: jnoel@a-sp.org

Co-Chair: Aleksy Konieczny
U.S. Steel Group, a unit of USX Corp.
5850 New King Court, Troy, MI 48098-2692
(248) 267-2541; fax: (248) 267-2581; e-mail: akonieczny@uss.com

Co-Chair: Mariana Forrest
DaimlerChrysler Corporation
2730 Research Drive, Rochester Hills, MI 48309
(248) 838-5256; fax: (248) 838-5338; e-mail: mgf@daimlerchrysler.com

Technology Development Manager: Joseph Carpenter
(202) 586-1022; fax: (202) 586-1600; e-mail: joseph.carpenter@ee.doe.gov
Field Technical Manager: Philip S. Sklad
(865) 574-5069; fax: (865) 576-4963; e-mail: skladps@ornl.gov

---

Contractor: U.S. Automotive Materials Partnership
Contract No.: DE-FC05-02OR22910

Objective

- Investigate the formability, springback, and weld properties of high-strength steel (HSS) and advanced HSS (AHSS) tailor-welded blanks (TWBs).
- Determine the fatigue properties of laser weld and mash seam welds in AHSS.
- Investigate the weight and cost savings potential for patch-type vs laser-welded TWBs.

Approach

- Prove the concept of using patch-type TWBs on door inner panels.
- Make stampings from automotive door inner dies to produce this type of door.
- Plan laser-weld and mash seam weld fatigue.

Accomplishments

- Determined that the patch-type tailored blank will not be one of the primary proposals for a lightweight door assembly.
- Determined the required fatigue test procedures and procured quotes for the work. Completed tension-compression fatigue testing at the University of Waterloo in Ontario.

Introduction

The tailor welding of sheet steel blanks, that is, the use of varying gauges and grades of steel within a specific flat panel "tailored" to provide specific characteristics in select areas, continues to gain favor in the product design community. Industry data show that production of TWBs has grown from just over 1 million in 1993 to nearly 24 million in 1999, with market potential estimated at 50 million blanks by the year 2003. TWBs have gained acceptance in the automotive industry as a means of simultaneously achieving cost and weight reduction. The application of high-strength low-alloy (HSLA) steel and AHSS, such as dual-phase and transformation-induced plasticity (TRIP) steels, offer the potential for further weight reduction. However, there is uncertainty regarding the weldability of these products and the resultant ductility of the weld and heat-affected zone. Manufacturing techniques must be developed and validated to produce reliable, high-volume HSS and AHSS TWBs.

The purpose of this focused 3-year project is to investigate the manufacturability and formability of HSS and AHSS TWBs and demonstrate that these products can produce a structure of significantly lower mass.

In addition to supporting the work of the Auto/Steel Partnership Lightweight Front End Project, the TWB Project has investigated wider application of patch-type blanks to reduce both the weight and the cost of automotive door assemblies for the Auto/Steel Partnership Lightweight Closures Project.

Project Details

The TWB team has worked with the Lightweight Closures Project to prove the concept of using patch-type TWBs on door inner panels. This type of tailored blank reduces weight because the spot-welded patch can be made to the smallest required irregular shape, whereas the laser weld must be a straight line, making the heavy metal member of the blank larger and heavier than necessary. The cost of spot welding the patch-type blank is also much less than the cost of laser welding.

The project team worked with the contractor, Oxford Automotive, to make stampings from automotive door inner dies to produce this type of door (Figure 1). Initial reviews by representatives from General Motors and DaimlerChrysler were generally positive; they made inquiries about repeating the stamping trials on dies for doors with more complex configurations.

Figure 1. Door inner hinge reinforcement made from a patch-type blank.

The stamping die tryout work with the contractor initially indicated a potential for this process to reduce the cost and weight of some door assemblies. However, the contractor was unable to overcome the problem of distortion at the sealing surface and in the areas of metal compression in the draw die. The Lightweight Closures Project and its contractor have determined that the patch-type tailored blank will not be one of their primary proposals for a lightweight door assembly. The Lightweight Closures team is now looking at other forms of laser-welded tailored blanks and hydroformed structures for mass reduction of door inner assemblies. The TWB team will continue to look for practical applications for this type of tailored blank.

Most of the work done by the project team in 2002 was associated with conducting a fatigue test program for mash-welded and laser-welded blanks for the Lightweight Front End Structures Project. The TWB team procured dual-phase (DP) 600 and 800 materials in the grades and gauges that will be used to form structural members in lighter-weight vehicles. The TWB team had these materials welded

in various grade and gauge combinations for test specimens (Table 1).

Table 1. Tailor-welded blank combinations for tension-compression test.

DQ 1.6 mm to DP 800 1.2 mm	T-C	Laser
DQ 1.6mm to DP 600 1.2 mm	T-C	Laser
DP 800 1.6 mm to DP 800 1.2 mm	T-C	Laser
DP 600 1.5 mm to DP 600 1.2 mm	T-C	Laser
DP 600 1.5 mm to DP 800 1.2 mm	T-C	Laser
DP 800 1.6 mm to DP 600 1.2 mm	T-C	Laser
DP 800 1.6 mm to DP 800 1.2 mm	T-C	Laser
DP 600 1.2 mm to DP 600 1.2 mm	T-C	Laser
DP 600 1.2 mm to DP 600 1.2 mm	T-C	Mash

DQ = draw quality.
DP = duel phase.

Fatigue test planning was done in conjunction with the Sheet Steel Fatigue Project, the Joining Technology Project, and the Lightweight Front End Structures Project. As they defined the materials they would use for TWBs in the motor compartment rails, the TWB team determined the required fatigue test procedures and procured quotes for this work. Tension-compression fatigue testing has been completed at the University of Waterloo in Ontario (see Figures 2, 3, and 4). The tests were performed on an MTS servo-controlled closed-loop machine. Differences in failure modes were noted and recorded. Reverse bending fatigue tests are also planned for additional fatigue data on these types of welds in AHSS. Test data will be furnished to the Lightweight Project initiatives and published on the Auto/Steel Partnership web site (www.a-sp.org).

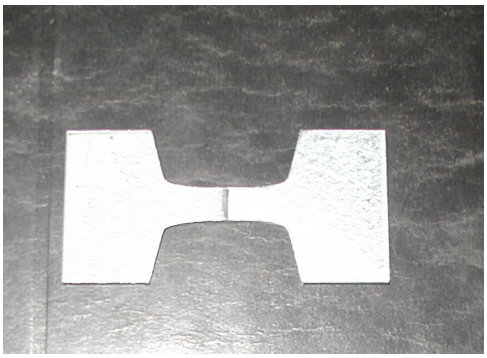

Figure 2. Tailor-welded blank fatigue test specimen.

Figure 3. Fatigue test specimen mounted in test machine grips with anti-rotation guide.

Figure 4. Test specimen mounted in the MTS test machine with an anti-buckling guide.

I. Tribology

Project Manager: Pat V. Villano
Auto/Steel Partnership
2000 Town Center Drive, Suite 320, Southfield, MI 48075-1123
(248) 945-4780; fax: (248) 356-8511; e-mail: pvillano@a-sp.org

Project Chairman: Alan Pearson
General Motors Corporation
Metal Fabricating Division
1240 Stevenson Hwy., Mail code 480-991-408, Troy, MI 48007-7025
(248) 528-7247: fax: (248) 528-4070; e-mail: alan.pearson@gm.com

Technology Development Manager: Joseph Carpenter
(202) 586-1022; fax: (202) 586-1600; e-mail: joseph.carpenter@ee.doe.gov
Field Technical Manager: Philip S. Sklad
(865) 574-5069; fax: (865) 576-4963; e-mail: skladps@ornl.gov

---

Contractor: U.S. Automotive Materials Partnership
Contract No.: DE-FC05-02OR22910

Objective

- Conduct stamping simulation tests to study the effects of tribology—the interrelationship of lubrication, friction, and wear—on the stamping performance of advanced high-strength steels. (Stamping performance is defined as minimizing die wear and maximizing dimensional stability. Understanding the contribution of lubricants to errors in spring back prediction when using finite element analysis will also improve dimensional performance.)

Approach

Phase 1—Friction Testing

- Select the sheet steel material grades for tests.
- Obtain the sheet steel materials from the member steel companies and ship them to TribSys Inc. for twist compression testing (TCT) and draw bead simulation (DBS) friction tests.
- Have Tribsys manufacture and supply dies and inserts to be used in the Phase 2 tool wear testing.
- Set up coil line for tool wear test at TribSys.

Phase 2—Tool Wear Testing

- Compare die wear rate with different lubricants applied to the high-strength steel materials selected for the tests.
- Restraining force will be compared with temperature, contact area, and wear on the draw beads.
- Correlate the data with the friction test results from Phase 1.

Accomplishments

- Selected lubricants to be applied to the sheet steel samples, obtained them from lubricant suppliers, and shipped them to TribSys.
- Obtained all steel sample material for TCT & DBS tests from steel suppliers and shipped it to TribSys.

- Completed TCT and DBS friction tests.
- Set up the complete coil line to be used for the tool wear test.
- Manufactured (at TribSys) all dies and die inserts required for the tool wear tests.
- Determined steel coil material specifications for the wear test. Three material grades were selected—DP 600, high-strength low-alloy (HSLA 340), and aluminum-killed draw-quality (AKDQ). All are 1.0 mm thick. The material will be supplied with three different coatings.
- Received one coil of HSLA 340 at TribSys.

Introduction

Lubricants have historically been used in forming sheet metal stampings to reduce friction, improve formability, and minimize die wear, as well as provide corrosion protection. The projected increase in the use of advanced high-strength steels (AHSS) forces a greater emphasis on understanding the process parameters associated with die wear, such as heat build-up and die scoring and dimensional stability caused by springback variation. The contribution of interfacial friction to springback variation is not known. AHSS may require different lubricants and/or die materials to minimize the friction and die wear.

In an attempt to reduce die weight, automobile manufacturers are using thinner, higher-strength steel panels. There are several issues associated with stamping parts from these steels. The springback of high-strength steel panels results in reduced process capability and greater variation in the vehicle assembly. The higher strength of these steels means that dies will be subjected to higher contact pressure and greater wear. Wear in the draw beads will affect the restraining force and result in greater variation, as well as down-time for repairs.

This project will examine how springback and die wear are affected by lubricant and die materials used with AHSS.

Tribology tests will be used to collect data and measure responses such as friction (retaining force), temperature, contact area, springback, and wear. These responses will be related to actual stamping practices, an important step in quantifying the problem and implementing possible solutions.

In Phase 1 of this project, the effect of lubricants on friction, springback, and wear from stamping AHSS will be examined using the DBS and TCT. Surface phenomena such as contact area and roughness will be examined and used to model the relationship between friction and springback.

In Phase 2, the wear test will be used to compare wear rates of draw beads with different lubricants and sheet materials. In this test, restraining force will be compared with temperature, contact area, and wear of the drawbeads. These data will be correlated using the TWT and DBS results from Phase 1.

Figure 1 shows the coil line setup for the tool wear test. Table 1 provides descriptions of the tooling to be used.

Table 1. List of tooling (dies and die inserts)

Item	Description	Quantity
1	G3500 TCT annular tools—1 in. OD, 0.750 in. ID	100
2	G3500 drawbeads—0.375 in. diameter × 2.75 in.	30
3	Ion nitrided G3500 drawbeads—0.375 in. diameter × 2.75 in.	30
4	G3500 wear test center insert—0.375 × 1.13 × 2.75 in.	30
5	G3500 wear test side insert—1.25 × 1.13 × 2.75 in.	20

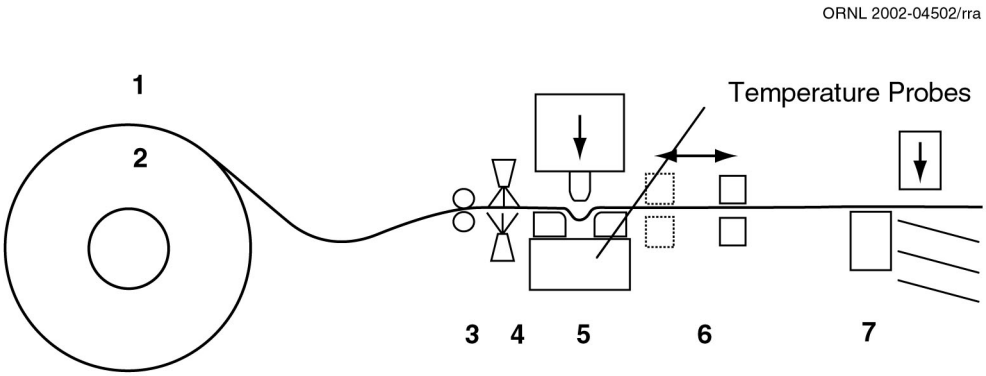

No.	Name	Description
1	Decoiler	48 in. × 4 in.—2000 lb max
2	Coil	2–2.5 in. coil–0.040 in. thick
3	Guide rollers	Vertical and horizontal guiding
4	Lubricator	Air brush spray top and bottom
5	Die set and inserts	Guided die set with bead inserts (3/set)
6	Feeder– 6 in. stroke	6000 lb hydraulic with hydraulic clamps
7	Cut-off	Synchronized with feeder

Figure 1. Tool wear test apparatus at TribSys.

Appendix A. ACRONYMS AND ABBREVIATIONS

ADFG	advanced drive file generation
A/SP	Auto/Steel Partnership
ABP	acrylobenzophenone
ACC	Automotive Composites Consortium
AFS	American Foundry Society
AHSS	advanced high-strength steel
AKDQ	aluminum killed draw-quality
Al	aluminum
ALCOA	Aluminum Company of America
ALM	Automotive Lightweighting Materials
ALTC	Automotive and Light Truck Committee
AMD	Automotive Metals Division
AN	acrylonitrile
ANL	Argonne National Laboratory
APAW	aluminum plasma arc welding
APC	American Plastics Council
ASTM	American Society for Testing and Materials
BCC	body-centered cubic
BHF	blank holder force
BIW	body-in-white
CAD	computer-aided design
CAE	computer-aided engineering
CAFE	Corporate Average Fuel Economy
CD	compact disk
CFC	carbon-fiber composite
CLM	cast light metals
CRADA	cooperative research and development agreement
CWRU	Case Western Reserve University
DOE	U.S. Department of Energy
DP	dual phase
DPF	direct powder forging
DQSK	drawing quality special-killed
E	experimental
EDS	energy-dispersive spectroscopy
EFLD	enhanced forming limit diagram
EGN	exfoliated graphite nanostructure
ELV	end-of-life vehicle
EMF	electromagnetic forming
FBL	feedback linearization
FCVT	FreedomCAR and Vehicle Technologies
FE	finite element
FEA	finite element analysis
FEM	finite element method

FLD	forming-limit diagram
FP2	Focal Project 2
FP3	Focal Project 3
FY	fiscal year
GASP	grazing angle surface polarimeter
GM	General Motors
HDG	hot dip galvanized
HDPE	high-density polyethylene
HSLA	high-strength low-alloy
HSS	high-strength steel
HTML	High Temperature Materials Laboratory
HVSC	Huron Valley Steel Corporation
ICS	Industrial Ceramic Solutions
IF	interstitial free
IIW	International Institute of Welding
IR	infrared
IRDI	Industrial Research and Development Institute
ISRM	intermediate strain rate machine
ITP	International Titanium Powders
LANL	Los Alamos National Laboratory
LBNL	Lawrence Berkeley National Laboratory
LCCF	low-cost carbon fiber
LIBS	laser-induced breakdown spectroscopy
LLDPE	linear low-density polyethylene
LLNL	Lawrence Livermore National Laboratory
MA	methylacrylate
MAP	microwave-assisted plasma
MMC	metal matrix composite
MMCC	metal matrix cast composites
MPCC	magnesium powertrain cast components
NCC	National Composites Center
NDE	nondestructive evaluation
NDT	nondestructive test
NRCAN	Natural Resources of Canada
NTRC	National Transportation Research Center
OAAT	Office of Advanced Automotive Technologies
ODS	oxygen dispersion strengthened
OEM	original equipment manufacturer
OIT	Office of Industrial Technologies
ORNL	Oak Ridge National Laboratory
P4	programmable powder preform process
P&S	press and sintering
PAN	polyacrylonitrile

PC	personal computer
PE	polyethylene
PID	proportional integral derivative
PM	powder metallurgy
PMC	polymer matrix composite
PMPRA	powder metallurgy particle-reinforced aluminum
PNNL	Pacific Northwest National Laboratory
PP	polypropylene
PQTI	Plasma Quench Titanium, Inc.
PRA	particle-reinforced aluminum
PVB	polyvinyl butyral
PVC	polyvinyl chloride
R&D	research and development
RH	relative humidity
ROI	return on investment
ROM	read-only memory
RVE	representative volume element
SA/RD	sales and administrative/research and development
SAE	Society of Automotive Engineers
SAMPE	Society for the Advancement of Material and Process Engineering
SCMD	structural cast magnesium development
SEM	scanning electron microscope
SHT	solution heat treatment
SNL	Sandia National Laboratories
SOM	solid-oxygen-conducting membrane
SRIM	structural reaction injection molding
TCM	technical cost model
TDM	Troy Design and Manufacturing
TGA	thermo-gravimetric
TRIP	transformation-induced plasticity
TWB	tailor welded blank
ULSAB	ultralight steel auto body
UM	University of Michigan
USAMP	U.S. Automotive Materials Partnership
USCAR	U.S. Council for Automotive Research
UT	University of Tennessee
UTS	ultimate tensile strength
UV	ultraviolet
YSZ	yttria-stabilized zirconia